Characterization of RIG-I-like receptor activation by *in vitro* transcribed mRNA vaccines and modulation by nucleoside modifications

Dissertation

zur

Erlangung des Doktorgrades (Dr. rer. nat.)

der

Mathematisch-Naturwissenschaftlichen Fakultät

der

Rheinischen Friedrich-Wilhelms-Universität Bonn

vorgelegt von

Katharina Isabell Maser

aus

Marburg

Bonn (Juni, 2025)

Angefertigt mit Genehmigung der Mathematisch-Naturwissenschaftlichen Fakultät

der Rheinischen Friedrich-Wilhelms-Universität Bonn

Gutachter/Betreuer: Prof. Dr. med. Gunther Hartmann

Gutachter: Prof. Dr. rer. nat. Michael Famulok

Tag der Promotion: 28.01.2026

Erscheinungsjahr: 2026

Abstract

The therapeutic potential of mRNA has been studied for decades, but the COVID-19 pandemic accelerated its development and approval for human use. A major challenge is the potential of mRNA to activate innate RNA-sensing receptors, triggering inflammatory responses that affect vaccine dosage and efficacy. The underlying immune mechanisms are not well understood, although this knowledge would greatly aid in optimizing *in vitro* transcribed (IVT)-mRNA and modulating its immunostimulatory effects.

In this study, the innate immune response to COVID-19 mRNA vaccines by BioNTech and Moderna, as well as to IVT-mRNA, was characterized *in vitro*. The cytosolic double-stranded RNA (dsRNA) sensing RIG-I-like receptors (RLRs), RIG-I and MDA5, were identified as the primary receptors responsible for mRNA-induced type I interferon responses. Mechanistically, RLRs were activated by unspecific dsRNA byproducts generated during *in vitro* transcription. LC/MS analysis revealed that 5′ triphosphate-dsRNA byproducts, capable of activating RIG-I, were not permissive to capping by Vaccinia Capping Enzyme. Various methods were explored to remove dsRNA byproducts and reduce RLR activation, such as oligo(dT)-purification and dephosphorylation.

Additionally, the study characterized species-specific differences in innate mRNA sensing between human and murine cells. In human cells, IVT-mRNA was primarily sensed by RIG-I, while MDA5 was the dominant sensor in murine cells.

Moreover, effects of nucleotide modifications, including Ψ, m1Ψ, 5moU, m5C, and m6A, on individual innate RNA receptors were investigated, focusing on RLRs. RLRs were differentially modulated by these modifications in human and murine cells. Reduced dsRNA content was the leading cause for lower RIG-I activation in response to modified IVT-mRNAs. However, 5moU directly impaired activation of specifically murine RIG-I, while human RIG-I was only slightly affected. Furthermore, Ψ and m1Ψ enhanced activation of murine but not human MDA5. Both human and murine MDA5 activation was completely abolished by 5moU, m5C, and m6A, even when pure dsRNA was used, indicating direct effects on MDA5.

Furthermore, mRNA translation and its modulation by nucleoside modifications were investigated. Some modifications, such as m1Ψ and 5moU, are known to enhance mRNA translation, for which the lower innate immune activation is assumed to be responsible. While RLR activation and type I interferon signaling did indeed restrict mRNA translation in human cells, as expected, the enhanced translation by nucleoside modifications only partially depended on this. Thus, it was revealed that nucleoside modifications enhance translation by directly affecting the translation machinery via currently unknown mechanisms.

In conclusion, the incorporation of either m1Ψ or 5moU has been identified as the most promising measure to reduce mRNA-induced innate immune responses while achieving maximal translation.

Overall, this study provides valuable insights into immune responses to mRNA vaccines, presents methods for modulating these responses, and highlights differences between experimental systems relevant to preclinical study design. Altogether, this could be applied to design mRNA therapeutics that achieve an optimal balance of antigen expression and adjuvant activity on the one hand, or entirely non-immunostimulatory mRNA on the other hand, which could be used for protein replacement or combined with exogenous adjuvants tailored to specific pathogens.

Table of Contents

1. Introduction

1.1 A short overview of the immune system

Various pathogens constantly threaten the human body. To detect and defend against these pathogens, the immune system utilizes numerous complex processes, which are divided into two branches: innate and adaptive.[1] The innate immune system is germline-encoded and is responsible for the immediate detection of pathogens, resulting in a broad defense response that counteracts infection. In contrast, the adaptive immune system utilizes somatic recombination to develop a specific response over time, potentially leading to long-lasting immunity. Together, these two systems enable the body to effectively combat infections and establish heightened protection against future encounters.

1.1.1 The innate immune system

The very first defense mechanisms of the innate immune system are physical barriers, such as the skin and mucosae, and directly antimicrobial molecules, such as the complement system. These proteins are constitutively present in the blood, and their expression is increased upon immune activation. Complement proteins are activated by binding pathogens either directly or via antibodies and can damage a foreign intruder or facilitate their phagocytosis by immune cells via opsonization.[1] Upon contact with our cells, pathogens or their components can also be detected by a diverse set of innate-immune pattern recognition receptors (PRRs), which detect conserved molecular patterns associated with microbial invaders or damaged cells, known as pathogen-associated molecular patterns (PAMPs) or damage-associated molecular patterns (DAMPs), respectively.[1] The discrimination of self vs. non-self is fundamental to prevent aberrant immune activation and autoinflammatory responses. Therefore, PRRs recognize PAMPs and DAMPs that are usually absent in healthy cells (e.g. cytosolic, double-stranded RNA as an intermediate of viral replication, or bacterial cell wall lipopolysaccharides (LPS)) or by detecting molecules in unusual locations (e.g. DNA in the cytosol).

PRRs, such as Toll-like receptors (TLRs) or RIG-I-like receptors (RLRs), are distributed across extracellular, intracellular, and endosomal compartments and enable comprehensive surveillance of the whole cell and its environment. Some PRRs, particularly the cytosolic antiviral receptors, are broadly expressed – that is, in most nucleated cells – while others are restricted to professional innate immune cells, such as macrophages, dendritic cells, and natural killer (NK) cells.[1] These cells are often strategically located at barrier sites and tissues, enabling a fast detection and defense response upon penetration of physical barriers.

Upon binding to the specific PAMP, the PRR is activated and initiates intracellular signaling cascades, culminating in the production of pro-inflammatory cytokines and chemokines, which alert neighboring cells and attract and activate cells of the innate and adaptive immune system.[1] In innate immune cells, PRR signaling leads to cell activation, that is, the initiation of cellular effector functions, such as phagocytosis of pathogens, release of antimicrobial proteins, elimination of infected cells, antigen presentation, and the expression of cell surface markers and cytokines.

The nature of these responses is tailored to the detected pathogen in order to enable an effective defense. For instance, PRRs specialized in detecting viral infections, typically nucleic acid sensors such as the cytosolic RLRs, induce type I interferons (IFN) and, to a lesser extent, other pro-inflammatory cytokines.[1] Type I IFNs act in an autocrine and paracrine manner via the interferon-α/β receptor (IFNAR) to establish an antiviral state in the infected cell itself and neighboring cells. This antiviral state aims to inhibit viral replication through mechanisms such as increased RNA degradation and reduced protein translation. Furthermore, type I IFNs attract immune cells specialized in eliminating infected cells, such as NK cells and cytotoxic $CD8^+$ T cells.[1] To facilitate their surveillance, type I IFNs enhance the expression of cell surface markers such as major histocompatibility complex (MHC) class I, which presents intracellular peptides and enables the identification of an infected cell. As a final measure, RLRs may induce programmed cell death of the infected cell to prevent the virus from spreading.

Besides restraining infections, another important role of the innate immune system is the initiation of adaptive responses.[1] PRR signaling is critical for the activation of dendritic cells, which are innate immune cells specialized in presenting the captured and processed antigens to T cells in the draining lymph node. T cell activation further requires co-stimulation in the form of cell surface molecules and cytokines from the antigen-presenting cell, which is likewise induced by PRR signaling. Additionally, the cytokines induced by the innate immune response shape the nature of adaptive responses.

Dysregulation or mutation of PRRs can lead to erroneous recognition of endogenous molecules, resulting in autoinflammatory diseases. For instance, type I interferonopathies represent a group of disorders characterized by excessive type I IFN signaling that causes systemic inflammation and tissue damage. These disorders include systemic lupus erythematosus and Aicardi-Goutières syndrome and are often associated with dysregulated or mutated TLRs, RLRs, or the cytosolic DNA sensor cGAS (cyclic GMP-AMP synthase).[2]

In summary, the innate immune system serves as the body's first line of defense against microbial threats and orchestrates rapid and effective responses to pathogen invasion. For localized infections, this may be sufficient to eliminate the pathogens. However, local inflammatory responses can cause tissue damage and thus should not be sustained for prolonged periods. Furthermore, some pathogens are able to persist against or evade the innate defense mechanisms. Therefore, another important role

of the innate immune system is to restrain infections until the adaptive response develops. Additionally, innate responses promote and shape the highly specific adaptive responses that lead to protective and long-lasting immunity. Understanding pattern recognition mechanisms can potentially improve the treatment of human disease and enable the development of innovative prophylactic and therapeutic strategies to be implemented in, for example, vaccination or cancer immunotherapies.

1.1.2 The adaptive immune system

Antigen presentation is fundamental to the adaptive immune response and involves loading peptides onto transmembrane proteins for extracellular display. These specialized proteins, called MHC (major histocompatibility complex) molecules, comprise two classes. MHC class I molecules are expressed on the surface of all nucleated cells and are loaded in the endoplasmic reticulum with peptides derived from the cytosolic degradation of intracellular proteins.[1] Thus, MHC class I molecules can present both harmless endogenous and viral or mutated peptides in the case of infection or cell damage. Peptide presentation on MHC class I molecules serves the surveillance by immune cells, such as cytotoxic $CD8^+$ T cells and NK cells, which eliminate infected or damaged cells. In contrast, MHC class II molecules are expressed only by professional antigen-presenting cells (APCs), such as conventional dendritic cells (cDCs), macrophages, and B cells.[1] MHC class II molecules are loaded with peptides in the endolysosome. These peptides can originate from extracellular sources via endocytosis, such as bacteria or cell debris that may also contain intracellular pathogens, or from intracellular sources through autophagy.

Innate cDCs are especially important for the initiation of the adaptive immune response.[1] cDCs are abundant at barrier sites, such as the skin or mucosal tissues, and constantly sample cellular debris and potential pathogens from their surroundings via macropinocytosis or receptor-mediated endocytosis. Upon sensing a PAMP, PRR signaling induces the maturation of cDCs into antigen-presenting cells (APCs). As such, they increase intracellular processing of sampled material and antigen presentation via MHC class I and II molecules. Simultaneously, the cells migrate to secondary lymphoid tissues, such as the draining lymph node, where the adaptive immune response is initiated. Additionally, a subset of cDCs is capable of cross-presentation, that is the presentation of extracellularly derived peptides on MHC class I. Cross-presentation is essential to induce adaptive immunity against intracellular pathogens because it enables the cDC to sample exogenous antigens and initiate an appropriate immune response without being infected itself.[1]

In the draining lymph node, the antigen-specific T cell receptor (TCR) of naive $CD8^+$ or $CD4^+$ T cells binds to the peptide:MHC-I or peptide:MHC-II complex, respectively, on the cDC. Due to somatic

recombination, each lymphocyte bears a unique receptor specific to an individual MHC:peptide complex. This polyclonality enables the detection of a vast array of antigens and is the basis for the adaptive immune response. During lymphocyte development, several selection mechanisms, including positive and negative selection, ensure that lymphocytes do not recognize endogenous peptides, thereby establishing central tolerance and preventing autoimmune reactions. Upon activation, T cells undergo significant proliferation, producing numerous clones of the same antigen specificity, and differentiate into effector T cells.[1] This process takes around 3 – 6 days before the effector T cells migrate to the site of infection.[1]

Besides binding to the MHC:peptide complex, the activation of naive T cells requires co-stimulation by cDCs. This is provided by cell surface proteins, such as CD80 and CD86, as well as pro-inflammatory cytokines. The production of these co-stimulatory proteins by cDCs is induced upon PRR signaling, and specific cytokines expressed by the cDC can polarize the adaptive response in a manner that is, ideally, tailored to the detected pathogen. These cytokines guide the differentiation of $CD4^+$ T cells into different T helper (T_H) cell subsets, such as T_H1 against intracellular, T_H17 against extracellular, or T_H2 against parasitic pathogens.[1] These T_H cell subsets are equipped with specialized effector functions and cytokines that shape an optimal immune response. $CD8^+$ T cells differentiate into cytotoxic T lymphocytes (CTL) and are specialized in killing infected or damaged cells.

Besides this cell-mediated immunity, the adaptive immune system provides humoral immunity in the form of antibodies. Antibodies are produced by differentiated B cells and function by neutralizing harmful substances, blocking cell entry of pathogens, and facilitating phagocytosis and complement activation via opsonization.[1] Similar to T cells, naive B cells possess a unique antigen-specific B cell receptor (BCR), a cell surface-bound immunoglobulin (Ig). Binding of the BCR to the respective antigen results in its internalization and processing, followed by presentation on MHC class II. This peptide:MHC-II complex is bound by effector T cells, usually specialized follicular helper T cells (T_{FH}), that have already been activated by the same antigen. This process occurs in dedicated areas known as germinal centers inside secondary lymphoid organs. The T_{FH} activates the B cell via co-stimulatory surface proteins, such as CD40L, and cytokines, such as interleukin-21 (IL-21), that induce B cell differentiation into an antibody-producing plasma cell.[1] While naive B cells produce only IgD and IgM antibodies, their differentiation induces a class switch directed by specific cytokines produced by the T_{FH} and shifts the B cell to the production of either IgG, IgA, or IgE. IgG is the most abundant antibody and confers broad protection in blood and tissues, while IgA is the only secreted antibody and is important for the protection of mucosal tissues.[1] IgE is specialized in the defense against parasites, such as helminths, by activating granulocytes, specifically mast cells and basophils, to release antimicrobial granules. Through the complex processes of somatic hypermutation and affinity maturation, the B cell will enhance the specificity and affinity of the produced antibodies.

The two-signal activation model of naive T and B lymphocytes, consisting of the peptide:MHC and TCR/BCR interaction, and co-stimulation provided by cDCs and T_{FH} cells in the form of surface proteins and cytokines, is another guardrail that helps to prevent autoimmune reactions in addition to central tolerance. Endogenous peptides are constantly presented on MHC molecules, but in the absence of PRR signaling and subsequent co-stimulation, lymphocytes that exhibit specificity for endogenous antigens will not be activated and often undergo anergy, a state of cellular unresponsiveness. Additionally, the absence of innate immune responses favors the differentiation of anti-inflammatory regulatory T cells.[1] Together, these processes establish peripheral tolerance to endogenous or harmless antigens.

While most of the antigen-specific effector T and B cells die after the infection has been cleared, known as clonal contraction, a small percentage differentiates into long-lived memory cells, which are capable of mounting a fast response upon recurrent infection without the need for cell-mediated activation and differentiation. Antibody-producing plasma cells that migrate to the bone marrow are long-lived and provide antigen-specific antibodies for up to several decades.[1] Together, this immunological memory provides enhanced protection against the respective pathogen by enabling fast and efficient immune responses and reducing the probability and severity of recurrent infection.

1.2 RNA-sensing receptors of the innate immune system

1.2.1 RIG-I-like receptors

The RIG-I-like receptors (RLRs) are a family of cytosolic PRRs comprising three members: RIG-I (retinoic acid-inducible gene I), MDA5 (melanoma differentiation-associated protein 5), and LGP2 (laboratory of genetics and physiology 2).[2,3] RLRs are broadly expressed in all nucleated cells and play a crucial role in detecting viral infections by recognizing double-stranded RNA (dsRNA). DsRNA is a hallmark of viral infection, as endogenous dsRNA is not abundant in the cytosol and is actively counteracted by mechanisms such as A-to-I editing.[4–6] Thus, cytosolic dsRNA can indicate viral infection with dsRNA viruses and occurs during the replication of single-stranded RNA viruses (ssRNA). Although many RNA viruses are detected by both RLRs, RIG-I and MDA5 also have non-redundant functions.[7] Amongst others, RIG-I is important for the defense against Orthomyxoviridae, such as Influenza virus A and B, and Paramyxoviridae, such as Sendai virus, whereas MDA5 is involved in the detection of Picornaviridae, such as Encephalomyocarditis virus (EMCV), and Coronaviridae, such as Severe Acute Respiratory Syndrome Coronavirus 2 (SARS-CoV-2).[8]

RLRs bind to dsRNA via their C-terminal domain (CTD) and a central DExD/H-Box RNA helicase domain. RIG-I and MDA5, but not LGP2, further possess two N-terminal caspase activation and recruitment domains (CARDs). Binding of dsRNA induces conformational changes that expose the CARD domains and enable interaction with MAVS (mitochondrial antiviral-signaling protein), an adapter protein downstream of RLR signaling that is located in the outer mitochondrial membrane.[9–11] Due to its lack of CARD domains, LGP2 cannot signal but is instead assumed to modulate RIG-I and MDA5 activation. Both RIG-I and MDA5 bind dsRNA in a sequence-independent manner but require distinct patterns for their activation, as explained below.

While transcription initially generates RNA with a 5′ triphosphorylated (ppp) end, eukaryotic mRNA is capped before translocation into the cytosol. Capping refers to the addition of a 7-methylguanosine (m7G) to the 5′ RNA end (cap-0) and subsequent 2′-O-methylation of the first and second nucleotide (cap-1 and cap-2, respectively).[12] Additionally, ribosomal and transfer RNAs are processed to 5′ monophosphorylated (p) ends and 2′-O-methylated at selected positions throughout the RNA sequence. Therefore, 5′ppp-dsRNA is a hallmark of viral infection. Via its CTD, RIG-I binds to the 5′ end of dsRNA while requiring a minimum of 18 bp double-stranded region and recognizes 5′ppp, pp, and, to a lesser extent, hydroxyl (OH) RNA ends, but it is not activated by 5′p-RNA.[13–20] A cap-0 structure on the 5′ end diminishes activation of RIG-I, whereas cap-1 and cap-2 completely abrogate it.[21] An ideal RIG-I agonist is blunt-ended, although RIG-I does tolerate 3′ but not 5′ overhangs.[14] RIG-I binds to dsRNA termini and translocates along the RNA length in an ATP hydrolysis-dependent manner, leading to CARD exposition and oligomerization of RIG-I. The subsequent dissociation of oligomerized RIG-I from the RNA is assumed to be critical for interaction with MAVS.[22] In line with this, ATPase activity of RIG-I and dsRNA-induced RIG-I signaling correlate closely, and the replacement of only one amino acid in the ATPase domain of RIG-I renders it inactive while maintaining RNA-binding capacity.[2,23,24]

In comparison, the ligand requirements for MDA5 activation have mainly remained elusive. While it is known that MDA5 binds to and oligomerizes on long dsRNA, the experimental evidence for the required RNA length varies considerably from 500 to up to 2000 bp dsRNA.[23,25] Additionally, while the dsRNA analog polyinosinic:polycytidylic acid (poly(I:C)) is a potent MDA5 ligand, its counterpart polyadenylic:polyuridylic acid (poly(A:U)) is not, indicating that activation of MDA5 requires currently unknown RNA characteristics other than merely long dsRNA, such as higher-order RNA structures.[26,27] Nevertheless, several studies show that MDA5 binds dsRNA internally and forms continuous filaments along the length of the dsRNA in an ATP hydrolysis-dependent manner.[28,29] This mechanism is presumed to be the basis for the length requirement of MDA5 activation. Furthermore, it remains ambiguous whether MDA5 is inhibited by 2′-O-methylation of the first nucleotide. Züst *et al.* reported increased cytokine induction and reduced viral replication of a coronavirus lacking functional 2′-O-methyltransferase in mice, which were indeed dependent on MDA5 but also TLR7.[30] In contrast, a different study by Szretter *et al.* found no effect of MDA5

deficiency on virulence of a West Nile virus mutant lacking 2′-O-methylation in primary cells and mice.[31] Additionally, Luthra *et al.* identified a viral 5′ cap-1 RNA capable of activating MDA5, suggesting that MDA5 is not generally inhibited by 2′-O-methylation.[32] Nevertheless, further investigation is required to clarify the role of 2′-O-methylation in MDA5 activation.

Both RIG-I and MDA5 induce the oligomerization of MAVS via CARD-CARD interactions, leading to the recruitment of TBK1 (TANK-binding kinase 1) and IKK (IκB kinase). These phosphorylate the transcription factors IRF3 (interferon regulatory factor 3), IRF7, and NFκB (nuclear factor kappa-light-chain-enhancer of activated B cells), which in turn induce the expression of type I IFNs and pro-inflammatory cytokines (Figure 1).

While type I IFN production is not unique to RLR activation, the corresponding signaling pathway will be explained in the following to delineate the functional outcomes associated with RLR activation. The best-characterized proteins of the type I IFN family are the multiple IFNα subtypes (13 in humans, 14 in mice) and the single IFNβ protein.[33] Type I IFNs bind to the ubiquitously expressed IFNAR that signals via the JAK-STAT (Janus kinase; signal transducers and activators of transcription) pathway, leading to the formation of the transcription factor complex ISGF3, which consists of STAT1, STAT2, and IRF9 (Figure 1).[33] By binding to interferon-stimulated response elements (ISRE), ISGF3 induces the transcription of several antiviral restriction factors, known as interferon-stimulated genes (ISGs). ISGs inhibit viral entry and replication, for example by increased RNA degradation and reduced protein translation. Additionally, type I IFNs attract and activate NK cells and CTLs that will eliminate infected cells and enhance the maturation of APCs and antigen-presentation. In addition to their constitutive expression, RIG-I and MDA5 are ISGs themselves, and their expression is enhanced by IFNAR signaling, creating a positive feedback loop. Finally, activation of MAVS can induce apoptotic cell death via several type I IFN-dependent and -independent mechanisms.[34–37]

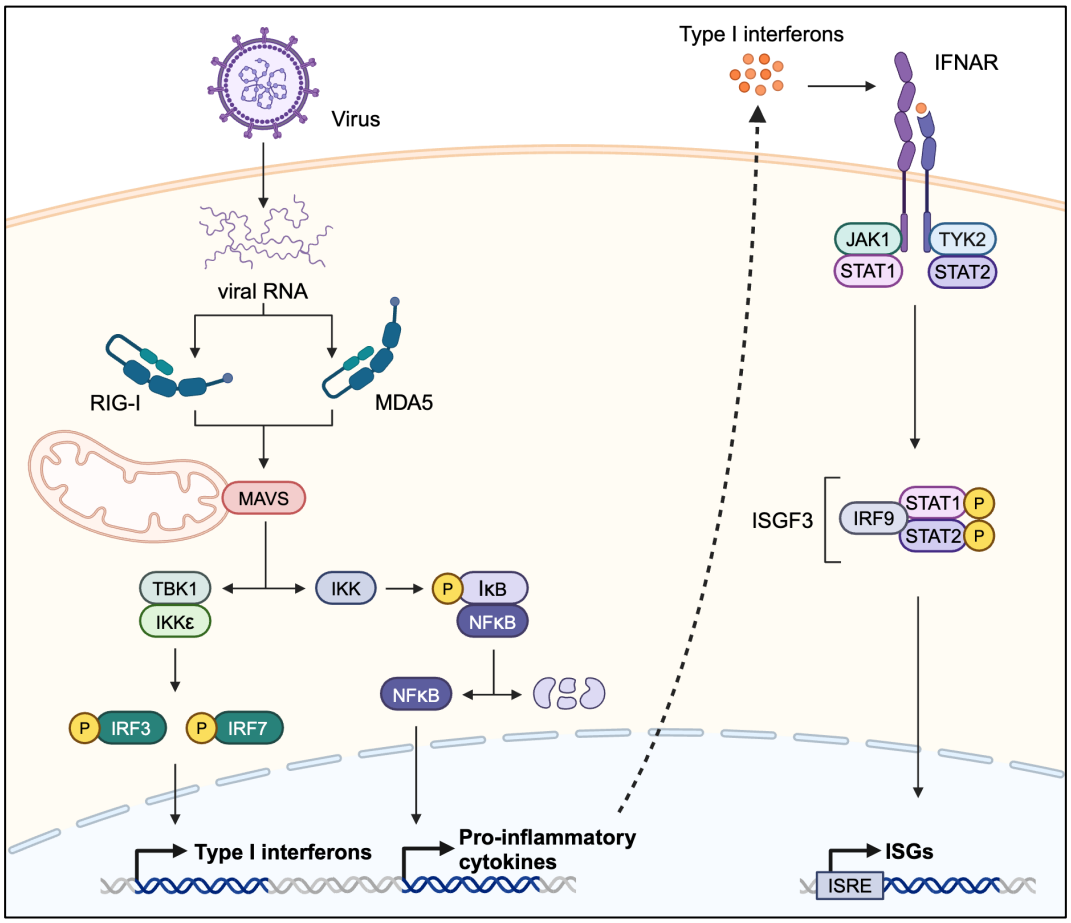

Figure 1: Signaling pathways of RIG-I-like receptors and type I IFN receptor
RIG-I and MDA5 sense cytosolic viral dsRNA and initiate signaling cascades by MAVS oligomerization. Activation of TBK1 and IKKε leads to phosphorylation of IRF3 and IRF7, which induce transcription of type I interferons. Simultaneously, activated IKK phosphorylates IκB leading to the release of NFκB, which induces transcription of pro-inflammatory cytokines. Type I interferons signal in an autocrine and paracrine manner via IFNAR and induce the transcription of interferon-stimulated genes (ISGs) via ISGF3.

1.2.2 Toll-like receptors

Toll-like receptors (TLRs) are transmembrane glycoproteins that consist of an extracellular leucine-rich repeat (LRR) in a horseshoe-like form that is responsible for PAMP recognition, a transmembrane region and an intracellular Toll/IL-1 receptor (TIR) domain that initiates downstream signaling.[38] This family comprises 10 and 12 different TLRs in humans and mice, respectively. While TLRs in the plasma membrane specialize in recognizing lipids and proteins, endosomal TLRs, such as TLR3, TLR7, TLR8, TLR9, and TLR13, recognize nucleic acids. Signaling of these TLRs requires homodimerization, which is supported by the acidic environment in the endosome.[39] In contrast to the broadly expressed RLRs, TLRs are restricted to specific cell types, such as immune or epithelial cells.

TLR9 senses unmethylated CpG motifs in bacterial DNA, and although TLR13 senses RNA, it recognizes a highly conserved sequence motif of bacterial ribosomal RNA that is not relevant to this study.[1] Moreover, TLR13 is not present in primates.[39]

TLR3 is mainly expressed in macrophages, cDCs, and intestinal epithelial cells. It senses dsRNA originating from engulfed dsRNA viruses or endocytosis of dying cells that contain replication intermediates of ssRNA viruses.[1,39] Physiological ligands include several viruses known to activate MDA5, such as West Nile virus and EMCV, and TLR3 is also activated by poly(I:C).[39] The minimal dsRNA length required for TLR3 activation is approximately 40 bp, but it was recently proposed that TLR3 can form multimeric complexes by binding to longer dsRNA laterally.[40] Upon ligand binding, TLR3 forms a homodimer, and the intracellular TIR domain recruits the adapter molecule TRIF (TIR-domain containing adapter-inducing interferon-β), which in turn activates several TRAF (TNF receptor-associated factor) proteins. Via the TRAF3-TBK1-IRF3 and the TRAF6-IKK-NFκB pathway, TLR3 induces the expression of type I IFNs and pro-inflammatory cytokines, respectively.[39]

In humans, TLR7 is primarily expressed in plasmacytoid DCs (pDCs) and B cells, whereas TLR8 is expressed in myeloid immune cells, including monocytes, macrophages, and cDCs. In mice, TLR7 is also expressed in these myeloid cells, whereas TLR8 is dysfunctional [39,41] pDCs are a subset of DCs specialized in producing type I IFNs upon viral infection.[1] TLR7 and TLR8 are essential for the recognition and defense against RNA viruses, such as Influenza A virus and SARS-CoV-2, and certain bacteria. Initially, TLR7 and TLR8 were believed to bind ssRNA. However, recent studies demonstrated that each receptor possesses two ligand binding sites that bind a single nucleotide and a short oligonucleotide, respectively, which are generated via RNA degradation by endosomal RNases.[42–46] While TLR7 binds to individual guanosines and trinucleotides of a NUN sequence (N = any nucleotide, U = uridine), TLR8 binds individual uridines and UN dinucleotides.[47] Engagement of both binding pockets seems to be required for efficient activation. RNase T2 and RNase 2 are the endosomal RNases responsible for TLR8 activation.[45,46] Both TLR7 and TLR8 as well as the upstream RNases seem to be inhibited by 2′-O-methylation.[46,48,49] TLR7 and TLR8 also recognize imidazoquinoline derivatives such as resiquimod (R848), that is used in antiviral and antitumor therapy as well as for basic research.[39] Activation of TLR7 and TLR8 leads to the recruitment of MyD88 (Myeloid differentiation primary response 88) and the downstream adapter molecules IRAK1 (IL-1 receptor associated kinase 1), IRAK4, and TRAF6 and subsequent activation of transcription factors NFκB, AP-1 and IRF5, which induce the pro-inflammatory cytokines IL-6, IL-12 and TNFα (tumor necrosis factor α).[38] In the case of TLR7, this response is specific to human B cells and murine myeloid cells. Conversely, TLR7-mediated induction of type I IFNs is specific to pDCs in both humans and mice and is mediated via the MyD88-IRAK1-TRAF6 IKK pathway, resulting in the activation of IRF7 and transcription of IFNα.[38,39]

1.2.3 Other RNA-sensing receptors and restriction factors

The innate immune system comprises several other antiviral RNA-sensing receptors besides RLRs and TLRs. Many of these do not induce downstream signaling pathways and cytokine induction but instead exhibit direct antiviral mechanisms aimed to restrict pathogen spread, such as reducing viral translation and are therefore termed *antiviral restriction factors*. These proteins are usually ISGs, meaning their expression is upregulated by IFNAR signaling, and together with many other non-sensing proteins, these factors contribute to the antiviral state. Two relevant sensors for this study are highlighted in this chapter to provide insight into the complexity of innate RNA sensing.

One of the best-studied of these proteins is protein kinase R (PKR), a cytosolic dsRNA sensor that, upon viral infection, induces a broad translational shutdown to prevent viral replication and spread. Activation of PKR is independent of RNA sequence and end structures and requires a minimal length of 30 bp to accommodate two PKR molecules.[50,51] Activated PKR dimerizes, auto-phosphorylates, and phosphorylates the eukaryotic translation initiation factor 2α (eIF2α).[51] eIF2α is involved in translation initiation by delivering the methionine-transfer RNA to the 40S ribosome subunit in a guanosine triphosphate (GTP)-dependent manner.[52] Regeneration of eIF2α:GDP to eIF2α:GTP requires help of eIF2B. However, phosphorylated eIF2α sequesters eIF2B, thereby reducing the concentration of active eIF2α and significantly decreasing cap-dependent translation. In contrast, certain mRNAs, for instance that of the activating transcription factor 4 (ATF4), are not affected by phosphorylation of eIF2α due to inherent regulatory elements.[52] ATF4 activates genes contributing to the integrated stress response that can ultimately lead to apoptotic cell death if the infection is not eliminated.[52,53]

OAS1 (2′-5′-Oligoadenylate synthetase 1) is a cytosolic dsRNA sensor that, upon activation, produces the second messenger 2-5A (2′-5′-linked oligoadenylate), which induces RNase L-mediated degradation of all cellular RNAs. Activation of OAS1 by dsRNA longer than 30 bp is independent of RNA sequence and end structures, although the involvement of 5′ triphosphate moieties has been suggested and remains an active area of research.[26,54,55] In addition to restricting viral replication via RNA degradation, cleavage by RNase L creates blunt-end 5′OH-RNA that activates RIG-I, although not with the same potency as 5′ppp/pp-RNA, but thereby still amplifying the immune response.[56] Of note, regular cellular RNases create 5′p-RNAs that are not recognized by RIG-I.

1.3 mRNA vaccines

1.3.1 Vaccination

Vaccination, or active immunization, is the process of eliciting protective immunity against a specific pathogen in an individual, usually achieved by delivering a respective antigen while triggering an immune response that mimics an infection. In 1796, Edward Jenner conducted one of the pioneering immunizations by deliberately infecting patients with cowpox, a virus causing a rather mild disease. He demonstrated that this procedure protected the individuals against subsequent infection by the much more threatening smallpox virus.[1] Jenner further coined the term 'vaccination' (Latin: *vacca* = cow). This breakthrough ultimately enabled the eradication of smallpox nearly two centuries later, as announced by the World Health Organization (WHO) in 1980.[57] Since then, groundbreaking discoveries in immunology have extended our understanding of vaccination mechanisms and accelerated the development of vaccines against various pathogens and different vaccine types. Today, vaccination remains the most effective measure to prevent or decrease the severity of infectious diseases.

The basic immunologic principle of vaccination mimics that of an infection and requires two events: The delivery of an antigen specific to the pathogen and immune activation to achieve the co-stimulation required for the adaptive immune response. Antigen delivery can be achieved in multiple ways, the most commonly used being the injection of live, attenuated pathogens, killed, inactivated pathogens, or pathogen subunits.[58] Besides, nucleic acids coding for pathogen-derived antigens can also be used. DNA encoding for a pathogen-derived protein can be delivered in the form of a recombinant plasmid or viral vector. Notably, the first mRNA-based vaccines have recently been approved for human application during the SARS-CoV-2 pandemic.[59,60]

The immune response and co-stimulation required for adaptive responses are either triggered via PAMPs delivered by the pathogen itself, in the case of live or inactivated vaccines, or by the addition of specific adjuvants. The most commonly used adjuvants are aluminum salts, which activate the innate sensor NLRP3 and induce inflammasome activation.[61] In addition, TLR ligands, such as the TLR4 ligand LPS-derivative monophosphoryl lipid A (MPL) and the TLR9 ligand unmethylated CpG dinucleotide-containing ssDNA are successfully employed in approved vaccines.[62–64] In general, the applicability of adjuvants is limited by their toxicity. For example, LPS has a high risk of inducing systemic inflammation and shock, which is why the less inflammatory and better tolerated MPL is used.[62,65,66] In the case of nucleic acid vaccines, both DNA and RNA can act as innate immune receptor ligands and thus potentially exert adjuvant function.[67,68]

Each vaccine type comes with specific benefits and disadvantages. While attenuated vaccines induce strong and broad protective immunity, acquired mutations can increase their pathogenicity and cause

disease, although these cases are rare.[58] In addition, these vaccines can be harmful to immunodeficient recipients. Therefore, inactivated or subunit vaccines are often safer, but the lack of active replication can lead to less effective induction of immunity. Furthermore, subunit vaccines require the thorough selection of an appropriate antigen and the addition of adjuvants.

Nucleic acid-based vaccines attract significant scientific and clinical interest because they are cost-effective and simple to design and produce.[58,69] DNA- and RNA-based approaches enable the fast development of vaccines against newly emerging pathogens, such as the SARS-CoV-2 virus, and the rapid adjustment of vaccines to extensively mutating pathogens, such as the Influenza virus. Their versatility even allows the development of customized treatments for individual patients, for example, in anti-tumor vaccination.

While nucleic acid vaccines can encode any desired protein, these vaccines face the challenge of entering the host cell for transcription (in the case of DNA vaccines) and translation (for both DNA and RNA vaccines). Due to their size and negative charge, nucleic acids cannot cross cell membranes without complexation or encapsulation.[70] The intracellular delivery of DNA for medical applications is commonly achieved through viral vectors, which have demonstrated effectiveness due to their natural capability to enter specific cell types and the nucleus.[71] Additionally, encapsulation of nucleic acids by carrier molecules, which aid uptake and prevent degradation by extracellular nucleases, is an efficient delivery technique. These vehicles, for example lipid nanoparticles (LNPs), also offer another level of adaptability. Depending on the specific composition, these carriers can achieve a particular biodistribution, regulate half-life, or target specific cell types, such as APCs.[72]

The production of mRNA via cell-free *in vitro* transcription, as explained in more detail in Chapter 1.3.3, is considerably faster than the production of protein or DNA vaccines. However, the lower stability of RNA requires storage at -20 to -80 °C, thereby complicating distribution logistics and increasing costs, but continuous efforts to improve formulations show promise in overcoming these obstacles.[58]

Besides vaccination, DNA virus- and retrovirus-based vectors have been successfully used for EMA- and FDA-approved clinical gene replacement and transgenic cell therapies, and similar applications are now under clinical development for mRNA technology, including protein replacement therapy, cancer immunotherapy, cellular reprogramming, and genome editing.[73–77]

1.3.2 The COVID-19 pandemic and first approved mRNA vaccines

The first cases of COVID-19 (Coronavirus disease 2019) caused by SARS-CoV-2 occurred in Wuhan, China, in December 2019, and shortly after, in March 2020, the WHO announced a pandemic outbreak.[78] Already one year later, in December 2020, the first COVID-19 vaccines were administered.[59,60] Until then, the virus had infected more than 150 million people and caused over three million deaths worldwide.[79] While COVID-19 is usually not fatal in young, immunocompetent people, it causes severe cold-like symptoms and infects multiple organs, leading to long-term damage, for example in the lungs and heart.[80] Furthermore, the disease is life-threatening for immunocompromised and aged individuals. This recent pandemic illustrates the relevance of ongoing advancements in vaccination technology, particularly in mRNA-based therapeutics. While the development of traditional protein-based vaccines usually takes several years until official approval, the COVID-19 mRNA vaccines developed by BioNTech/Pfizer and Moderna were approved just 11 months after obtaining the genomic sequence of SARS-CoV-2, which is the fastest vaccine development in medical history.[79] Furthermore, these vaccines are the first-ever approved mRNA-based therapies.

The vaccines by BioNTech and Moderna utilize a codon-optimized mRNA encoding the stabilized prefusion spike glycoprotein of SARS-CoV-2.[59,60] This spike protein is essential for virus cell entry via ACE2 (angiotensin-converting enzyme 2) on bronchial epithelial cells and endothelial cells of several other organs.[81] The spike protein naturally contains an endogenous N-terminal signal peptide, which enables the extracellular display and secretion of the protein after translation of the mRNA vaccine and subsequent uptake and processing by APCs.[82] Both vaccines induce robust spike-specific $CD4^+$ and $CD8^+$ T cell responses and antibody titers and demonstrated up to 94 % efficacy at preventing COVID-19 in phase III clinical trials.[79] The side effects included moderate local inflammation and mild systemic symptoms such as fever, fatigue, and muscle pain. Both mRNA vaccines incorporate N1-methyl-pseudouridine instead of uridine to reduce mRNA-induced inflammation and enhance translation.[83]

To efficiently deliver intact mRNA, it is encapsulated in a carrier vehicle, usually lipid-nanoparticles (LNPs) (Figure 2). These consist of ionizable lipids, cholesterol, phospholipids, and PEGylated lipids.[79] Ionizable lipids bind the negatively charged mRNA and form a spherical structure. They remain neutrally charged at physiological pH, reducing overall toxicity and prolonging circulation half-life.[79] At the acidic pH inside endosomes, protonation of the ionizable lipids facilitates fusion with the endosomal membrane and delivery of the mRNA to the cytosol. Although the exact mechanisms of endosomal escape remain unclear, the generated osmotic pressure is assumed to result in endosomal rupture.[79] Cholesterol stabilizes the particle and promotes cellular uptake. Phospholipids aid in fusion with endosomal membranes and influence biodistribution based on their

charge.[79] Finally, the PEGylated lipids (polyethylene glycol-conjugated lipids) regulate particle size, half-life, biodistribution, and cellular uptake.

After administration of the LNP-encapsulated mRNA, local cells internalize the particles by receptor-mediated endocytosis and macropinocytosis (Figure 2). After endosomal escape into the cytosol, the mRNA engages with the endogenous translation machinery, generating the respective protein. The cells then present corresponding peptides derived from proteasomal degradation on their MHC class I molecules, which induces activation of cytotoxic $CD8^+$ T cells (Figure 2). Additionally, any extracellularly displayed or secreted proteins can be internalized and processed by dendritic cells and B cells. Peptide presentation on MHC class II molecules results in activation and differentiation of $CD4^+$ T cells and B cells. Similar to the immune responses during an infection, as explained in Chapter 1.1, these processes induce the generation of cellular and humoral protective immunity.

Interestingly, the currently approved mRNA vaccines do not contain additional adjuvants. The innate immune activation and co-stimulation required for lymphocyte activation are presumed to be caused by immune stimulatory properties of the LNPs and/or the mRNA contained within.[67,68,84] However, the underlying mechanisms remain largely unknown and will be discussed in more detail in Chapter 1.4.

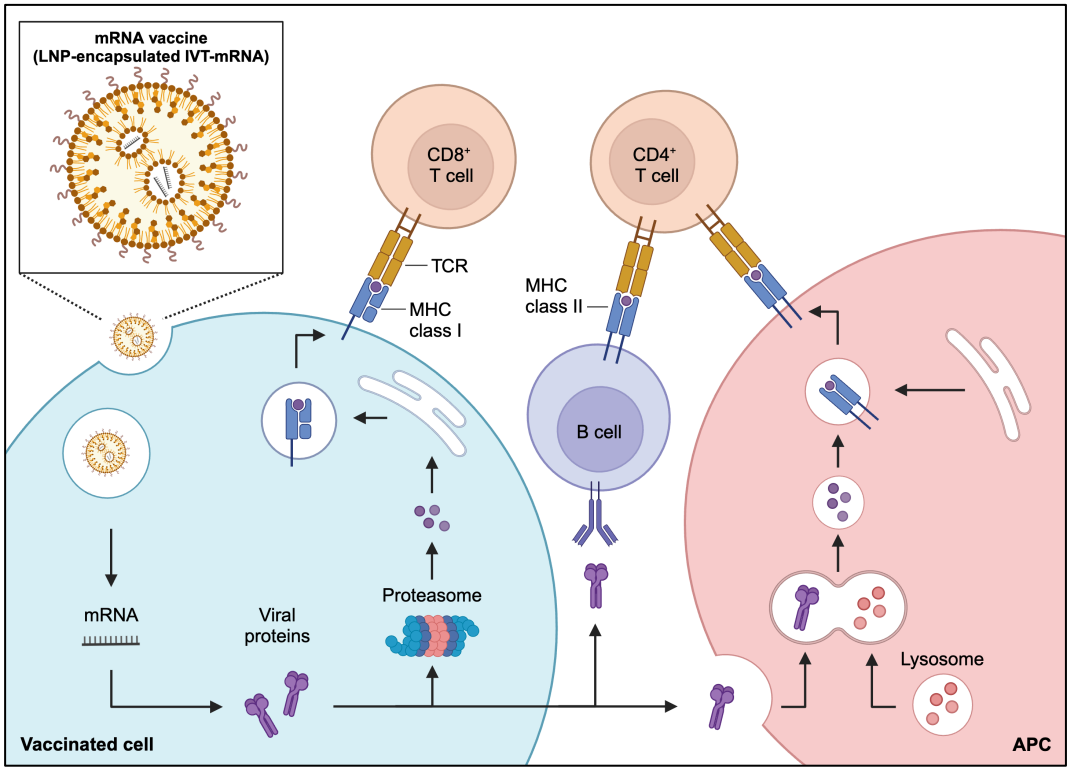

Figure 2: Induction of adaptive immune responses to antigens delivered by mRNA vaccines
LNP-encapsulated IVT-mRNA is endocytosed by target cells. The mRNA escapes into the cytosol and is translated into pathogen-derived, e.g. viral, proteins, which is degraded by the (immuno)proteasome. Peptides are translocated into the endoplasmic reticulum, loaded onto MHC class I molecules and presented to cytotoxic $CD8^+$ T cells. Alternatively, the proteins are secreted and endocytosed by naive B cells and APCs. After endolysosomal degradation, the peptides are loaded onto MHC class II molecules and presented to $CD4^+$ T cells. Co-stimulatory surface markers are not indicated. APC = antigen-presenting cell, BCR = B cell receptor, IVT-mRNA = *in vitro* transcribed mRNA, LNP = lipid nanoparticle, MHC = major histocompatibility complex, TCR = T cell receptor.

1.3.3 *In vitro* transcription of mRNA

mRNA therapeutics exploit the endogenous translation machinery by delivering an exogenous mRNA into the cytosol. The first proof-of-concept of *in vitro* protein expression from *in vitro* transcribed (IVT)-mRNA was already demonstrated in 1980, followed by *in vivo* studies in 1990, and the first mRNA-based vaccination against influenza in mice in 1993.[85–87] However, the success of the mRNA technology was restrained by its instability and proinflammatory potential. In the following decades, several molecular biology and immunology discoveries led to the optimization of mRNA design and increased its therapeutic applicability.

Artificial mRNA is produced via *in vitro* transcription, a cell-free process utilizing a DNA template, nucleoside triphosphates (NTPs), and a bacteriophage-derived RNA polymerase that transcribes the mRNA from the template in an appropriate buffer (Figure 3). The most commonly used polymerase is derived from the T7 bacteriophage due to its high fidelity, yield, and ability to incorporate modified nucleosides.[88–90] The T7 polymerase recognizes a specific promoter sequence in the DNA template and initiates transcription preferentially by incorporating a guanosine triphosphate (GTP).[91–94] Furthermore, promoters ending in GGG were shown to enhance transcription, so most IVT-mRNAs start with this sequence (Figure 3). If the incorporation of modified nucleotides is desired, the respective NTP can be substituted by a modified analog, either completely or in any other desired ratio.

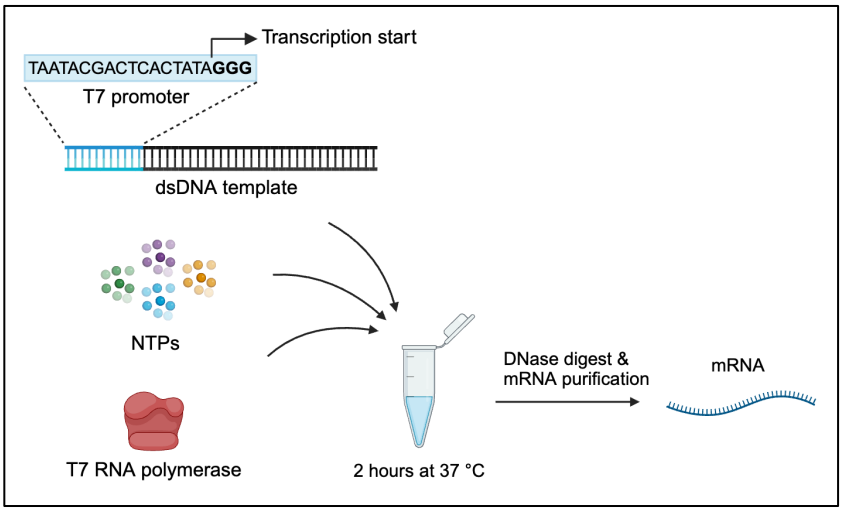

Figure 3: Production of mRNA via *in vitro* transcription
During *in vitro* transcription, the T7 RNA polymerase binds to the T7 promoter sequence in a dsDNA template and starts transcription by incorporating GTP. The reaction is usually carried out for two hours at 37 °C. The DNA template is then digested, and the mRNA is purified.

A typical mRNA is composed of the protein-coding sequence (CDS) flanked by untranslated regions (UTRs) that increase mRNA stability and regulate translation (Figure 4). To achieve efficient translation, the CDS is usually optimized for codon usage without altering the protein sequence and is combined with naturally occurring UTRs from highly expressed genes, such as α- and β-globin.[79] A 3′ poly(A) tail enhances mRNA stability and is critical for translation by binding the poly(A)-binding protein PABP, which binds to the eukaryotic translation initiation factor 4G (eIF4G) thereby delivering the mRNA to the translation initiation complex.[95] All of these components are usually encoded in the DNA template. Alternatively, the poly(A) tail can be added enzymatically after the transcription via a poly(A)-polymerase. However, this method is more laborious and produces poly(A) tails of heterogenous length.[79] The DNA template is usually a linearized plasmid but can also be generated via polymerase chain reaction (PCR). After *in vitro* transcription, the DNA template is digested using DNases, and the mRNA is purified by conventional methods, such as phenol/chloroform precipitation.

Eukaryotic mRNA usually harbors a 5′ cap-1 structure that protects the mRNA from degradation, marks mRNA as "self", and regulates mRNA processing and translation. During the latter, the cap structure is bound by eIF4E, which is complexed to eIF4G, forming an mRNA loop to the poly(A) tail characteristic of eukaryotic translation.[95] The 5′ mRNA cap consists of a 7-methylguanosine (m7G) linked via a 5′ – 5′ triphosphate bond to the first nucleotide (cap-0), which is methylated at the 2′-O position (cap-1) (Figure 4).[12]

For IVT-mRNA, the 5′ cap can be added co-transcriptionally or after the reaction by respective enzymes. Co-transcriptional capping uses a cap analog that is utilized by the T7 polymerase to initiate transcription. Given that the T7 polymerase preferentially initiates transcription with GTP, first-generation cap analogs consist of a GTP linked to m7G, resulting in cap-0 IVT-mRNA.[77,91–94] However, this cap analog is frequently incorporated in reverse orientation, leading to poor translational activity.[77] Second-generation cap analogs harbor a 3′-O-methylation on the m7G to prevent reverse incorporation and are known as anti-reverse cap analogs (ARCA).[77,96] Still, competition with generic GTP during transcription initiation reduces the incorporation efficiency of cap analogs.[97] The most widely used cap analog today, CleanCap®, was developed by TriLink and comprises an N1-methyl-modified dinucleotide linked to the m7G cap (Figure 4). This design forms cap-1 mRNA, which demonstrates enhanced translation compared to cap-0 IVT-mRNA (Figure 4).[97,98] Furthermore, the dinucleotide improves CleanCap® incorporation by reducing competition with generic nucleotides during transcription initiation, resulting in higher capping efficiency compared to ARCA.[97] CleanCap® is available with two dinucleotide versions: CleanCap® GG (two guanosines) or CleanCap® AG (adenosine followed by guanosine), requiring accordingly designed DNA templates and resulting in IVT-mRNA starting with either guanosine or adenosine as the 5′ initial nucleotide.[97] CleanCap® AG achieves an incorporation efficiency of over 95 %, while CleanCap® GG achieves 70 – 90 %, attributed to the T7 polymerase's preference for guanosine

initiation, reducing competition during transcription initiation with AG templates.[99,100] Besides, CleanCap® comes with or without 3′-O-methylation on the m7G to prevent reverse incorporation. Notably, the COVID-19 mRNA vaccine by BioNTech incorporates the CleanCap® AG with 3′-O-methylation.[101]

Enzymatic capping is performed after the *in vitro* transcription by utilizing two enzymes derived from the vaccinia virus.[102,103] In a reaction including GTP and the methyl donor S-adenosylmethionine (SAM), the vaccinia virus capping enzyme first removes the γ-phosphate group of the 5′ppp-RNA end, then adds a GTP via 5′ – 5′ triphosphate linkage and methylates it at the N7 position. Then, the methyltransferase creates a cap-1 structure by 2′-O-methylation of the first nucleotide. Enzymatic capping is employed for the COVID-19 mRNA vaccine by Moderna.[104] Enzymatically capped mRNA usually starts with 5′ guanosine to achieve maximal mRNA yield during *in vitro* transcription.[91–94]

While co-transcriptional capping enables a rapid one-step approach for mRNA synthesis, the transcription will occasionally initiate with a generic nucleotide instead of the cap analog, leading to the presence of uncapped transcripts, which are immunogenic and poorly translated.[13,26,95,97] Nevertheless, TriLink reported a 94 % capping efficiency using their CleanCap® analog.[97] In contrast, enzymatic capping requires a post-transcriptional capping reaction but results in up to 99 % capping efficiency.[105]

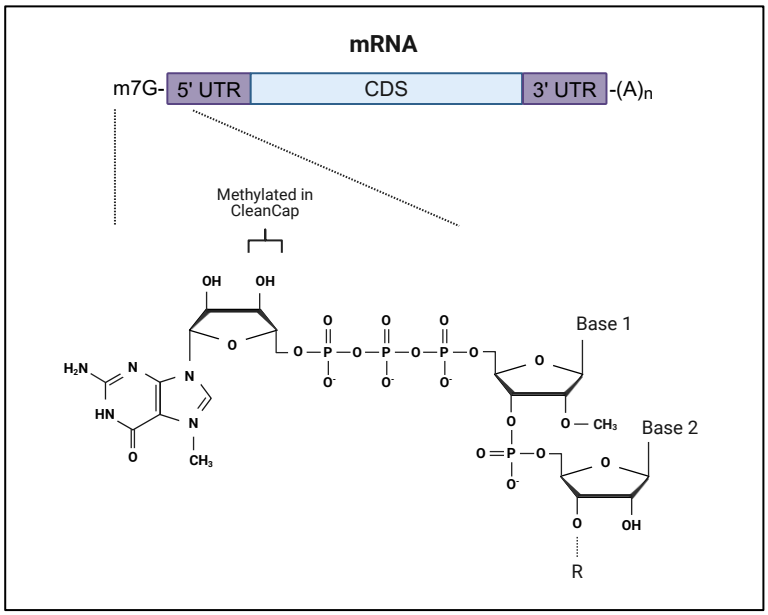

Figure 4: mRNA scheme and 5′ cap-1 structure
mRNA is composed of a CDS flanked by 5′ and 3′ UTRs and a poly(A) tail. The 5′ cap-1 structure consists of a 7-methyl-guanosine (m7G) bound to the first 2′-O-methylated nucleotide via 5′-5′ triphosphate linkage. The co-transcriptional cap analog CleanCap® (3′Ome) has an additional methyl group at the 3′-O position of the m7G to prevent reverse incorporation and keep structural consistency with the previously used ARCA (anti-reverse cap analogue). CDS = coding sequence, UTR = untranslated region.

1.4 Innate immune activation by *in vitro* transcribed mRNA

1.4.1 Innate immune activation by *in vitro* transcribed mRNA and double-stranded RNA byproducts

The tolerability and therapeutic applicability of IVT-mRNA is largely defined by its inflammatory potential. While a certain degree of immune activation could exert adjuvant-like effects, excessive inflammation limits applicable dosages and vaccine efficacy. Therefore, understanding the mechanisms leading to mRNA-induced immune responses is of high interest for the development of mRNA therapeutics.

As explained in Chapter 1.2, the innate immune system possesses several PRRs that sense single- or double-stranded RNA. While the target mRNA is putatively single-stranded, *in vitro* transcription generates several unspecific dsRNA byproducts. For instance, certain RNA polymerases including T7 have been found to produce short abortive transcripts (Figure 5).[89] After transcription of the first nucleotides, the T7 polymerase performs a conformational change to release the promoter region and enable stable elongation of the RNA transcript.[106] Apparently, this process fails in up to 44 % of initiation events leading to a considerable number of short transcripts in the range of 2 – 13 nt.[106,107] These can anneal to complementary regions within the mRNA resulting in double-stranded regions and might even act as primers for RNA-templated transcription. Additionally, complementarity within the 3′ end of the mRNA can lead to a hairpin formation that is bound by the T7 polymerase, which starts RNA-templated transcription along the mRNA (Figure 5).[108–110] The resulting 3′ extended (or loop-back) transcripts can be up to twice the length of the initial mRNA and form long double-stranded regions. Furthermore, the T7 polymerase is capable of promoter-independent transcription of the antisense DNA strand, thereby producing an RNA complementary to the target mRNA leading to the formation of a full-length duplex (Figure 5).[25] Moreover, the presence of further currently unknown mechanisms and RNA species is conceivable. Therefore, while IVT-mRNA primarily consists of the target mRNA, it also contains a diverse mixture of ss- and dsRNA species of different length and secondary structure. Additionally, intramolecular secondary structures of the target mRNA may provide immunogenic double-stranded regions.

Activation of PRRs by IVT-mRNA has been investigated by several studies. For example, by overexpressing the respective receptors in HEK 293 cells, Karikó *et al.* demonstrated that IVT-mRNA activates TLR3, TLR7 and TLR8.[111,112] Activation of TLR3 and TLR7 by IVT-mRNA was further confirmed *in vivo* in mice.[113,114] TLR7 and TLR8 are activated by ssRNA species, such as the target mRNA, while TLR3 likely senses dsRNA byproducts. In line with this, Karikó *et al.* found that elimination of dsRNA byproducts via HPLC purification reduced, but did not abolish, mRNA-induced cytokine induction in human DCs.[115]

Likewise, RIG-I is activated by dsRNA byproducts generated during *in vitro* transcription. While initial studies using IVT-RNAs speculated that RIG-I could also sense 5′-phosphorylated ssRNA, Schlee et al. later conclusively demonstrated that the dsRNA byproducts were responsible for activating RIG-I, as an IVT produced with only three NTPs, which was incapable of forming dsRNA byproducts, along with a chemically synthesized 5′ppp-ssRNA, did not activate RIG-I.[14,116] Later on, Karikó *et al.* confirmed the activation of RIG-I by IVT-mRNA.[117] Nevertheless, the exact mechanisms and byproducts leading to RIG-I activation by IVT-mRNA remain elusive.

In contrast, the ligand requirements for MDA5 activation are insufficiently characterized, and it remains unclear whether *in vitro* transcription generates dsRNA byproducts capable of activating MDA5. Previous studies investigating MDA5 activation utilized double-stranded constructs, thereby preventing any conclusions relevant to IVT-mRNA and its byproducts.[23,28,29] While Mu *et al.* reported that a 512 bp full-length duplex formed by transcription of the antisense DNA strand was sensed by MDA5, other studies demonstrate that dsRNA longer than 2000 bp is required for MDA5 activation.[23,25] Nevertheless, during the course of this study, another group demonstrated that the COVID-19 mRNA vaccine developed by BioNTech is capable of activating MDA5 *in vivo* in mice.[67] In conclusion, the potential of IVT-mRNA to activate MDA5 and the underlying mechanisms require further investigation.

Lastly, PKR and OAS1 were found to be activated by dsRNA byproducts of IVT-mRNA, but the functional outcomes have not yet been characterized in detail.[118,119]

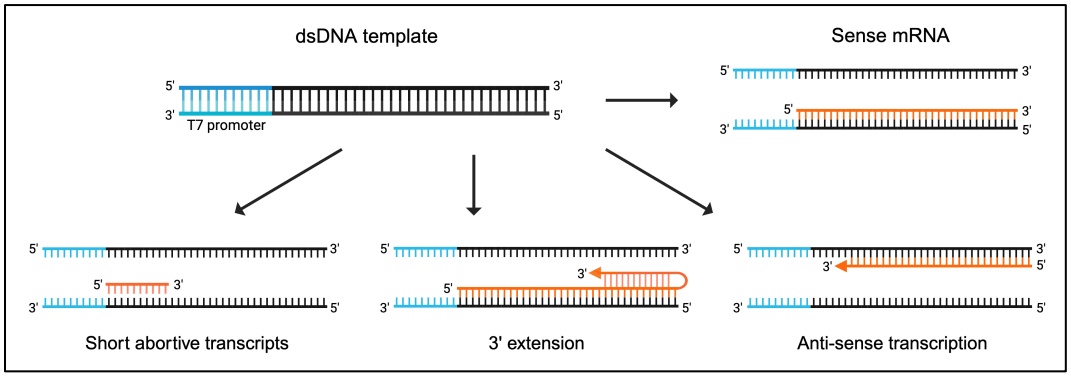

Figure 5: *In vitro* transcription produces double-stranded dsRNA byproducts
During *in vitro* transcription, the T7 polymerase transcribed the sense mRNA from a dsDNA template. Several mechanisms lead to the production of unspecific, double-stranded RNA byproducts. In the case of an unsuccessful conformation change of the polymerase, the transcription terminates prematurely and produces short abortive transcripts. Complementarity within the 3′ mRNA end can lead to formation of a hairpin and RNA-templated transcription, creating 3′ extended transcripts. Additionally, promoter-independent transcription of the antisense DNA strand leads to the production of complementary RNA and a full-length duplex.

1.4.2 Innate immune activation as obstacle and opportunity for mRNA therapeutics

IVT-mRNA is capable of activating several RNA-sensing PRRs of the innate immune system. Since these PRRs are naturally involved in fighting viral infections, their activation leads to antiviral and pro-inflammatory responses that could be detrimental to the efficacy of mRNA therapeutics. For example, excessive immune stimulation causes local inflammation, elevates adverse side effects, and reduces applicable vaccine dosages, thereby reducing protein production. Likewise, antiviral restriction mechanisms induced by immune activation can reduce mRNA vaccine efficacy. For example, the type I IFN-induced antiviral state reduces overall mRNA translation and increases mRNA degradation via restrictive ISGs such as IFIT1, PKR, and OAS1. In line with this, Pollard *et al.* reported enhanced translation of IVT-mRNA in murine *Ifnar*$^{-/-}$ bone marrow-derived DCs, indicating that type I IFNs restrict mRNA translation.[114] Furthermore, some ISGs, such as the IFITM family, inhibit viral entry into the cell and might likewise reduce the uptake of mRNA-LNPs. In addition, excessive type I IFN signaling can negatively affect lymphocyte effector mechanisms, proliferation, and survival.[120–122] Indeed, it was shown that IFNAR signaling restricts T cell activation in response to mRNA vaccines in mice.[114]

In contrast, induction of adaptive immune responses requires activation of the innate immune system. While many vaccine types require the addition of adjuvants, the currently approved mRNA vaccines do not include any adjuvants, and it was hypothesized that immunogenic properties of the IVT-mRNA and/or the LNP particle activate innate mechanisms to induce co-stimulation.[123] Indeed, mRNA-induced maturation of human APCs was demonstrated *in vitro*.[124,125] Strikingly, a few studies indicated a role of specifically RLRs for mRNA vaccine efficacy. For instance, mRNA-induced activation of splenic B lymphocytes was reduced in *Mavs*$^{-/-}$ mice.[126] Additionally, a recent study by Li *et al.* reported a decreased induction of spike-specific CD8^{+} T cells in *Mda5*$^{-/-}$ mice after vaccination with the COVID-19 mRNA vaccine by BioNTech.[67] This effect seemed mediated by MDA5-induced type I IFN production and was not observed for other receptors, such as TLR3 and TLR7. Therefore, activation of PRRs such as MDA5 by IVT-mRNA can be advantageous for vaccination efficacy by providing adjuvant-like immune stimulation. This effect might be mediated for example by type I IFNs, which act on several cell types involved in the adaptive immune response. For instance, DCs enhance antigen presentation on MHC I and II and upregulate cell surface molecules, such as CD80, CD86, BAFF, and APRIL, needed for co-stimulation of T and B cells in response to type I IFN.[122,127,128] Furthermore, type I IFNs enhance APC cross-presentation to CD8^{+} T cells and upregulation of chemokine receptors that promote APC migration to secondary lymphoid organs.[129] In addition, moderate IFNAR signaling was shown to promote lymphocyte proliferation, differentiation, survival, class switch, and antibody production.[127–129] Lastly, type I

IFNs reduce the anti-inflammatory functions of regulatory T cells.[130] In line with these processes, two studies demonstrated the requirement of type I IFNs for the adjuvant effect of TLR3-ligand poly(I:C) and TLR7-ligand poly(U)$_{21}$ for protein-based vaccines in mice.[131,132]

In conclusion, the activation of innate immune responses by IVT-mRNA can be both advantageous and detrimental to therapeutic efficacy. Optimally, in an antiviral vaccine, this response would need to occur in a critical window: it should be strong enough to achieve antiviral co-stimulation yet not reach levels that would completely restrict antigen translation through antiviral restriction factors. In contrast, some other therapeutic applications of IVT-mRNA, like protein replacement therapy, could conceivably aim at maximum protein production without inducing any inflammatory responses. Therefore, understanding the underlying mechanisms of PRR activation by IVT-mRNA will enable optimized mRNA design tailored to the respective medical application.

1.4.3 Incorporation of modified nucleosides modulates innate immune activation by *in vitro* transcribed mRNA

An effective measure to reduce innate immune activation by IVT-mRNA is the incorporation of modified nucleosides, first demonstrated in 2005 and 2008 by Katalin Karikó and Drew Weissman.[111,117] This discovery is considered essential to the success of mRNA vaccines and was awarded the Nobel Prize in Physiology or Medicine in 2023.[133] The initial idea originated from the fact that eukaryotic RNA is extensively modified and non-immunogenic. Therefore, some of the most abundant, naturally occurring modifications were tested in IVT-mRNA. These include pseudouridine (Ψ), N1-methyl-pseudouridine (m1Ψ), 5-methoxy-uridine (5moU), 5-methyl-cytidine (m5C), and N6-methyl-adenosine (m6A) (Figure 6). Ψ, a rotational isomer of uridine, is the most abundant eukaryotic RNA modification and is present in almost all RNA types.[134] Compared to uridine, Ψ provides an additional hydrogen bond donor at the N1 position, which, in addition to the conventional pairing with adenine, enables wobble base-pairing with guanine, cytosine, and uracil.[135] Due to this and the higher flexibility of the C5-C1′ base-ribose bond compared to N1-C1′ in uridine, Ψ is thought to regulate RNA stability and secondary structures, particularly in tRNA.[135] Additionally, it modulates mRNA translation, for example by promoting read-through stop codons.[134] Similarly, the Ψ-derivative m1Ψ is also presumed to regulate RNA stability due to the C5-C1′ bond, but provides only two hydrogen bond donors for base pairing with adenine, equivalent to uridine (Figure 6). M1Ψ is naturally present in archaeal rRNA and tRNA.[136–138] However, given that the currently used detection methods do not differentiate between Ψ and m1Ψ, m1Ψ might be present in other species as well. The modification 5moU is found in bacterial tRNA and is presumed to enhance translational fidelity, but the exact functions are poorly understood.[137] Besides, m5C is

moderately abundant in eukaryotic RNA species, primarily mRNA, and improves its stability. In addition, m5C promotes nuclear export and regulates translation and RNA-protein interactions.[134] Lastly, m6A is the most abundant modification in eukaryotic mRNA, but is also present in other RNA species such as tRNA and rRNA.[139,140] It regulates RNA stability and translation and is exploited as an immune evasion mechanism by some viruses.[141–143]

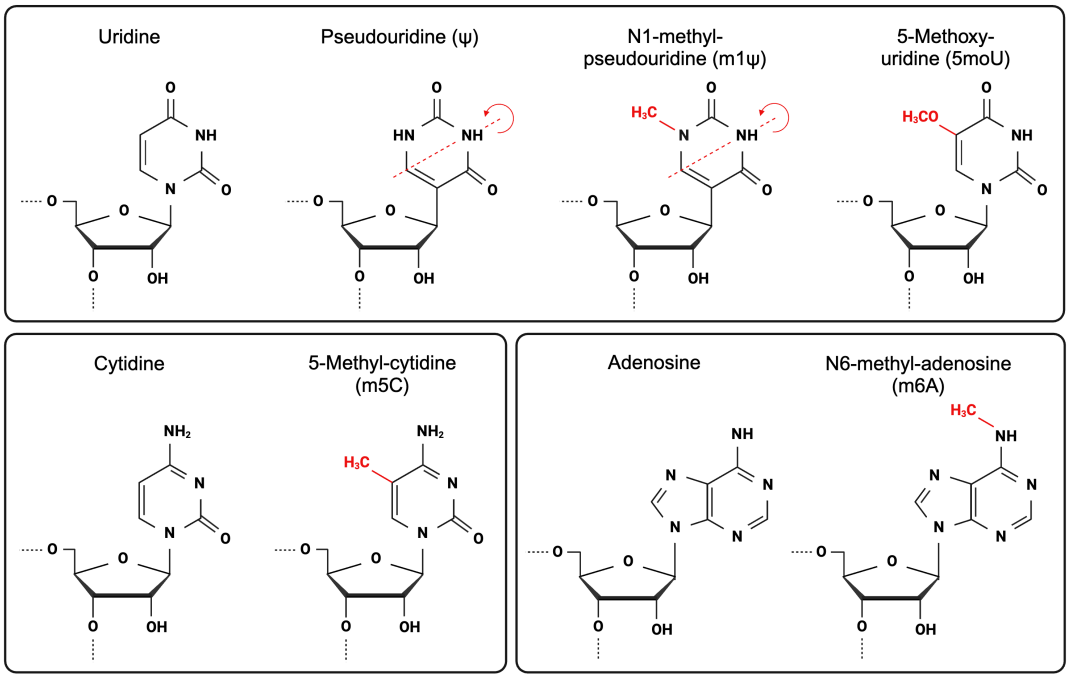

Figure 6: Natural nucleoside modifications
Nucleotide modifications under investigation for incorporation into mRNA vaccines. Upper panel: uridine, pseudouridine (Ψ), N1-methyl-pseudouridine (m1Ψ), 5-methoxy-uridine (5moU). Lower left panel: cytidine, 5-methyl-cytidine (m5C). Lower right panel: adenosine, N6-methyl-adenosine (m6A).

All of these modifications were found to generally reduce mRNA-induced innate immune responses, but the extent varied between modifications and experimental settings.[83,144] Interestingly, only a few studies investigated the effect of modified nucleosides on the activation of individual PRRs. An overview of the respective studies and their findings is presented in Table 1. Furthermore, the underlying mechanisms leading to reduced innate immune responses to mRNA incorporating modified nucleosides have not been investigated by most studies, although several hypotheses exist. For the ssRNA sensors TLR7 and TLR8, the modifications Ψ, m5C, and m6A presumably interfere directly with receptor binding, signaling conformation, or degradation by upstream RNases. Indeed, it was reported that after the elimination of dsRNA byproducts via HPLC purification, the residual inflammatory potential of the target mRNA is abolished by incorporation of Ψ.[115] In contrast, modulation of dsRNA-sensing receptors can be mediated by two different mechanisms. On the one hand, several studies demonstrated that certain nucleoside modifications reduce the generation of

dsRNA byproducts during *in vitro* transcription.[25,144–146] The resulting reduced dsRNA content in modified IVT-mRNA could be responsible for the reduction of innate immune responses. Alternatively, direct impediments of receptor activation, as observed for TLR7 and TLR8, are also conceivable. Unfortunately, most studies investigated nucleoside modifications using single-stranded IVT-RNA, thereby preventing any conclusions regarding these two mechanisms, and incorporated only selected modifications rather than providing a comprehensive panel (Table 1). While the incorporation of Ψ was shown to inhibit the activation of most PRRs (Table 1), the underlying mechanisms remain unknown. Furthermore, the effect of certain modifications, especially m1Ψ and 5moU, on the activation of individual PRRs has not been characterized in detail yet (Table 1). While m1Ψ is assumed to exhibit similar immune modulation as Ψ, several studies demonstrated that m1Ψ-modified mRNA induces even less innate immune responses than Ψ alone, indicating further currently unknown mechanisms.[83,136] Given that several studies demonstrated the potential of specifically m1Ψ and 5moU to reduce the inflammatory capacity of mRNA, which resulted in the incorporation of m1Ψ in the COVID-19 mRNA vaccines, understanding the modulation of individual PRRs by these modifications is of great interest.[83,144] Therefore, a systematic side-by-side investigation of PRR activation by RNA incorporating commonly used nucleoside modifications is required.

Furthermore, given the broad expression profile of RLRs, compared to the cell type-specific expression of TLRs, RLRs are of great relevance for mRNA vaccines. Therefore, RLR stimulation by IVT-mRNA and its modulation by nucleoside modifications requires extensive investigation. Additionally, two previous studies indicated a role of RLR activation for the adjuvant-like effect of mRNA vaccines, further highlighting their significance.[67,126]

Of note, besides reducing mRNA-induced innate immune responses, several nucleoside modifications, particularly Ψ, m1Ψ, and 5moU, were found to increase mRNA translation, thereby presenting another highly useful feature for mRNA therapeutics. While the underlying mechanisms are not completely understood, it has been proposed that this mainly results from reduced innate immune stimulation and antiviral restriction.[117,118] However, direct effects of nucleoside modifications on the translational machinery have also been proposed. For example, Svitkin *et al.* reported that m1Ψ promotes translation initiation and decelerates ribosome movement, thereby causing increased ribosome loading on individual mRNAs.[147] Lastly, modulation of mRNA secondary structure by nucleoside modifications has been suggested to affect translation.[148] Therefore, while the inflammatory potential of IVT-mRNA is an essential determinant for its therapeutic applicability, the effects of nucleoside modifications in IVT-mRNA have to be investigated for both immune stimulation and translation.

Table 1: Inhibitory effect of modified nucleosides on activation or binding of PRRs by/to *in vitro* transcribed RNA species. Overview of relevant publications regarding modulation of PRR activation by nucleoside modifications. The extent of the inhibitory effect on PRR activation is indicated as follows: none (-), mild (+), moderate (++), and strong (+++). Modifications that the respective study has not investigated are indicated with (/). All studies used *in vitro* transcribed RNA species. If the RNA length was not stated, the encoded protein is included for estimation. MEF = murine embryonic fibroblast, RRL = rabbit reticulocyte lysate.

PRR	Study & experimental setup	Ψ	m1Ψ	5moU	m5C	m6A
TLR3	Karikó *et al.* (2005)*:* IL-8 production of TLR3-HEK293 cells in response to 1571 nt mRNA.[111]	+	/	/	+	+++
TLR7	Karikó *et al.* (2005): IL-8 production of TLR7-HEK293 cells in response to 1571 nt mRNA.[111]	+++	/	/	+++	+++
	Hornung *et al.* (2006): IFNα production by human primary pDCs in response to 24 nt ssRNA.[13]	+++	/	/	/	/
TLR8	Karikó *et al.* (2005): IL-8 production of TLR8-HEK293 cells in response to 1571 nt mRNA.[111]	+++	/	/	+	+++
RIG-I	Hornung *et al.* (2006): IFNα production by human primary monocytes in response to 24 nt ssRNA.[13]	+++	/	/	/	/
	Karikó *et al.* (2008): IFNβ production of wildtype and *Rig-I*$^{-/-}$ MEFs in response to 1866 nt mRNA.[117]	++	/	/	/	/
	Peisley *et al.* (2013): Filament formation of recombinant RIG-I on 136 bp dsRNA based on electron microscopy and EMSA assay.[149]	+	/	/	/	+
	Durbin *et al.* (2016): • RIG-I precipitation after pulldown using 106 nt ssRNA from Huh7 lysate. • RIG-I conformation change based on limited trypsin digestion of HEK293 lysate incubated with 106 nt ssRNA.[150]	- ++	+ ++	/ /	- +	++ +
	Nelson *et al.* (2020): ISG54 reporter activity in wildtype and *Rig-I*$^{-/-}$ A549 cells in response to erythropoietin-encoding mRNA.[126]	/	++	/	/	/
MDA5	Mu *et al.* (2018): IFNβ reporter activity in MDA5-HEK293T cells in response to • 512 nt ssRNA, • 512 nt dsRNA.[25]	++ -	++ -	/ /	++ -	- -
PKR	Anderson *et al.* (2010): Phosphorylation of PKR in HEK293T cells in response to firefly luciferase-encoding mRNA.[118]	+	/	/	+	-
	Svitkin *et al.* (2017): Phosphorylation of eIF2α in RRL, Krebs lysate, and HeLa S10 extract in response to a ~2 kb and a ~1.5 kb mRNA.[147]	/	++	/	++	/
OAS1	Anderson *et al.* (2011): Production of 2-5A by recombinant OAS1 in response to a HPLC-purified firefly luciferase-encoding mRNA.[119]	+++	/	/	/	+++

1.4.4 Bartok and Hartmann groups collaboratively identify RIG-I-like receptors as primary sensors of mRNA vaccines and uncover species-specific differences between humans and mice

Shortly after the COVID-19 mRNA vaccines by BioNTech and Moderna were approved in Germany in early 2021, the groups of Prof. Dr. Eva Bartok and Prof. Dr. Gunther Hartmann of the University Hospital Bonn started a collaborative effort to characterize the innate immune responses induced by these mRNA vaccines. A portion of this thesis (mainly Results Chapter 3.1) is part of this highly collaborative project. To put these results into the broader context, a selection of data generated by other scientists of the Bartok and Hartmann groups will be presented in the following chapter to enable a comprehensive discussion of these collaborative findings as well as to better introduce the rationale and experimental setups of follow-up projects presented in Chapter 3.2 and 3.3. To this end, the following figures were extracted from the unpublished manuscript and rearranged for display.

Since purchasing vaccines for basic research during the early stages of the pandemic, when available material was needed for vaccinations, would have posed ethical problems, the residual vaccine left over in vials after vaccination was used. Therefore, numerous members of the Bartok and Hartmann groups, particularly Dr. Madeleine Gräf and Maximilian Appel, MD, collected the leftover vaccine vials from clinics in the Bonn area over several months. The contents were pooled to accumulate sufficient volumes and either used on the same day where possible or stored at -80 °C for later experiments.

The innate immune response to the COVID-19 mRNA vaccines was investigated *in vivo* in mice. To characterize the potential activation of RNA-sensing receptors, 5 µg BioNTech vaccine and 16.6 µg Moderna vaccine were administered intramuscularly in 8 to 20-week-old C57BL/6 mice, and serum cytokines were assessed after 24 hours (Figure 7A). The vaccine dosage was based on the official instructions for humans, stating that one dose of the Moderna vaccine consists of approximately 3.3 times more RNA than the BioNTech vaccine.[59,60] These experiments were performed by the Hartmann group members Dr. Marcel Renn, Patrick Müller, and Yu Pan Tan, and data was analyzed by Prof. Dr. Eva Bartok. The results showed significant MDA5-dependent IFNα serum levels induced by the COVID-19 mRNA vaccines by BioNTech and Moderna (Figure 7B-C). This finding demonstrates the presence of MDA5-activating dsRNA in the COVID-19 mRNA vaccines, in line with concurrent publications and further *in vitro* data presented in Chapter 3.1.[67] Interestingly, the IFNα levels induced by the BioNTech vaccine were substantially higher than those induced by the Moderna vaccine, which will be elaborated upon in subsequent sections.

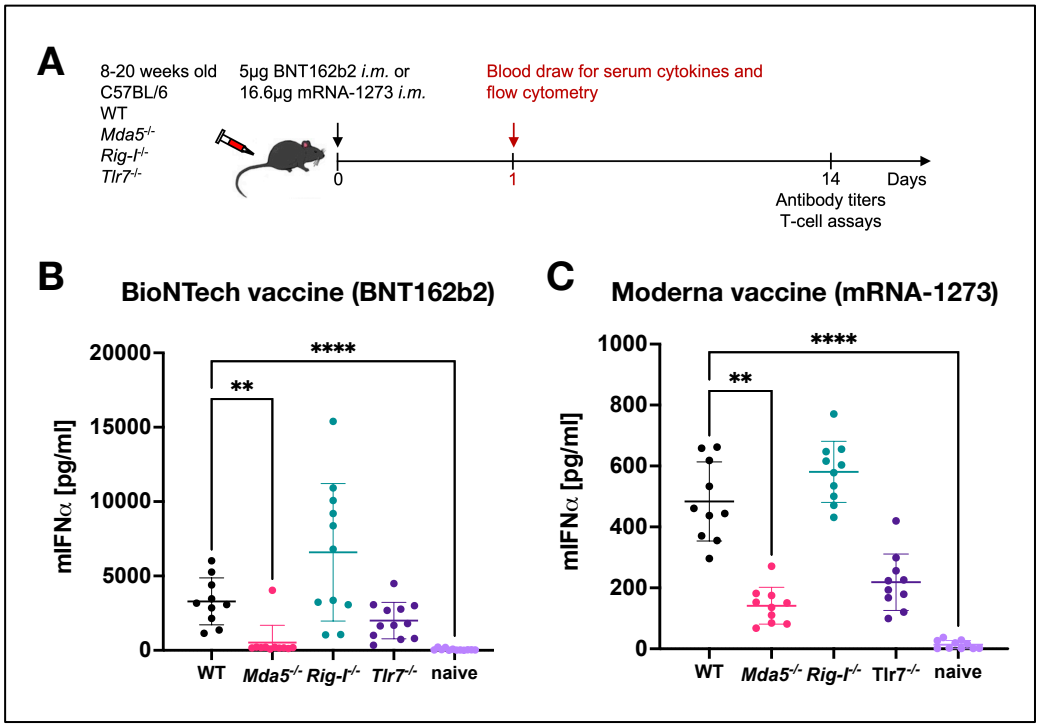

Figure 7: COVID-19 mRNA vaccines by BioNTech and Moderna induce an MDA5-dependent IFNα response *in vivo* in mice. (A) Schematic overview of the experiment. Mice of indicated genotypes were injected intramuscularly (i.m.) with 5 µg BioNTech vaccine (BNT162b2) or 16.6 µg Moderna vaccine (mRNA-1273). (B-C) IFNα release in serum was measured using the LEGENDplex™ Mouse Anti-Virus Response Kit (BioLegend, #740622). Mean ± SEM of 10-12 mice. Statistical comparisons were performed using one-way ANOVA with Dunnett's post-hoc test. * $p < 0.05$, ** $p < 0.01$, *** $p < 0.005$, **** $p < 0.001$. WT = wildtype. Data by Dr. Marcel Renn, Patrick Müller, and Yu Pan Tan. Data analysis by Prof. Dr. Eva Bartok. Figures from unpublished manuscript, rearranged and renumbered for display.

Additionally, the induction of adaptive immune responses by the COVID-19 mRNA vaccines in mice was investigated at 14 days after administration by the previously mentioned researchers (Figure 8A). Using a SARS-CoV-2 spike protein ELISA, the levels of spike-specific IgG were assessed. Furthermore, the $CD8^+$ T cell response was characterized by stimulating splenocytes with a SARS-CoV-2 peptide mix and quantifying $IFN\gamma^+$ $CD8^+$ T cells by flow cytometry. Both vaccines induced significant spike-specific IgG levels and $CD8^+$ T cell responses, confirming the vaccine's efficiency in inducing an adaptive immune response, which is in line with previous publications (Figure 8B-E).[67,101,104,151] Strikingly, mice deficient in MDA5 exhibited reduced spike-specific IgG and $IFN\gamma^+$ $CD8^+$ T cell levels, indicating that MDA5 activation contributes to vaccine efficiency. Together with a concurrent report by Li et al., these results demonstrate an adjuvant-like effect of MDA5 activation by dsRNA contained within mRNA vaccines.[67] This phenomenon was further investigated *in vitro*, as presented in Chapter 3.1.3. Interestingly, despite the varying degrees of IFNα induction by BioNTech's and Moderna's vaccines observed in Figure 7, the efficiency in inducing adaptive responses appeared to be similar between the two vaccines. (Figure 8B-E).

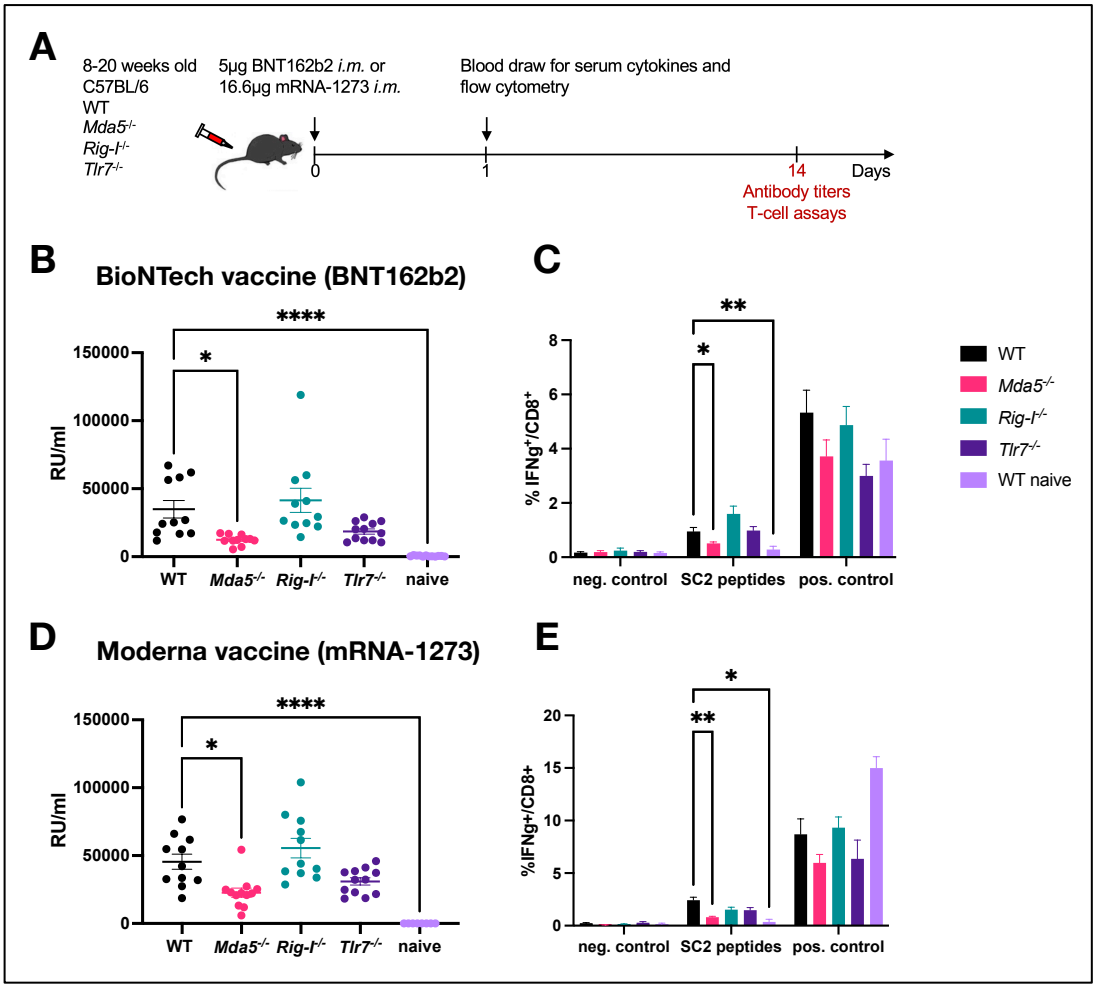

Figure 8: MDA5 contributes to COVID-19 mRNA vaccination outcomes in mice
(A) Schematic overview of the experiment. Mice of indicated genotypes were injected intramuscularly (i.m.) with 5 µg BioNTech vaccine (BNT162b2) or 16.6 µg Moderna vaccine (mRNA-1273). (B,D) SARS-CoV-2 Spike protein-specific IgG levels in the serum at day 14 post-vaccination, quantified using the Anti-SARS-CoV-2-QuantiVac-ELISA (IgG) kit (Euroimmun #EI 2606-9601-10G). (C,E) Intracellular IFNγ staining in $CD8^+$ T cells from splenocytes at day 14 post-vaccination, after the indicated restimulation overnight using the Quant-T-Cell SARS-CoV-2 kit (Euroimmun #ET 2606-3003). Mean ± SEM of 10-12 mice. Statistical comparisons were performed using one-way ANOVA with Dunnett's post-hoc test. * $p < 0.05$, ** $p < 0.01$, *** $p < 0.005$, **** $p < 0.001$. WT = wildtype. SC2 = SARS-CoV-2. Data by Dr. Marcel Renn, Patrick Müller, and Yu Pan Tan. Data analysis by Prof. Dr. Eva Bartok. Figures from unpublished manuscript, rearranged and renumbered for display.

Besides the *in vivo* experiments in mice, the innate immune response to the COVID-19 mRNA vaccines was also investigated in gene-edited human primary cells and cell lines. Specifically, Dr. Thomas Zillinger from the Hartmann group transfected transdifferentiated macrophage-like BLaER1 cells with mRNA isolated from BioNTech's or Moderna's vaccine. In addition, Sofía Beatriz Soler from the Bartok group stimulated primary monocyte-derived macrophages with the formulated vaccines. IFNα and CXCL10 responses were quantified via ELISA. CXCL10 is an interferon-induced protein that provides a highly sensitive measure of type I IFN responses.[1]

In contrast to the results obtained from mice, the cytokine response to the COVID-19 mRNA vaccines in human cells mainly depended on RIG-I, with only minor involvement of MDA5 (Figure

9). This finding was also confirmed in human skeletal muscle cells and human dermal fibroblasts by Dr. Thomas Zillinger and Sofía Beatriz Soler (data not shown), altogether confirming that the strong RIG-I dependency is not a peculiarity of the BlaER1 cell model but extends to human cells in general. Along with the previously presented *in vivo* data and data presented in Chapter 3.1, these results demonstrate a species-specific difference in mRNA sensing, such that human cells primarily employ RIG-I for mRNA sensing while murine cells utilize MDA5. This finding has significant implications for the translatability of murine *in vivo* experiments in preclinical research. Prompted by this observation, species-specific differences in sensing of nucleoside-modified mRNA as well as nucleoside-modified RLR ligands were further investigated throughout this thesis, extending the comparison of RLR activation and species selectivity to other common mRNA nucleoside modifications beyond N1-methyl-pseudouridine (m1Ψ), namely pseudouridine (Ψ), 5-methoxy-uridine (5moU), N6-methyl-adenosine (m6A), and 5-methyl-cytidine (m5C).

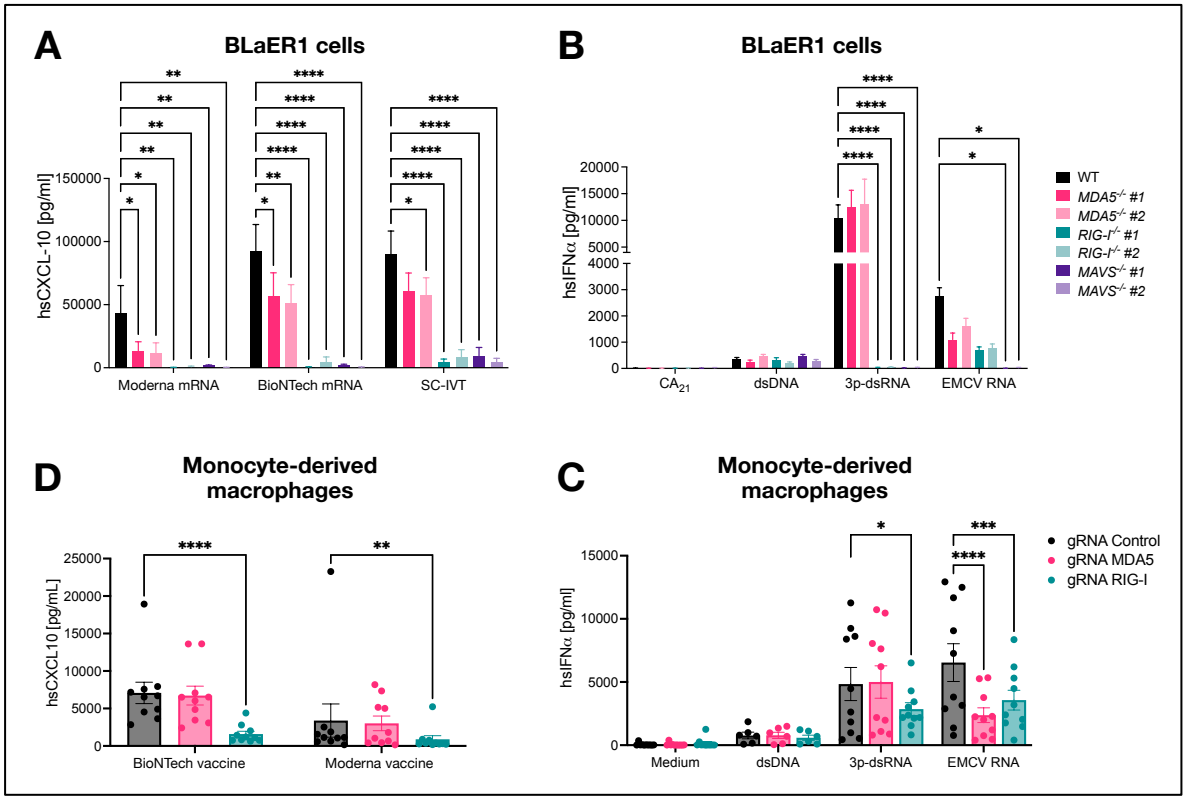

Figure 9: COVID-19 mRNA vaccines predominantly activate RIG-I in human cells. (A,B) Transdifferentiated BLaER1 cells were transfected with mRNA isolated from COVID-19 mRNA vaccines by BioNTech and Moderna, *in vitro* transcribed mRNA (SC-IVT), or indicated controls. (A) CXCL10 and (B) IFNα release were quantified via ELISA. Mean ± SEM of 5 independent experiments. (C,D) Monocyte-derived macrophages were stimulated with formulated COVID-19 mRNA vaccines by BioNTech and Moderna or indicated controls. (C) CXCL10 and (D) IFNα release were quantified via ELISA. Mean ± SEM of 10 donors. Statistical comparisons were performed using (A,B) two-way or (C,D) one-way ANOVA with Dunnett's post-hoc test. * $p < 0.05$, ** $p < 0.01$, *** $p < 0.005$, **** $p < 0.001$. WT = wildtype.
Data by Dr. Thomas Zillinger (A,B) and Sofía Beatriz Soler (C,D). Data analysis by Prof. Dr. Eva Bartok. Figures from unpublished manuscript, rearranged and renumbered for display.

Subsequently, Dr. Thomas Zillinger demonstrated how RNA purification contributes to the differences in IFNα levels induced by BioNTech's and Moderna's COVID-19 mRNA vaccine. The higher IFNα induction by mRNA isolated from BioNTech's vaccine compared to Moderna's was once more demonstrated in human peripheral blood mononuclear cells (PBMCs, Figure 10A). Purification of full-length, polyadenylated mRNA via oligo(dT)-coated magnetic beads (Figure 10B) and concurrent removal of immunogenic dsRNA byproducts significantly reduced IFNα induction by mRNA isolated from BioNTech's vaccine (Figure 10C). In line with this, the unbound poly(A)-fraction induced higher IFNα levels than the total BioNTech mRNA, indicating an enrichment of immunogenic dsRNA. In contrast, mRNA isolated from Moderna's vaccine was unaffected (Figure 10D). These results suggest that Moderna applies oligo(dT)-purification during their vaccine manufacturing, as indicated in a previous publication, and that this purification results in reduced IFNα induction compared to BioNTech's vaccine, which seems not to employ this purification method.[101,104]

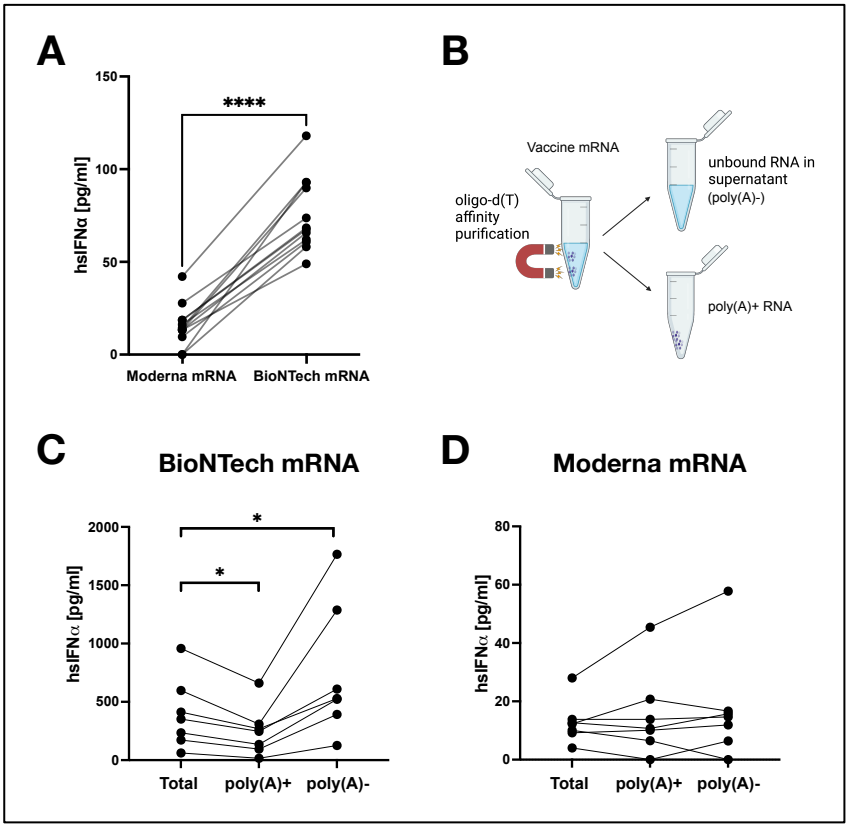

Figure 10: RNA purification contributes to the differences in the type I interferon response between BioNTech and Moderna COVID-19 mRNA vaccine. (A) Direct comparison of IFNα release from PBMCs transfected with RNA isolated from BioNTech's or Moderna's COVID-19 mRNA vaccine. Mean of 10 donors. (B) Schematic overview of the oligo-d(T) purification. (D,C) IFNα release from PBMCs stimulated with RNA purified from (D) BioNTech's or (C) Moderna's COVID-19 mRNA vaccine and purified as indicated in (C). Mean of 7 donors. Lines connect individual donors. Statistical comparisons were performed using (A) student's T-test or (C,D) one-way ANOVA with Dunnett's post-hoc test. * $p < 0.05$, ** $p < 0.01$, *** $p < 0.005$, **** $p < 0.001$. Data by Dr. Thomas Zillinger. Data analysis by Prof. Dr. Eva Bartok. Figures from unpublished manuscript, rearranged and renumbered for display.

Both COVID-19 mRNA vaccines contain a nucleoside-modified mRNA, in which all uridines have been replaced with N1-methyl-pseudouridine (m1Ψ), in order to reduce the activation of innate RNA receptors, such as TLRs (see Chapter 1.4.3). The effect of m1Ψ on activation of RLRs has remained elusive and was investigated during this collaborative project of the Bartok and Hartmann groups. To this end, an unmodified and m1Ψ-modified mRNA comprising 3189 bp of the SARS-CoV-2 genomes' 3′ end was *in vitro* transcribed, referred to as SC-IVT (SARS-CoV-2 *in vitro* transcript, see Figure 17A for schematic illustration). A cap-1 structure was added enzymatically to the mRNA to structurally mimic the COVID-19 vaccine mRNA. Several gene-edited primary cells and cell lines were stimulated with this mRNA, and RLR activation was quantified based on IFNα ELISA.

As exemplified by data generated by Dr. Thomas Zillinger using human BLaER1 cells (Figure 12), activation of human RIG-I was reduced by incorporation of m1Ψ into SC-IVT. Additionally, a weak activation of human MDA5 was observed by the unmodified but not m1Ψ-modified SC-IVT, indicating that incorporation of m1Ψ reduces activation of human MDA5 (Figure 12). These findings were additionally confirmed by Sofía Beatriz Soler using gene-edited human primary cells (data not shown). The role of m1Ψ for the activation of murine RLRs was investigated using primary murine cells and is presented in the results section of this thesis (Chapter 3.1.5, Figure 24).

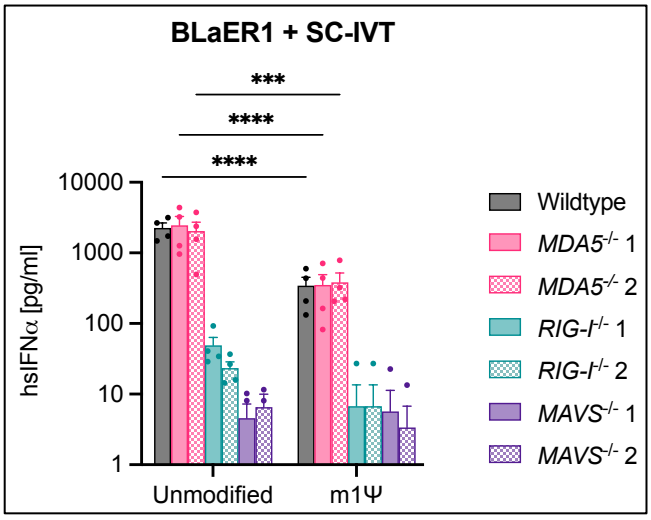

Figure 11: N1-methyl-pseudouridine (m1Ψ) reduces mRNA-induced RIG-I activation in human cells. Transdifferentiated BLaER1 cells were transfected with unmodified or m1Ψ-modified SC-IVT. IFNα release was quantified via ELISA. Mean ± SEM of 4 independent experiments. Statistical comparisons were performed using two-way ANOVA with Tukey's multiple comparisons correction. Only comparisons between stimuli are displayed. * $p < 0.05$, ** $p < 0.01$, *** $p < 0.005$, **** $p < 0.001$. WT = wildtype. Data by Dr. Thomas Zillinger.

In summary, this collaborative research project by the groups of Prof. Dr. Eva Bartok and Prof. Dr. Gunther Hartmann demonstrated that mRNA vaccines can exhibit adjuvant-like effects via immunogenic dsRNA contaminants activating innate RNA-sensing receptors, such as MDA5. Furthermore, the innate sensing of *in vitro* transcribed mRNA differs between humans and mice, which has essential implications for preclinical research and the development of mRNA therapeutics. Lastly, oligo(dT)-purification was identified as an efficient method to reduce type I IFN induction by mRNA vaccines. These findings are complemented by data presented in Chapter 3.1. Altogether, this sets the stage for further investigations into the role of nucleoside modifications in innate receptor activation by mRNA and other nucleic acid receptor agonists, as presented in Chapter 3.2 and 3.3.

1.5 Aim of the Study

The COVID-19 pandemic brought mRNA technology to the medical forefront, as immediate action was required to control it. Rapid mRNA vaccine development was only possible due to the significant scientific advancements in mRNA technology in previous decades. However, many of the specific molecular mechanisms induced by the administration of mRNA therapeutics, particularly their effects on the innate immune system, have remained poorly defined.

In this study, the innate immune activation by the COVID-19 mRNA vaccines by BioNTech and Moderna, as well as non-modified and nucleoside-modified IVT-mRNAs, is investigated, focusing particularly on the potential activation of the cytosolic RNA receptors RIG-I and MDA5. Additionally, the mechanisms of mRNA-induced RLR activation, for example by dsRNA byproducts or the effects of 5′ capping, are characterized. Furthermore, the modulation of RLR activation by incorporating commonly used nucleotide modifications into mRNA is explored, and the underlying modulation mechanisms are deciphered using defined RLR ligands. Finally, mRNA translation and its modulation by nucleoside modifications and innate immune responses is assessed. In all these pursuits, the experiments are specifically designed to identify potential differences between human and murine cells.

Altogether, this study aims to elucidate innate immune responses induced by IVT-mRNA and strives to facilitate the design of future mRNA therapeutics by providing mechanistic insight into the modulation of mRNA inflammatory potential by incorporation of nucleoside modifications.

2. Material and Methods

2.1 Material

2.1.1 Mouse strains

Name	Source
C57BL/6J	Jackson Laboratory, RRID: IMSR_JAX:000664
Ifnar$^{-/-}$ B6.129S2-Ifnar1$^{tm1Agt/Mmjax}$	Jackson Laboratory, RRID: MMRRC_032045-MU
Mavs$^{-/-}$ B6.129-*Mavs*$^{tm1Zjc/J}$	Shizuo Akira (University of Osaka)[152]
Mda5$^{-/-}$ B6.Cg-Ifih1$^{tm1.1Cln/J}$	Jackson Laboratory, RRID: IMSR_JAX:015812
Rig-I$^{-/-}$ B6.Ddx58$^{tm1.1IKCKP}$	Martin Schlee (Institute of Clinical Chemistry and Clinical Pharmacology, University Hospital Bonn)
Tlr7$^{-/-}$ B6.129P2-Tlr7^{tm1Aki}	Winfried Barchet (Institute of Clinical Chemistry and Clinical Pharmacology, University Hospital Bonn). Originally from Shizuo Akira (University of Osaka).[153]

2.1.2 Cell lines

Name	Source
BLaER1	Thomas Graf (Center for Genomic Regulation, Barcelona)[154,155]
Gene-edited BLaER1	Thomas Zillinger (Institute of Clinical Chemistry and Clinical Pharmacology, University Hospital Bonn)
THP-1	Clinics for Anesthesiology and Intensive Care (University Hospital Bonn). Originally from ATCC, TIB-202.
Gene-edited THP-1 (*MDA5*$^{-/-}$ *RIG-I*$^{-/-}$)	Thomas Zillinger (Institute of Clinical Chemistry and Clinical Pharmacology, University Hospital Bonn)
Transduced THP-1 (stable overexpression of RLRs)	This study
THP-1 Dual	Martin Schlee (Institute of Clinical Chemistry and Clinical Pharmacology, University Hospital Bonn). Originally from Invivogen, thpd-nfis.
Gene-edited THP-1 Dual (*PKR*$^{-/-}$)	Martin Schlee (Institute of Clinical Chemistry and Clinical Pharmacology, University Hospital Bonn)
HEK 293	Moritz Kebschull (Cardiology, University Hospital Bonn).
Gene-edited HEK 293	Thomas Zillinger (Institute of Clinical Chemistry and Clinical Pharmacology, University Hospital Bonn)
HEK 293 FT	Thermo Fisher Scientific, R70007
Murine GM-CSF-expressing J558	Winfried Barchet (Institute of Clinical Chemistry and Clinical Pharmacology, University Hospital Bonn).[156]
L929	Winfried Barchet (Institute of Clinical Chemistry and Clinical Pharmacology, University Hospital Bonn).
VeroE6	Beate Kümmerer (Institute of Virology, University Hospital Bonn)

2.1.3 Bacterial and viral strains

Name	Source	Cat. No.
Encephalomyocarditis virus (EMCV)	Winfried Barchet, Bonn[157]	-
E. coli Stbl3 (plasmid cloning)	Thermo Fisher Scientific	C737303

2.1.4 Chemicals, reagents and commercial buffers

Name	Source	Cat. No.
$(MgCO_3)_4Mg(OH)_2*5H_2O$	Carl Roth	3520.2
0.9 % NaCl	Fresenius	PZN00827194
1,4-Dithiothreitol (DTT)	Carl Roth	6908.2
17ß-Estradiol	Merck	3301-1GM
5-methoxyuridine	Tebu-bio	N-1093-1
5-methylcytidine	Jena Biosciences	NU-1138L
6X TriTrack Loading Dye	Thermo Fisher Scientific	R1161
Acetyl-Coenzyme A (95 % HPLC)	Genaxxon Bioscience	M3210.0100
Adenosine-triphosphate (ATP)	Carl Roth	K054.3
Agar	Carl Roth	X969.2
Ampuwa H_2O	Fresenius Kabi Deutschland GmbH	30201763
BD OptEIA™ TMB Substrate Reagent Set	BD Biosciences	555214
Bovine serum albumin	Carl Roth	8076.4
Buffer RLT	Qiagen	79216
Buffer RW1	Qiagen	1053394
Chloroquine	Sigma Aldrich	C6628
Coelenterazine (1 mg/ml)	PJK Biotech	102172
Cypridina Luciferin (Vargulin)	NanoLight Technology	305-1
D-Luciferin	Synchem	S039
DEPC	Carl Roth	K028.3
dNTP-Set 1 (100 mM)	Carl Roth	K039
DOTAP	Carl Roth	L787.2
Dulbecco's Modified Eagle Medium (DMEM)	Gibco (Thermo Fisher Scientific)	41965-039
Dulbecco's Phosphate Buffered Saline (DPBS)	Gibco (Thermo Fisher Scientific)	14190-094
Ethanol (≥ 99.5 %)	Carl Roth	5054.4
Ethidium bromide solution	Carl Roth	2218.2
Fetal Calf Serum (FCS)	Gibco (Thermo Fisher Scientific)	10270-106
Ficoll	VWR	17-1440-03
Formamide	Carl Roth	6749.3
GeneRuler DNA Ladder Mix (0.5 μg/μl)	Thermo Fisher Scientific	SM0331
Geneticin™ Selective Antibiotic	Thermo Fisher Scientific	10131035
KCl	Carl Roth	6781.1
LB medium	Carl Roth	X968.3
LiCl solution	Thermo Fisher Scientific	AM9480
Lipofectamine 2000	Thermo Fisher Scientific	11668019
MEM Non-Essential Amino Acids (NEAA, 10 mM)	Gibco (Thermo Fisher Scientific)	11140-050
Methanol	Carl Roth	8388.5
$MgSO_4*7H_2O$	Carl Roth	P027.1
My-Budget 5X EvaGreen® qPCR-Mix II (ROX)	Bio-Budget Technologies	80-5820000
N1-methylpseudouridine	Jena Biosciences	NU-890L
N6-methyladenosine	Jena Biosciences	NU-1101L
Opti-MEM™ Reduced Serum Medium	Gibco (Thermo Fisher Scientific)	31985-070
Penicillin / Streptomycin	Gibco (Thermo Fisher Scientific)	15140-122
Pharm Lyse™ Erythrocyte Lysing Buffer	BD Biosciences	555899
PNPP (4-Nitrophenylphosphate)	Sigma Aldrich	20-106
Poly-L-arginine, 5 - 15 kDa	Sigma-Aldrich	P4463
Polybrene	Sigma Aldrich	H9268

Powdered milk	Carl Roth	T145.3
Pseudouridine	Jena Biosciences	NU-1139L
Puromycin hydrochloride	Cayman Chemical	13884
R848 (Resiquimod)	Invivogen	tlrl-r848-1
Recombinant Human Interleukin-3 (rh IL-3)	PeproTech	200-03
Recombinant Human Macrophage Colony Stimulating Factor (rh M-CSF)	PeproTech	300-25
Recombinant Mouse Interferon-Alpha	PBL Assay Science	12100-1
RiboLock RNase Inhibitor (40 U/μl)	Thermo Fisher Scientific	EO0381
RiboRuler High Range RNA Ladder	Thermo Fisher Scientific	SM1821
Roti®-Aqua-P/C/I	Carl Roth	X985.1
Roti®-Phenol / Chloroform / Isoamylalkohol	Carl Roth	A156.1
ROTIPHORESE®50x TAE buffer	Carl Roth	CL86.3
RPMI Medium 1640	Gibco (Thermo Fisher Scientific)	21875-034
Saponin	Carl Roth	4185.1
Sodium Acetate	Sigma Aldrich	127-09-3
Sodium Ascorbate	Sigma-Aldrich	11140
Sodium chloride (NaCl)	Carl Roth	9265.2
Sodium hydroxide (NaOH)	Carl Roth	6771.3
Sodium Pyruvate	Gibco (Thermo Fisher Scientific)	11360-070
Supersignal® Chemiluminescent Substrate	Thermo Fisher Scientific	34075
SYBR Safe DNA Gel Stain	Thermo Fisher Scientific	S33102
TBST tablets (RNase free)	Carl Roth	1248.1
*Trans*IT®-LT1 Transfection Reagent	Mirus	MIR 2304
Trichlormethan / Chloroform (≥ 99 %)	Carl Roth	3313.1
Tricine	Carl Roth	6977.1
Tris	Carl Roth	AE15.3
TRIzol	Thermo Fisher Scientific	15596026
Trypsin-EDTA (0.05 %)	Gibco (Thermo Fisher Scientific)	25200056
Tween® 20	Carl Roth	9127.1
UltraPure™ 1 M Tris-HCl-Puffer, pH 7.5	Thermo Fisher Scientific	15567027
UltraPure™ EDTA, pH 8.0 (0.5 M)	Thermo Fisher Scientific	15575020
Zombie Aqua™ Fixable Viability Kit	BioLegend	423102
Zymo Wash Buffer	Zymo Research	1003-3-24

2.1.5 Non-commercial buffers

Name	Composition
(dT) Binding buffer	100 mM Tris-HCl, 500 mM LiCl, 0.5 % LiDS, 1 mM EDTA, 5 mM DTT
2X HEPES-buffered saline, pH 7.07	50 mM HEPES, 280 mM NaCl, 10 mM KCl, 1.5 mM Na2HPO4, 12 mM sucrose
ELISA Assay Buffer	1 X PBS, 10 % FCS
ELISA Coating Buffer, pH 6.5	90 mM Na_2HPO_4, 130 mM NaH_2PO_4
ELISA Wash Buffer	1 X PBS, 0.1 % Tween 20
Elution buffer	20 mM Tris-HCl, 1 mM EDTA
FACS buffer	PBS, 2 mM EDTA, 2 % FCS
Firefly luciferase substrate solution	20 mM tricine, 2.67 mM $MgSO_4$*$7H_2O$, 0.1 mM EDTA pH 8.0, 33.3 mM DTT, 0.53 mM ATP, 0.27 mM Acetyl-CoA, 0.5 mM D-Luciferin, 0.265 mM $(MgCO_3)_4Mg(OH)_2$*$5H_2O$, 5 mM NaOH
Gaussia / Cypridina luciferase buffer	100 mM Tris pH 7.7, 300 mM Sodium ascorbate
Human IFNα ELISA Assay Buffer	1 X PBS, 0.1 % Tween 20, 0.5 % BSA

Low-salt buffer	20 mM Tris-HCl, 200 mM LiCl, 1 mM EDTA
PNPP buffer, pH 9.0	2 mg/ml PNPP, 100 mM Tris, 100 mM NaCl, 10 mM $MgCl_2$
Saponin Lysis Buffer	50 mM Tris pH 7.4, 100 mM NaCl, 0.5 % Saponin
Tail buffer, pH 8.5	100 mM Tris, 5 mM EDTA, 0.2 % SDS, 200 mM NaCl
Wash I buffer	20 mM Tris-HCl, 500 mM LiCl, 0.1 % LiDS, 1 mM EDTA, 5 mM DTT
Wash II buffer	20 mM Tris-HCl, 500 mM LiCl, 1 mM EDTA

2.1.6 Antibodies

Name	Source	Cat. No.
Brilliant Violet 785™ rat anti-mouse CD86 (Clone GL-1)	BioLegend	105043
Brilliant Violet 421™ hamster anti-mouse CD11c (Clone N418)	BioLegend	117343
APC rat anti-mouse CD40 (Clone 1C10)	eBioscience	17-0401-82
Rat Anti-Mouse IFN-Alpha, Clone RMMA-1 (MAb)	PBL Assay Science	22100-1
Anti-Mouse IFN-Alpha, Rabbit Serum (PAb)	PBL Assay Science	32100-1
Goat-anti-rabbit IgG (H+L) HRP	Bio-Rad	1706515
Anti-dsRNA monoclonal antibody J2	Jena Bioscience	RNT-SCI-10010500
Goat-anti-mouse IgG-HRP	Bio-Rad	1706516
FITC rat anti-mouse CD11b (Clone M1/70)	BD Biosciences	553310
PE/Cyanine7 hamster anti-mouse CD69 (Clone H1.2F3)	BioLegend	104512
Purified rat anti-mouse CD16/32 (Fc Block™, Clone 2.4G2)	BD Biosciences	553142
APC/Cyanine 7 rat anti-mouse MHC II (Clone M5/114.15.2)	BioLegend	107627

2.1.7 Enzymes

Name	Source	Cat. No.
AscI	New England Biolabs	R0558S
BcoDI	New England Biolabs	R0542S
DNase I, RNase-free (1 U/µl)	Thermo Fisher Scientific	EN0521
DreamTaq DNA Polymerase	Thermo Fisher Scientific	EP0705
EcoRI-HF	New England Biolabs	R3101S
Polyphosphatase	Lucigen	RP8092H
Proteinase K	Carl Roth	7528.5
Q5 High-Fidelity DNA Polymerase	New England Biolabs	M0491L
RevertAid Reverse Transcriptase (200 U/µl)	Thermo Fisher Scientific	EP0442
RNase If	New England Biolabs	M0243S
SacI	Thermo Fisher Scientific	FD1894
Terminator Exonuclease	Biozym	162370
TURBO DNase	Thermo Fisher Scientific	AM2238
Vaccinia 2′-O-methyltransferase	New England Biolabs	M2080
Vaccinia Capping Enzyme	New England Biolabs	M0366

2.1.8 Oligonucleotides

IDT = Integrated DNA Technologies

Name	Sequence [5′ → 3′]	Source
9.2S RNA	AGCUUAACCUGUCCUUCAA	Biomers, Ulm, Germany
Control ssRNA (= Mock)	CACACACACACACACACAC	Biomers, Ulm, Germany
CpG1826-PTO	TCCATGACGTTCCTGACGTT	Invivogen, tlrl-1826
CpG2006-PTO	TCGTCGTTTTGTCGTTTTGTCGTT	Invivogen, tlrl-2006
Forward primer for 512B template	GGGAGAAGCTCTCTTACACCTGATTCATTTCCA	IDT
Forward primer for 512B template including T7 promoter primer	TAATACGACTCACTATAGGGAGAAGCTCTCTTACACCTGATTCATTTCCA	IDT
Forward primer for DNA template of antisense EGFP-Fluc	TAATACGACTCACTATAGGGGGAGGCAAACACTTTATTAT	IDT
Herring testes (HT) DNA	-	Promega, D1811
Ifnar genotyping forward primer	CGAGGCGAAGTGGTTAAAAG	IDT
Ifnar genotyping reverse primer #1	ACGGATCAACCTCATTCCAC	IDT
Ifnar genotyping reverse primer #2	AATTCGCCAATGACAAGACG	IDT
Mda5 genotyping forward primer	CTTCTGTTCTTCCTGGGAGACC	IDT
Mda5 genotyping reverse primer #1	GGGACTATTGACAGTCGAAGAC	IDT
Mda5 genotyping reverse primer #2	CTTGGCTTCCTCCTAAACTCAG	IDT
mm-Hprt forward primer	GCCCCAAAATGGTTAAGGTT	IDT
mm-Hprt reverse primer	CAAGGGCATATCCAACAACA	IDT
mm-Ifi44 forward primer	TCGATTCCATGAAACCAATCAC	IDT, Liehl *et al.*[158]
mm-Ifi44 reverse primer	CAAATGCAGAATGCCATGTTTT	IDT, Liehl *et al.*[158]
mm-Ifit1 forward primer	CTGAGGCCCACATTTGAGAT	IDT
mm-Ifit1 reverse primer	TGTTGTTCAGTGCCTTCTGG	IDT
mm-Ifit3 forward primer	CTGAACTGCTCAGCCCACAC	IDT, Liehl *et al.*[158]
mm-Ifit3 reverse primer	TGGACATACTTCCTTCCCTGA	IDT, Liehl *et al.*[158]
mm-Ifnb forward primer	ATGGTGGTCCGAGCAGAGAT	IDT
mm-Ifnb reverse primer	CCACCACTCATTCTGAGGCA	IDT
mm-Isg15 forward primer	AGTGCTCCAGGACGGTCTTA	IDT
mm-Isg15 reverse primer	TGCCTGCAGTTCTGTACCACA	IDT
mm-Rsad2 forward primer	AACCCCCGTGAGTGTCAACTA	IDT
mm-Rsad2 reverse primer	AACCAGCCTGTTTGAGCAGAA	IDT
mm-Siglec1 forward primer	TCTCGGCTCCTGTGGTCCTAAG	IDT
mm-Siglec1 reverse primer	TCCACAGTGCAGATGAACACGG	IDT
mm-Usp18 forward primer	CGTGCTTGAGAGGGTCATTTG	IDT, Liehl *et al.*[158]
mm-Usp18 reverse primer	GGTCGGGAGTCCACAACTTC	IDT, Liehl *et al.*[158]
Poly(I:C) HMW	$(I)_n$:$(C)_n$	Invivogen, tlrl-pic
Random hexamer primers	-	IDT, 51-01-18-01
Reverse primer for 512B template	GGGAGAATGTCGAATGGGTATTCCACAGAC	IDT
Reverse primer for 512B template including T7 promoter primer	TAATACGACTCACTATAGGGAGAATGTCGAATGGGTATTCCACAGAC	IDT
Reverse primer for DNA template of antisense EGFP-Fluc	GGGAGAACGCGTTTAATTAAATTTGTCGAC	IDT
Synthetic ssRNA antisense (for LCMS)	AAGAUGAACUUCAGGGUCAGCGUC	Biomers
Synthetic ssRNA antisense + 3 nt overhang (for LCMS)	AAGAUGAACUUCAGGGUCAGCGUCAAA	Biomers
Synthetic ssRNA sense (for LCMS)	GACGCUGACCCUGAAGUUCAUCUU	Biomers

Template for 24 nt ssRNA (antisense DNA strand)	AAGCTGACCCTGAAGTTCATCCCCTATAGTG AGTCGTATTA	IDT
Template for 24 nt ssRNA (sense DNA strand)	TAATACGACTCACTATAGGGGATGAACTTCA GGGTCAGCTT	IDT
Template for 56 nt hairpin dsRNA (antisense DNA strand)	GGGACGCTGACCCAGAAGATCTACTATTTC TAGTAGATCTTCTGGGTCAGCGTCCCTATAG TGAGTCGTATTACAA	IDT
Template for 56 nt hairpin dsRNA (sense DNA strand)	TTGTAATACGACTCACTATAGGGACGCTGAC CCAGAAGATCTACTAGAAATAGTAGATCTTC TGGGTCAGCGTCCC	IDT

2.1.9 Commercial assays

Name	Source	Cat. No.
Human IL-12 (p70) ELISA Set	BD	555183
Human IP-10 (CXCL10) ELISA Set	BD	550926
Human TNF alpha ELISA Set	BD	555212
IFN alpha Human Matched Antibody Pair	Thermo Fisher Scientific	BMS216MST
Mouse IL-12 (p40) ELISA Set	BD	555165
PureLink™ HiPure Plasmid Midiprep Kit	Thermo Fisher Scientific	K210005
Quantseq 3′ mRNA-Seq Library Prep Kit FWD for Illumina	Lexogen	015.24
Rabbit Reticulocyte Lysate System, Nuclease Treated	Promega	L4960
TranscriptAid T7 High Yield Transcription Kit	Thermo Fisher Scientific	K0441

2.1.10 Equipment

Name	Source	Cat. No.
ACQUITY UPLC BEH C18 Column	Waters	186002350
ACQUITY-UPLC system	Waters	-
Attune NxT Flow Cytometer	Thermo Fisher Scientific	RRID:SCR_019590
Bead Mixer Mill	VWR	412-0167
Cytation™ 3 Cell Imaging Multi-Mode Reader	BioTek	BTCYT3MV
Envision Reader	PerkinElmer	-
Epoch spectrophotometer	BioTek	17287989
FlexCycler^2	Thistle Scientific	844-00069
Microplate 96-well Med. Binding (for ELISA)	Greiner Bio-One	655001
NanoDrop 8000	Thermo Fisher Scientific	ND-8000-GL
Nytran SuPerCharge (SPC) Nylon Blotting Membrane, 0.45 µm, 11 × 14 cm, sheet	Sigma-Aldrich	WHA10416230
Odyssey XF Imager	LI-COR	-
Oligo d(T)$_{25}$ Magnetic Beads	NEB	S1419S
QuantStudio™ 5 Real-Time PCR System, 384-well	Thermo Fisher Scientific	A28140
TC20 automated cell counter	Bio-Rad	1450102
Tissue Culture Plate 96F	TPP	92696
UVIlink UV crosslinker	Biocom Direct	CL-508.G
UVP GelStudio PLUS imager	Analytik Jena	-
Xevo TQ-S Quadrupole	Waters	-
Zymo-Spin IIICG Silica Columns	Zymo Research	C1006-250-G

2.1.11 Software

Name	Source
BioRender	BioRender.com
Cutadapt	Martin *et al.*[159]
DESeq2	Love *et al.*[160]
FASTQC	Github, https://github.com/s-andrews/FastQC
FlowJo 10.8	BD Life Sciences, RRID:SCR_008520
Gen5 2.09	Biotek, RRID:SCR_017317
HT-Seq	Putri *et al.*[161]
ImageJ	Imagej.net
Office (Word, Excel, Powerpoint)	Microsoft
Papers Citation Program	Readcube
Prism 10	GraphPad Software, RRID:SCR_002798
Samtools	Danecek *et al.*[162]
STAR Aligner	Dobin *et al.*[163]

2.2 Methods

2.2.1 Cell culture

The standard medium utilized for both cell lines and primary cells was either RPMI or DMEM supplemented with 10 % heat-inactivated fetal calf serum (FCS), 1 mM sodium pyruvate, 100 U/ml penicillin, 100 µg/ml streptomycin, and 0.1 mM non-essential amino acids, and will be referred to as "complete RPMI" or "complete DMEM", respectively. Any deviation will be indicated at the respective location. All cells were incubated at 37 °C and 5 % CO_2. Cell lines were passaged once or twice per week based on their proliferation rate. For passaging, adherent cells were rinsed with PBS and detached by incubation with 0.05 % trypsin-EDTA for 2 – 3 minutes (min) at room temperature (RT). To preserve cells, aliquots were frozen in FCS containing 10 % dimethyl sulfoxide (DMSO) using a freezing container filled with isopropanol to achieve a cooling rate of approximately -1 °C/min. This freezing method was employed for all cells except THP-1 cells, which exhibited improved survival rates if frozen in FCS containing only 5 % DMSO.

2.2.2 Trans-differentiation of human BLaER1 cells into macrophage-like cells

The human BLaER1 (B cell Leukemia C/EBPαER clone 1) cell line is derived from a B cell precursor leukemia patient and has been stably transfected with the transcription factor C/EBPα fused to the estrogen receptor binding domain and green fluorescent protein (GFP) by utilizing the squirrel monkey retrovirus.[154,164] This enables the trans-differentiation of the pre-B cells into macrophage-like cells as follows. 1 x 10^7 cells were seeded into a 10 cm cell culture dish with 15 ml complete RPMI, 100 nM 17-β-estradiol, 10 ng/ml interleukin-3 (IL-3), and 10 ng/ml M-CSF (macrophage colony-stimulating factor). Following 6 days of incubation at 37 °C and 5 % CO_2, cells were harvested by collecting supernatants and incubating dishes with 4 ml PBS containing 2 mM EDTA at 37 °C for 20 min. Cells were detached by repetitive pipetting, transferred to the supernatant-containing tubes and centrifuged at 300 rcf for 5 min. Pellet was resuspended in complete RPMI and counted using the automated TC20 cell counter. Finally, 7 x 10^4 cells/well were plated in 100 µl into a flat-bottom 96-well plate and incubated until stimulation.

2.2.3 Generation of GM-CSF-containing J588 cell supernatant

J558 cells transduced with a murine GM-CSF expression vector were cultured in T-175 cell culture flasks in complete RPMI including 1 mg/ml geneticin (G-418) until 100 % confluency.[156] Supernatants were harvested, centrifuged at 2,000 rcf and 4 °C for 20 min and filtered using a 0.22 µm pore-sized filter. Optimal working concentration of GM-CSF-containing supernatants were determined by titration series on BMDCs (Chapter 2.2.4) and flow cytometric analysis based on expression of CD11c and MHC class II. Supernatants were aliquoted and stored at -20 °C.

2.2.4 Generation of bone marrow and bone marrow-derived dendritic cells

Mice were euthanized by cervical dislocation. Femur and tibia were isolated, cut, and placed in a perforated 0.5 ml tube within a 2 ml receiver tube. A brief centrifugation for 5 - 10 sec at 3000 rcf extracted the bone marrow. The resulting pellets were resuspended in 1 ml erythrocyte lysis buffer and incubated for 5 min at RT. The cell suspension was transferred to a tube containing 10 ml complete RPMI, followed by centrifugation for 5 min at 300 rcf. The cells were resuspended in complete RPMI and counted using the TC20 cell counter. If bone marrow was to be stimulated, 2×10^5 cells/well were plated in 100 µl into a flat-bottom 96-well plate and incubated until stimulation. For generation of BMDCs, 5×10^6 cells were seeded into 10 cm cell culture dishes containing 12 ml complete RPMI supplemented with 13 % GM-CSF-containing J588 cell supernatant (Chapter 2.2.3). After 4 days of incubation at 37 °C and 5 % CO_2, 8 ml cell suspension were replaced with complete RPMI containing 13 % GM-CSF including a centrifugation step to retain all cells. On day 6, cells were harvested and counted as described for BLaER1 cells (Chapter 2.2.2). Finally, 2×10^5 cells/well were plated in 100 µl into a flat-bottom 96-well plate and incubated at 37 °C and 5 % CO_2 until stimulation.

2.2.5 Generation of bone marrow-derived macrophages (BMM)

Bone marrow-derived macrophages (BMMs) were generated similarly to BMDCs (Chapter 2.2.4) but were cultured in petri dishes and complete RPMI supplemented with 30 % L929-conditioned medium instead of GM-CSF. The L929-conditioned medium was generated by incubating 2×10^6 L929 cells in complete DMEM in T-175 cell culture flasks for 10 days. Supernatants were collected and filtered using a 0.22 µm pore-sized filter. BMMs were harvested after 7 days (no medium change in between) using the procedure described for BLaER1 cells (Chapter 2.2.2). 1×10^5 cells/well were plated in 100 µl DMEM into a flat-bottom 96-well plate and incubated at 37 °C and 5 % CO_2 until stimulation.

2.2.6 Isolation of peripheral blood mononuclear cells (PBMCs)

Whole blood or buffy coats were diluted to a convenient volume using 0.9 % NaCl. 13 ml Ficoll were added to a 50 ml tube, and 25 ml of blood cell suspension were gently layered on top. Samples were centrifuged at 800 rcf for 20 min with brakes set to level 1. Cell layer was transferred to a new tube, washed in 50 ml 0.9 % NaCl and centrifuged at 450 rcf for 7 min. Supernatant was discarded, cell pellet resuspended in 10 ml erythrocyte lysis solution and incubated for 5 min at RT. Cell suspension was again washed using 0.9 % NaCl and resuspended in complete RPMI. Cells were counted using the TC20 cell counter and 4×10^5 cells/well were plated into a flat-bottom 96-well plate. Stimulation was performed within the following 2 h. Optional chloroquine treatment was performed 30 min prior to transfection using a final concentration of 10 µM.

2.2.7 RNA isolation from COVID-19 mRNA vaccines

Leftover vials of COVID-19 mRNA vaccines by BioNTech/Pfizer and Moderna were kindly provided by company physicians of the University Hospital Bonn, the Johanniter Hospital Bonn, and the WCCB716 COVID-19 vaccination center Bonn. Residual vial contents were pooled, and RNA was isolated by addition of 1 volume ROTI®Aqua-Phenol followed by vortexing for 20 sec and centrifugation at 12,000 rcf for 5 min. Upper aqueous phase was transferred to a fresh tube, mixed with 1 volume chloroform and once more vortexed and centrifuged. Upper aqueous phase was transferred and mixed with 0.1 volume 3 M sodium acetate (pH 5.2) and 2 volumes cold ethanol to precipitate the RNA. Samples were incubated for > 10 min at -80 °C and centrifuged at 16,000 rcf and 4 °C for 30 min. Pellets were washed twice with 70 % cold ethanol, air-dried and resuspended in DEPC-treated H_2O. RNA was dissolved via incubation at 55 °C for 10 min and quantified spectrophotometrically using a NanoDrop spectrophotometer.

2.2.8 Transformation of competent bacteria

50 µl of chemically competent *E. coli* strain Stbl3 was mixed with 10 pg plasmid DNA and incubated on ice for 30 min. Heat shock was performed at 42 °C for 1 min followed by a 2-minute incubation on ice. 950 µl LB medium were added and bacteria were incubated on a standard heating block at 37 °C and 450 rpm for 60 min. Following a 3-minute centrifugation at 3,000 rcf, pellet was spread an agar plate containing the respective antibiotic and incubated on an orbital shaker at 37 °C and 90 rpm overnight. Colonies were picked into 150 ml LB medium and incubated overnight as above.

2.2.9 Plasmid DNA preparation

Plasmids were purified using the PureLink™ HiPure Plasmid Midiprep Kit according to the manufacturer's instructions.

2.2.10 Generation of DNA templates for *in vitro* transcription

pEF-BOS plasmids containing the T7 promoter sequence followed by those of SC-IVT, EGFP-Fluc and mCherry mRNAs, respectively, were kindly provided by Dr. Thomas Zillinger and Dr. Christine Wuebben (Institute of Clinical Chemistry and Clinical Pharmacology). Templates were generated by restriction enzyme digestion of plasmids, using AscI and SacI for SC-IVT, EcoRI for EGFP Fluc, and BcoDI for mCherry. Enzymes and plasmids were used in a 1:10 ratio in the provided buffer and incubated at 37 °C for 30 min. A 5 µl aliquot was extracted to confirm successful digestion via agarose gel electrophoresis (Chapter 2.2.13). Templates were purified using phenol/chloroform purification as described in 2.2.7 using ROTI®-Phenol instead of ROTI®Aqua-Phenol. DNA templates for the 24 nt ssRNA and the 56 nt hairpin dsRNA were ordered from Integrated DNA Technologies. Strands were annealed in 50 mM KCl and 16 mM Tris-HCl by heating to 95°C for

2 min, followed by 72°C for 1 min, and cooled by 1°C per cycle over 57 cycles. Sense and antisense templates of 512B RNAs were generated by standard polymerase chain reaction (PCR) using Q5 DNA polymerase. Primers amplify the first 512 nt of the human MDA5 coding sequence. A pLenti-hMDA5 plasmid was kindly provided by Dr. Thomas Zillinger and used as PCR template. The T7 promoter was included in the forward primer for the sense 512B template and in the reverse primer for the antisense 512B template.[25] Template of the antisense EGFP-Fluc (for generation of the ds-mRNA) was also produced via PCR and respective primers from the pEF-BOS EGFP-Fluc plasmid.

2.2.11 *In vitro* transcription and isolation of mRNA

In vitro transcription was performed using the TranscriptAid T7 High Yield kit according to the manufacturer's instructions and the reaction was incubated at 37 °C for 2 h. To incorporate nucleoside modifications, respective nucleotides were substituted for their modified analog. The DNA template was digested by adding 1.5 µl TURBO DNase and additional incubation at 37 °C for 30 min. RNA was isolated as described in Chapter 2.2.7. A few exceptions to this procedure are described below. All non-messenger RNAs were transcribed for a duration of 4 h. The short 24 nt ssRNA and 56 nt hairpin dsRNA were generated using 5 µM template. The ss512B was generated using 200 ng template. The ds512B was generated by combining 200 ng of sense and antisense template each into a single reaction. After purification of the ds512B, residual ssRNA was digested using RNase If according to the manufacturer's instructions. RNase If was deactivated by adding 20 µl of 20 mg/ml proteinase K solution and incubating at 37 °C for 30 min followed by RNA purification as described before.

2.2.12 Enzymatic mRNA capping

Enzymatic capping of mRNA was performed using the vaccinia one-step capping system according to the instructions of NEB. Briefly, 15 µg mRNA were adjusted to 14 µl using H_2O and denatured at 65 °C for 5 min followed by immediate cooling on ice. Capping reaction was prepared according to the manual and incubated at 37 °C for 1 hr. Capped mRNA was purified as described in Chapter 2.2.7.

2.2.13 Agarose gel electrophoresis

2 % agarose gels were prepared in TAE buffer including 1:100,000 SYBR Safe DNA gel stain. For RNA gel electrophoresis, 500 ng RNA or 4 µl of RiboRuler High Range RNA Ladder were mixed with DEPC-treated H_2O and 2X loading dye (95 % formamide, 5 mM EDTA, and a spatula tip of orange G) in a volume of 12 µl and denatured at 70 °C for 5 min. For DNA gel electrophoresis, 500 ng DNA or 5 µl aliquots of restriction enzyme digestions were mixed with 6X TriTrack loading Dye. 4 µl of GeneRuler DNA Ladder Mix were used. Samples were loaded and gel was run at 6 V/cm

for 30 – 60 min. Gels were imaged via the UVP GelStudio PLUS imager by Analytik Jena using blue LED light for excitation and 510 – 560 nm “SYBR Green” emission filter.

2.2.14 Oligo(dT)-purification

200 µl oligo(dT)$_{25}$ magnetic beads were equilibrated in 400 µl binding buffer at RT for 2 min and buffer was subsequently aspirated. 20 µg IVT-mRNA were mixed with 1 ml binding buffer, added to the beads and incubated on a rotary shaker at RT for 10 min. Supernatants were collected as poly(A)- fraction and precipitated using isopropanol as described in 2.2.7. Beads were washed twice with 1 ml wash buffer I, once with 1 ml wash buffer II and once with 1 ml low-salt buffer. Beads were mixed with 200 µl elution buffer and incubated at 50 °C and 300 rpm on a heater block for 2 minutes. Eluted mRNA was transferred to a fresh tube and quantified using a NanoDrop spectrophotometer.

2.2.15 Anti-dsRNA dot blot

RNA was diluted in DEPC-H_2O and 2 µl were pipetted onto a Nytran Supercharge membrane. RNA was crosslinked using 130 kJ UV illumination and air-dried for 10 min. Membrane was pre-wetted in PBS and blocked in RNase-free TBST containing 5 % milk for 1 h at RT. Following two washing steps in RNase-free TBST, the membrane was incubated in 2 % milk / TBST and 1:1,000 anti-dsRNA antibody J2 overnight at 4 °C. After three 15-min washes in TBST, the membrane was incubated in 1 % milk / TBST and 1:5,000 goat anti-mouse IgG-HRP for 2 h at RT, protected from light. The membrane was washed thrice for 15 min each and developed using 500 µl Supersignal ECL reagents. Imaging was performed using the chemiluminescence channel of the Odyssey XF Imager. Membrane was washed again, incubated in RNase-free TBST containing 1:10,000 EtBr for 10 min and imaged using the 600 nm channel. Images were analyzed using ImageJ.

2.2.16 Polyphosphatase and terminator exonuclease digestions

Polyphosphatase digestion was performed prior to transfection of RNA. Briefly, the desired RNA amount was added to a 20 µl reaction mix as indicated in Table 14 and incubated at 37 °C for 30 min. Samples were then diluted with Opti-MEM to the desired volume and utilized for transfection, as described in Chapter 2.2.18. If subsequent digestion with terminator exonuclease was desired, higher amounts of RNA (up to 5 µg) were digested per 20 µl reaction. After incubation, samples were diluted with 30 µl DEPC-H_2O and purified using phenol/chloroform purification as described in Chapter 2.2.7. Terminator exonuclease digestion was performed as described in Table 13 and incubated at 30 °C for 60 min. RNA was purified using phenol/chloroform purification as before.

Table 14: Polyphosphatase digestion

Reagent	Quantity
H_2O	To 20 µl
10X Reaction Buffer	2 µl
RNA	Up to 5 µg
RiboLock RNase Inhibitor	0.5 µl
Polyphosphatase	1 µl

Table 13: Terminator exonuclease digestion

Reagent	Quantity
H_2O	To 20 µl
10X Reaction Buffer A	2 µl
RNA	Up to 10 µg
Terminator Exonuclease	1 µl

2.2.17 Generation of EMCV RNA

VeroE6 cells were cultured in T-75 cell culture flasks in complete DMEM. At 80 % confluency, cells were infected using an aliquot of EMCV virus-containing supernatants collected from previous infections of VeroE6 cells. After 10 – 16 h of incubation at 37 °C and 5 % CO_2, medium was aspirated, and cells were collected for RNA isolation using 3 – 5 ml TRIzol per T-75 flask. Isolation was performed according to the TRIzol manual.

2.2.18 Transfection of nucleic acids

For cytosolic delivery, the transfection reagent Lipofectamine 2000 was utilized for all stimuli in this study except poly(I:C), which was transfected using TransIT LT-1. The general procedure was identical for both reagents and is described further below. Prior to stimulation, the cells were seeded in 96-well flat-bottom plates. For each well, 12.5 µl of serum-free Opti-MEM were mixed with 0.25 µl transfection reagent and incubated at RT for 5 – 10 min. Meanwhile, the desired quantity of nucleic acid was prepared in 12.5 µl Opti-MEM. Both solutions were combined and incubated at RT for 20 min. Finally, 25 µl transfection mix per 96-well were added to the cells followed by overnight incubation at 37 °C and 5 % CO_2. For endosomal delivery to human PBMCs, poly-L-arginine transfection was used. For endosomal delivery to murine primary cells, DOTAP (1,2-dioleoyl-3-trimethylammonium-propane) was used. The procedures were similar to Lipofectamine 2000, but reaction mixes were prepared using PBS instead of Opti-MEM and 0.18 µl poly-L-arginine or 1 µl DOTAP, respectively, instead of Lipofectamine 2000.

2.2.19 Enzyme-linked immunosorbent assay (ELISA)

Murine interferon-α (mIFNα): ELISA plates were coated with 50 µl coating buffer pH 6.5 containing 1 µg/ml rat anti-mouse IFNα antibody, sealed and incubated overnight at 4 °C. The plates were then washed three times with 200 µl ELISA wash buffer. Unspecific binding sites were blocked with 50 µl assay buffer for 1 h at RT, followed by three washing steps. 50 µl of samples or mIFNα standard (two-fold serial dilution starting at 5000 pg/ml) prepared in assay buffer were added and incubated overnight at 4 °C. Following three washing steps, 50 µl of assay buffer containing 100 U/ml rabbit anti-IFNα antibody were added to each well and incubated at RT for 3 h. After

seven washing steps, 50 µl assay buffer containing 1:5,000 goat anti-rabbit IgG-HRP were added to each well and incubated for 1 – 3 h at RT, protected from light. Plates were washed seven times and developed as described below. **Human interferon-α:** The assay was performed according to the manufacturer's instructions but with halved volumes. Additional adjustments included blocking of unspecific binding sites for 0.5 – 1 h at RT and diluting the HRP-Conjugate at 1:2,500 instead of 1:1,000. **Human CXCL10, human IL12p70, human TNFα, murine IL12p40:** The assays were performed according to the manufacturer's instructions but with halved volumes and concentrations. All ELISAs were developed using 50 µl of BD TMB substrate at RT and reactions were stopped with 25 µl 1 M H_2SO_4 upon visible color development in 4 – 5 standard wells. Absorbance was measured at 450 nm with λ correction at 570 nm using the BioTek Epoch spectrophotometer.

2.2.20 Fluorescence-activated cell sorting (FACS)

For FACS analysis, BMDCs were washed with PBS and incubated with 50 µl PBS containing 2 mM EDTA per 96-well at 37 °C for 30 min. Cells were harvested by repetitive pipetting and transferred to a round-bottom plate. Each staining described below was performed in 30 µl per 96-well followed by a washing step using 200 µl FACS buffer and centrifugation at 500 rcf for 5 min at 4 °C. Live/dead staining was performed using 1:500 Zombie Aqua solution in PBS and incubated at RT for 15 min, protected from light. After washing, Fc block was utilized at a 1:200 dilution in FACS buffer and incubated at RT for 20 min, protected from light. Lastly, surface markers (CD11b, CD11c, CD69, CD86, CD40) were used diluted 1:200 in FACS buffer and incubated at RT for 20 min, protected from light, followed by two washing steps. Cells were measured using the Attune NxT flow cytometer. Compensation was performed using OneCompBeads and single marker staining. Data was analyzed using FlowJo 10.8 by gating for single, live cells and quantifying expression of CD69, CD86, and CD40 within the $CD11b^+CD11c^+$ cell population.

2.2.21 Quantification of fluorescent proteins by microscopy

Expression of fluorescent proteins was imaged using respective channels and 4-fold magnification of the Cytation™ 3 reader and cell counts were quantified using the Gen5 software. $EGFP^+$ or $mCherry^+$ cell count was normalized to total cell count obtained using digital phase contrast.

2.2.22 Lentiviral transduction and stimulation of THP-1 cells

Lentiviral vectors expressing human and murine RLRs in junction to an IRES-EGFP-2A-Puromycin cassette were provided by Dr. Thomas Zillinger. Transduction of THP-1 *RIG-I*$^{-/-}$ *MDA5*$^{-/-}$ cells was performed in T-25 cell culture flasks using virus-containing supernatants that were diluted 1:2 with complete RPMI and included 8 µg/ml polybrene as transduction enhancer. Medium was replaced after 12 h. After 36 h, medium was exchanged to complete RPMI containing 5 µg/ml puromycin.

After several passages, positive cells were selected via flow cytometric cell sorting. For stimulation, 8 x 10^4 THP-1 or THP-1 dual cells were plated in a flat-bottom 96-well plate in 100 µl complete RPMI and stimulated as described in Chapter 2.2.18.

2.2.23 Luciferase assays

To quantify the activity of firefly luciferase, supernatants were aspirated, and cells were lysed in 100 µl saponin lysis buffer per 96-well. After incubation for 20 min, 25 µl were transferred to a white 96-well round-bottom plate and mixed with 25 µl firefly luciferase substrate solution. To quantify the activities of Gaussia/Lucia or Cypridina luciferases, 25 µl of cell supernatants were transferred to a white 96-well round-bottom plate and mixed with 25 µl buffer containing 100 mM Tris pH 7.4, 300 mM sodium ascorbate and either 1 µg/ml coelenterazine or 1 µM Cypridina luciferin, respectively. Luminescence was measured immediately using the EnVision plate reader.

2.2.24 Secreted alkaline phosphatase (SEAP) assay

SEAP activity was quantified by mixing 30 µl cell supernatant with 30 µl PNPP buffer in a transparent 96-well round-bottom plate and incubating for 2 h at RT. Absorbance was measured at 405 nm using the BioTek Epoch spectrophotometer.

2.2.25 Reporter assay in HEK 293 cells

4 x 10^4 HEK 293 cells were plated in flat-bottom 96-well plates in 100 µl complete DMEM and incubated for 18 h at 37 °C and 5 % CO_2. Plasmids were kindly provided by Dr. Thomas Zillinger. Plasmid quantities indicated in Table 15 were transfected using LT-1 as described in Chapter 2.2.18. After 8 h, medium was changed and cells were transfected with desired stimuli, as described above. Following 20-h incubation, luciferase activities were quantified as described in 2.2.23.

Table 15: Reporter plasmid mix per 96-well

Plasmid	[ng]
pGL3-IFNβ-Gluc	85
pLKO.1-EF1α-Cluc	3
pMAX-GFP	10
pLenti-hMDA5	2

2.2.26 RNA isolation for quantitative PCR

Supernatants were aspirated, and cells were lysed in 60 µl RLT buffer per 96-well. Lysates were mixed with 60 µl 70 % EtOH, loaded onto a Zymo-Spin silica column, placed in a collection tube, and centrifuged at 10,000 rcf for 1 min. Flowthrough was discarded, and columns were washed with 350 µl RW1 buffer followed by 350 µl Zymo wash buffer using the previous centrifugation settings. Columns were centrifuged at maximum speed for 2 min and transferred to an elution tube. 30 µl H_2O were added and incubated for 2 min. RNA was eluted by centrifugation at 10,000 rcf for 1 min and quantified using a NanoDrop spectrophotometer.

2.2.27 cDNA synthesis / reverse transcription

In a volume of 10 µl, genomic DNA was removed by digesting 200 ng RNA with DNase I according to the manufacturer's instructions and incubation for 30 minutes at 37 °C. DNase inactivation and primer annealing were carried out simultaneously by adding 2.5 µl of 15.625 mM EDTA containing 20 µM random hexamer primers followed by incubation at 65 °C for 10 min. 7.5 µl of the reverse transcription master mix, as specified in the RevertAid manual, were added to achieve a final volume of 20 µl. The mixture was incubated at 42 °C for 60 minutes and reverse transcriptase was heat-inactivated at 70 °C for 5 minutes. The volume was adjusted to 100 µl H_2O and samples were ready for use in quantitative PCR experiments.

2.2.28 Real-time quantitative polymerase chain reaction (RT-qPCR)

In a total volume of 10 µl, 1 X EvaGreen qPCR Mix was combined with 5 µM forward and reverse primers each and 2 µl cDNA (see 2.2.27). The replication efficiencies of each primer pair were assessed by cDNA dilution series and ranged between 1.8- to 2.2-fold. Each reaction was performed as triplicates in a 384-well plate, sealed with an optical sealing sheet and centrifuged at 300 rcf for 5 min. The qPCR was performed according to the program outlined in Table 16 using a QuantStudio™ 5. Fluorescent intensity was quantified during the final temperature step of each qPCR cycle and during the melting curve stage. Experiment quality and cycle threshold (Ct) values were evaluated through visual examination of amplification and melting curves. The relative expression of the gene of interest (GOI) was determined by normalizing to a housekeeping gene (HKG), accounting for primer efficiencies using the following equation:

$$Relative\ Gene\ Expression = \frac{Primer\ efficiency\ GOI^{-(Ct\ GOI)}}{Primer\ efficiency\ HKG^{-(Ct\ HKG)}}$$

Table 16: RT-qPCR program

Step	°C	Min:sec	°C/sec	Cycles
Initial denaturation	95	10:00	1.6	
Denaturation	95	00:15	1.6	40 X
Annealing	60	00:20	1.6	
Extension	72	00:20	1.6	
Melt Curve Analysis	95	00:15	1.6	
	60	01:00	1.6	
	95	00:15	0.075	

2.2.29 Generation of littermates, genotyping & RNA sequencing analysis

Littermates were generated by mating C57BL/6J wildtype mice with either *Mda5*$^{-/-}$ (B6.Cg-Ifih1$^{tm1.1Cln/J}$) or *Ifnar*$^{-/-}$ (B6.129S2-Ifnar1$^{tm1Agt/Mmjax}$) mice, respectively, and subsequently mating the heterozygous offspring. For DNA isolation and genotyping, ear punch tissue samples were incubated in tail buffer at 55 °C overnight. Samples were centrifuged at 14,000 rcf for 10 min. DNA in the supernatant was precipitated with 1 volume EtOH and centrifugation as above. Pellets were washed in 70 % EtOH and resuspended in H_2O. Genotyping was performed according to the instructions from the Jackson Laboratory using a standard PCR reaction with Dreamtaq polymerase and appropriate primers. For sample collection, mice were euthanized by cervical dislocation, and 0.5 cm^2 liver pieces were harvested and flash-frozen in liquid nitrogen. Tissues were homogenized in 1 ml TRIzol using 2 mm ceramic beads and a bench-top bead beater (2x 20 sec, 30 Hz). RNA was isolated as described in the TRIzol manual. RNA sequencing was performed by the NGS Core Facility (University Hospital Bonn) using Lexogen 3′ Sequencing kits. Data analysis was performed by the author. Briefly, reads were preprocessed using FASTQC and cutadapt, and aligned to the mouse Genome Reference Consortium Build 39 using STAR. BAM files were indexed using Samtool and mapped reads were annotated using a Gencode primary assembly GTF file (vM27) and STAR. Quantification was performed via HT-Seq. Differential expression analysis was performed in R using DESeq2. Total read counts that were normalized to the library size were extracted and statistically analyzed in Prism 10.

2.2.30 LC/MS

LC-MS analysis was conducted on an ACQUITY UPLC system (Waters), interfaced with an Xevo TQ-S Quadrupole (Waters) and utilizing an electrospray ionization source in negative mode. Chromatographic separation was carried out on an ACQUITY UPLC BEH C18 column (2.1 x 50 mm, 1.8 µm particle size) maintained at 60°C. The analytes were separated using a gradient of 16.6 mM triethylamine (TEA), 100 mM hexafluoroisopropanol (HFIP), and 10% methanol (MeOH) as eluent A, and 16.6 mM TEA, 100 mM HFIP, and 95% MeOH as eluent B, with a flow rate of 0.3 mL/min. The gradient was separated as follows: 0 to 5% B over 8 minutes, 5 to 10% B over 6 minutes, and 10 to 40% B over 2 minutes. Sample preparation was performed in 200 mM TEAA with 20 mM EDTA.

2.2.31 *In vitro* translation in rabbit reticulocyte lysate

In vitro translation of EGFP-Fluc mRNA in rabbit reticulocyte lysate was performed according to the manufacturer's instructions. After incubation at 30 °C for 90 min, 25 µl sample were transferred to a white round-bottom 96-well plate and firefly luciferase activity was quantified as described in Chapter 2.2.23.

2.2.32 Software and data analysis

All statistical tests were calculated using GraphPad Prism 10. Schematic illustrations were designed at BioRender.com. Bibliography was created using Readcube Papers. Other software and data analysis are indicated at the respective locations above.

3. Results

3.1 mRNA vaccines induce innate immune responses through activation of RIG-I-like receptors

3.1.1 COVID-19 mRNA vaccines are sensed by RIG-I-like receptors

To investigate the innate immune responses induced by COVID-19 mRNA vaccines, members of the Bartok and Hartmann groups collected leftover vaccine vials from clinics. In addition to the experiments conducted by other scientists presented in Chapter 1.4.4, the activation of RIG-I-like receptors (RLRs) was characterized in primary murine cells *in vitro*.

To this end, murine bone marrow-derived dendritic cells (BMDCs) were stimulated with the vaccines for 24 and/or 48 hours, and IFNα production was quantified via ELISA. These cells represent a suitable model system due to their robust cytokine responses to RLR ligands, such as the RIG-I ligand 5′ppp-dsRNA, and the MDA5 ligands poly(I:C) and RNA derived from Vero cells infected with the picornavirus EMCV (Encephalomyocarditis virus) (Figure 12A). Additionally, BMDCs derived from RIG-I- or MDA5-deficient knockout mice enabled the discrimination of individual RLR responses to mRNA vaccines and functional outcomes associated with RIG-I or MDA5 activation (Figure 12A).

In line with the *in vivo* data presented in Chapter 1.4.4, an MDA5-dependent IFNα response by BMDCs was observed after stimulation with the COVID-19 mRNA vaccine developed by BioNTech (BioNTech vaccine) (Figure 12B). However, the IFNα levels were only slightly above the technical detection limit of the ELISA. In contrast, the COVID-19 mRNA vaccine produced by Moderna (Moderna vaccine) did not induce a detectable IFNα response (Figure 12B).

Given that the BioNTech vaccine induced higher cytokine responses than the Moderna vaccine in previous experiments (Chapter 1.4.4), it was hypothesized that the IFNα response to the Moderna vaccine by BMDCs was below the technical detection limit of the ELISA. Furthermore, concurrent experiments by Sofía Beatriz Soler demonstrated that the cytokine response to the vaccines was stronger in human macrophages than DCs (Chapter 1.4.4 and data not shown). Therefore, the experiment was repeated using primary murine bone marrow-derived macrophages (BMMs). Indeed, BMMs demonstrated a more potent IFNα response to the control stimuli and BioNTech vaccine than BMDCs, confirming the previous hypothesis (Figure 12). Accordingly, an MDA5-dependent IFNα response was also detectable for the Moderna vaccine in BMMs (Figure 12D). In line with previous data (Figure 7B and Chapter 1.4.4), the IFNα response to the BioNTech vaccine was up to four-fold greater than that induced by the Moderna vaccine in BMMs.

These findings confirm that both COVID-19 mRNA vaccines contain RNA species capable of activating MDA5, and that murine cells sense mRNA vaccines primarily via MDA5, in line with previous *in vivo* experiments (Chapter 1.4.4).

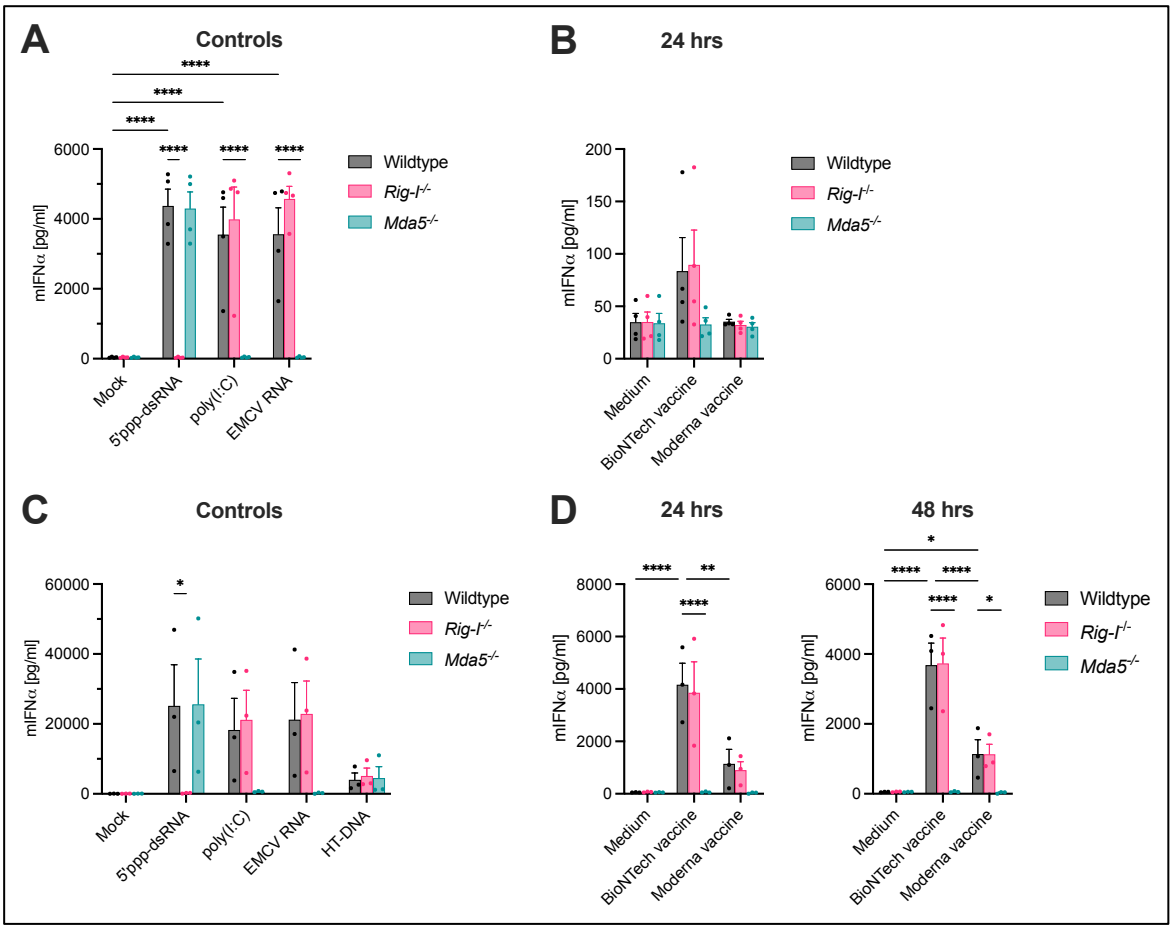

Figure 12: COVID-19 mRNA vaccines activate MDA5 in BMDCs and BMMs
(A) BMDCs were transfected with indicated stimuli using Lipofectamine or LT-1 for poly(I:C). (B) BMDCs were stimulated with 8 µg/ml of indicated COVID-19 mRNA vaccines. (C-D) Stimulation of BMMs analogous to A – B. Production of IFNα was quantified via ELISA. Mean + SEM of at least three independent experiments. Statistical significance was calculated by two-way ANOVA with Tukey's multiple comparisons correction. Comparisons between stimuli are depicted exclusively for wildtype cells. Within each stimulus, only comparisons of genotypes to the wildtype are displayed. * $p < 0.05$, ** $p < 0.01$, *** $p < 0.001$, **** $p < 0.0001$. EMCV = encephalomyocarditis virus, HT-DNA = herring testes DNA.

The lack of detectable IFNα production in BMDCs after stimulation with the Moderna COVID-19 mRNA vaccine could potentially be attributed either to an absence of innate immune activation in this cell type or to the overall weaker IFNα levels induced in BMDCs compared to BMMs. Therefore, the BMDC experiments were repeated using increased vaccine doses. Additionally, providing a more sensitive readout, qPCR was performed on mRNA isolated from stimulated BMDCs to quantify the mRNA expression levels of *Ifnb* and a panel of interferon-stimulated genes (ISGs) (Figure 13). As anticipated, an MDA5-dependent upregulation of all tested genes was evident following stimulation with the BioNTech vaccine, with the majority exhibiting statistical significance. Furthermore, the detectable upregulation of *Ifit1*, *Rsad2*, and *Siglec1* by the Moderna

vaccine confirmed the induction of MDA5-dependent innate immune responses in BMDCs by this vaccine and validated the higher type I IFN induction by BioNTech vaccine compared to Moderna vaccine on the level of ISGs.

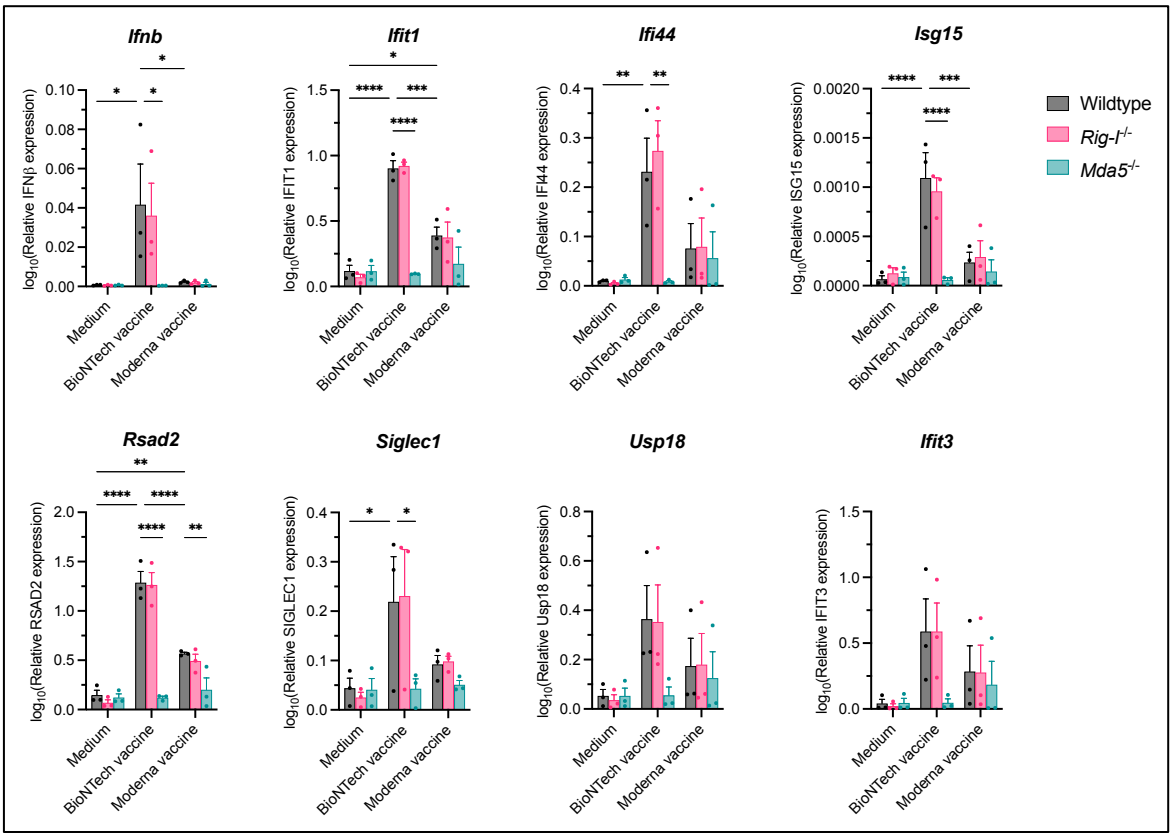

Figure 13: COVID-19 mRNA vaccines induce MDA5-dependent upregulation of *Ifnb* and ISGs in BMDCs
BMDCs were stimulated with 16 µg/ml of indicated mRNA vaccines. Expression of *Ifnb* and a set of interferon-stimulated genes was quantified by RT-qPCR. Mean + SEM of three independent experiments. Statistical significance was calculated by two-way ANOVA with Tukey's multiple comparisons correction. Comparisons between stimuli are depicted exclusively for wildtype cells. Additionally, within each stimulus, only comparisons of genotypes to the wildtype are displayed. * $p < 0.05$, ** $p < 0.01$, *** $p < 0.001$, **** $p < 0.0001$.

The evident dependency of the type I IFN response to COVID-19 mRNA vaccines on the cytosolic RNA sensor MDA5 strongly suggests its mediation by RNA molecules contained within the vaccines. However, empty lipid nanoparticles (LNPs), which are the vaccine delivery vehicles devoid of RNA, have been reported to provoke innate immune responses, including type I IFN production, through mechanisms that remain not fully understood.[84,165,166] While an unspecific uptake and delivery of extracellular nucleic acids by empty LNPs is conceivable, inflammatory responses induced by the individual vehicle components themselves are also possible. However, based on the present data, this LNP-induced type I IFN response seems to be negligible compared to the mRNA-induced response. Nevertheless, to mitigate potential bias by distinct vaccine formulations and to standardize the comparison between BioNTech and Moderna, RNA was isolated from the vaccines using phenol/chloroform extraction, followed by validation of mRNA integrity

via agarose gel electrophoresis (Figure 14A) and transfection into BMDCs and BMMs using the transfection reagent Lipofectamine 2000.

As expected, a significant MDA5-dependent IFNα induction was observed in BMDCs and BMMs in response to mRNA purified from BioNTech vaccine (Figure 14B-C). Additionally, weak IFNα levels were induced in response to mRNA purified from Moderna vaccine in both cell types (Figure 14B-C). While the previously depicted upregulation of ISGs in BMDCs indicated an MDA5-dependent type I IFN response to the intact COVID-19 mRNA vaccine by Moderna (Figure 13), the IFNα levels were presumably below the ELISA detection limit (Figure 12B, D). Interestingly, mRNA-induced IFNα levels were higher when complexed to Lipofectamine, even at 20-fold reduced mRNA doses compared to LNP-formulated vaccines (Figure 14B-C). However, the relative RLR activation was preserved, and mRNA isolated from BioNTech vaccine induced significantly higher IFNα levels than mRNA from Moderna, indicating that this difference is caused by a distinct immunostimulatory potential of the mRNA rather than LNP composition *per se*.

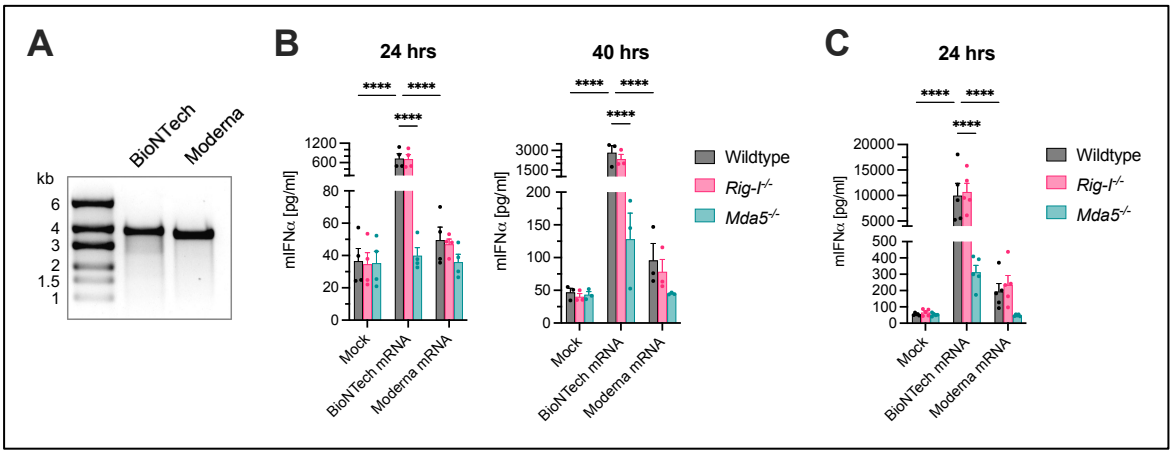

Figure 14: mRNA purified from COVID-19 vaccines induces MDA5-dependent IFNα response

(A) Agarose gel electrophoresis showing integrity of 1 µg/lane mRNA after isolation from COVID-19 vaccines. Image is representative of three independent purifications. (B) BMDCs were transfected with 0.8 µg/ml of mRNA isolated from indicated COVID-19 mRNA vaccines complexed to Lipofectamine 2000. IFNα production was quantified after 24 and 40 hours via ELISA. (C) Stimulation of BMMs analogous to (B). Mean + SEM of at least three independent experiments. Statistical significance was calculated by two-way ANOVA with Tukey's multiple comparisons correction. Comparisons between stimuli are depicted exclusively for wildtype cells. Within each stimulus, only comparisons of genotypes to the wildtype are displayed. **** $p < 0.0001$.

The initial experiments presented in Chapter 1.4.4 revealed a species-specific difference in the sensing of mRNA vaccines: While the COVID-19 mRNA vaccine-induced CXCL10 response in human monocyte-derived macrophages and BLaER1 cells was mainly dependent on RIG-I (Figure 9), the IFNα response of mice relied primarily on MDA5 (Figure 7). In line with this, the IFNα production of murine BMDCs and BMMs after *in vitro* stimulation with COVID-19 mRNA vaccines or purified mRNA was dependent on MDA5 (Figure 12B, D; Figure 13; Figure 14B, C). Nevertheless, a residual IFNα signal was observed in MDA5-deficient BMDCs and BMMs in

response to mRNA purified from BioNTech vaccine (Figure 14B, C), suggesting an additional involvement of another RNA sensor. Since state-of-the-art capping methods are known to leave between 1 and 6 % uncapped transcripts,[97,167] potential engagement of RIG-I by 5′ppp- or 5′pp-RNA was investigated via polyphosphatase (PP) digestion of purified vaccine mRNAs before transfection into BMMs. Since RIG-I does not recognize cap-1 or 5′p-RNAs,[18,21] removal of accessible 5′ γ- and β-phosphate groups by PP treatment is expected to abolish RIG-I-dependent IFNα responses, as confirmed using a 5′ppp-dsRNA control (Figure 15A). Additionally, RNA from cells infected with EMCV, known for its potent MDA5 activation, ensured that PP treatment did not compromise RNA integrity and innate immune stimulation independent of 5′ppp ends.

As expected, the MDA5-dependent IFNα response to mRNA purified from COVID-19 vaccines was unaffected by PP digestion (Figure 15B). However, the weak IFNα response in MDA5-deficient cells to BioNTech mRNA was effectively reduced by PP treatment, indicating that the residual signal may be due to activation of RIG-I by uncapped RNA species bearing 5′ppp or 5′pp.

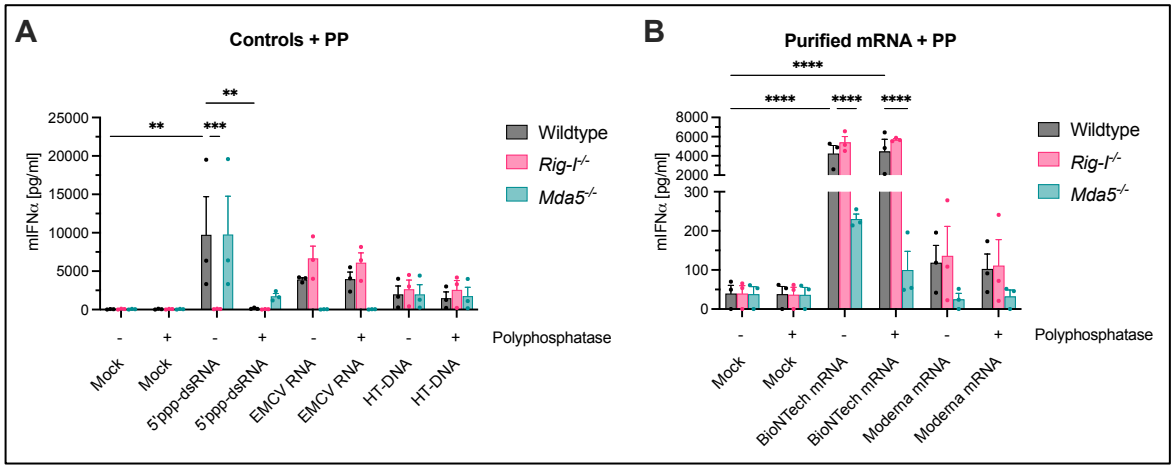

Figure 15: RIG-I activation through 5′ppp-RNA contributes to IFNα levels induced by COVID-19 vaccines in BMMs
BMMs were transfected with indicated controls (A) or 0.8 μg/ml of mRNA isolated from indicated COVID-19 mRNA vaccines (B) with or without polyphosphatase (PP) treatment. IFNα production was quantified after 24 hours via ELISA. Mean + SEM of five independent experiments. Statistical significance was calculated by two-way ANOVA with Tukey's multiple comparisons correction. Comparisons between stimuli are depicted exclusively for wildtype cells. Within each stimulus, only comparisons of genotypes to the wildtype are displayed. * $p < 0.05$, ** $p < 0.01$, *** $p < 0.001$, **** $p < 0.0001$. EMCV = encephalomyocarditis virus, HT-DNA = herring testis DNA.

In addition to murine BMDCs and BMMs, human peripheral blood mononuclear cells (PBMCs) were utilized to further investigate the species-specific differences and individual roles of RIG-I and MDA5 in the sensing of COVID-19 mRNA vaccines. PBMCs were stimulated with two batches of purified mRNA from COVID-19 vaccines, with or without PP treatment, and IFNα as well as CXCL10 production was quantified via ELISA. CXCL10, also known as IP10, is an interferon-induced protein and thus provides heightened sensitivity for detecting type I IFN responses.

Transfection of mRNA purified from BioNTech vaccine induced significant IFNα and CXCL10 levels in PBMCs (Figure 16B, D). While IFNα production in response to purified Moderna mRNA was apparently below the ELISA detection limit in these experiments (Figure 16B), the more sensitive CXCL10 ELISA readout confirmed the presence of immunostimulatory RNA (Figure 16D). All measured cytokine levels were considerably reduced after PP treatment, indicating that they were primarily mediated by recognition of 5′polyphosphate-bearing RNA and thus indicating that RIG-I rather than MDA5 may be activated in these cells (Figure 16B, D). This data underscores that the sensing of mRNA vaccines is primarily mediated via RIG-I in human cells, in line with experiments using primary human monocyte-derived macrophages and BLaER1 cells presented in Chapter 1.4.4, Figure 9.

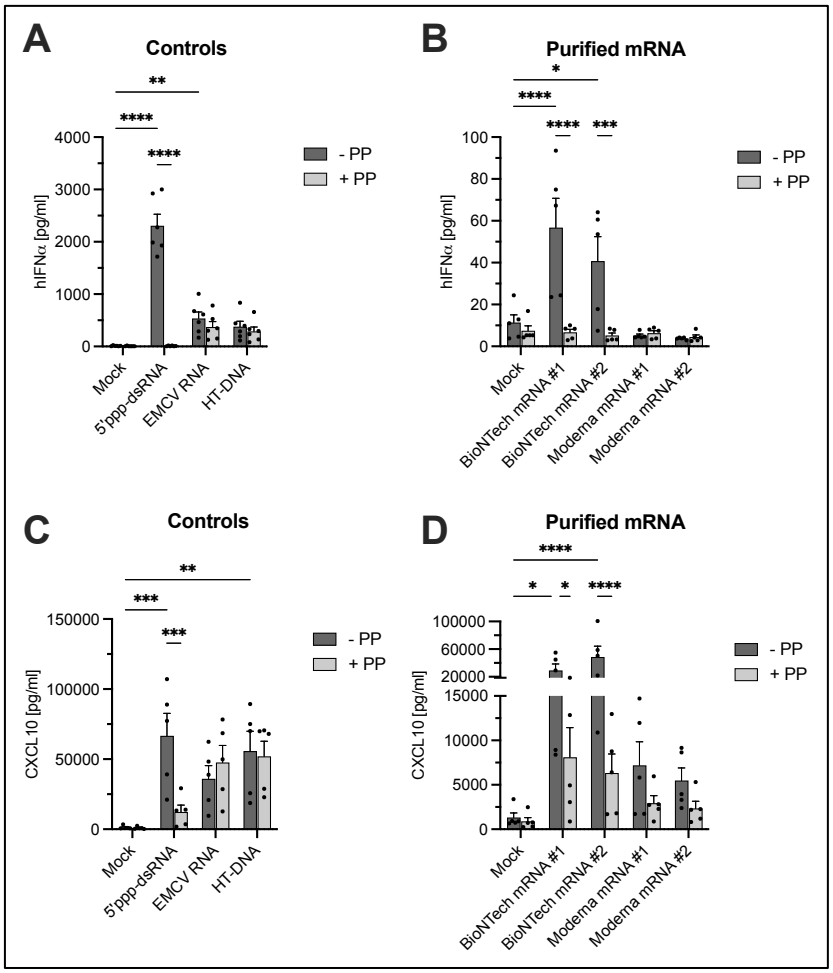

Figure 16: Innate immune activation by COVID-19 vaccines in human PBMCs depends predominantly on RIG-I. PBMCs were transfected with (A, C) indicated controls or (B, D) 0.8 μg/ml of two mRNA batches isolated from indicated COVID-19 mRNA vaccines with or without polyphosphatase (PP) treatment. (A - B) IFNα and (C - D) CXCL10 production was quantified after 24 hours via ELISA. Mean + SEM of six donors. Statistical significance was calculated by two-way ANOVA with Tukey's multiple comparisons correction. Only comparisons to Mock and between treatments are displayed. * $p < 0.05$, ** $p < 0.01$, *** $p < 0.001$, **** $p < 0.0001$. EMCV = encephalomyocarditis virus, HT-DNA = herring testis DNA.

In conclusion, the present findings confirm that COVID-19 mRNA vaccines induce type I IFN responses by activating RIG-I-like receptors. This innate immune response is independent of delivery vehicles and relies predominantly on the RNA molecules contained within the vaccines. The engagement of both MDA5 and RIG-I indicates the presence of long dsRNA stretches and uncapped 5′ppp-dsRNA, respectively. The BioNTech vaccine consistently induced higher type I IFN responses compared to Moderna, in line with the previously indicated different purification techniques presented in Chapter 1.4.4, Figure 10, which will be further explored in Chapter 3.1.2. Furthermore, the presented data confirm the species-specific innate sensing of mRNA vaccines in human and murine cells presented in Chapter 1.4.4. While murine cells predominantly responded to mRNA vaccines through MDA5 activation, cytokine responses of human PBMCs exhibited sensitivity to phosphatase treatments, indicating that rather RIG-I may be the primary sensor.

3.1.2 Byproducts generated during *in vitro* transcription are responsible for innate immune activation by mRNA vaccines

While both RIG-I and MDA5 sense double-stranded RNA, the main product of an *in vitro* transcription is single-stranded. In the case of IVT-mRNA generation, this product is the mRNA molecule itself. However, the process of *in vitro* transcription is also known to generate unspecific double-stranded RNA (dsRNA) byproducts, which are presumably responsible for the innate immune activation by mRNA vaccines.[25,109,110,115] Thus, it is plausible that RLRs are activated by these byproducts and/or intramolecular secondary structures of the mRNA.

Previous studies demonstrated that mRNA purification and elimination of byproducts via HPLC or ethanol-cellulose chromatography reduce the dsRNA content of IVT-mRNA and their immunostimulatory potential.[115,145] Oligo(dT)-purification is another method to isolate full-length mRNA molecules with accessible poly(A)-tails, while removing non-polyadenylated byproducts, and is thought to likewise reduce the dsRNA content of IVT-mRNA.[168–170] Indeed, previous experiments by Dr. Thomas Zillinger demonstrated that oligo(dT)-purified RNA isolated from BioNTech's vaccine induced lower type I IFN responses in human PBMCs compared to the unpurified RNA (Chapter 1.4.4, Figure 10). Additionally, the type I IFN response to Moderna's vaccine, which has been oligo(dT)-purified according to the corresponding publication, was not reduced by additional purification.[104] Thus, these initial experiments confirm that RIG-I activation in human cells is mainly mediated by dsRNA byproducts generated during the *in vitro* transcription. Following this observation, the effect of oligo(dT)-purification on activation of MDA5 was investigated in murine BMDCs. To this end, oligo(dT)-conjugated beads were utilized to purify mRNA isolated from BioNTech's COVID-19 vaccine. In addition, an *in vitro* transcribed mRNA

comprising 3189 bp of the SARS-CoV-2 genomes' 3′ end, including its 3′ UTR and a 42 nt poly(A)-tail, termed SC-IVT (SARS-CoV-2 in vitro transcript), was used to reproduce the findings observed with the vaccine mRNA and extent the conclusions to IVT-mRNA in general (Figure 17A). Analogous to the COVID-19 mRNA vaccines by BioNTech and Moderna, the nucleotide uridine was replaced with N1-methyl-pseudouridine (m1Ψ) during the *in vitro* transcription of the SC-IVT. Additionally, a 5′ cap-1 structure was added via enzymatic capping, the method that is also utilized by Moderna.[104]

Transfection into BMDCs enabled the comparison of innate immune activation by the initial mRNA preparation, the poly(A)+ fraction, and the remaining poly(A)- RNA. For both mRNAs, purification of poly(A)+ mRNA significantly reduced IFNα induction in BMDCs compared to the initial, unpurified mRNA (Figure 17B). Furthermore, the remaining poly(A)- RNA fraction exhibited a slightly increased IFNα induction, indicating an enrichment of immunostimulatory RNA. These findings confirm that the MDA5-mediated IFNα response of murine BMDCs to mRNA vaccines depends on RNA species other than the full-length mRNA, likely unspecific byproducts generated during *in vitro* transcription that are not captured by oligo(dT)-purification.

To investigate the dsRNA content of the COVID-19 mRNA vaccines and the SC-IVT, as well as the effect of oligo(dT) purification, an RNA dot blot using the anti-dsRNA antibody J2 was performed. As mentioned before, Moderna already employs oligo(dT)-purification during the manufacturing of their COVID-19 mRNA vaccine, which was hypothesized to cause the significantly lower innate immune stimulation by the Moderna vaccine compared to BioNTech vaccine observed in preceding experiments.[104,126] In line with this, the dot blot revealed notably lower amounts of dsRNA in mRNA isolated from Moderna vaccine compared to BioNTech (Figure 17C). Additionally, after oligo(dT)-purification, the poly(A)- fractions of BioNTech mRNA and the SC-IVT exhibited a notable increase in dsRNA content, in line with their enhanced immunostimulatory capacity (Figure 17). In contrast, the poly(A)- yield of Moderna mRNA was too low for downstream analysis (Figure 17C), confirming the efficiency of initial purification techniques employed by Moderna. These data strongly support the notion that removal of dsRNA byproducts via oligo(dT)-purification employed by Moderna causes the reduced innate immune stimulation by Moderna vaccine compared to BioNTech.

Altogether, the present data confirms dsRNA byproducts of *in vitro* transcription as a major source of innate immune activation by mRNA vaccines and highlights oligo(dT)-purification as a promising tool to eliminate undesired inflammatory RNA species from mRNA therapeutics.

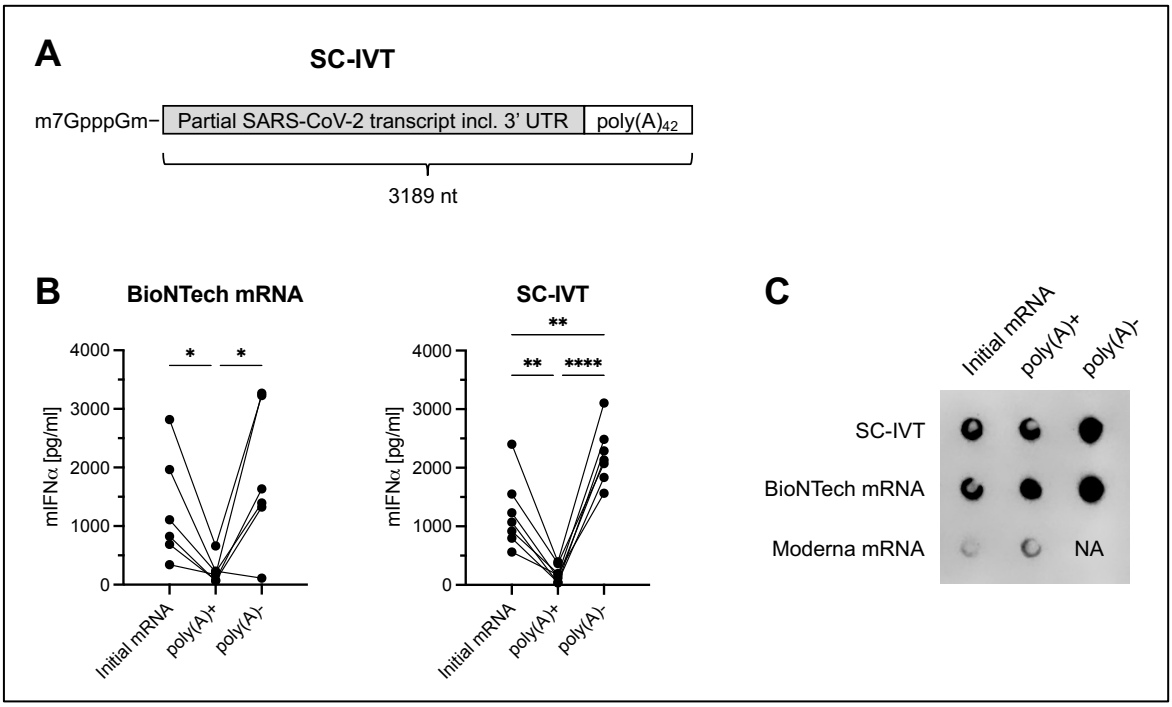

Figure 17: *In vitro* transcription byproducts without (accessible) poly(A)-tail are responsible for IFNα induction by mRNA vaccines. (A) Schematic illustration of the SARS-CoV-2 *in vitro* transcript (SC-IVT). (B) BMDCs were transfected with 0.8 μg/ml of indicated RNA. IFNα production was quantified after 24 hours via ELISA. Each data point represents one of at least six independent experiments. Statistical significance was calculated by one-way ANOVA with Tukey's multiple comparisons correction. * $p < 0.05$, ** $p < 0.01$, *** $p < 0.001$, **** $p < 0.0001$. (B) Anti-dsRNA dot blot of indicated RNAs. NA = not available.

3.1.3 MDA5 activation by mRNA vaccines upregulates dendritic cell markers required for induction of adaptive immunity

To investigate the functional implications of mRNA vaccine-induced RLR activation for vaccination efficiency, the expression of relevant activation markers on BMDCs after stimulation with the individual vaccines was assessed via flow cytometry. The panel comprised antibodies against CD69 (cluster of differentiation 69), CD40, and CD86, all of which are upregulated upon DC activation and are involved in the induction of adaptive immune responses. CD69 is an early activation marker for all leukocytes. Its function is to retain the otherwise circulating immune cells in lymphoid tissues, such as the draining lymph node, by inducing internalization of S1P1R (sphingosine-1-phosphate receptor 1), the chemokine receptor responsible for lymphoid egress, thus prolonging the interaction of immune cells in lymphoid tissues following an infection.[1] CD40 is a cell surface protein expressed by all antigen-presenting cells (APC), including dendritic cells (DCs). Binding to CD40L (CD40 ligand) on lymphocytes further promotes activation and antigen presentation of APCs.[1] CD86, also known as B7.2, contributes to the required co-stimulation for the activation of lymphocytes by DCs.[1]

The mean fluorescence intensity (MFI) is the average fluorescence signal emitted by antibody-stained cells in the respective channel, indicating the magnitude of protein expression, and has been calculated for each marker in the $CD11b^+CD11c^+$ DC population.

In earlier experiments, the Moderna COVID-19 mRNA vaccine exhibited a lower type I IFN response than the BioNTech vaccine. This reduced innate immune stimulation likely contributed to a higher supportable dosage of the Moderna vaccine. Accordingly, based on the official dosage instructions, one dose of Moderna vaccine contains ~3.3 times the amount of RNA compared to BioNTech vaccine (100 µg versus 30 µg, respectively).[59,60] To provide a more realistic comparison, the subsequent stimulation of BMDCs was performed with accordingly adjusted vaccine quantities. All tested cell surface markers were upregulated on BMDCs in response to BioNTech COVID-19 mRNA vaccine as well as the purified mRNA (Figure 18). The Moderna vaccine and purified mRNA still exhibited less innate immune stimulation than BioNTech, despite adjusted dosages, and an upregulation of activation markers was not detectable. However, the model mRNA SC-IVT confirmed the results observed with BioNTech vaccine and purified mRNA (Figure 18). In line with preceding experiments, the upregulation of cellular activation markers was dependent on MDA5 in all cases. Conceivably, this MDA5-mediated APC activation could contribute to the effectiveness of the vaccine *in vivo*. In line with this, the *in vivo* experiments presented in Chapter 1.4.4 demonstrated lower induction of spike-specific IgG and $IFN\gamma^+$ $CD8^+$ T cells by the COVID-19 mRNA vaccines from BioNTech and Moderna in mice deficient in MDA5 compared to wildtype (Figure 8).

Additionally, BMDCs deficient in the IFNα/β receptor (IFNAR) were included to investigate whether MDA5-dependent upregulation of DC activation markers was mediated by the production of type I IFN and auto-/paracrine IFNAR signaling or other signaling pathways downstream of MDA5. The absence of activation marker upregulation on IFNAR-deficient cells indicates that it is indeed mediated by type I IFN production and IFNAR signaling following MDA5 activation (Figure 18). In line with this, *in vivo* data provided by Dr. Marcel Renn, Patrick Müller, and Yu Pan Tan, demonstrated similarly reduced levels of spike-specific IgG and $IFN\gamma^+$ $CD8^+$ T cells in IFNAR-deficient and MDA5-deficient mice compared to wildtype in response to Moderna's vaccine (data not shown), indicating the importance of MDA5-induced type I IFN signaling. However, this IFNAR-dependency was not observed for BioNTech's vaccine, thus hindering definitive conclusions about the mechanism by which MDA5 activation contributes to the effectiveness of the COVID-19 mRNA vaccines, and emphasizing the need for further investigation.

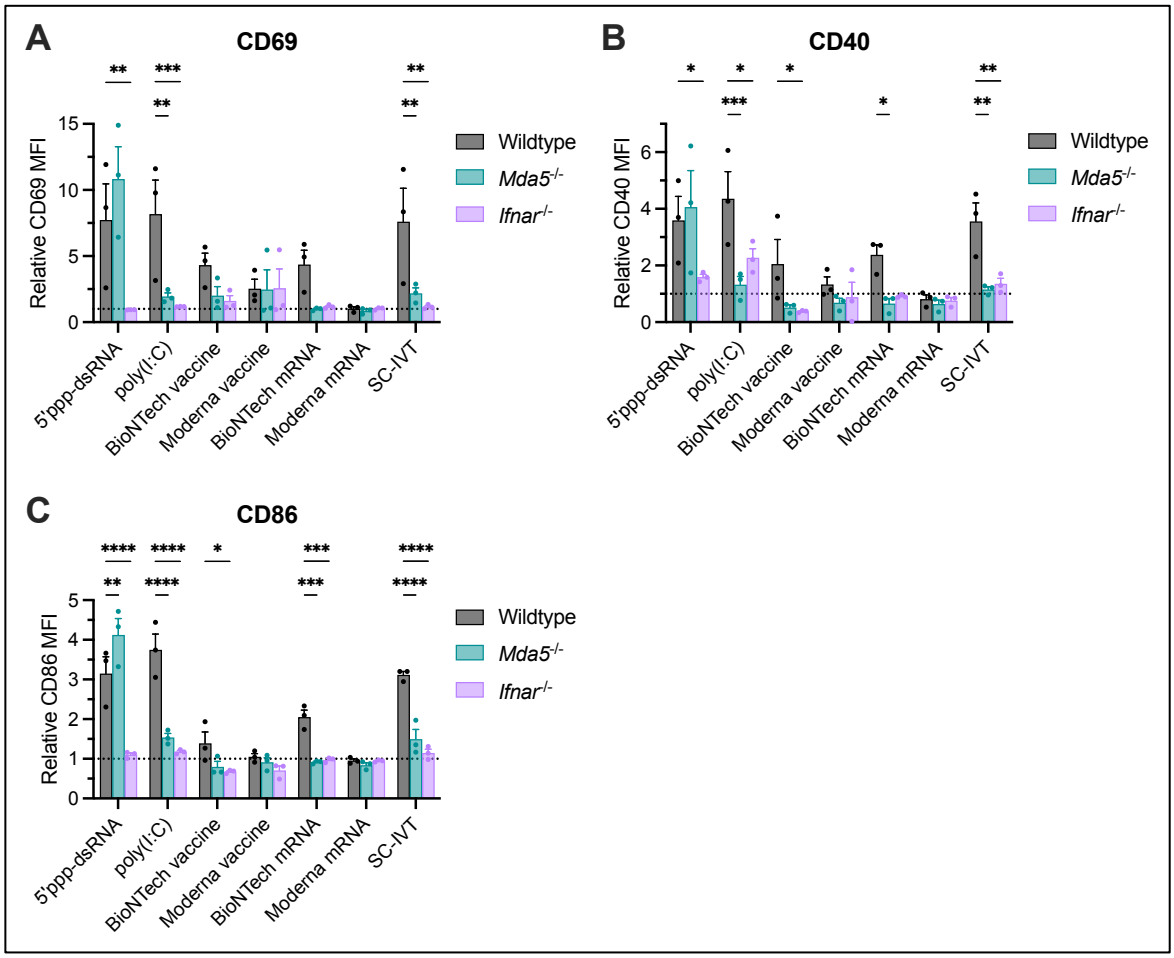

Figure 18: MDA5 activation by mRNA vaccines upregulates dendritic cell activation markers via IFNAR signaling
BMDCs were stimulated with either 8 µg/ml BioNTech vaccine, 16 µg/ml Moderna vaccine, 0.8 µg/ml purified vaccine mRNA, 0.8 µg/ml SC-IVT, or indicated controls. Cells were harvested after 18 hours, stained and analyzed via flow cytometry. Mean fluorescence intensity (MFI) of (A) CD69, (B) CD40, and (C) CD86 was measured on $CD11b^+CD11c^+$ cells. Whole vaccines were normalized to the unstimulated control whereas transfected RNAs were normalized to the mock transfection. Dotted line indicates the relative background level at y = 1. Mean + SEM of three independent experiments. Statistical significance was determined by comparing knockouts to the wildtype control within each stimulus using two-way ANOVA with Dunnett's multiple comparisons test. * $p < 0.05$, ** $p < 0.01$, *** $p < 0.001$, **** $p < 0.0001$. SC-IVT = 3 kb SARS-CoV-2 *in vitro* transcript.

While RLRs are constitutively expressed in all cell types, their expression is enhanced by type I IFN signaling in an antiviral feed-forward mechanism.[1] Therefore, the previous data could potentially result from a reduced expression of MDA5 in IFNAR-deficient cells. To address this specific question, existing RNA-sequencing data from an experiment conducted as part of a different project were utilized. Here, RNA was isolated from liver sections of wildtype, *Mda5*$^{-/-}$, and *Ifnar*$^{-/-}$ littermate mice, and 3′ RNA sequencing was performed. Although the primary purpose of this sequencing was unrelated to the current study, the resulting data set includes gene expression levels that are relevant to the conclusions of this research. Notably, the sample collection, processing, and RNA sequencing data analysis were performed by the author, ensuring the reliability and relevance of the data.

To investigate the general effect of IFNAR-deficiency on expression of RLRs, transcript counts of MDA5 (*Ifih1*) and RIG-I (*Ddx58*) were extracted from the differential expression analysis and plotted individually (Figure 19). As expected, expression of MDA5 was completely abolished in liver cells of *Mda5*$^{-/-}$ littermates, while expression of RIG-I was not negatively affected (Figure 19A). In fact, RIG-I transcript counts were even increased in the absence of MDA5, potentially as a result of currently unknown compensation mechanisms between RLRs. Interestingly, both MDA5 and RIG-I expression were reduced in liver cells of *Ifnar*$^{-/-}$ littermates, in line with known antiviral feed-forward mechanisms (Figure 19B). However, sufficient levels of MDA5 transcripts remain in the absence of IFNAR, validating the conclusion that mRNA-induced upregulation of DC activation markers is mediated by MDA5-induced type I IFN and subsequent IFNAR signaling. Nevertheless, MDA5 expression remains to be quantified in *Ifnar*$^{-/-}$ BMDCs to investigate cell type-specific effects as well as the IFNAR-dependent feedback mechanisms following MDA5 activation.

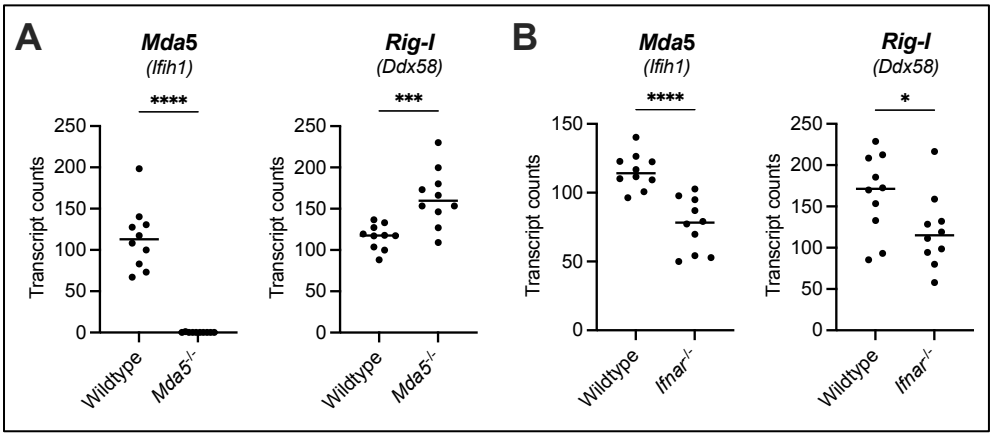

Figure 19: RIG-I-like receptor expression levels in liver samples of *Mda5*$^{-/-}$ and *Ifnar*$^{-/-}$ littermate mice. RNA was isolated from liver samples of wildtype and *Mda5*$^{-/-}$, or wildtype and *Ifnar*$^{-/-}$ littermate mice, respectively, and 3′ RNA sequencing was performed. Transcript counts of MDA5 and RIG-I were quantified using HTSeq and normalized to the library size using DESeq2. Each dot represents an individual mouse, and the depicted line indicates the mean value across a cohort of 10 mice. Statistical significance was determined using Student's t-test. * $p < 0.05$, ** $p < 0.01$, *** $p < 0.001$, **** $p < 0.0001$.

3.1.4 Role of 5′ cap for RIG-I-like receptor activation by *in vitro* transcribed mRNA

Efficient mRNA translation necessitates the presence of a 5′ cap-1 structure.[77] However, it is well established that RIG-I activation requires a double-stranded 5′ end with free tri- or diphosphate groups and that the addition of a 7-methyl-guanosine (cap-0) and 2′O methylation of the first nucleotide (cap-1) interferes with RIG-I activation.[13,14,21,171] In preceding experiments, phosphatase digestion of mRNA purified from BioNTech COVID-19 mRNA vaccine indicated that RIG-I is activated by uncapped 5′ppp or 5′pp-RNAs (Chapter 3.1.1, Figure 15 and 16), in line with reports stating that state-of-the-art capping methods leave approximately 1 – 6 % uncapped transcripts.[97,167] To confirm this hypothesis and extend the conclusions to other mRNA sequences besides the SARS-CoV-2 spike protein, the polyphosphatase experiments were repeated in human transdifferentiated macrophage-like BLaER1 cells using an IVT-mRNA encoding enhanced green fluorescent protein (EGFP) and firefly luciferase (Fluc), referred to as EGFP-Fluc mRNA (Figure 20). This RNA was subsequently capped enzymatically. Two BLaER1 cell clones of each MDA5, RIG-I, and MAVS knockout were included to eliminate potential clonal off-target incidents introduced during the CRISPR procedure. 5′ppp-dsRNA was used as a positive control for RIG-I activation, and poly(I:C) for MDA5 (Figure 20B). Of note, while high molecular weight poly(I:C) is primarily a ligand for MDA5, it also induces RIG-I-dependent IFNα in human cells (unpublished observations by the Bartok and Hartmann groups).

Indeed, the RIG-I-dependent IFNα response to m1Ψ-modified 5′ cap-1 EGFP-Fluc mRNA was significantly reduced after polyphosphatase treatment, confirming that RIG-I activation is mediated by uncapped transcripts (Figure 20C).

To further confirm the findings observed with COVID-19 mRNA vaccines, phosphatase experiments were also performed in BMMs using the mRNA SC-IVT. Since activation of MDA5 is not dependent on 5′ppp ends, it was not affected by polyphosphatase treatments of the SC-IVT, as expected (Figure 20E). In contrast, IFNα levels in MDA5-deficient cells were reduced after polyphosphatase digestion, confirming that RIG-I is partially responsible for mRNA-induced IFNα production in BMMs and that it is indeed activated by inefficiently capped RNA species.

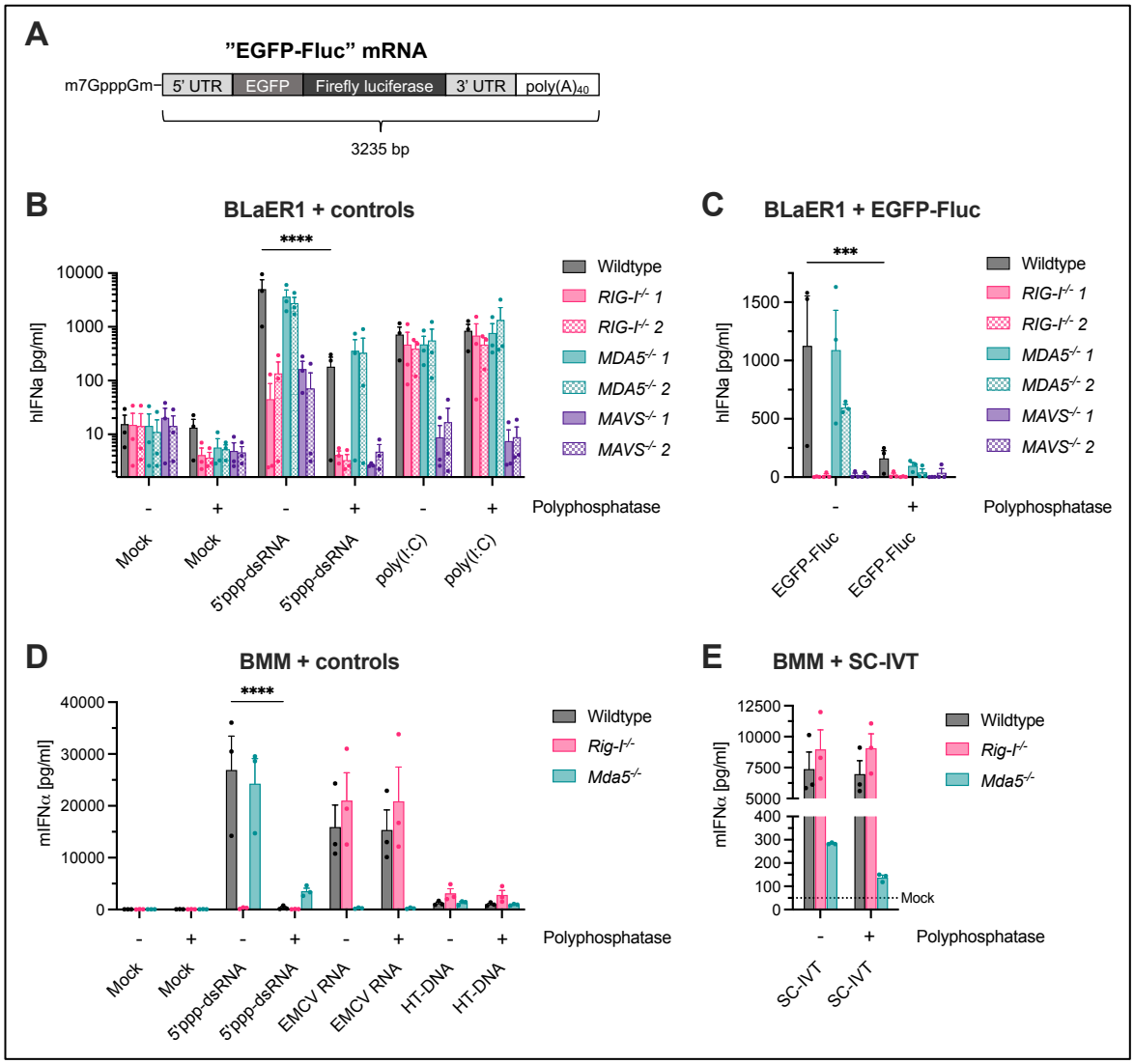

Figure 20: RIG-I is activated by uncapped 5′ppp or 5′pp transcripts contained within *in vitro* transcribed mRNA
(A) Schematic illustration of EGFP-Fluc mRNA. (B-C) BLaER1 cells were transfected with (B) indicated controls or (C) 0.8 µg/ml of m1Ψ-modified 5′ cap-1 EGFP-Fluc mRNA with or without polyphosphatase treatment. (D-E) BMMs were transfected with (D) indicated controls or (E) 0.8 µg/ml of m1Ψ-modified 5′ cap-1 SC-IVT with or without polyphosphatase treatment. IFNα production was quantified after 24 hours via ELISA. Mean + SEM of three independent experiments. Statistical significance was calculated by two-way ANOVA with Tukey's multiple comparisons correction. Only comparisons of phosphatase treatments within stimuli are shown selectively for wildtype cells. * $p < 0.05$, ** $p < 0.01$, *** $p < 0.001$, **** $p < 0.0001$. EMCV = encephalomyocarditis virus, HT-DNA = herring testis DNA, SC-IVT = SARS-CoV-2 *in vitro* transcript.

While 5′ cap structures are known to interfere with activation of RIG-I, their effect on MDA5 remains ambiguous. Previous studies indicated an inhibition of MDA5 activation by 5′ cap-1 structures based on a heightened MDA5-dependent IFN response to coronavirus mutants lacking ribose 2′-O-methyltransferase.[30] However, direct experimental evidence on MDA5 inhibition by cap structures is missing. Therefore, a direct comparison of innate immune activation by uncapped and capped mRNAs was performed in BLaER1 cells and BMDCs.

Using enzymatic capping after the *in vitro* transcription enabled the production of 5′ppp and cap-1 mRNA originating from a single IVT preparation. Therefore, the individual mRNAs did not differ

except for their 5′ end. As a control for capping efficiency, mRNA translation was quantified. Since BlaER1 cells constitutively express an EGFP-transgene, EGFP-Fluc mRNA was used and firefly luciferase activity was measured as readout for translation. BMDCs were stimulated with a corresponding mRNA encoding only EGFP, and EGFP$^+$ cell count was analyzed via fluorescence microscopy using the Cytation™3 reader.

For both mRNAs, 5′ cap-1 significantly increased mRNA translation compared to the uncapped analogue, confirming the success of the capping procedure (Figure 21A, C). Interestingly, the presence of a 5′ cap structure did not negatively affect activation of RIG-I in BLaER1 cells nor activation of MDA5 in BMDCs as demonstrated by similar IFNα levels (Figure 21B, D). In fact, 5′ cap-1 even slightly enhanced activation of MDA5 by the EGFP mRNA, possibly by stabilizing against 5′ exonuclease-mediated degradation, but did not reach significance (Figure 21D).

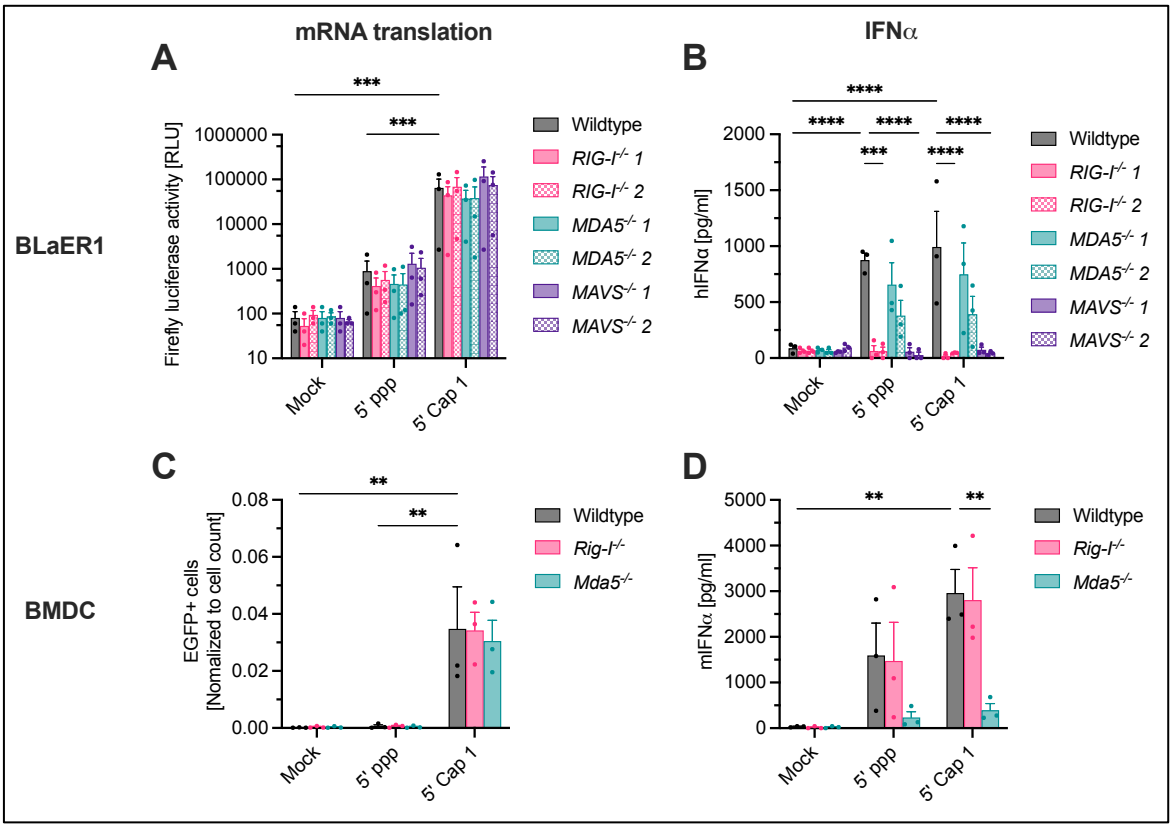

Figure 21: 5′ capping of *in vitro* transcribed mRNA does not affect activation of RIG-I-like receptors
(A - B) BLaER1 cells were transfected with 0.8 μg/ml of m1Ψ-modified EGFP-Fluc mRNA bearing indicated 5′ ends. After 18 hours, (A) firefly luciferase activity was quantified in BLaER1 cell lysates and (B) IFNα production was measured via ELISA. (C – D) BMDCs were transfected with 0.8 μg/ml of m1Ψ-modified EGFP mRNA bearing indicated 5′ ends. After 18 hours, (C) EGFP$^+$ cell count was quantified via microscopic imaging and normalized to the total cell count obtained from digital phase contrast, and (D) IFNα production was measured via ELISA. Mean + SEM of three independent experiments. Statistical significance was calculated by two-way ANOVA with Tukey's multiple comparisons correction. Comparisons between stimuli are depicted exclusively for wildtype cells. Within each stimulus, only comparisons of genotypes to the wildtype are displayed. For BLaER1 cells, only the higher p value of two corresponding clones is indicated. * $p < 0.05$, ** $p < 0.01$, *** $p < 0.001$, **** $p < 0.0001$.

Preceding experiments using the COVID-19 mRNA vaccines and IVT-mRNAs (Figure 15, Figure 16, Figure 20) demonstrated that both current capping techniques yield uncapped transcripts capable of activating RIG-I, which likewise challenges any conclusions regarding effects of 5′ cap on MDA5 activation. During co-transcriptional capping, which is used for the BioNTech COVID-19 vaccine, uncapped transcripts arise from transcription initiation with a regular nucleotide instead of the cap analogue.[77] Furthermore, primer-independent transcription can be a source of uncapped transcripts.[25] In contrast, enzymatic capping should theoretically act on any 5′ppp-RNA. However, the equal RIG-I-dependent type I IFN responses to uncapped and capped IVT-mRNAs indicate that the immunostimulatory RNA species are unaffected by the capping procedure. Therefore, it was hypothesized that the vaccinia capping enzyme might be unable to act on double-stranded 5′ppp RNA ends. To investigate this, short synthetic RNA oligos of 24 nt length were capped enzymatically and subsequently analyzed via LC/MS. A direct comparison of ss- and dsRNA was performed along with a mock antisense strand control to exclude potential competitive effects (Figure 22A-C). Additionally, the effect of a 3′ overhang on the 5′ppp end was investigated (Figure 22D). The deconvoluted ESI^- mass was investigated for the main peak assigned to the sense RNA strand (Figure 22, sense strand highlighted in blue). The mass of the corresponding antisense strands as well as the UV traces are shown in the appendix (Chapter 5.1, Figure 52, Figure 53).

The untreated RNA sense strand exhibited a mass of ~ 7847 Da, which was ~ 23 Da higher than the expected mass (Figure 22, I). This deviation corresponds to the hybridization of a Na^+ molecule to the RNA, which is occasionally observed in LC/MS analysis. For the untreated dsRNA, the retention time of the sense and antisense strands were so similar that they could not be separated based on individual peaks. However, since the antisense strand possesses a 5′OH instead of a 5′ppp end, the strands could be differentiated based on their masses within the same peak (Figure 22C, I). Therefore, the observed masses of the untreated controls were correct in all cases.

After the capping treatment, both the ssRNA alone and with mock antisense exhibited two masses corresponding to the 5′ cap-0 RNA and a small amount of 5′pp-RNA (Figure 22A-B, II). This finding validated the high resolution and suitability of the LC/MS method and confirmed the capping success. The 5′pp-RNA results from the individual enzymatic activities of the vaccinia capping enzyme, which are a phosphatase, guanylyl transferase, and guanine methyltransferase, which are employed in this order.[172] Therefore, while the majority of RNA was dephosphorylated and subsequently capped, a few residual dephosphorylated but uncapped transcripts remained. In contrast, the dsRNA sample presented only one mass corresponding to 5′pp-RNA (Figure 22C, II), indicating that the vaccinia capping enzyme is indeed unable to cap double-stranded RNA, whereas the phosphatase activity of the enzyme can act on both ss- and dsRNA. Interestingly, the dsRNA with a 3′ overhang of three nucleotides was completely unaltered by the vaccinia enzyme, indicating that the phosphatase activity is impeded by 3′ overhangs (Figure 22D, II).

To further investigate the phosphatase activity of the vaccina capping enzyme, a capping reaction without GTP was performed, thus disabling the guanylyl transferase activity (Figure 22, III). As expected, ssRNA alone, ssRNA with mock antisense, and dsRNA were processed into 5′pp-RNAs, confirming that the vaccinia phosphatase activity is active on both ss- and dsRNA (Figure 22A-C, III). In contrast, the overhang-bearing dsRNA maintained a 5′ppp end, confirming that a 3′ overhang abolishes the vaccinia phosphatase activity (Figure 22D, III). Of note, while RIG-I is known to preferably bind blunt-end 5′ppp- and 5′pp-dsRNA, it also tolerates a 3′ overhang, indicating that such RNA species would be capable of activating RIG-I, if present in mRNA preparations.[14]

Finally, the activity of the polyphosphatase (PP) was investigated on ss- and dsRNA (Figure 22, IV). Both ss- and dsRNA were processed to 5′p-RNAs by the enzyme (Figure 22A-C, IV), in line with the reduced RIG-I activation after PP digestion presented in preceding chapters mRNAs (Figure 15, Figure 16, Figure 20). Interestingly, even the 3′ overhang did not impede PP digestion (Figure 22D, IV).

These findings demonstrate that PP enzymatic activity is active irrespective of 5′ppp end structure, while vaccinia capping enzyme is unable to cap double-stranded 5′ppp ends, which are a requirement for RIG-I activation. This explains why vaccinia capping was not able to substantially reduce RIG-I activation of IVT-mRNAs, and is in line with the RIG-I activity of IVT-mRNA and vaccine mRNA being sensitive to PP treatment.

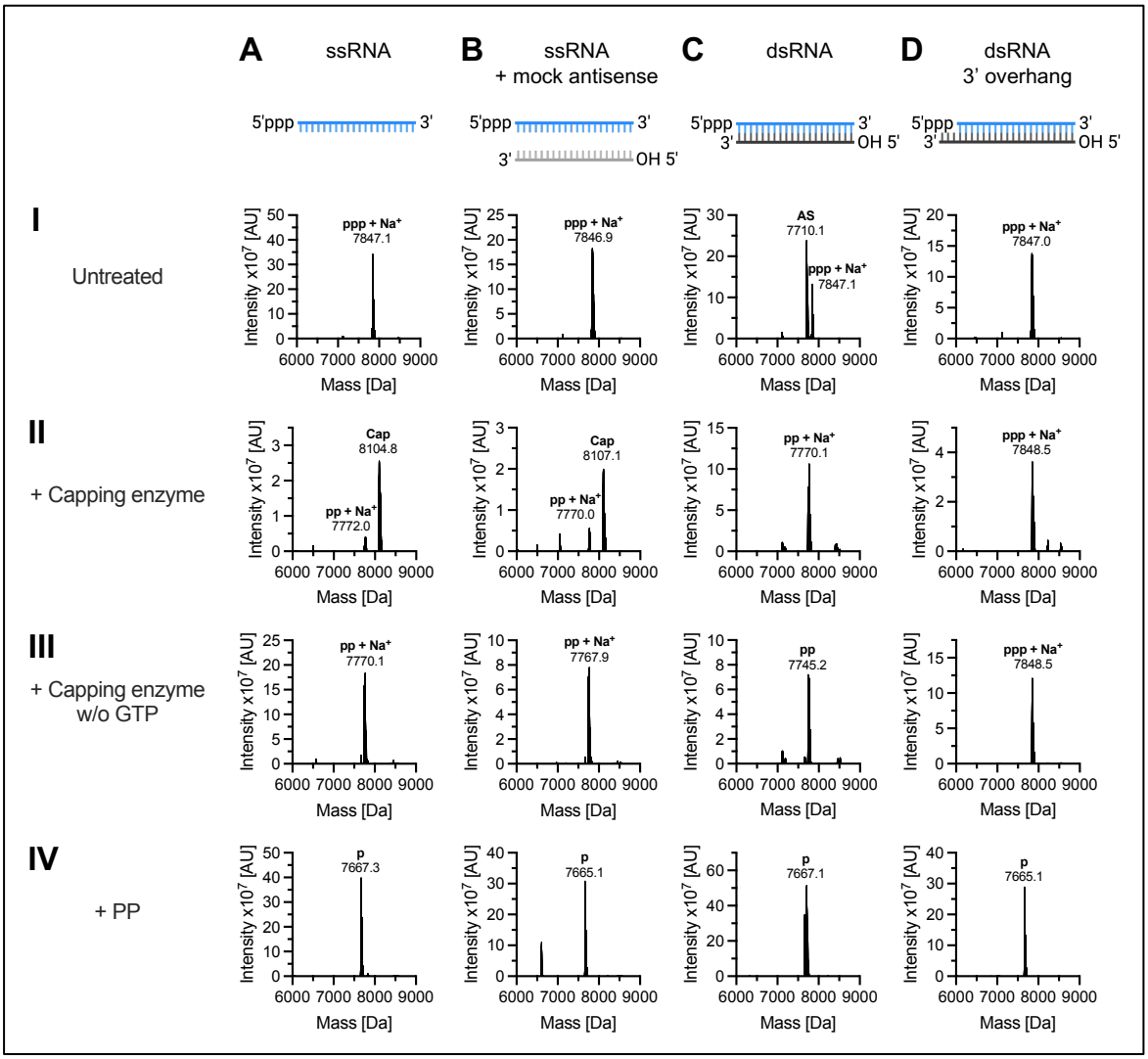

Figure 22: Double-stranded RNA is not processed by the vaccinia capping enzyme and retains 5′ppp or 5′pp ends
Synthetic 24 nt RNAs indicated in I – IV were treated as indicated in A – D and subjected to LC/MS analysis. Data depict the deconvoluted ESI^- masses of the main peak assigned to the RNA sense strand (highlighted in blue). (I) ssRNA, (II) ssRNA with mock antisense, (III) blunt-end dsRNA, (IV) dsRNA with a 3 nt 3′ overhang. (A) Untreated RNAs, (B) standard capping using the vaccinia capping enzyme, (C) capping without GTP, (D) polyphosphatase (PP) digestion. Data are representative of three independent experiments.

While RIG-I activation requires a 5′ppp double-stranded RNA end, MDA5 is known to bind long dsRNA stretches that can also occur within higher-order RNA structures.[27] Therefore, such MDA5 ligands, if contained within IVT-mRNA, might possess a single-stranded 5′ end that is accessible for 5′ capping by the vaccinia enzyme. To investigate this possibility and further investigate a potential impediment of MDA5 activation by 5′ cap structures, a method to select successfully capped RNAs from IVT preparations was employed. After enzymatic capping, the SC-IVT was subjected to polyphosphatase (PP) digestion, which trims any remaining uncapped 5′ppp or 5′pp transcripts to 5′p ends. Following this, the RNA was digested with 5′ Terminator Exonuclease (TE), an exonuclease that specifically degrades 5′p-RNAs but does not affect 5′ppp, pp, cap-0 or cap-1 RNA species. These consecutive treatments enrich IVT preparations for successfully capped RNAs. As a

control, uncapped SC-IVT was processed analogously. The significantly higher RNA recovery of capped SC-IVT compared to uncapped confirmed the procedure's selectivity and a successful enrichment of capped RNA (Figure 23A). Nevertheless, a small proportion of the uncapped mRNA was recovered for some samples, likely due to incomplete digestion by one of the enzymes. Indeed, the recovery was further reduced by a prolonged treatment duration (data not shown).

After the digestion, the capped RNAs were transfected into BMDCs, and IFNα production was measured. As expected, PP treatment of capped SC-IVT did not negatively affect activation of MDA5 compared to untreated (Figure 23B). Furthermore, the capped SC-IVT treated with both PP and TE induced similar MDA5-dependent IFNα levels as the untreated and PP-digested analogs. Since the combination of PP and TE treatment enriches 5′ capped mRNA, these findings contradict the reported inhibitory effect of 5′ cap-1 structures on MDA5 activation, in line with the previous experiments demonstrating no differential MDA5 activation by 5′ppp or 5′ cap-1 mRNA (Figure 21).[30]

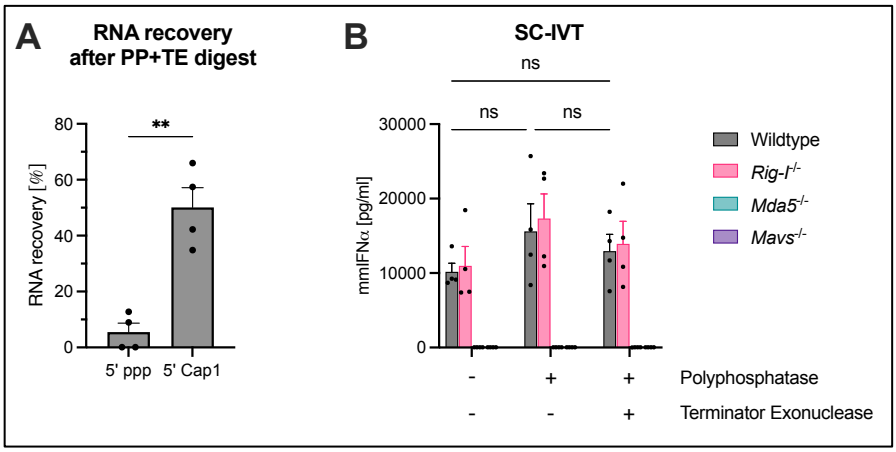

Figure 23: Enrichment of 5′ cap-1 mRNA does not affect MDA5 activation
(A) RNA recovery after consecutive digestion of SC-IVT mRNA harboring indicated 5′ ends with polyphosphatase (PP) and terminator exonuclease (TE). Mean + SEM of four independent purifications. Statistical significance was determined using Student's t-test. (B) BMDCs were transfected with 0.8 μg/ml of m1Ψ-modified 5′ cap-1 SC-IVT mRNA after indicated enzymatic treatments. IFNα production was quantified after 24 hours via ELISA. Mean + SEM of four independent experiments. Statistical significance was determined using two-way ANOVA with Tukey's multiple comparisons test and is shown for wildtype cells only. ** $p < 0.01$

In summary, these data demonstrate that RIG-I is activated by residual uncapped RNAs resulting from the inability of the vaccinia capping enzyme to process dsRNA. In contrast, while no negative impact of 5′ capping on MDA5 activation was observed, further investigation is required to define the exact effects of 5′ cap on MDA5.

3.1.5 N1-methyl-pseudouridine (m1Ψ) enhances mRNA-induced activation of murine MDA5 while reducing activation of murine RIG-I

The COVID-19 mRNA vaccines by BioNTech and Moderna contain an m1Ψ-modified *in vitro* transcribed (IVT)-mRNA coding for the SARS-CoV-2 pre-fusion spike protein. In preceding experiments, this mRNA was found to activate RIG-I-like receptors. Intriguingly, the type I IFN response to m1Ψ-modified mRNA in mice and murine cells was primarily dependent on MDA5, while IFNα production from human cells was mainly mediated by RIG-I (Chapter 1.4.4, Chapter 3.1.1). Furthermore, previous experiments demonstrated that the activation of human RIG-I and human MDA5 by IVT-mRNA is reduced by the incorporation of m1Ψ (Chapter 1.4.4, Figure 11). Following these observations, the effects of m1Ψ on the activation of murine RLRs and potential species-specific differences were investigated by stimulating murine BMDCs with unmodified and m1Ψ-modified SC-IVT.

In line with preceding findings, the m1Ψ-modified SC-IVT induced a strong MDA5-dependent IFNα response by BMDCs (Figure 24). In contrast, the unmodified SC-IVT elicited a significantly weaker IFNα response (approximately 6.5 times lower), which was mediated by activation of both RIG-I and MDA5 (Figure 24). These findings indicate that unmodified IVT-mRNA is a ligand for both murine RIG-I and MDA5, and that the incorporation of m1Ψ inhibits the activation of murine RIG-I while enhancing activation of murine MDA5. Considering that previous experiments revealed a reduction of human RLR activation by m1Ψ, murine RIG-I seems to be similarly affected by m1Ψ as human RIG-I. In contrast, the enhanced activation of murine MDA5 by m1Ψ is different from the human system.

In conclusion, the collaborative project pursued by Bartok and Hartmann groups uncovered two notable species-specific differences in the mRNA sensing mechanisms of human and murine cells: Firstly, the relative involvement of RIG-I and MDA5 differs, meaning that murine cells utilize both sensors to detect unmodified IVT-mRNA, whereas human cells predominantly rely on RIG-I for mRNA sensing. Secondly, the incorporation of m1Ψ exerts contrasting effects on MDA5 activation in the two species, diminishing activation in human cells while enhancing it in murine cells.

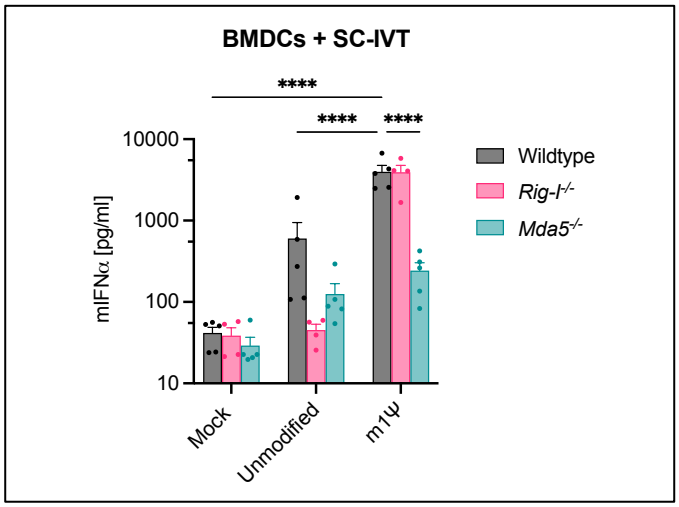

Figure 24: Incorporation of m1Ψ enhances activation of murine MDA5 by *in vitro* transcribed mRNA. BMDCs were transfected with indicated controls or 0.8 μg/ml of unmodified or m1Ψ-modified SC-IVT. IFNα production was quantified after 18 hours via ELISA. Mean + SEM of five independent experiments. Statistical significance was calculated using two-way ANOVA with Tukey's multiple comparisons correction. Comparisons between stimuli are depicted exclusively for wildtype cells. Within each stimulus, only comparisons of genotypes to the wildtype are displayed. * $p < 0.05$, ** $p < 0.01$, *** $p < 0.001$, **** $p < 0.0001$.

3.1.6 Endosomal Toll-like receptors do not contribute to the innate immune response induced by m1Ψ-modified mRNA vaccines

After reaching the target cells, mRNA vaccines are taken up by several mechanisms, including receptor-mediated endocytosis and macropinocytosis, and traffic through endosomal compartments, where they can interact with RNA-sensing Toll-like receptors (TLRs).[113,173] The relevant RNA-sensing TLRs are TLR3, TLR7, and TLR8, and previous studies based on *in vitro* overexpression experiments reported that these TLRs are indeed activated by transfection of IVT-mRNA.[111,112] Furthermore, *in vivo* activation of TLR3 and TLR7 by unmodified mRNA vaccines has been confirmed in mice.[113,114] However, activation of TLR7 and TLR8, and, to a lesser extent, TLR3, was shown to be abolished by incorporation of pseudouridine (Ψ), a precursor of the N1-methyl-pseudouridine (m1Ψ) that is integrated into the COVID-19 mRNA vaccines.[111] Therefore, it has remained questionable whether m1Ψ-modified IVT-mRNA would activate endosomal TLRs. So far, the effect of m1Ψ on endosomal TLRs has not been explicitly investigated.

In preceding experiments, IFNα production by BMDCs and BMMs was completely dependent on RLRs. However, expression of pattern recognition receptors and specific cytokine induction differ significantly between cell types. For example, while murine TLR7 is expressed in certain myeloid cells and plasmacytoid dendritic cells (pDC), the employed signaling pathways and resulting cytokine secretion differ considerably between the cell types (see Chapter 1.2.2).[39] In myeloid cells,

activation of TLR7 induces the pro-inflammatory cytokines IL-6, IL-12, and TNFα, but induction of IFNα is specific to pDCs.[38,39] Consequently, the preceding experiments performed in BMDCs and BMMs were not suitable to measure IFNα induction by TLR7 by mRNA vaccines. Thus, the experiments were repeated using BMMs, and the induction of IL-12p40 was measured as a TLR7-specific readout. Additionally, murine bone marrow was stimulated with mRNA isolated from the COVID-19 vaccines. Bone marrow is a heterogeneous cell population that includes pDCs, which would be the likely source of TLR7-dependent IFNα *in vivo.*

TLR3 is expressed by macrophages and DCs alike, and its engagement leads to the production of type I IFNs in both cell types.[39] Consequently, TLR3 activation by COVID-19 mRNA vaccines or the model mRNA SC-IVT could have been detectable in preceding experiments. However, the inherent LNPs of the COVID-19 mRNA vaccines and the transfection reagent Lipofectamine 2000 are multi-component lipoplexes specially designed for endosomal escape of the RNA into the cytosol and thus might not be optimal to study engagement of TLRs.[173] Therefore, the following experiments were performed using only the cationic lipid DOTAP (1,2-dioleoyl-3-trimethylammonium-propane), which is less proficient in endosomal escape, thus prolonging potential interaction with TLRs.

DOTAP was used to deliver mRNA isolated from COVID-19 vaccines by BioNTech and Moderna to BMMs and murine bone marrow. IFNα production by the heterogenous bone marrow population reflects engagement of TLR7, whereas IL-12p40 production by BMMs can be induced through the activation of TLR3 and/or TLR7. Of note, TLR8 is dysfunctional in mice and is therefore addressed in later sections of this study using primary human cells (Chapter 3.2.5).[41]

The TLR7/8-specific ligands R848, which is an imidazoquinoline derivate, and 9.2S-RNA, a short ssRNA, in conjunction with TLR7-deficient cells confirmed endosomal delivery and functional TLR7 signaling by induction of specific cytokines in BMMs and bone marrow (Figure 25).[174,175] Meanwhile, the TLR9-ligands CpG2006-PTO and CpG1826-PTO, DNA oligos containing CpG motifs and stabilizing phosphothioate (PTO) backbones, induced IL-12p40 and IFNα in all genotypes.[176]

In BMMs, no IL-12p40 induction was observed following endosomal stimulation with mRNA isolated from COVID-19 vaccines (Figure 25A). Similarly, no IFNα response was observed from bone marrow stimulated with vaccine mRNA (Figure 25B). Taken together, these data indicate that endosomal TLRs do not substantially contribute to the vaccine mRNA-induced innate immune response in murine BMDM and bone marrow cells.

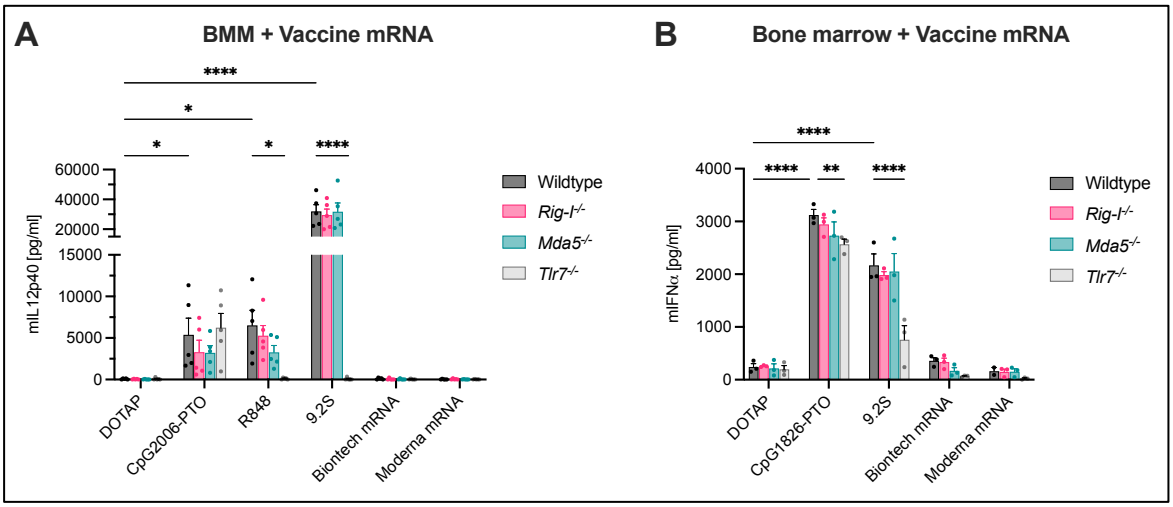

Figure 25: DOTAP-transfected COVID-19 vaccine mRNA does not activate TLR7

(A) BMMs or (B) murine bone marrow was transfected with indicated controls or 0.8 μg/ml mRNA isolated from COVID-19 vaccines using DOTAP. Production of IL12p40 or IFNα was quantified after 24 hours via ELISA. Mean + SEM of at least three independent experiments. Statistical significance was calculated by two-way ANOVA with Tukey's multiple comparisons correction. Comparisons of stimuli to Mock are depicted exclusively for wildtype cells. Within each stimulus, only comparisons of genotypes to the wildtype are displayed. * $p < 0.05$, ** $p < 0.01$, *** $p < 0.001$, **** $p < 0.0001$.

Since TLR7 is inhibited by Ψ-modified mRNA,[111] the SC-IVT was utilized to investigate whether m1Ψ had similar effects. Indeed, the unmodified SC-IVT induced strong TLR7-dependent IL12p40 levels in BMMs and IFNα production in bone marrow, whereas the m1Ψ-modified version did not (Figure 26). These findings demonstrate that activation of TLR7 by IVT-mRNA is inhibited by incorporation of m1Ψ and further confirm that COVID-19 mRNA vaccines by BioNTech and Moderna do not activate TLR7 due to the incorporation of m1Ψ. Of note, no effect of 5′ end cap structures was observed on TLR7 activation (Figure 26).

The IFNα response of murine bone marrow to unmodified SC-IVT completely depended on TLR7 (Figure 26B). Nevertheless, DOTAP-transfected m1Ψ-modified SC-IVT induced weak IFNα levels that were slightly above background and not mediated by TLR7 or RLRs. This could indicate a low-level activation of other sensors, possibly TLR9 by incompletely degraded dsDNA template, or cGAS through DOTAP-induced cell damage.

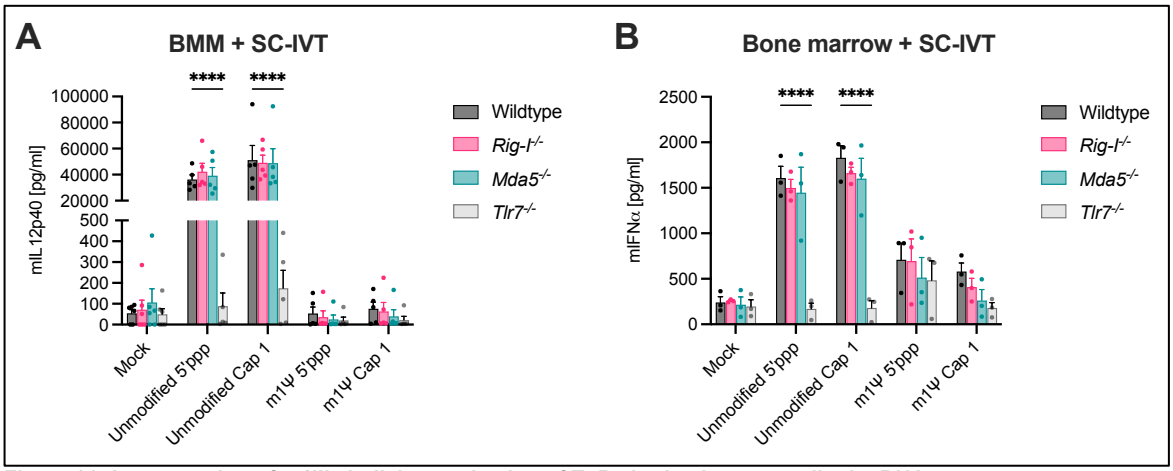

Figure 26: Incorporation of m1Ψ abolishes activation of TLR7 by *in vitro* transcribed mRNA
(A) BMMs or (B) murine bone marrow were transfected with 0.8 µg/ml of an *in vitro* transcribed m1Ψ-modified 3 kb SARS-CoV-2 mRNA (SC-IVT) using DOTAP. Production of IL12p40 or IFNα was quantified after 24 hours via ELISA. Mean + SEM of at least three independent experiments. Statistical significance was calculated by comparing knockouts to the wildtype using two-way ANOVA with Dunnett's multiple comparisons correction. * $p < 0.05$, ** $p < 0.01$, *** $p < 0.001$, **** $p < 0.0001$.

In conclusion, TLR7 is not involved in the sensing of m1Ψ-modified mRNA vaccines in murine cells. While TLR7 is activated by unmodified IVT-mRNA, its activation is abrogated by incorporation of m1Ψ, as has been previously described for Ψ.[111] TLR7 is known to sense RNA degradation products, and it remains to be elucidated whether TLR7 itself or upstream RNases are inhibited by Ψ and m1Ψ.[43,177] While the absence of an IL-12p40 response to unmodified mRNA in TLR7-deficient bone marrow cells contradicts an engagement of TLR3 (Figure 26B), further experiments including TLR3-specific controls, such as DOTAP-transfected poly(I:C), and TLR3-deficient cells are required for definite conclusions.

All in all, these findings are in line with previous reports and highlight TLRs as important innate sensors for mRNA vaccines, depending on the choice of incorporated nucleoside modification and composition of lipid nanoparticles used for delivery.[111,113]

3.2 Modulation of RIG-I-like receptor activation by mRNA incorporating modified nucleosides

3.2.1 Innate immune activation by *in vitro* transcribed mRNA vaccines is modulated by nucleoside modifications in a species-specific manner

The modified nucleoside N1-methyl-pseudouridine (m1Ψ) is incorporated into the mRNA molecule in the COVID-19 mRNA vaccines to decrease innate immune responses while simultaneously enhancing mRNA translation.[83] Several other nucleoside modifications have demonstrated similar effects and are commonly used in the research and development of mRNA therapeutics. These include pseudouridine (Ψ), 5-methoxy-uridine (5moU), 5-methyl-cytidine (m5C), and N6-methyl-adenosine (m6A) (Chapter 1.4.3, Figure 6).[83,144]

While the effects of nucleoside modifications on TLR activation have been largely characterized (Chapter 1.4.3, Table 1), details on the modulation of RLR activation remain scarce. Data from this thesis (Chapter 3.1) and other Bartok and Hartmann group members (Chapter 1.4.4) demonstrate that m1Ψ-modified mRNA induces potent RLR-dependent immune responses, thus challenging the prevalent notion that m1Ψ generally abolishes innate immune activation by mRNA vaccines. Additionally, a species-specific modulation of RLR activation by m1Ψ has been revealed in collaboration with the Bartok group (Chapter 1.4.4, Figure 11; Chapter 3.1.5, Figure 24). Understanding PRR activation by mRNA vaccines is fundamental to developing mRNA therapeutics with optimized immunostimulatory properties tailored to the specific application, such as vaccination or protein replacement therapy. Therefore, this study aimed to characterize the modulation of RLR activation by the incorporation of commonly used nucleoside modifications in IVT-mRNA.

To simultaneously investigate the effect of nucleoside modification on the innate immune response and protein translation, the EGFP-Fluc mRNA was generated by *in vitro* transcription, and specific nucleotides were substituted with modified analogs. The mRNA was capped enzymatically to enable concurrent investigation of mRNA translation, as presented in Chapter 3.3.

RNA integrity was assessed using agarose gel electrophoresis, revealing slight variations in gel migration patterns between nucleoside-modified and unmodified mRNAs (Figure 27A). This consistent electrophoretic behavior, observed throughout the study and across various RNA sequences (data not shown), suggests that the modifications slightly alter the charge and/or molecular conformation of the RNA rather than its molecular size (e.g., due to incomplete transcription).[178] Therefore, in vitro transcription successfully yielded full-length RNA for both modified and unmodified sequences.

EGFP-Fluc mRNAs were transfected into murine BMDCs, primary human PBMCs, and human BLaER1 cells, followed by measurement of cytokine responses via ELISA. BMDCs produced higher levels of IFNα in response to m1Ψ-modified mRNA compared to unmodified mRNA (Figure 27B), consistent with earlier findings (Chapter 3.1.5, Figure 24). Notably, Ψ-modified mRNA elicited an even stronger IFNα response, further challenging the notion that these modifications universally suppress mRNA-induced innate immune responses. In human BLaER1 cells and PBMCs, m1Ψ significantly reduced IFNα and CXCL10 production compared to the unmodified mRNA (Figure 27C-D), in line with previous findings demonstrating a reduced activation of RIG-I by m1Ψ (Chapter 1.4.4, Figure 11). Ψ-modified mRNA likewise elicited reduced IFNα and CXCL10 levels compared to unmodified mRNA, but to a lesser extent than observed for the m1Ψ-modified mRNA (Figure 27C-D). Thus, Ψ, like m1Ψ, modulates the mRNA-induced type I IFN response in a species-specific manner. In contrast, for all other tested modifications, the modulation of mRNA-induced innate immune responses was similar between the tested cell types and species (Figure 27B-D). The 5moU-modified mRNA induced the lowest cytokine levels, thereby successfully reducing the mRNA-induced immune response to almost background levels. The modification m5C did not significantly affect cytokine responses to mRNA, whereas m6A induced a slightly reduced cytokine production (Figure 27B-D).

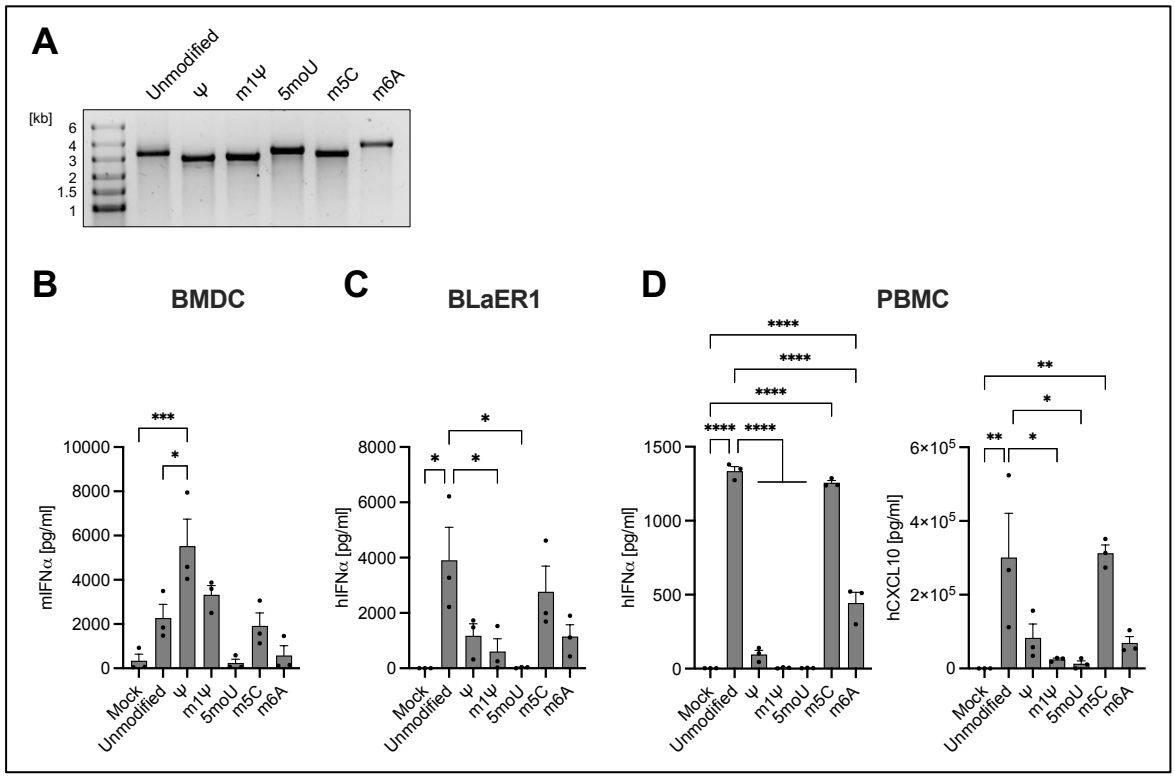

Figure 27: Innate immune response to *in vitro* transcribed mRNA is modulated by nucleoside modifications in a species-specific manner (A) Integrity of EGFP-Fluc mRNA incorporating indicated nucleoside modifications visualized by agarose gel electrophoresis. (B) BMDCs, (C) BLaER1 cells, and (D) PBMCs were transfected with 0.8 μg/ml of EGFP-Fluc mRNA incorporating indicated nucleoside modifications. IFNα and CXCL10 production was quantified after 18 hours via ELISA. Mean + SEM of at least three independent experiments or donors, respectively. Statistical significance was calculated by one-way ANOVA with Tukey's multiple comparisons correction. Only comparisons to Mock and unmodified mRNA are shown. * $p < 0.05$, ** $p < 0.01$, *** $p < 0.001$, **** $p < 0.0001$.

To elucidate the individual engagement of RIG-I and MDA5 in human and murine cells and their potentially different modulation by modified nucleosides, modified EGFP-Fluc mRNA was again transfected into BMDCs and BLaER1 cells, including MDA5, RIG-I, and MAVS knockout cells.

The IFNα production of human BLaER1 cells in response to EGFP-Fluc mRNA was primarily dependent on RIG-I (Figure 28A), in line with preceding experiments using COVID-19 vaccine mRNA and the SC-IVT (Chapter 1.4.4, Figure 9; Chapter 3.1.4, Figure 20). Activation of human RIG-I was reduced by incorporation of m1Ψ (Figure 28A), consistent with previous findings (Chapter 1.4.4, Figure 11). Additionally, human RIG-I activation by EGFP-Fluc mRNA was reduced by the incorporation of Ψ and 5moU, but remained largely unaffected by m5C and m6A (Figure 28A). Although 5moU was most effective in reducing mRNA-induced innate immune activation, a residual RIG-I-dependent IFNα response was still detectable in response to 5moU-modified mRNA (Figure 28A). In RIG-I-deficient BLaER1 cells, a weak MDA5-dependent IFNα production in response to unmodified mRNA was detectable (Figure 28A). This activation of human MDA5 seemed to be slightly reduced by Ψ and abolished by all other modifications, in line with previous findings demonstrating a decreased activation of human MDA5 by m1Ψ (Chapter 1.4.4, Figure 11). Of note, m5C-modified mRNA activated human MDA5 only in one of two *RIG-I*$^{-/-}$ BLaER1 cell clones, necessitating further investigation.

The IFNα response of murine BMDCs to EGFP-Fluc mRNA was primarily dependent on MDA5 (Figure 28B), in line with the preceding *in vivo* and *in vitro* experiments using the COVID-19 mRNA vaccines and the SC-IVT (Chapter 1.4.4, Figure 7; Chapter 3.1.1, Figure 12; Chapter 3.1.5, Figure 20). Although previous experiments using the SC-IVT demonstrated an enhanced activation of murine MDA5 by m1Ψ (Chapter 3.1.5, Figure 24), the IFNα levels of wildtype BMDCs in response to unmodified and m1Ψ-modified EGFP-Fluc mRNA remained similar (Figure 28B). However, the unmodified mRNA activated both RIG-I and MDA5 in BMDCs, while IFNα levels induced by m1Ψ-modified mRNA were solely dependent on MDA5 (Figure 28B). Thus, m1Ψ again enhanced activation of murine MDA5 (Figure 28B), albeit to a lesser extent than what was observed for the SC-IVT (Chapter 3.1.5, Figure 24). An enhanced activation of murine MDA5 could also be observed for Ψ and to an even greater extent than for m1Ψ (Figure 28B). In contrast, activation of murine MDA5 was abolished by 5moU, m5C, and m6A (Figure 28B), as was the case for human MDA5 (Figure 28A). As mentioned before, a minor RIG-I-dependent IFNα response to unmodified mRNA was notable in MDA5-deficient BMDCs (Figure 28B). This activation of murine RIG-I by EGFP-Fluc mRNA was abolished by m1Ψ, Ψ, and 5moU, enhanced by m5C, and reduced by m6A (Figure 28B), which was similar to the results observed for human RIG-I in BLaER1 cells (Figure 28A) and is consistent with data obtained by stimulating murine BMDCs with the m1Ψ-modified SC-IVT (Chapter 3.1.5, Figure 24).

These findings further confirm a strong species-specific preference for the engagement of RIG-I or MDA5 for mRNA sensing in human and murine cells, respectively. Furthermore, RIG-I and MDA5 are differentially modulated by nucleoside modifications, the most striking difference being that Ψ and m1Ψ reduce activation of RIG-I in both species as well as of human MDA5, but enhance activation of murine MDA5.

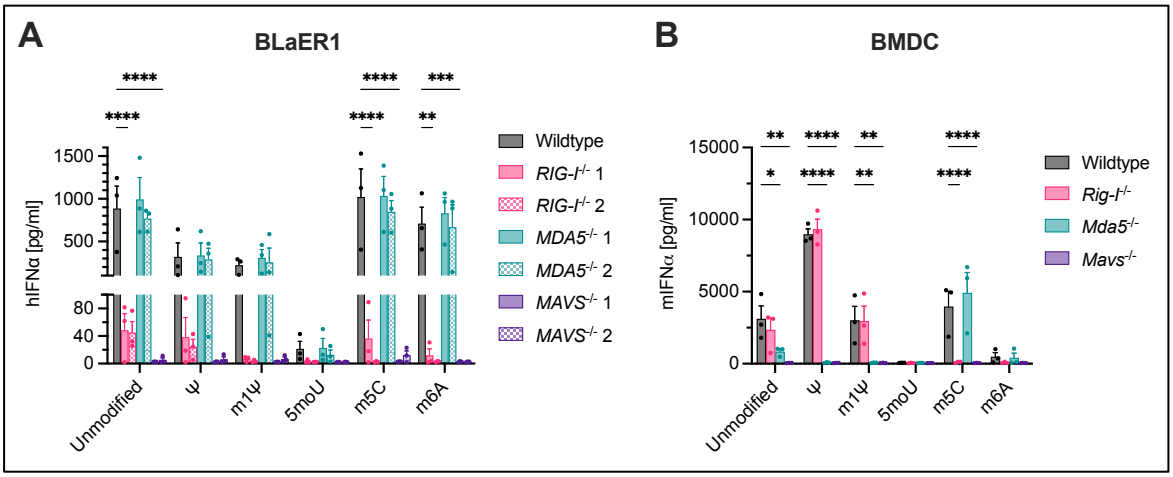

Figure 28: RIG-I is the dominant sensor for mRNA vaccines in human cells, while murine cells primarily engage MDA5 (A) BLaER1 cells and (B) BMDCs were transfected with 0.8 µg/ml of EGFP-Fluc mRNA incorporating indicated nucleoside modifications. IFNα production was quantified after 18 hours via ELISA. Mean + SEM of three independent experiments. Statistical significance was determined by comparing wildtype and knockout clones using two-way ANOVA with Tukey's multiple comparisons correction. For BLaER1 cells, only the higher p value of two corresponding clones is shown. * $p < 0.05$, ** $p < 0.01$, *** $p < 0.001$, **** $p < 0.0001$.

3.2.2 Modified nucleosides differentially modulate the generation of double-stranded RNA byproducts during *in vitro* transcription

While certain nucleoside modifications have been found to reduce innate immune activation by IVT-mRNA, the underlying mechanisms remain largely unknown. Preceding experiments demonstrated that double-stranded byproducts generated during *in vitro* transcription are responsible for the activation of RLRs by mRNA vaccines, as evidenced by the reduced RLR-dependent IFNα responses to oligo(dT)-purified compared to unpurified IVT-mRNA (Chapter 1.4.4, Figure 10; Chapter 3.1.2, Figure 17). Similarly, HPLC or ethanol/cellulose purifications have been found to reduce innate immune responses to mRNA vaccines by eliminating dsRNA byproducts.[115,145] Besides, the incorporation of certain nucleoside modifications in mRNA vaccines has been found to reduce the generation of dsRNA byproducts during *in vitro* transcription, which is believed to cause the observed reduction in innate immune activation by some modifications. Specifically, a reduction of dsRNA content by nucleoside modifications has been indicated for m1Ψ, 5moU, and m5C, albeit

to varying extents.[25,144–146] In contrast, previous studies regarding Ψ provide ambiguous experimental evidence on its modulation of dsRNA content.[25,115,144] Only one study investigated the modulation of dsRNA formation by m6A and found no differences compared to unmodified.[25]

However, other studies indicate a direct interference of nucleoside modifications with binding or conformational changes of innate receptors as the underlying mechanism for the reduced induction of innate immune responses by modified mRNAs.[111,150]

Given the limitations of previous studies in comparing only a few nucleoside modifications at a time and utilizing different techniques, the present thesis aimed to provide a comprehensive side-by-side comparison of dsRNA content across all nucleoside modifications presented. Furthermore, it was explored whether the dsRNA content correlates with the modulation of RLR activation by modified mRNA, as observed in Chapter 3.2.1, Figure 28.

The dsRNA content of EGFP-Fluc mRNA was investigated via dot blot and anti-dsRNA antibody J2 staining (Figure 29A). A subsequent staining with ethidium bromide (EtBr) verified equal sample loading (Figure 29B). To quantify the relative modulation of dsRNA content by nucleoside modifications, the area under the curve (AUC) was calculated and normalized to the unmodified mRNA (Figure 29D). All tested nucleoside modifications reduced the dsRNA content in EGFP-Fluc mRNA to different extents, except for Ψ, which contained approximately 30 % more dsRNA than the unmodified control (Figure 29A, C, D). The modifications m1Ψ, m5C, and m6A caused a moderate reduction of dsRNA content of approximately 10 %, 30 %, and 40 %, respectively (Figure 29A, C, D). The incorporation of 5moU resulted in the significantly lowest dsRNA content, achieving a reduction of 80 % compared to unmodified (Figure 29D), in line with its effectively reduced innate immune stimulation. While the increased dsRNA content in Ψ-modified mRNA could explain its potent MDA5 activation in murine BMDCs (Figure 28B), it conflicts with the reduced activation of both RIG-I and MDA5 in human BLaER1 cells (Figure 28A). Of note, identical RNA batches were used in all experiments, therefore eliminating any potential batch-dependent variations. This divergence could indicate a direct inhibitory effect of Ψ on human RLRs or a modulation of not only dsRNA quantity but also quality, leading to a differential generation of RLR ligands. Additionally, secondary effects via other RNA sensors, such as PKR or OAS, could be involved and necessitate further investigation.

Despite the ambiguity observed for Ψ, the dsRNA content of modified mRNAs generally seemed to correlate with the extent of mRNA-induced innate immune responses. To analyze this, a Spearman correlation coefficient was calculated based on the anti-dsRNA signal of EGFP-Fluc mRNA at 100 ng depicted in Figure 29C, and the IFNα levels of wildtype BLaER1 cells or BMDCs depicted in Figure 28, respectively. The results demonstrated a positive correlation between dsRNA content and IFNα induction, with $r_s = 0.35$ for BLaER1 cells and $r_s = 0.7$ for BMDCs (Figure 29E, F). However, statistical significance was observed only for the BMDC data ($p = 0.15$ for BLaER1 cells,

p = 0.0013 for BMDCs). These findings confirm that the modulation of dsRNA content by the investigated nucleoside modifications is indeed contributing to the altered innate immune activation by modified mRNA. Nevertheless, a direct impairment of RNA receptor binding or activation by the nucleoside modifications is also possible and will be further investigated during this study.

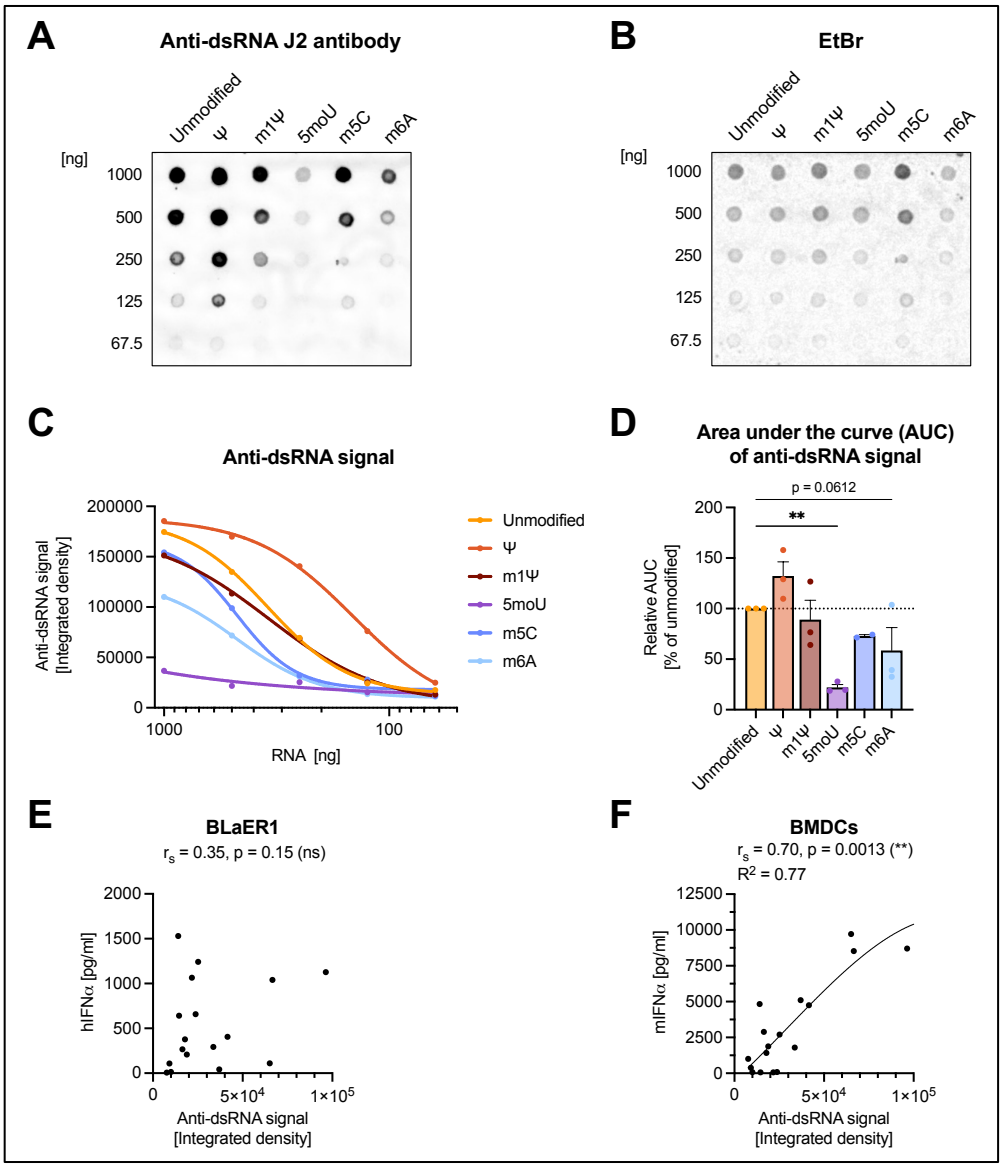

Figure 29: Modified nucleosides modulate the generation of dsRNA byproducts during *in vitro* mRNA transcription, partially correlating with innate immune activation. (A) Anti-dsRNA antibody J2 signal of an EGFP-Fluc mRNA dot blot incorporating indicated nucleoside modifications. (B) Ethidium bromide (EtBr) staining of dot blot depicted in (A). Images are representative of three independent experiments. (C) Integrated density of the anti-dsRNA signal of EGFP-Fluc mRNA dot blots. Mean of three independent experiments. (D) Area under the curve (AUC) of the anti-dsRNA signal depicted in (C) normalized to unmodified mRNA. Mean + SEM of three independent experiments. For m5C, one data point was identified as outlier based on EtBr staining and removed from the analysis. Statistical significance was determined by comparing each data set to the unmodified control using one-way ANOVA. (E, F) Spearman correlation coefficient (r_s) and corresponding p value was calculated for the anti-dsRNA signal of all mRNAs at 100 ng depicted in (B) and the corresponding IFNα levels produced by wildtype BLaER1 cells or BMDCs depicted in Figure 28, respectively. A curve was fitted to the data points by comparing several regression models (linear, exponential, sigmoidal, and first to third order polynomial) and choosing the model with highest R^2 (i.e. best fit, in this case third order polynomial for BMDCs). The quality of fit of the regression model is indicated by the coefficient of determination (R^2). None of the tested regression models provided a sufficient fit ($R^2 > 0.5$) for the BLaER1 data and the curves were thus omitted from the visualization. * $p < 0.05$, ** $p < 0.01$.

The experimental evidence in the literature on Ψ's modulation of dsRNA byproducts is ambiguous, with studies reporting a reduction in dsRNA[25], equal dsRNA levels[115], or dsRNA increase,[144] as observed in the present study. Additionally, a sequence-dependent modulation of dsRNA content by Ψ has been proposed before based on the comparison of nine different mRNAs.[115] To investigate IVT-specific effects for the tested nucleoside modifications, the dot blot was repeated with a different RNA. Since Mu *et al.* previously demonstrated a reduction of dsRNA content by incorporation of Ψ into a 512 nt RNA, this RNA was utilized using the exact same sequence and methodology of the original publication and is referred to as ss512B.[25]

Consistent with the findings of Mu *et al.*, the Ψ-modified ss512B exhibited an approximately 30 % reduced AUC for dsRNA content compared to its unmodified control in a J2 dot blot (Figure 30A, B), indicating an IVT-specific modulation of dsRNA content by Ψ.[25] Of note, the two IVTs tested thus far exhibited a slightly different uridine content, with 0.18 % for the EGFP-Fluc mRNA and 0.25 % for the ss512B, and it remains to be investigated whether this factor contributes to the differential modulation of dsRNA content by Ψ. Possibly in line with this notion, m1Ψ reduced the anti-dsRNA signal AUC of ss512B to a greater extent (~60 %, Figure 30A, B) than what was observed for the EGFP-Fluc mRNA (~10 %, Figure 29C, D). All other modifications exhibited a similar reduction of dsRNA content in ss512B (Figure 30A, B) as observed in the EGFP-Fluc mRNA (Figure 29), indicating that the effects of these modifications are independent of IVT sequence. The relative modulation of anti-dsRNA signal AUC was approximately 85 % for 5moU, 15 % for m5C, and 55 % for m6A (Figure 30A, B).

It is worth mentioning that the incorporation of nucleoside modifications could potentially interfere with the binding affinity of the J2 antibody, thus leading to false results. Although the anti-dsRNA dot blot is well established, the effect of nucleoside modifications on J2 binding affinity has not been characterized for most modifications. In fact, the confirmation of unaltered J2 binding affinity using a double-stranded modified RNA has been performed only for m1Ψ.[145] Therefore, the complementary antisense strand of ss512B was *in vitro* transcribed for each nucleoside modification and annealed to the correspondingly modified strands, followed by digestion of single-stranded RNA using RNase If, resulting in a fully-modified 512 nt double-stranded RNA termed ds512B. While most modifications did not significantly alter J2 binding affinity, 5moU-modified ds512B exhibited a significant reduction in anti-dsRNA signal AUC of approximately 45 % (Figure 30C-D), indicating that 5moU negatively affects J2 binding. Thus, the actual dsRNA content of 5moU-modified EGFP-Fluc mRNA and 5moU-modified ss512B may be higher than previously observed in Figure 29 and Figure 30A, respectively. In conclusion, accurate quantification of dsRNA content in IVT-mRNA via J2 dot blot requires the interpolation from a standard dilution series of an equally modified dsRNA. This potential inaccuracy in estimating the dsRNA content of 5moU-modified IVTs complicates conclusions about the extent to which 5moU-mediated reduction in innate immune

activation by IVT-mRNA is influenced by a decrease in dsRNA content versus direct effects on receptor binding or activation. Therefore, further experiments are required to elucidate the underlying mechanism, which will be presented in the following chapters. Nevertheless, 5moU-modified mRNA induced the lowest IFNα levels of all tested modifications (Figure 27, Figure 28), thus representing a promising modification for mRNA therapeutics, irrespective of the causative factor.

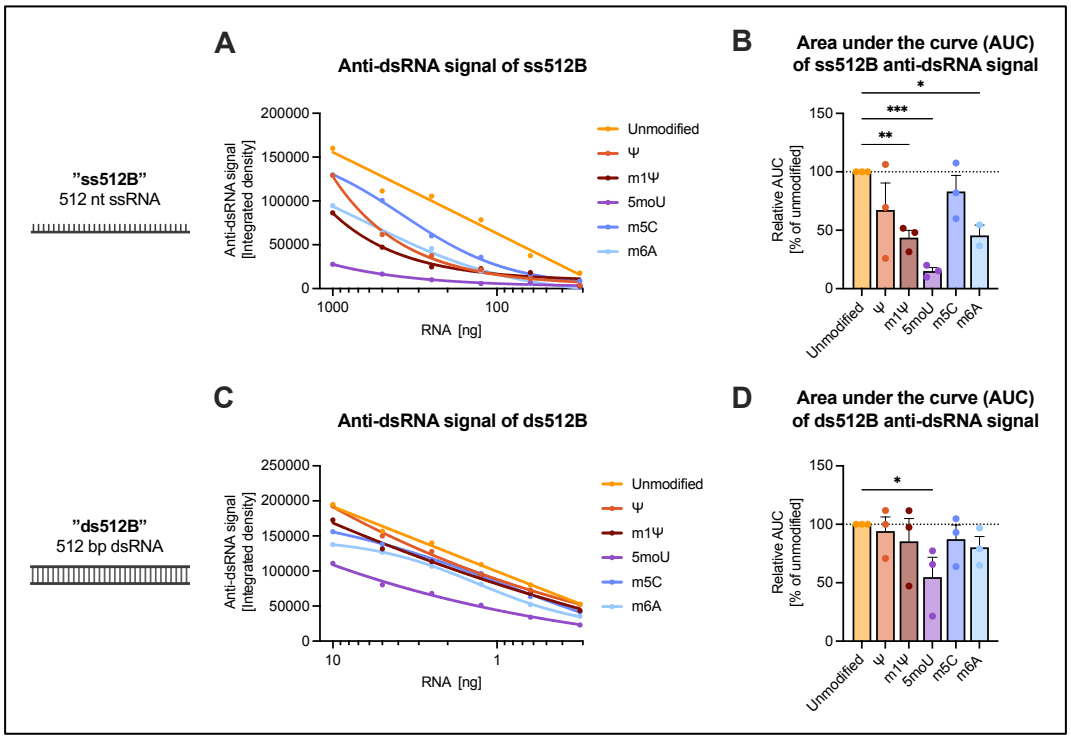

Figure 30: Modulation of dsRNA content in a 512 nt *in vitro* transcript and J2 affinity by nucleoside modifications Integrated density of the anti-dsRNA signal of (A) ss512B and (C) ds512B dot blots. (B, D) Area under the curve (AUC) of the anti-dsRNA signal depicted in (A) and (C), respectively, normalized to unmodified mRNA. Mean + SEM of three independent experiments. For m6A-modified ss512B, one data point was identified as outlier based on EtBr staining and removed from the analysis. Statistical significance was determined by comparing each data set to the unmodified control using one-way ANOVA. * $p < 0.05$, ** $p < 0.01$, *** $p < 0.001$.

In summary, nucleoside modifications differentially reduce the generation of dsRNA byproducts during *in vitro* transcription. While 5moU-modified IVTs exhibited the lowest anti-dsRNA signals, a 5moU-modified dsRNA demonstrated a reduced binding affinity of the J2 antibody compared to unmodified dsRNA, thus challenging the estimation of dsRNA content in 5moU-modified IVTs. The correlation of reduced dsRNA and RLR activation supports the notion that the reduction of dsRNA byproducts is in part responsible for reduced innate immune activation by modified mRNA vaccines. Nevertheless, the differential RLR activation in human and murine cells in response to Ψ- and m1Ψ-modified mRNA indicates further effects that are independent of overall dsRNA content. Additionally, Ψ had ambiguous effects on the dsRNA content of different RNAs indicating correlations to RNA length, sequence, or other currently unknown influences.

3.2.3 Modulation of RIG-I activation by nucleoside modifications

The reduction of immunogenic dsRNA byproducts by incorporation of nucleoside modifications into IVT-mRNA has been implicated as the main reason for the modulated innate immune responses to modified mRNA vaccines. Nevertheless, some findings indicate the presence of direct effects of nucleoside modifications on binding or activation of innate RNA receptors. For example, the ssRNA receptor TLR7 is directly inhibited by m1Ψ, as demonstrated in Chapter 3.1.5, Figure 26. Furthermore, Durbin *et al.* indicated reduced binding affinities of RIG-I to modified RNAs.[150]

In the following, the goal was to characterize whether the reduction of RIG-I activation by nucleoside modifications is mediated solely by a reduced dsRNA content or whether direct impediments with RIG-I binding or activation are involved. To this end, a short single-stranded 24 nt ssRNA, which itself is not sensed by RIG-I, was used to estimate the generation of double-stranded byproducts capable of activating RIG-I. Additionally, a double-stranded hairpin RNA of 56 nt (26 bp + 4 nt loop) was utilized as an optimal RIG-I ligand to investigate the direct effects of nucleoside modifications on RIG-I activation independent of IVT byproducts. The RNAs were transfected into BLaER1 cells and BMDCs to enable the comparison of human and murine RIG-I. Due to their different potency in activating RIG-I, as determined by dose-response titrations (Figure 32 and data not shown), different concentrations of ss- and dsRNA were used.

When incorporated into the 24 nt ssRNA, the modifications modulated RIG-I-dependent IFNα production similarly as observed previously using the EGFP-Fluc mRNA in both species (Figure 31A-B). Again, all uridine modifications significantly reduced activation of RIG-I in both species. While the reduction of RIG-I-mediated IFNα levels by uridine modifications ranged from 40 to 80 % in human BLaER1 cells, murine RIG-I was far more affected and murine IFNα levels were reduced by at least 99 % (Figure 31A-B). The 5moU-modified RNA was once more the least immunogenic in both species (Figure 31A-B). The modification m5C had no effect on RIG-I-dependent IFNα levels in human BLaER1 cells, but caused a reduction of approximately 50 % in murine BMDCs (Figure 31A-B). The m6A-modified RNA reduced RIG-I activation by 60 % in BLaER1 cells and by 80 % in BMDCs.

In contrast, the RIG-I-dependent IFNα response of human BLaER1 cells to the 26 bp dsRNA was largely unaffected by most nucleoside modifications (Figure 31C). Only 5moU caused a slight but significant reduction of human RIG-I activation of approximately 25 %. In murine BMDCs, the modulation pattern of RIG-I activation by modified nucleosides remained similar to that of the 24 nt ssRNA, although the extent of inhibition was considerably less pronounced (Figure 31D). Ψ and m1Ψ reduced murine RIG-I activation by approximately 35 % and 65 %, respectively. Similarly, m5C and m6A reduced murine RIG-I activation by approximately 20 % and 40 %, respectively.

In contrast, the 5moU-modified dsRNA did not activate murine RIG-I (Figure 31D), as observed for the 5moU-modified ssRNA (Figure 31B).

These findings demonstrate that the reduced activation of RIG-I by modified nucleosides is mainly mediated by a reduction of dsRNA content rather than direct inhibition, especially for human RIG-I (Figure 31C-D). In contrast, murine RIG-I seems to exhibit some sensitivity to nucleoside modifications even in dsRNA ligands, with its activity being completely abrogated by 5moU. By comparison, human RIG-I presented only a minor impediment by 5moU (Figure 31C). Finally, given the preceding ambiguous effects of Ψ on dsRNA content of IVTs, the present findings once again suggest a reduction of dsRNA content by Ψ for the 24 nt ssRNA. Of note, the dsRNA content of these short RNAs could not be investigated via dot blot because the J2 antibody requires at least 40 bp of dsRNA for binding.[179]

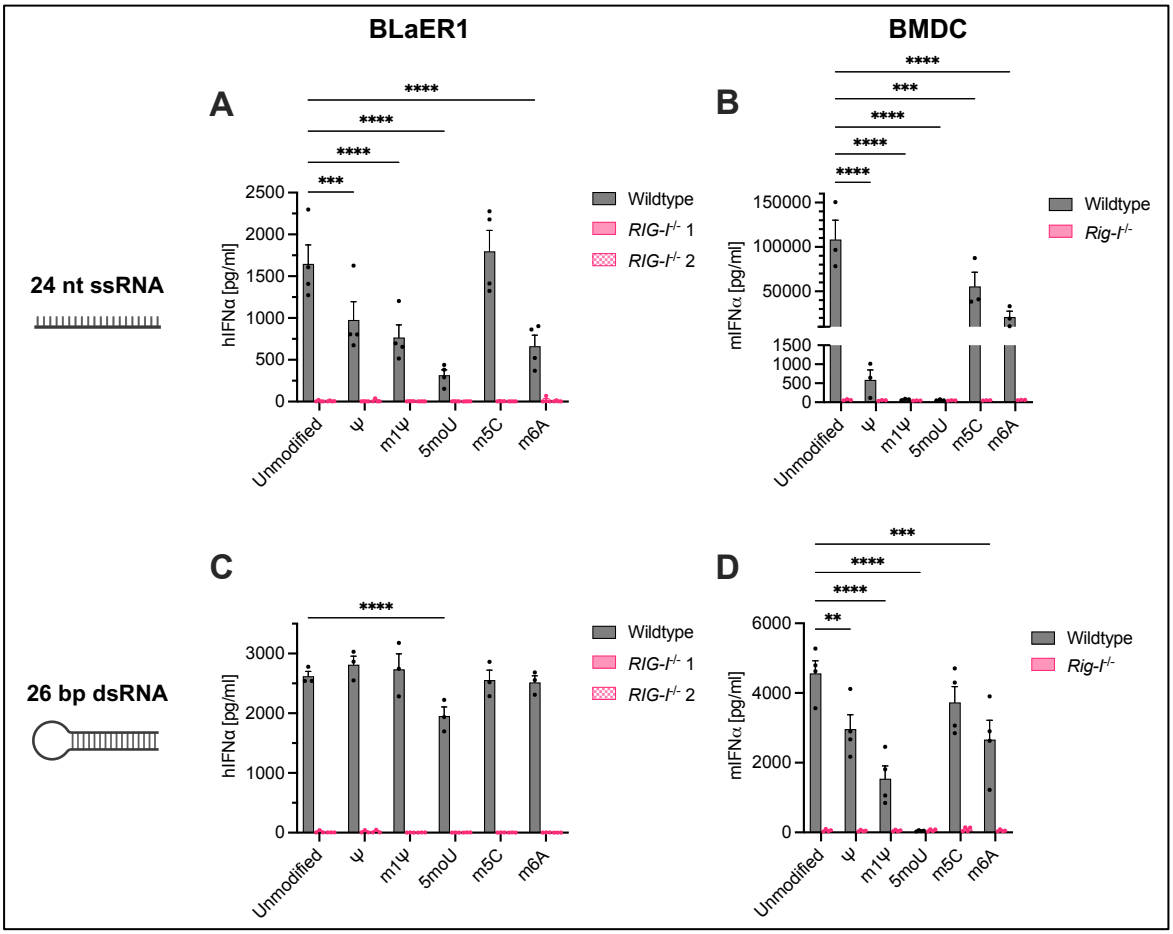

Figure 31: Direct modulation of RIG-I activation by nucleoside modifications

(A), (C) BLaER1 cells were transfected with (A) 250 ng/ml 24 nt ssRNA or (C) 100 ng/ml 26 bp dsRNA incorporating indicated nucleoside modifications. (B), (D) BMDCs were transfected with (B) 1000 ng/ml 24 nt ssRNA or (D) 100 ng/ml 26 bp dsRNA incorporating indicated nucleoside modifications. IFNα production was quantified after 18 hours via ELISA. Mean + SEM of at least three independent experiments. Statistical significance was determined by comparing each modification to the unmodified control within wildtype cells using two-way ANOVA with Dunnett's multiple comparisons test. For BLaER1 cells, only the higher p value of two corresponding clones is shown. * $p < 0.05$, ** $p < 0.01$, *** $p < 0.001$, **** $p < 0.0001$.

Next, a dose-response titration of the 26 bp dsRNA was assessed in BLaER1 cells and BMDCs. For all modifications except 5moU, activation of human RIG-I in BLaER1 cells remained unaffected by nucleoside modifications across several orders of magnitude of dsRNA concentration (Figure 32A, B), in line with the preceding results. For 5moU, the area under the curve (AUC) of the IFNα response was reduced by approximately 30 % compared to the unmodified dsRNA (Figure 32B). Strikingly, no activation of murine RIG-I was observed in BMDCs in response to 5moU-dsRNA, even at high concentrations of up to 2000 ng/ml (Figure 32C, D), indicating a strong direct impairment of murine RIG-I activation by 5moU. In addition, Ψ and m1Ψ reduced the RIG-I-mediated IFNα response of BMDCs, decreasing the AUC by approximately 30 % and 35 %, respectively (Figure 32C, D), in line with previous findings of this study. Activation of murine RIG-I via dsRNA was unaffected by m5C, in line with previous results (Figure 31D, Figure 32B). Although a reduced activation of murine RIG-I by m6A-modified dsRNA was observed in the previous experiment using 100 ng/ml (Figure 31D), no consistent reduction could be observed throughout the titration curve or the AUC (Figure 32C, D).

In summary, these findings confirm that the previously observed reduction of human RIG-I activation by ssRNA incorporating Ψ, m1Ψ, 5moU, or m6A, is primarily mediated by a decrease of dsRNA byproducts. For 5moU, additional direct impairment of human RIG-I is also contributing to the reduced response. M5C did not affect human RIG-I activation by either mechanism. As expected, the reduced dsRNA content likewise affected activation of murine RIG-I. However, murine RIG-I was directly impaired by Ψ, m1Ψ, and 5moU, the latter, in particular, completely blocking activation of murine RIG-I by currently unknown mechanisms.

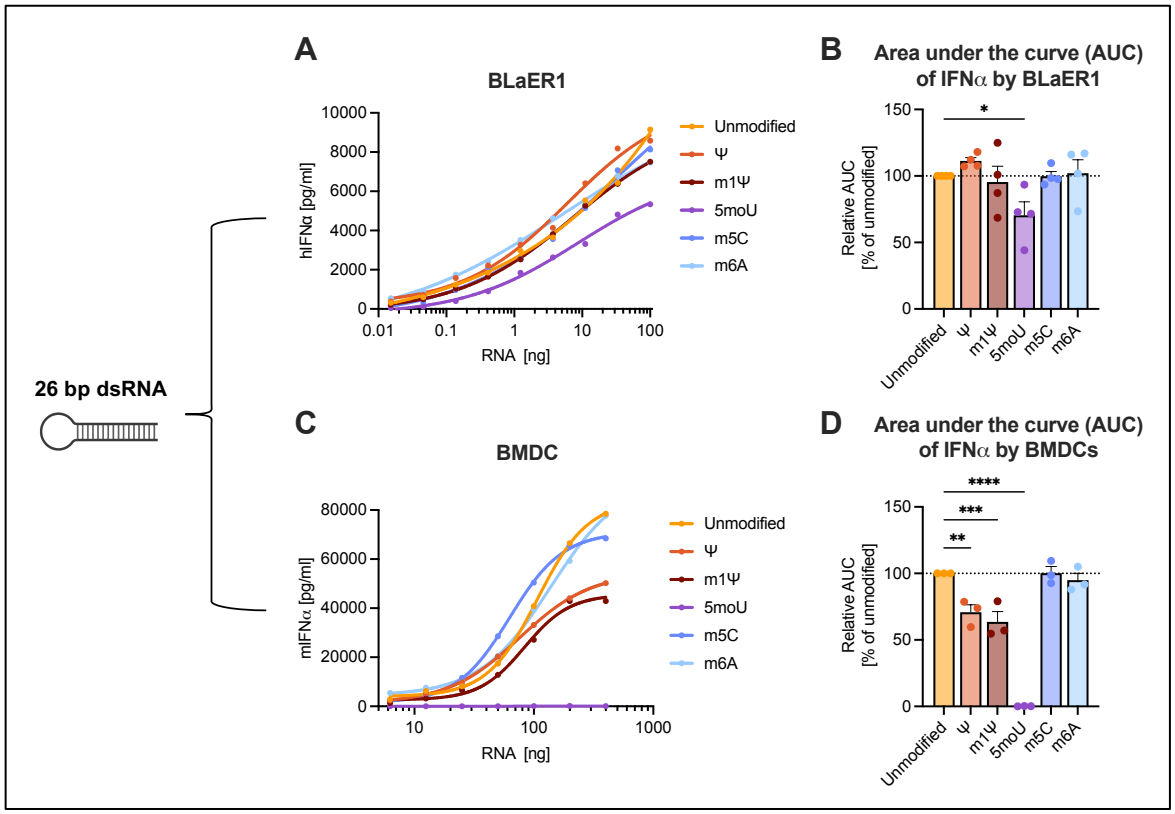

Figure 32: Activation of murine RIG-I is completely abolished by incorporation of 5moU
(A) BLaER1 cells and (C) BMDCs were transfected with indicated amounts of 26 bp dsRNA incorporating indicated nucleoside modifications. IFNα production was quantified after 18 hours via ELISA. Mean of at least three independent experiments. (B, D) Area under the curve (AUC) of IFNα response depicted in (A) and (C), respectively, normalized to unmodified mRNA. Mean + SEM of at least three independent experiments. Statistical significance was determined by comparing each data set to the unmodified control using one-way ANOVA. * $p < 0.05$, ** $p < 0.01$, *** $p < 0.001$, **** $p < 0.0001$.

The prior findings indicate a differential modulation of human and murine RIG-I by nucleoside modifications. However, human and murine RIG-I were tested in the context of the human and murine cells, respectively, meaning that other species-specific or cell type-dependent effects could in part (or totally) be responsible for these differences rather than the activities of human and murine RIG-I themselves. To enable a more direct comparison, human or murine RIG-I was expressed in human MDA5$^{-/-}$ RIG-I$^{-/-}$ THP-1 cells via lentiviral transduction. Subsequently, these cell lines were transfected with the 24 nt ssRNA or the 26 bp dsRNA incorporating the nucleoside modifications of interest, and CXCL10 production was measured via ELISA as a readout for RIG-I activation. To assess the relative modulation of human and murine RIG-I activation by the modifications, CXCL10 levels were normalized to the unmodified control RNA.

Using the 24 nt ssRNA, the inhibition of RIG-I activation by uridine modifications was confirmed for both species (Figure 33A). Reduction of human RIG-I activation by uridine modifications ranged from 30 to 70 % (Figure 33A), in line with the preceding results (40 to 80 % reduction in BLaER1 cells, Figure 31A). Murine RIG-I was again significantly more affected than human RIG-I, and the CXCL10 response was reduced by 95 % (Figure 33A), in line with what was observed previously

(99 % reduction in BMDCs, Figure 31B). M5C did not affect activation of human RIG-I but reduced activation of murine RIG-I by 30 % (Figure 33A), likewise in line with previous data (no effect in BLaER1 cells, 50 % reduction in BMDCs, Figure 31A-B). While m6A reduced activation of both human and murine RIG-I, the latter was again more strongly affected (20 % versus 70 % reduction, (Figure 33A), similar to what was observed previously (60 % reduction in BLaER1 cells, 80 % reduction in BMDCs, Figure 31A-B).

Likewise, the RIG-I-dependent CXCL10 response to the 26 bp dsRNA confirmed the preceding findings observed in human BLaER1 cells and murine BMDCs. Human RIG-I was unaffected by nucleoside modifications in the dsRNA ligand, but exhibited a weak inhibition of approximately 25 % by 5moU (Figure 33B), in line with previous results (25 % reduction in BLaER1 cells, Figure 31C). In contrast, murine RIG-I exhibited direct mechanistic sensitivities to all uridine modifications. Ψ and m1Ψ reduced murine RIG-I activation by approximately 10 % and 45 %, respectively (Figure 33B), similar to preceding results (35 % and 65 % reduction in BMDCs, Figure 31D). Importantly, 5moU once again abrogated activation of murine RIG-I (Figure 33B), in line with the data from BMDCs (Figure 31D). M5C and m6A did not affect activation of human nor murine RIG-I by the dsRNA (Figure 33B), in line with the dose-response titration using BLaER1 cells and BMDCs (Figure 32).

In summary, the species-specific modulation of RIG-I activation by nucleoside modifications initially observed in human BLaER1 cells and murine BMDCs could be reproduced within one cell type by lentivirally expressing the receptors in MDA5$^{-/-}$ RIG-I$^{-/-}$ THP-1 cells. These data indicate that the observed differences between human and murine RIG-I are indeed substantially mediated by differences in the receptors themselves.

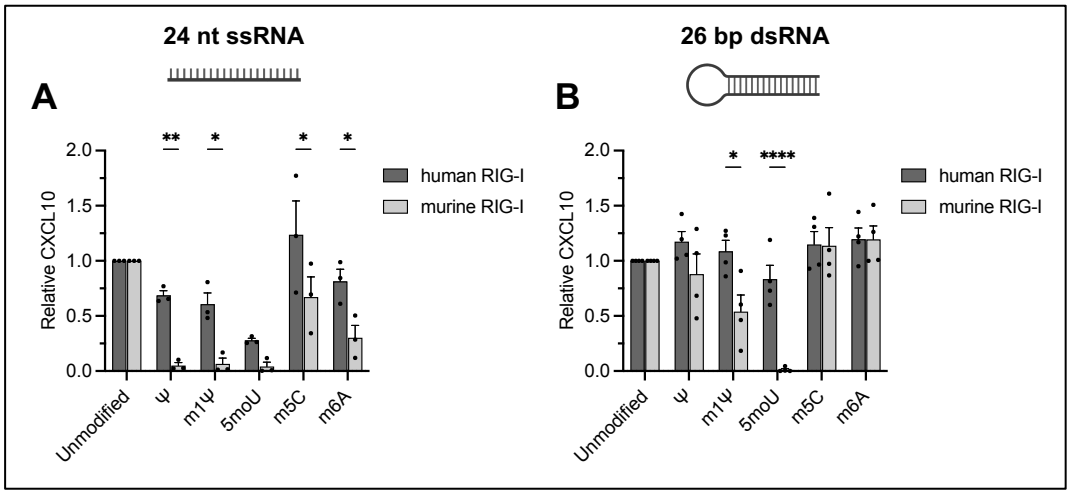

Figure 33: Human and murine RIG-I exhibit different sensitivities to modified nucleosides
MDA5$^{-/-}$ RIG-I$^{-/-}$ THP-1 cells were lentivirally transfected with either human or murine RIG-I under the EF1α promoter and stimulated with (A) 1.5 μg/ml 24 nt ssRNA or (B) 100 ng/ml 26 bp dsRNA incorporating indicated nucleoside modifications. CXCL10 production was quantified after 24 hours via ELISA and normalized to the unmodified control. Mean + SEM of at least three independent experiments. Statistical significance was determined by comparing the human and murine RIG-I response for each modification using two-way ANOVA. * $p < 0.05$, ** $p < 0.01$, *** $p < 0.001$, **** $p < 0.0001$.

In summary, the presented findings demonstrate that the reduction of RIG-I activation by nucleoside modifications is majorly mediated by a reduced generation of IVT byproducts, especially for human RIG-I. However, in addition to the effects of reduced dsRNA content, human RIG-I seems to be directly affected by 5moU, and murine RIG-I seems to be directly affected by all tested uridine modifications. Strikingly, 5moU completely abrogates the activation of murine RIG-I over a broad range of concentrations (two orders of magnitude) including any feasible concentration for *in vivo* application. These findings extent the differences in human and murine RIG-I responses to m1Ψ-modified mRNA already shown in collaboration with AG Bartok and Hartmann to other important uridine modifications, including the previously unknown species-specific inhibitory function of 5moU on murine RIG-I, and emphasize the importance of nucleoside modifications for the modulation of potentially immunostimulatory byproducts generated during *in vitro* transcription.

3.2.4 Modulation of MDA5 activation by nucleoside modifications

In preceding results of this study, the incorporation of m1Ψ reduced the dsRNA content of EGFP-Fluc mRNA by approximately 10 % (Chapter 3.2.2, Figure 29C, D). However, the activation of murine MDA5 was enhanced by this mRNA (Chapter 3.2.1, Figure 28B). A similar phenomenon was observed for the SC-IVT: data by Dr. Thomas Zillinger confirmed a reduction of dsRNA by m1Ψ (data not shown), but activation of murine MDA5 was significantly enhanced, to an even greater extent than observed for EGFP-Fluc mRNA (Chapter 3.1.5, Figure 24). These findings indicate a direct effect of m1Ψ on murine MDA5 that is independent of overall dsRNA content.

In the following, the mechanisms causing modulation of MDA5 activation by nucleoside modifications were assessed. Analogous to the experiments focusing on RIG-I, single-stranded and double-stranded ligands were utilized to assess the individual contribution of reduced dsRNA formation or direct inhibitory effects of nucleoside modifications on MDA5. A major challenge in this investigation is the fact that an optimal ligand for MDA5 has not yet been described. In a preceding study, Mu *et al.* utilized the ss512B to study the modulation of MDA5 activation by nucleoside modifications.[25] They found that during *in vitro* transcription, a promoter-independent antisense transcription caused the formation of a full-length 512 bp duplex (ds512B).[25] Using transient MDA5 overexpression in HEK 293T cells, Mu *et al.* reported that this ds512B activated MDA5, which was reduced by the incorporation of Ψ, m1Ψ, and m5C, but not m6A. Of note, 5moU was not investigated by Mu *et al.* Furthermore, MDA5 activation was apparently not directly affected by these modifications but only via a reduction of the full-length duplex formation.

Given the heterogeneity of MDA5 modulation by nucleoside modifications in human and murine cells observed in preceding chapters, the first aim was to reproduce the findings of Mu *et al.* by transfecting ss512B and ds512B in human BLaER1 cells and murine BMDCs. Due to their different potency in activating MDA5, as determined by dose-response titrations (Figure 35), different concentrations of ss- and dsRNA were used. Although the 512B RNA has been introduced as an MDA5 ligand by Mu *et al.*, the IFNα production by BLaER1 cells in response to ss512B and ds512B was mediated primarily by RIG-I (Figure 34A, C).[25] In BMDCs, the unmodified ss512B induced generally low IFNα levels, which were also dependent on RIG-I (Figure 34B). While the IFNα response by BMDCs was higher for the ds512B, no MDA5 activation could be observed (Figure 34D). Only the incorporation of Ψ and m1Ψ seemed to shift the activation from RIG-I to MDA5 (Figure 34B, D), consistent with previous findings of this study and of the Bartok and Hartmann groups (Chapter 1.4.4, Chapter 3.1.5, Chapter 3.2.1), indicating that these modifications directly enhance activation of murine MDA5. Of note, the modulation of ss/ds512B-induced RIG-I activation by nucleoside modifications was in line with preceding findings.

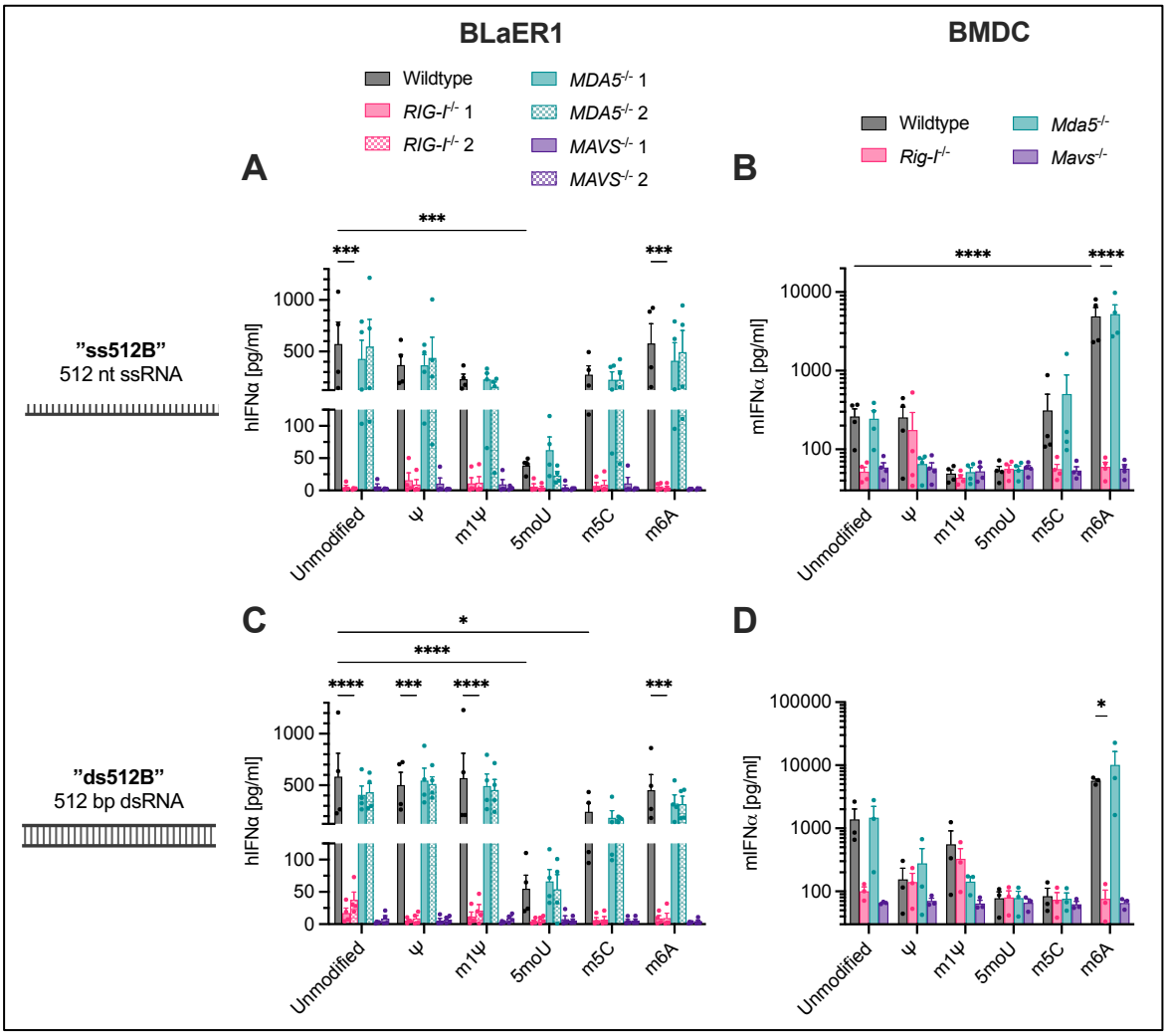

Figure 34: Putative MDA5 ligand primarily activates RIG-I in BLaER1 cells and BMDCs
(A), (C) BLaER1 cells were transfected with (A) 500 ng/ml ss512B or (C) 0.05 ng/ml ds512B incorporating indicated nucleoside modifications. (B), (D) BMDCs were transfected with (B) 1000 ng/ml ss512B or (D) 0.05 ng/ml ds512B. IFNα production was quantified after 18 hours via ELISA. Mean + SEM of at least three independent experiments. Statistical significance was determined using two-way ANOVA with Tukey's multiple comparisons correction. Comparisons of modifications to unmodified are only depicted for wildtype cells. Within each stimulus, only comparisons of RIG-I and MDA5 knockouts to the wildtype are displayed. For BLaER1 cells, only the higher p value of two corresponding clones is shown. * $p < 0.05$, ** $p < 0.01$, *** $p < 0.001$, **** $p < 0.0001$.

Given the weak IFNα response of BMDCs to ss- and ds512B, a range of RNA concentrations was assessed to investigate the maximal innate immune stimulation by these RNAs. Interestingly, RNA concentrations above those used in earlier experiments only caused reduced IFNα production in both cell types, indicating cytotoxic effects or potential PKR-mediated translational arrest (Figure 35). Therefore, these findings confirm that the settings used in Figure 34 were ideal to study activation of RIG-I and MDA5 by both ss- and ds512B and that the absence of MDA5 activation cannot be attributed to an insufficient RNA concentration. Instead, these data indicate that these RNAs are in fact not MDA5 but RIG-I ligands.

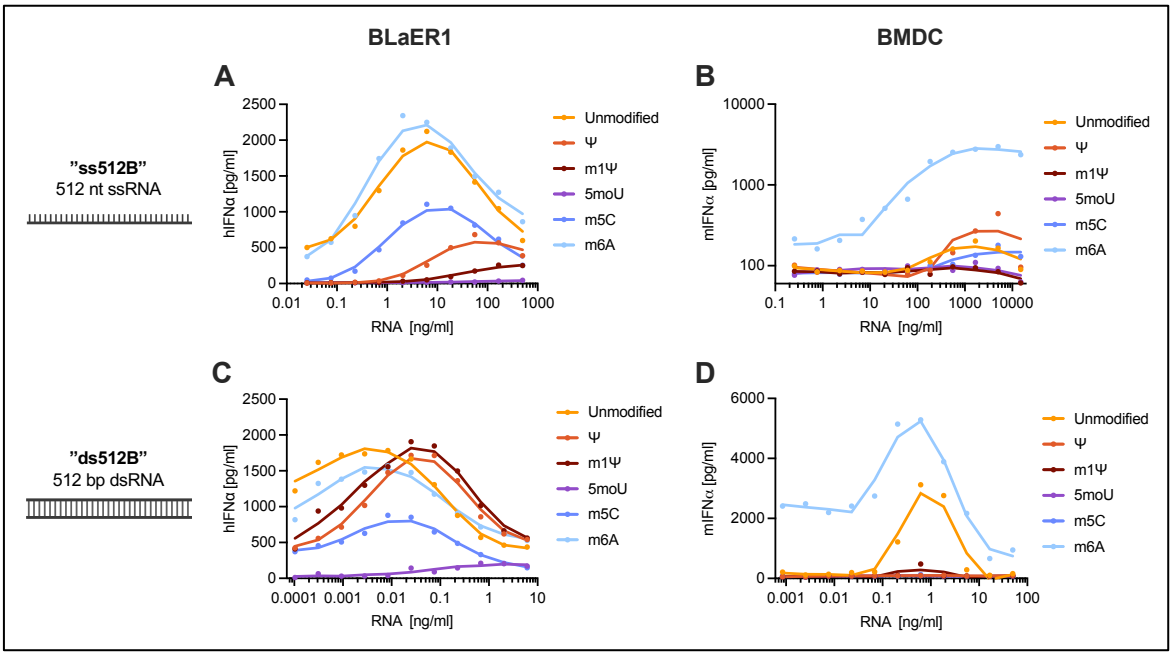

Figure 35: Quantitative analysis of 512B-induced immune stimulation in BLaER1 cells and BMDCs
(A, C) BLaER1 cells or (B, D) BMDCs were transfected with indicated amounts of (A-B) ss512B or (C-D) ds512B incorporating indicated nucleoside modifications. IFNα production was quantified after 18 hours via ELISA. Mean of at least three independent experiments.

In analogy to Figure 33, the potential activation of MDA5 by ss- and ds512B independent of RIG-I activation and possible cell type-mediated effects was investigated by lentiviral transduction of MDA5$^{-/-}$ RIG-I$^{-/-}$ THP-1 cells with either human or murine MDA5. These cell lines were then stimulated with the ss- and ds512B, and CXCL10 responses were quantified using ELISA. While this setting is analogous to the experiments focusing on RIG-I presented in the preceding chapter, CXCL10 production was not normalized to the unmodified control to enable the estimation of overall signal strength of the MDA5 response. Additionally, THP-1 cells stably transfected with GFP are depicted to estimate the background CXCL10 level for comparison.

The functional overexpression of human and murine MDA5 was confirmed using poly(I:C) and EMCV RNA, which induced CXCL10 production in cells transduced with human or murine MDA5 but not in GFP-expressing cells (Figure 36A). Furthermore, the absence of endogenous RIG-I activity was validated by transfection of the RIG-I ligand 5′ppp-dsRNA.

In line with preceding results, the ss512B RNA induced nearly no MDA5 activation, despite a weak CXCL10 induction by human MDA5 in response to Ψ- and m5C-modified ss512B (Figure 36B), indicating either insufficient amounts of the putatively MDA5-activating duplex byproduct, or the inability of named byproduct to activate MDA5 at all. Murine MDA5 did not respond to transfection of ss512B or ds512B (Figure 36B-C), in contrast to the previously observed MDA5 response in BMDCs to the Ψ-modified ss512B and m1Ψ-modified ds512B (Figure 34B, D). The unmodified and Ψ-modified ds512B induced a significant activation of human MDA5 (Figure 36C), in contrast to the results observed for BLaER1 cells (Figure 34C). This ds512B-induced activation of human

MDA5 seemed to be abolished by all other modifications (Figure 36C). Although the ds512B was able to activate human MDA5 in this setting, the CXCL10 levels were at least one order of magnitude lower than those observed for poly(I:C) and EMCV RNA, respectively (Figure 36A, C). Together with the absence of MDA5 activation in BLaER1 cells and BMDCs, these findings indicate that the ds512B is not an optimal ligand for MDA5, thus challenging previous observations published by Mu *et al.* regarding the modulation of MDA5 activation by nucleoside modifications.[25]

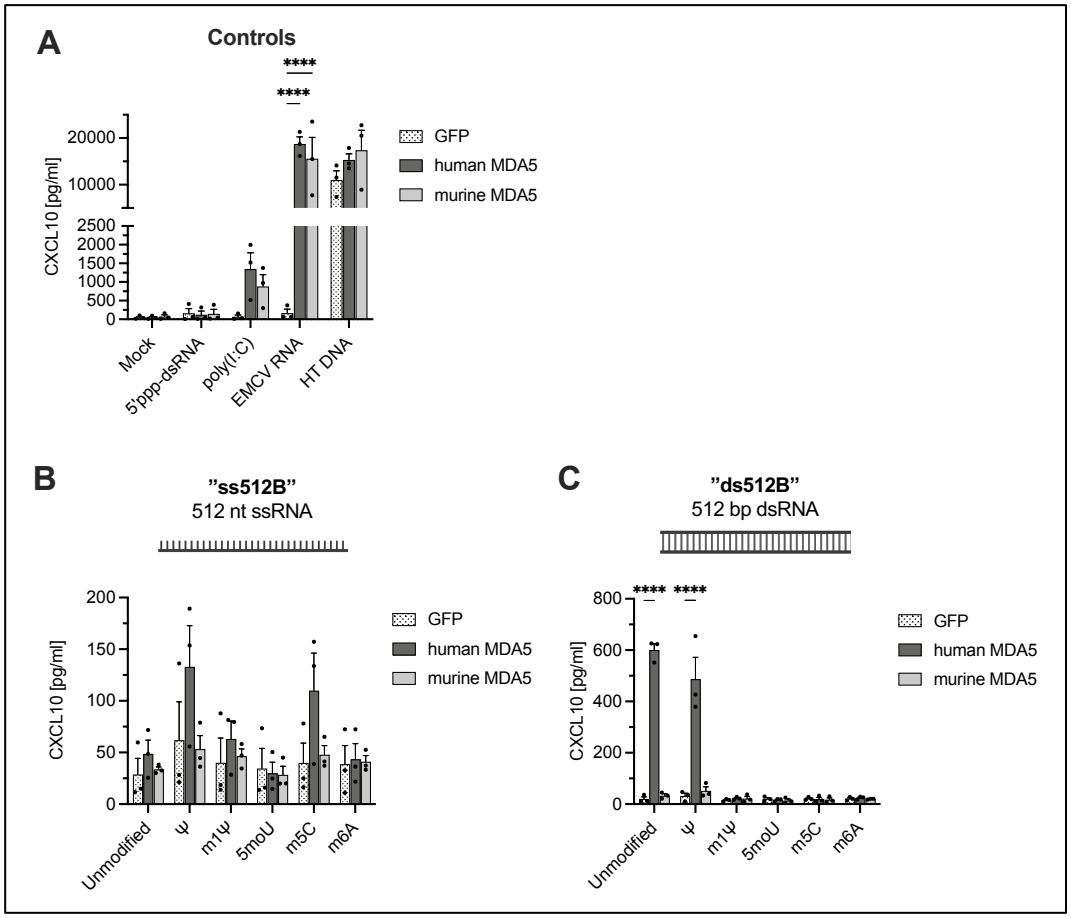

Figure 36: ds512B does not activate murine MDA5 and induces only weak activation of human MDA5
THP-1 cells deficient in endogenous MDA5 and RIG-I were stably transfected with either human or murine MDA5 and stimulated with (A) controls, (B) 2.5 μg/ml ss512B, or (C) 0.5 ng/ml ds512B incorporating indicated nucleoside modifications. CXCL10 production was quantified after 24 hours via ELISA. Mean + SEM of three independent experiments. Statistical significance was determined by comparing human and murine MDA5 to the GFP control, respectively, using two-way ANOVA and Dunnett's multiple comparisons test. **** $p < 0.0001$.

Apart from the evident contradiction concerning the activity of ds512B as MDA5 ligand, the effects of nucleotide modifications on MDA5 activation proposed by Mu *et al.* also conflict with the data presented in this study.[25] Of note, Mu *et al.* only investigated human MDA5, and comparing their findings to murine data of this study would be inappropriate, since any divergence could potentially be attributed to species-specific differences of MDA5, as observed previously for RIG-I.

Nevertheless, Mu *et al.* suggested an inhibition of human MDA5 activation by incorporation of Ψ and m5C into ss512B.[25] However, ss512B-mediated activation of human MDA5 in the overexpression model based on MDA5$^{-/-}$ RIG-I$^{-/-}$ THP-1 cells was enhanced by Ψ and m5C (Figure 36B), contradicting the effects proposed by Mu *et al*.[25]

Since Mu *et al*. used transient MDA5 overexpression in HEK 293T cells, a plausible explanation would be that the observed immune response to ss512B and its modulation by nucleoside modifications was in fact mediated by the unintentional activation of endogenous RIG-I. HEK 293 cells are indeed capable of mounting RIG-I-dependent immune responses.[180] To test this hypothesis, the experiments by Mu *et al.* were repeated by transiently expressing either human MDA5 or the negative control GFP in wildtype and *RIG-I*$^{-/-}$ HEK 293 cells together with reporter plasmids and stimulating the cells with modified ss512B. Subsequently, innate immune activation was quantified based on the activity of Gaussia luciferase (Gluc) expressed under the control of the IFNβ promoter and was normalized to the signal of Cypridina luciferase (Cluc), which was controlled by the EF1α promoter as a measure of overall translation.

The transfection of a 5′ppp-dsRNA confirmed the absence of functional RIG-I in *RIG-I*$^{-/-}$ HEK 293 cells (Figure 37A). Likewise, poly(I:C) and EMCV RNA validated the successful overexpression and activation of human MDA5 in both cell lines. Strikingly, the wildtype HEK cells indeed exhibited a similar IFNβ-reporter profile in response to ss512B as previously described by Mu *et al.*, such as a reduction of immune response by Ψ, m1Ψ, and m5C, but not m6A.[25] However, this response was independent of the overexpression of MDA5 (Figure 37B). Furthermore, no response to ss512B was observed in *RIG-I*$^{-/-}$ HEK cells, confirming that the results presented by Mu *et al.* were obscured by activation of endogenous RIG-I and did not reflect activation of human MDA5. Therefore, it is evident that wildtype HEK cells are not suitable to study the activation of MDA5 and that the ss- and ds512B are not MDA5 ligands. Of note, a very weak activation of human MDA5 could be observed for the m1Ψ-modified ss512B (1.6-fold compared to the corresponding GFP-expressing control), in contrast to previous observations from human BLaER1 cells and overexpression of human MDA5 in MDA5$^{-/-}$ RIG-I$^{-/-}$ THP-1 cells, which did not exhibit human MDA5 activation by m1Ψ-modified ss512B nor ds512B (Figure 34A,C; Figure 36B-C).

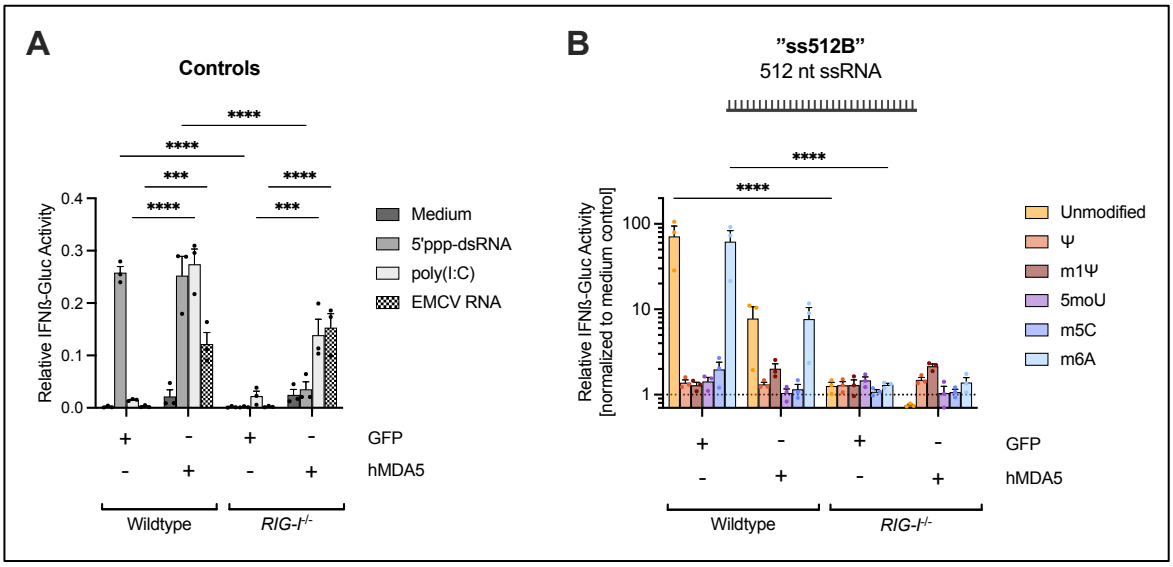

Figure 37: Activation of endogenous RIG-I invalidates MDA5 overexpression studies in HEK 293 wildtype cells
Wildtype or *RIG-I*$^{-/-}$ HEK 293 cells were transiently transfected with GFP- or hMDA5-expressing plasmids as well as EF1α-Cypridina-luciferase (Cluc) and IFNβ-Gaussia-luciferase (Gluc) reporter plasmids. After 8 hours, the cells were additionally stimulated with either (A) indicated controls or (B) 1 µg/ml ss512B incorporating indicated nucleoside modifications. Luciferase activities were measured 20 hours after stimulation, and Gluc was normalized to Cluc. Mean + SEM of three independent experiments. Statistical significance was determined using two-way ANOVA. Comparisons are shown for wildtype vs. *RIG-I*$^{-/-}$ and GFP vs. hMDA5 expression; comparisons between individual stimuli are not shown. * $p < 0.05$, ** $p < 0.01$, *** $p < 0.001$, **** $p < 0.0001$. hMDA5 = human MDA5.

Since Kato *et al.* previously reported a dsRNA length requirement of >2000 bp for activation of MDA5, it was hypothesized that the ds512B does not provide sufficient length for MDA5 activation.[23] Therefore, the potential modulation of MDA5 activation via direct mechanistic impairments by nucleoside modifications was investigated using a longer dsRNA than the previously utilized 512B RNA. To this end, the corresponding antisense strand of the EGFP-Fluc mRNA was *in vitro* transcribed and annealed to the sense mRNA, resulting in an approximately 3.2 kb-long dsRNA, termed ds-mRNA. This ds-mRNA was then transfected into *RIG-I*$^{-/-}$ and *MAVS*$^{-/-}$ BLaER1 cells and BMDCs to investigate the activation of MDA5 while excluding RIG-I.

Indeed, the unmodified ds-mRNA induced MDA5-dependent IFNα responses in both cell types and therefore validated its suitability to study the direct effects of nucleoside modifications on MDA5 (Figure 38). In line with preceding findings, the MDA5-dependent IFNα levels of human BLaER1 cells and murine BMDCs were not reduced by Ψ or m1Ψ, indicating that both human and murine MDA5 are not directly inhibited by these modifications (Figure 38). In fact, Ψ significantly enhanced activation of both human and murine MDA5, whereas m1Ψ significantly enhanced activation specifically of murine MDA5 (Figure 38). Given that a similar effect has also been observed using the putatively single-stranded EGFP-Fluc mRNA, although m1Ψ reduced the total dsRNA content of this mRNA, murine MDA5 activation seems to be directly enhanced by Ψ and m1Ψ via currently unknown mechanisms. Besides, the modifications 5moU, m5C, and m6A completely abolished

activation of MDA5 in both BLaER1 cells and BMDCs (Figure 38), indicating a direct mechanistic inhibition of human and murine MDA5 binding or activation by these modifications.

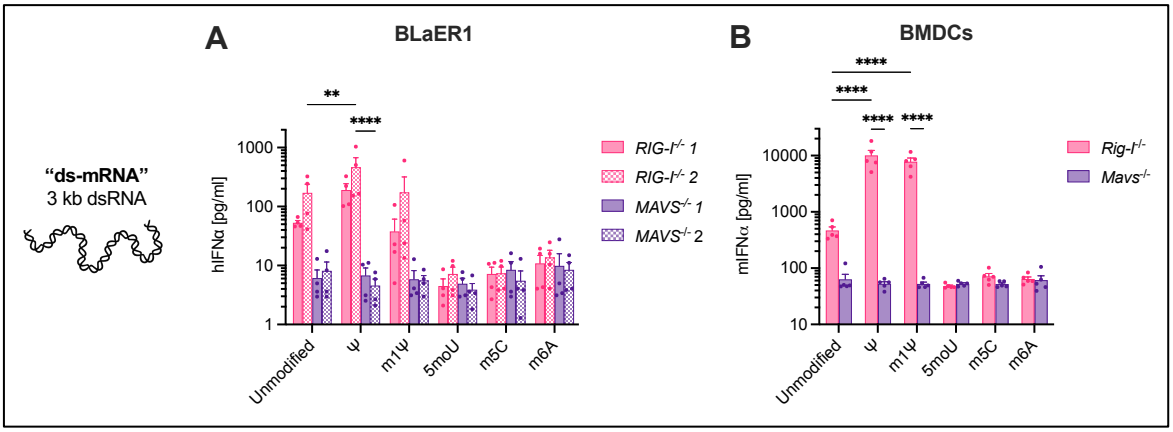

Figure 38: MDA5 activation by a 3 kb dsRNA is abrogated through 5moU, m5C, and m6A
(A) BLaER1 cells and (B) BMDCs were transfected with 1 μg/ml of a 3 kb dsRNA ("ds-mRNA") incorporating indicated nucleoside modifications. IFNα production was quantified after 18 hours via ELISA. Mean + SEM of at least four independent experiments. Statistical significance was determined using two-way ANOVA with Tukey's multiple comparisons correction. Comparisons between stimuli are depicted exclusively to the unmodified control. * $p < 0.05$, ** $p < 0.01$, *** $p < 0.001$, **** $p < 0.0001$.

To further investigate potential differences in the modulation of human and murine MDA5 by nucleoside modifications, the putatively single-stranded EGFP-Fluc mRNA and the ds-mRNA were transfected into the MDA5$^{-/-}$ RIG-I$^{-/-}$ THP-1 cells stably expressing either human or murine MDA5. This time, the CXCL10 induction was normalized first to the GFP-expressing cells and subsequently to the unmodified RNA, to specifically investigate the relative modulation of MDA5 by nucleoside modifications. All modifications seemed to reduce activation of human and murine MDA5 when incorporated into the EGFP-Fluc mRNA, with the exception of Ψ for murine MDA5 (Figure 39A). The CXCL10 response to the ds-mRNA largely confirmed the preceding findings of this study, whereas Ψ and m1Ψ enhance activation of murine MDA5, while human MDA5 activation was only enhanced by Ψ (Figure 39B). In addition, the enhancing effect of Ψ was significantly stronger for murine MDA5 compared to human MDA5 (Figure 39B), in line with results obtained using BLaER1 cells and BMDCs (Figure 38). In contrast, human MDA5 activation was actually reduced by m1Ψ-modified ds-mRNA (Figure 39B), contradicting the MDA5 response previously observed in BLaER1 cells transfected with the m1Ψ-modified ds-mRNA (Figure 38A). Further experiments are required to investigate this discrepancy. Besides, 5moU, m5C, and m6A abrogated activation of both human and murine MDA5 by ds-mRNA via currently unknown direct interactions (Figure 39B).
When investigating the modulation of MDA5 activation by nucleoside modifications, the use of single-stranded mRNA does not enable a differentiation between modulation by altered dsRNA

content or by direct mechanistic effects. However, all effects observed using ds-mRNA indicate direct mechanistic modulation of MDA5 activation by nucleoside modifications.

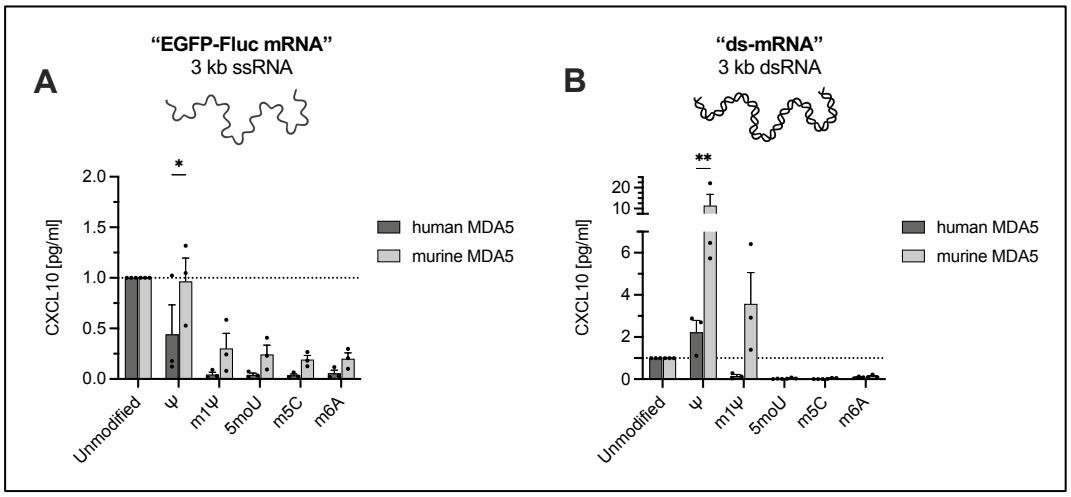

Figure 39: Comparing sensitivities of human and murine MDA5 to modified nucleosides
THP-1 cells deficient in endogenous MDA5 and RIG-I were stably transfected with either human or murine MDA5 and stimulated with (A) 1 μg/ml EGFP-Fluc mRNA or (B) 1 μg/ml ds-mRNA incorporating indicated nucleoside modifications. CXCL10 production was quantified after 24 hours via ELISA. Mean + SEM of three independent experiments. Statistical significance was determined by comparing human and murine MDA5 to the GFP control, respectively, using two-way ANOVA and Dunnett's multiple comparisons test. ** $p < 0.01$, **** $p < 0.0001$.

Investigating the modulation of MDA5 activation by nucleoside modifications reveals that single-stranded mRNA is insufficient to differentiate between modulation by altered dsRNA content and direct mechanistic effects. In contrast, the consistent effects observed with ds-mRNA conclusively demonstrate that some nucleoside modifications directly modulate MDA5 activation. The presented findings suggest that activation of both human and murine MDA5 is enhanced by Ψ, whereas m1Ψ specifically enhances activation of murine MDA5 and inhibits human MDA5. Additionally, the enhancing effect of Ψ appears to be much stronger for murine than for human MDA5. Strikingly, 5moU, m5C, and m6A were found to completely abolish activation of MDA5 in both species. While the underlying mechanisms remain unknown, these effects seem to be independent of dsRNA byproducts, indicating direct mechanistic inhibition of receptor binding or activation.

3.2.5 Modulation of Toll-like receptor activation by nucleoside modifications

While the preceding chapters identified certain nucleoside modifications as promising tools to reduce the activation of RLRs by IVT-mRNA, the immunostimulatory capacity of mRNA vaccines is determined by the sum of all innate immune RNA receptors in the cell. Thus, the EGFP-Fluc mRNA was investigated for potential TLR activation and corresponding modulation by nucleoside modifications. Although previous research regarding TLRs and modified nucleosides exists, some modifications used in this study have not yet been investigated before, such as m1Ψ and 5moU.[111] During the preceding investigation of innate immune responses to the COVID-19 mRNA vaccines, the effect of m1Ψ on TLR activation has been collaboratively investigated by the Bartok and Hartmann groups, and part of this data is presented in Chapter 3.1.5. In the following, the aim was to identify those modifications that are most efficient in inhibiting both RLR and TLR activation in primary human cells, in order to improve the design of future mRNA therapeutics.

To do so, human PBMCs were stimulated with the EGFP-Fluc mRNA using two different transfection reagents: Lipofectamine 2000 for a mainly cytosolic delivery, enabling investigation of RIG-I and MDA5, and poly-L-arginine for a primarily endosomal delivery to study activation of TLR3, TLR7, and TLR8.[181] Additionally, to identify TLR-specific responses, each condition was performed with and without the prior addition of chloroquine (CQ), a drug that prevents endosomal acidification required for TLR activation.[182] Finally, different cytokines were measured via ELISA to enable individual conclusions about the engaged receptors.

IFNα is produced by RIG-I and MDA5 in response to cytosolically delivered RNA, whereas its induction after endosomal delivery indicates activation of TLR7 in specifically pDCs.[38] In line with the important role of RIG-I for mRNA sensing in human cells observed in preceding chapters, the IFNα response to cytosolically delivered mRNA resembled the RIG-I-dependent cytokine patterns observed in BLaER1 cells, with a significant reduction by uridine modifications and m6A (Figure 40A). In contrast, endosomal delivery of the TLR7/8 ligands 9.2S and R848, as well as mRNA, induced very low levels of IFNα, which were nevertheless specific for activation of TLR7, as confirmed by their absence in chloroquine-treated conditions (Figure 40B). Despite the generally weak response, IFNα production was abolished by all uridine modifications, in line with a previous study reporting Ψ-mediated inhibition of TLR7.[111] The inhibition of TLR7 by m1Ψ has already been demonstrated in Chapter 3.1.5, and by others of the Bartok and Hartmann group (data not shown), and is once more confirmed by the present results. Together, these findings demonstrate that activation of TLR7 is inhibited by Ψ, m1Ψ, and 5moU. Of note, a previous study reported inhibitory effects of m5C and m6A on TLR7, which were not observed during this study.[111]

While TLR8 is inactive in mice, it plays a major role in innate nucleic acid sensing of human cells. To investigate potential TLR8 engagement, two cytokines were measured: IL12p70, which is a highly selective readout for human TLR8 activation, and TNFα, a more sensitive readout for TLR8 activation, which is, however, also induced by TLR3, TLR7, RIG-I, and MDA5, albeit to a lesser extent.[38,46,183] As expected, a strong induction of IL12p70 and TNFα was observed in response to endosomal delivery of unmodified mRNA, indicating activation of TLR8 and possibly TLR3 and TLR7 (Figure 40B-C). The IL12p70 and TNFα responses to endosomally delivered mRNA were absent in chloroquine-treated samples, confirming the specific engagement of endosomal TLRs. Of note, the TNFα response to R848 was not affected by chloroquine, likely due to a combination of insufficient chloroquine concentration and too short incubation time prior to transfection, in line with previous studies describing a minor effectiveness of chloroquine on TLR8 activation by R848 compared to nucleic acids.[46,184] The mRNA-induced IL12p70 and TNFα levels were significantly reduced by uridine modifications and m5C, but not m6A (Figure 40B-C). Previous literature demonstrated an inhibition of TLR8 activation by Ψ, m5C, and m6A.[111,185] While the present data support the preceding findings regarding Ψ and m5C, it contradicts an inhibition of TLR8-dependent cytokines by m6A, thus requiring further investigation. Nevertheless, this study provides the first-ever evidence that activation of TLR7 and TLR8 is inhibited by 5moU.

Of note, some donors presented a weak induction of TNFα in response to cytosolic mRNA delivery (Figure 40C). Given the previous findings using human cells, this response was likely mediated by RIG-I, but not MDA5.

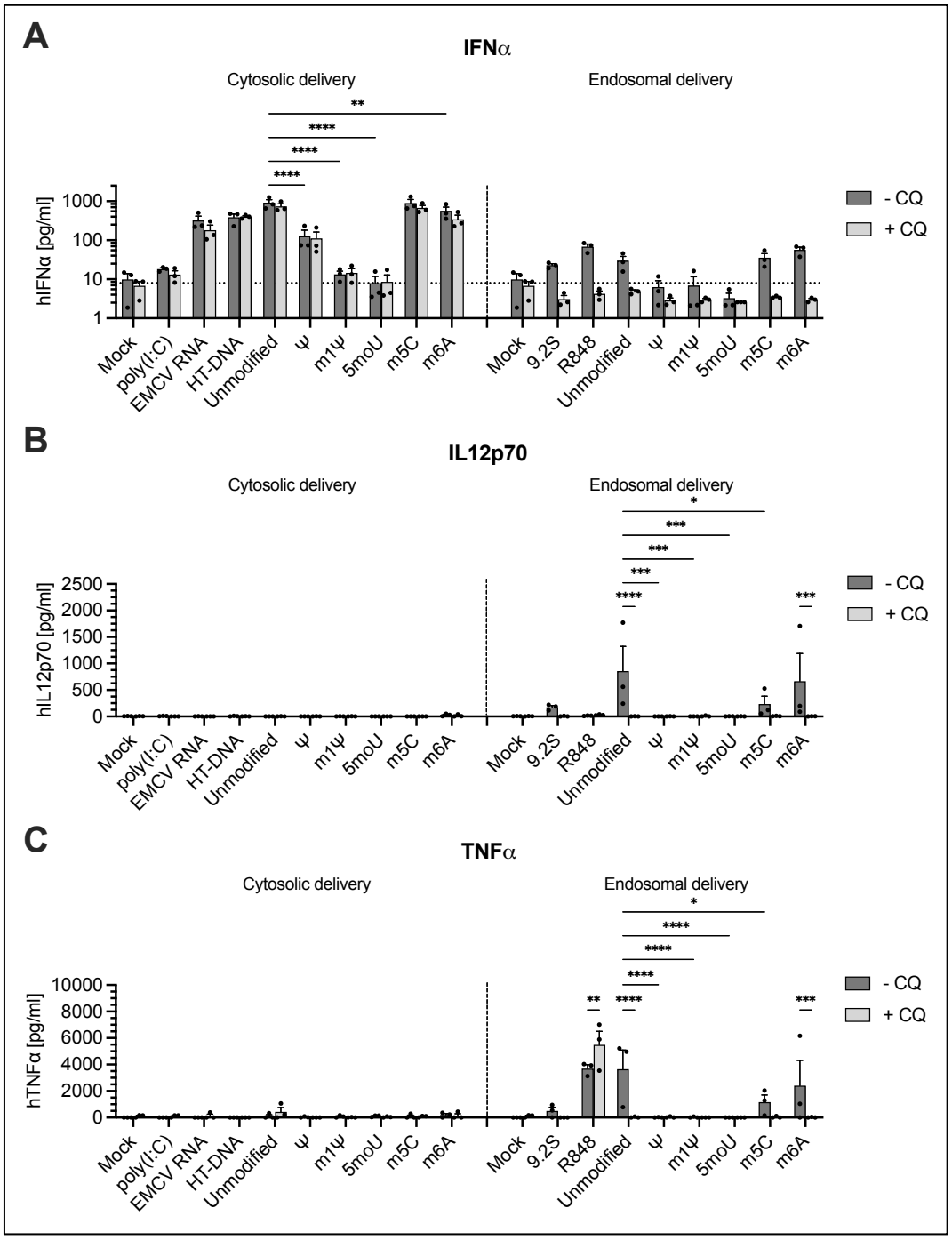

Figure 40: 5moU abolishes mRNA-induced activation of both RLRs and TLRs in human PBMCs
PBMCs were incubated with medium or 10 μM chloroquine (CQ) for 30 minutes and stimulated with indicated controls or 1 μg/ml EGFP-Fluc mRNA incorporating indicated nucleoside modifications. After 18 hours, IFNα, TNFα, and IL12p70 levels were measured via ELISA. Mean + SEM of three independent donors. The dotted line indicates the detection limit. Statistical significance was determined using two-way ANOVA. Comparisons are shown for "- CQ" vs. "+ CQ" and modified vs. unmodified mRNA. * $p < 0.05$, ** $p < 0.01$, *** $p < 0.001$, **** $p < 0.0001$.

In summary, this study demonstrates that activation of TLR7 and TLR8 by IVT-mRNA is abolished by the uridine modifications Ψ, m1Ψ, and 5moU. Given that Karikó *et al.* reported a similar inhibition by 5-methyluridine and 2-thiouridine, the present findings support the conclusion that TLR7 and TLR8 are generally susceptible to uridine modifications.[111] This hypothesis is strongly supported by the fact that both TLR7 and TLR8 were shown to preferentially bind to short uridine-containing RNA degradation products generated by endosomal RNases.[42,43,45,46,186] Besides, TLR8 additionally requires the release of individual uridine from ssRNA.[42]

Since previous literature negates a strong inhibitory effect of Ψ on activation of TLR3, the IFNα response of the present experiments was likely dependent on TLR7.[111] Therefore, the modulation of TLR3 by nucleoside modifications requires further investigation using more appropriate cell systems, such as MDA5$^{-/-}$ HT-29 cells.

Finally, while the activation of TLR7 and TLR8 seems to be completely abolished by uridine modifications in general, RLRs still induce significant immune responses to Ψ- and m1Ψ-modified mRNA in human cells, albeit to a lesser extent than to unmodified mRNA. Given that 5moU was the most effective modification for reducing RLR-dependent cytokine responses and likewise abrogated activation of TLR7 and TLR8, this modification seems a promising candidate for future mRNA therapeutics aiming for minimal innate immune stimulation, such as protein replacement therapy.

3.3 Translation of mRNA incorporating modified nucleosides and effects of innate immune activation

3.3.1 Modulation of mRNA translation by nucleoside modifications

An important contribution to the success of nucleotide modifications besides their reduction of mRNA-induced innate immune responses is their potential to enhance mRNA translation. This phenomenon further improves mRNA vaccine effectiveness by enabling lower dosages and reducing side effects for the patient. Karikó *et al.* were the first group to report that Ψ, and to a lesser extent m5C, increased translation of IVT-mRNA but concurrently found that m6A-modified mRNA was not translated.[117] Although m6A is the most abundant modification in eukaryotic mRNA,[139,140] its negative effect on translation of IVT-mRNA has been confirmed by several subsequent studies.[185,187] Later publications demonstrated that m1Ψ outperforms Ψ regarding enhanced translation and reduced innate immune activation.[83,144,188] However, the available studies on 5moU are limited and while they agree on a generally enhanced translation of 5moU over unmodified mRNA, the extent of which varies and it remains unclear whether 5moU might even exhibit a superior translation over m1Ψ.[144,189]

Since the investigation of mRNA-induced innate immune activation alone is not sufficient to determine the optimal modification for therapeutic application, the mRNA translation was assessed for all tested modifications and cell types. Furthermore, since innate sensing of mRNA was different between human and murine cells, the aim was to rule out any species-specific differences regarding mRNA translation. To do so, EGFP-encoding mRNA incorporating respective nucleoside modifications was transfected into human PBMCs and murine BMDCs. Since human BLaER1 cells already stably express GFP, an mCherry-encoding mRNA was used instead. After transfection, cells were imaged using the Cytation 3 and the mean fluorescent intensity was calculated for EGFP and mCherry, respectively.

Consistent with current literature, uridine modifications were potent enhancers of mRNA translation based on fluorescent protein expression in all tested cell types and achieved 2- to 140-fold increased translation compared to unmodified mRNA (Figure 41). Interestingly, while 5moU-modified mRNA produced the highest mCherry levels in human BLaER1 cells, it was inferior to m1Ψ-modified mRNA in PBMCs and murine BMDCs. In line with previous literature, m5C only moderately increased mRNA translation (1- to 4-fold) while incorporation of m6A abrogated translation in all cell types (Figure 41).[117,185,187] Finally, the modulation of mRNA translation by modified nucleotides was consistent between human and murine cells. Furthermore, the high innate immune activation by Ψ- and m1Ψ-modified mRNAs in BMDCs, as observed in earlier experiments, did not seem to negatively affect their translation (Figure 41C, D).

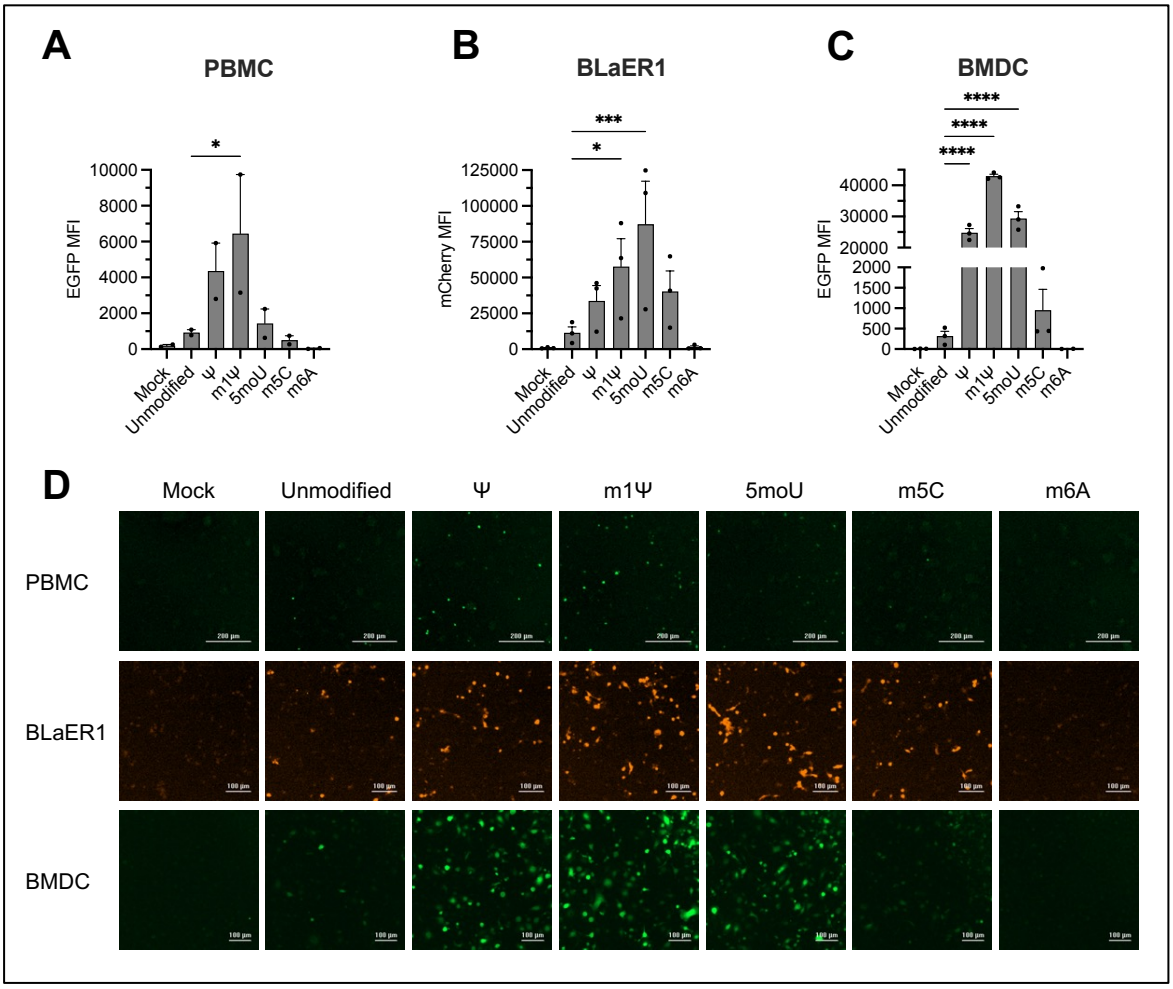

Figure 41: Fluorescent protein expression from EGFP and mCherry mRNAs incorporating modified nucleosides
(A) PBMCs, (B) BLaER1 cells and (C) BMDCs were transfected with 0.8 μg/ml EGFP mRNA or mCherry mRNA, respectively, incorporating indicated nucleoside modifications. After 18 hours, fluorescent protein expression was quantified via microscopic imaging. Mean fluorescent intensity of $EGFP^+$ or $mCherry^+$ cells, respectively. Mean + SEM of two donors or three independent experiments, respectively. An outlier has been excluded from the analysis of m6A-mRNA in BMDCs. Statistical significance was determined by comparing every condition to the unmodified control using one-way ANOVA. * $p < 0.05$, ** $p < 0.01$, *** $p < 0.001$, **** $p < 0.0001$. (D) Microscopy images corresponding to (A-C) representative of two donors or three independent experiments, respectively. Scale bar represents 200 μm for PBMCs and 100 μm for BLaER1 cells and BMDCs.

In order to validate the preceding findings using another mRNA sequence and readout, the EGFP-Fluc mRNA was transfected into PBMCs, BLaER1 cells, and BMDCs, and firefly luciferase activity was quantified as a measure of mRNA translation. In line with preceding results, uridine modifications were the most effective at enhancing mRNA translation (ranging between 5- to 90-fold increase compared to unmodified), while the positive effect of m5C was only moderate (2- to 10-fold increase), and m6A abrogated translation (Figure 42). In contrast to Figure 41B, translation of 5moU was not superior to m1Ψ in BLaER1 cells in this setting, with m1Ψ producing the highest luciferase activity in all cell types (Figure 42).

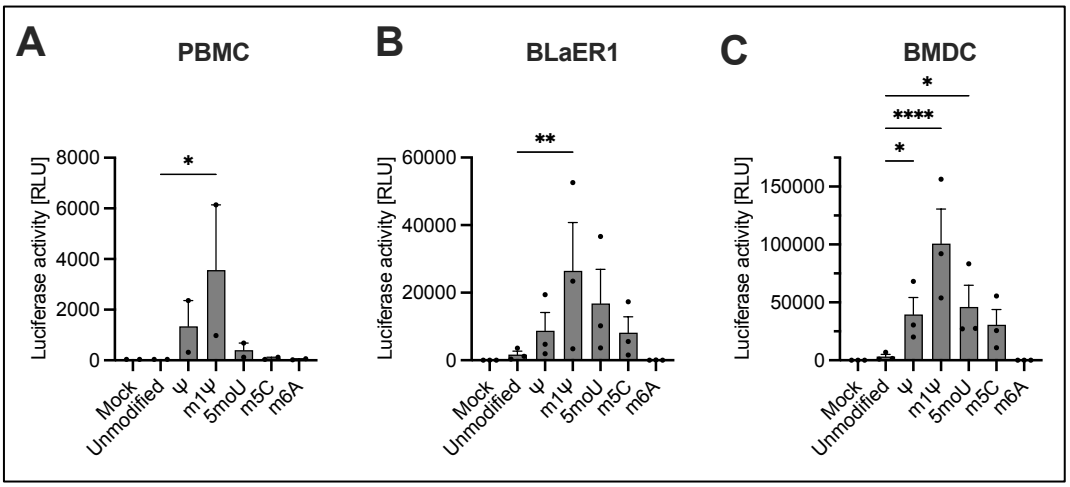

Figure 42: Luciferase expression from EGFP-Fluc mRNA incorporating modified nucleosides
(A) PBMCs, (B) BLaER1 cells and (C) BMDCs were transfected with 0.8 μg/ml EGFP-Fluc mRNA incorporating indicated nucleoside modifications. After 18 hours, firefly luciferase activity was quantified. Mean + SEM of two donors or three independent experiments, respectively. Statistical significance was determined by comparing every condition to the unmodified control using one-way ANOVA. * $p < 0.05$, ** $p < 0.01$, *** $p < 0.001$, **** $p < 0.0001$.

3.3.2 Improved translation of modified mRNAs is only partially caused by reduced signaling of MAVS and IFNAR

The proposed mechanisms leading to the enhanced translation by nucleoside modifications are diverse and only partially understood. Since innate nucleic acid sensing and the consecutive antiviral signaling are associated with translation inhibition and RNA degradation, it has been hypothesized that the reduced innate immune stimulation by modified mRNAs is in part responsible for their enhanced translation. Therefore, activation of TLRs and RLRs by mRNA vaccines and subsequent type I IFN signaling is assumed to be detrimental for effective translation. However, the direct experimental evidence for this phenomenon and its extent is limited.

Besides, direct effects of nucleoside modifications on the translational machinery have been proposed. For example, Svitkin *et al.* reported that m1Ψ increases translation by enhancing translation initiation and ribosome density, the latter caused by a decelerated ribosome movement along the mRNA.[147] Similarly, modulation of mRNA secondary structure by nucleoside modifications was hypothesized to affect translation.[148]

To further elucidate the role of RLR activation for mRNA translation, a side-by-side comparison of IFNα production and luciferase activity in wildtype and two MAVS-deficient clones of human BLaER1 cells after transfection with a range of EGFP-Fluc mRNA concentrations was performed.

The observed IFNα production of wildtype BLaER1 cells was in line with preceding experiments (Figure 27C, Figure 28A), with unmodified and m5C-modified mRNA being the most immunogenic, followed by m6A, Ψ, and m1Ψ (Figure 43A). The 5moU-modified mRNA again did not induce any

detectable IFNα, even at higher concentrations of 10 µg/ml. In line with preceding data, no mRNA-induced IFNα production was detectable in either of the *MAVS*$^{-/-}$ BLaER1 cell clones.

The modulation of mRNA translation by nucleoside modifications in wildtype BLaER1 cells was consistent across a range of mRNA concentrations, with uridine modifications once again exhibiting the highest translation efficiency (Figure 43A). A similar translation pattern was also observed in both *MAVS*$^{-/-}$ BLaER1 cell clones, indicating that a large part of the translation modulation by nucleoside modifications is independent of MAVS signaling (Figure 43A). Nevertheless, an increased translation in *MAVS*$^{-/-}$ compared to wildtype BLaER1 cells could be observed for unmodified and m5C-modified mRNA, and slightly for Ψ-modified mRNA, demonstrating that the translation of these mRNAs is indeed restricted via MAVS-mediated antiviral mechanisms. In line with preceding results and previous literature (Figure 41, Figure 42),[117,185,187] m6A-modified mRNA was not translated even at high mRNA concentrations in neither wildtype nor MAVS-deficient BLaER1 cells (Figure 43A).

To visualize the relative increase in translation due to the absence of MAVS, the fold change of luciferase activity in *MAVS*$^{-/-}$ BLaER1 cells relative to wildtype cells was calculated (Figure 43B). Indeed, unmodified and m5C-modified mRNA exhibited an up to 15- and 20-fold increase of mRNA translation in *MAVS*$^{-/-}$ cells, respectively, in congruence with their strong RIG-I-mediated innate immune stimulation. Additionally, Ψ- and m1Ψ-modified mRNAs exhibited a slight increase in translation, whereas 5moU- and m6A-modified mRNAs were unaffected by the absence of MAVS, in line with the low innate immune stimulation conferred by 5moU and generally abrogated translation by m6A (Figure 43B). As expected, these effects were proportional to RNA concentrations.

To investigate whether the translational restriction correlated with the extent of mRNA-induced MAVS signaling, a Spearman correlation analysis was performed for the relative increase in mRNA translation due to MAVS deficiency and mRNA-induced innate immune stimulation based on the IFNα production in wildtype BLaER1 cells. Of note, m6A-modified mRNA was excluded from this analysis due to the general absence of translation, which is evidently caused by effects other than MAVS-mediated restriction. Indeed, a highly significant, positive correlation was found between the two parameters, confirming that MAVS signaling proportionally restricts mRNA translation (r_s = 0.57 and 0.63, $p < 0.0001$, Figure 43C). Additionally, to visualize the trend of the correlation, several regression models (linear, exponential, sigmoidal, first to third order polynomial) were compared and the model exhibiting the highest R^2 (i.e. best fit) is depicted (in this case third order polynomial, Figure 43C).

Given that the translation differences between modified mRNAs persisted even in the absence of MAVS signaling, and the significant but moderate positive correlation between MAVS signaling and translational restriction, these findings suggest that MAVS signaling only partially contributes

to the enhanced translation of modified mRNAs and that other restriction mechanisms and/or a direct positive modulation of the translational machinery are also involved.

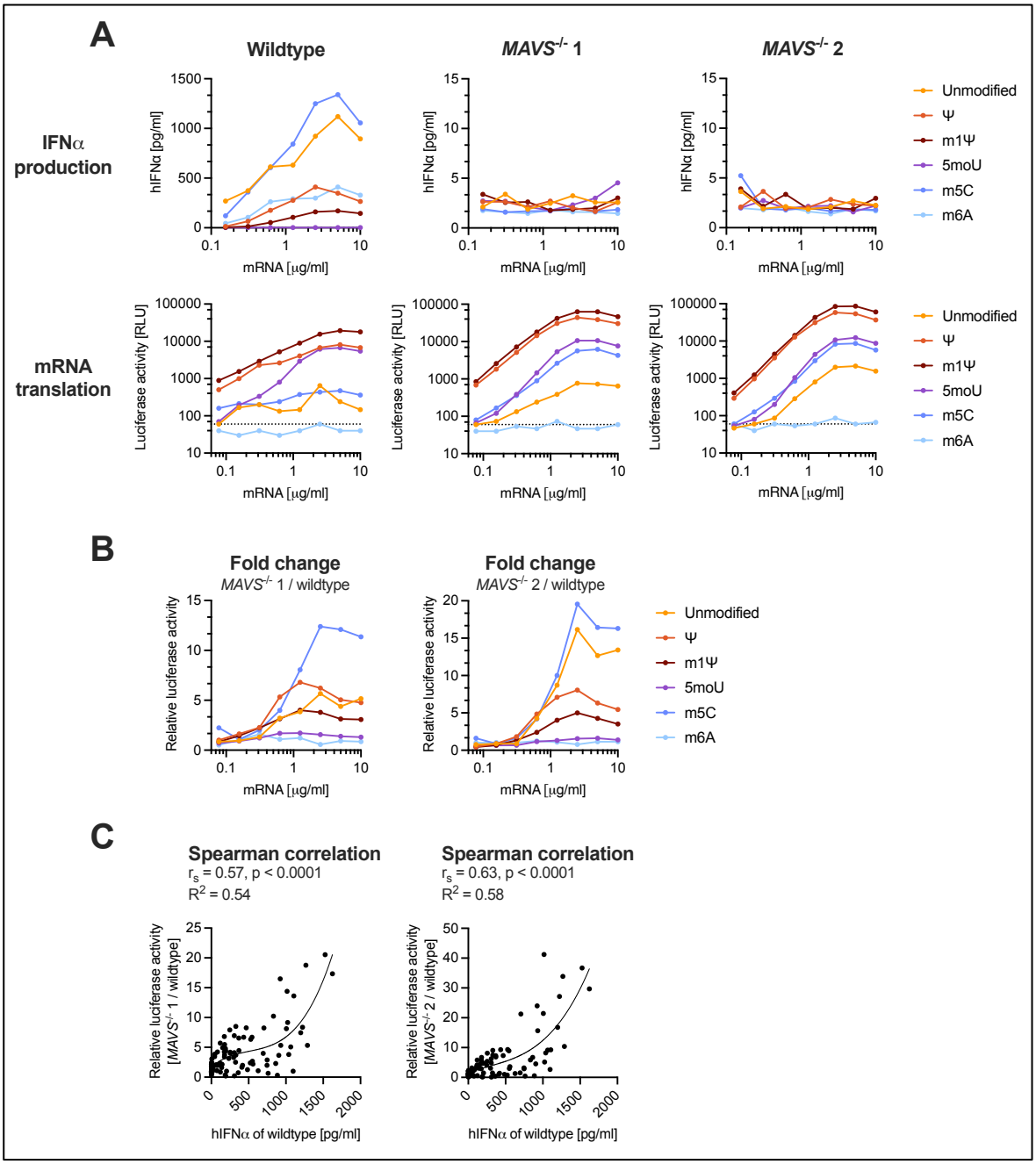

Figure 43: Increased mRNA translation in *MAVS*$^{-/-}$ BLaER1 cells correlates with IFNα production of wildtype cells
(A) Wildtype BLaER1 cells and two *MAVS*$^{-/-}$ BLaER1 clones were transfected with EGFP-Fluc mRNA at concentrations ranging from 0.08 µg/ml to 10 µg/ml. After 18 hours, IFNα production was measured via ELISA and mRNA translation was quantified based on luciferase activity. Mean of three independent experiments. Dotted line indicates technical detection limit of the luciferase assay at 60 RLU. (B) Fold change of luciferase activity in *MAVS*$^{-/-}$ relative to wildtype BLaER1 cells based on data depicted in (A). (C) Spearman correlation coefficient (r_s) and corresponding p-value was calculated for the fold change of luciferase activity in *MAVS*$^{-/-}$ cells depicted in (B) and IFNα production by wildtype cells depicted in (A). Data of m6A was excluded from the analysis due to the general absence of translation. A curve was fitted to the data points by comparing several regression models (linear, exponential, sigmoidal, and first to third order polynomial) and choosing the model with highest R^2 (i.e. best fit, in this case third order polynomial). The quality of fit of the regression model is indicated by the coefficient of determination (R^2).

To investigate the extent to which the translational restriction was mediated by type I IFN secretion and subsequent IFNAR signaling or by other pathways downstream of MAVS, the experiments were repeated in BLaER1 cells and two *IFNAR*$^{-/-}$ cell clones. Activation of IFNAR and the JAK-STAT signaling pathway leads to the formation of ISGF3, a complex consisting of the transcription factors STAT1, STAT2, and IRF9. These induce the transcription of interferon-stimulated genes (ISGs), which contribute to the antiviral state and further enhance the expression of type I IFNs.[1]

In line with this, the IFNα responses of *IFNAR*$^{-/-}$ cells to mRNA were considerably reduced compared to wildtype cells (Figure 44A). Similar to the preceding findings regarding MAVS, the absence of IFNAR slightly increased translation of unmodified, Ψ-, and m5C-modified mRNAs (Figure 44A). However, the calculated fold change of mRNA translation in *IFNAR*$^{-/-}$ cells demonstrated an increase of only up to 2.8-fold relative to wildtype cells (Figure 44B), which was notably lower than the fold change of up to 20-fold observed for MAVS-deficiency (Figure 43B).

Nevertheless, a significantly positive correlation was observed for the relative increase of translation in *IFNAR*$^{-/-}$ cells and the IFNα production of BLaER1 wildtype cells, indicating that IFNAR signaling proportionally restricts mRNA translation (r_s = 0.54 and 056, $p < 0.0001$, Figure 44C), similar to what was observed for MAVS signaling (r_s = 0.57 and 0.63, $p < 0.0001$, Figure 43C).

Together, these findings indicate that the translational repression in human BLaER1 cells is induced by innate immune responses to mRNA that are mediated by MAVS and IFNAR signaling. However, MAVS signaling caused a higher translational restriction compared to IFNAR, indicating the involvement of other antiviral mechanisms downstream of MAVS. Although type I IFNs are the primary cytokines induced by the RLR-MAVS pathway, IFNAR-independent mechanisms could for example depend on NFκB-induced mediators. Additionally, previous studies reported that activated IRF3 is capable of directly inducing the transcription of several ISGs independent of IFNAR-mediated JAK-STAT signaling.[190] Furthermore, MAVS signaling has been found to directly induce apoptosis via recruitment and activation of caspase-8.[34,36] Therefore, various mechanisms could contribute to MAVS-mediated translational restriction independent of IFNAR signaling.

Furthermore, since MAVS deficiency also eliminates the production of IFNα, this system concurrently abolishes both the signaling pathways downstream of MAVS and IFNAR, therefore displaying an additive effect that is likely even further amplified by antiviral feedback mechanisms. Therefore, the investigation of isolated restrictive effects of MAVS signaling independent of IFNAR signaling would require a comparison of *IFNAR*$^{-/-}$ and *IFNAR*$^{-/-}$ / *MAVS*$^{-/-}$ cells.

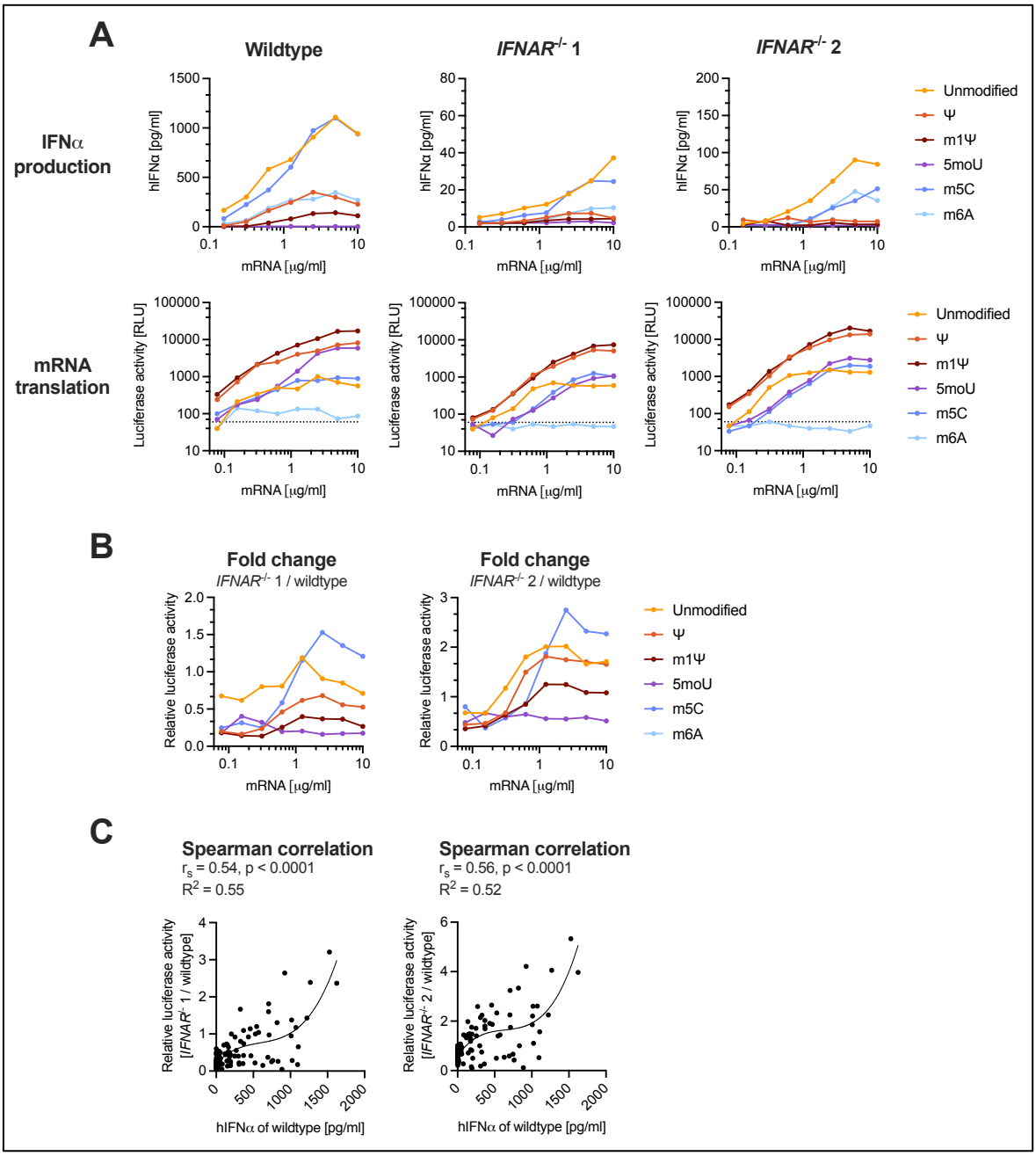

Figure 44: Increased mRNA translation in *IFNAR*$^{-/-}$ BLaER1 cells correlates with IFNα production of wildtype cells
(A) Wildtype BLaER1 cells and two *IFNAR*$^{-/-}$ BLaER1 clones were transfected with EGFP-Fluc mRNA at concentrations ranging from 0.08 µg/ml to 10 µg/ml. After 18 hours, IFNα production was measured via ELISA and mRNA translation was quantified based on luciferase activity. Mean of three independent experiments. Dotted line indicates technical detection limit of the luciferase assay at 60 RLU. (B) Fold change of luciferase activity in *IFNAR*$^{-/-}$ relative to wildtype BLaER1 cells based on data depicted in (A). (C) Spearman correlation coefficient (r_s) and corresponding p-value was calculated for the fold change of luciferase activity in *IFNAR*$^{-/-}$ cells depicted in (B) and IFNα production by wildtype cells depicted in (A). Data of m6A was excluded from the analysis due to the general absence of translation. A curve was fitted to the data points by comparing several regression models (linear, exponential, sigmoidal, and first to third order polynomial) and choosing the model with highest R^2 (i.e. best fit, in this case third order polynomial). The quality of fit of the regression model is indicated by the coefficient of determination (R^2).

Given that the innate RNA sensing via RLRs and their modulation by nucleoside modifications evidently differs between human and murine cells, the restriction of mRNA translation by MAVS and IFNAR signaling was investigated in murine BMDCs.

Unfortunately, m1Ψ-modified mRNA unexpectedly induced very low IFNα levels in this set of experiments compared to all preceding experiments, although the functional translation, which was again higher compared to all other modifications, confirmed RNA integrity and incorporation of m1Ψ (Figure 45A, D). Given this discrepancy, conclusions drawn regarding m1Ψ-modified mRNA should be approached with heightened caution and further investigation and validation are necessary. Despite this, all other modifications exhibited expected levels of mRNA-induced IFNα and mRNA translation in line with preceding results of this study, with an enhanced IFNα response by Ψ in wildtype BMDCs (Figure 45A, D). Furthermore, IFNα production was abolished by the absence of MAVS and IFNAR, respectively, in line with preceding observations for human BLaER1 cells.

Interestingly, no notable increase in mRNA translation in *Mavs*$^{-/-}$ or *Ifnar*$^{-/-}$ BMDCs was observed for any of the tested modifications (Figure 45A, D), which was confirmed by the calculated fold change (Figure 45B, E). Only m5C-modified mRNA exhibited a translational increase of approximately 2.8-fold in *Mavs*$^{-/-}$, but not *Ifnar*$^{-/-}$ BMDCs, relative to wildtype cells (Figure 45B). Interestingly, while innate mRNA sensing in murine BMDCs is primarily mediated by MDA5, incorporation of m5C specifically resulted in engagement of RIG-I as predominant receptor instead (Chapter 3.2.1, Figure 28B). Furthermore, it is especially intriguing that no effect was observed for the highly immunogenic unmodified and Ψ-modified mRNAs. In line with the absence of translational increase in *Mavs*$^{-/-}$ or *Ifnar*$^{-/-}$ BMDCs, there was no correlation with mRNA-induced IFNα responses in wildtype cells, as calculated by Spearman correlation analysis (Figure 45C, F).

Therefore, MAVS and IFNAR signaling did not proportionally restrict mRNA translation in murine BMDCs, in stark contrast to the results observed in human BLaER1 cells. It remains to be investigated whether this discrepancy is mediated by a species-specific or cell type-dependent difference. Besides, due the fact that RIG-I is the main mRNA sensor in human cells, and that, in murine BMDCs, the only mRNA exhibiting MAVS-mediated translational restriction was also recognized by RIG-I, it is tempting to speculate that RIG-I specifically might provoke a stronger translational restriction than MDA5.

In summary, the cooperative translational restriction of MAVS and IFNAR was successfully demonstrated in human BLaER1 cells. Nevertheless, several open questions, such as the precise role of MAVS and IFNAR, or species-, cell type- and receptor-mediated differences remain and require further investigation. Besides, the enhanced translation of modified mRNAs was sustained even in the absence of MAVS or IFNAR, demonstrating that the attenuated innate immune response only partially accounts for this effect. This suggests the involvement of additional antiviral restriction mechanisms and/or improved translation efficiency due to nucleoside modifications.

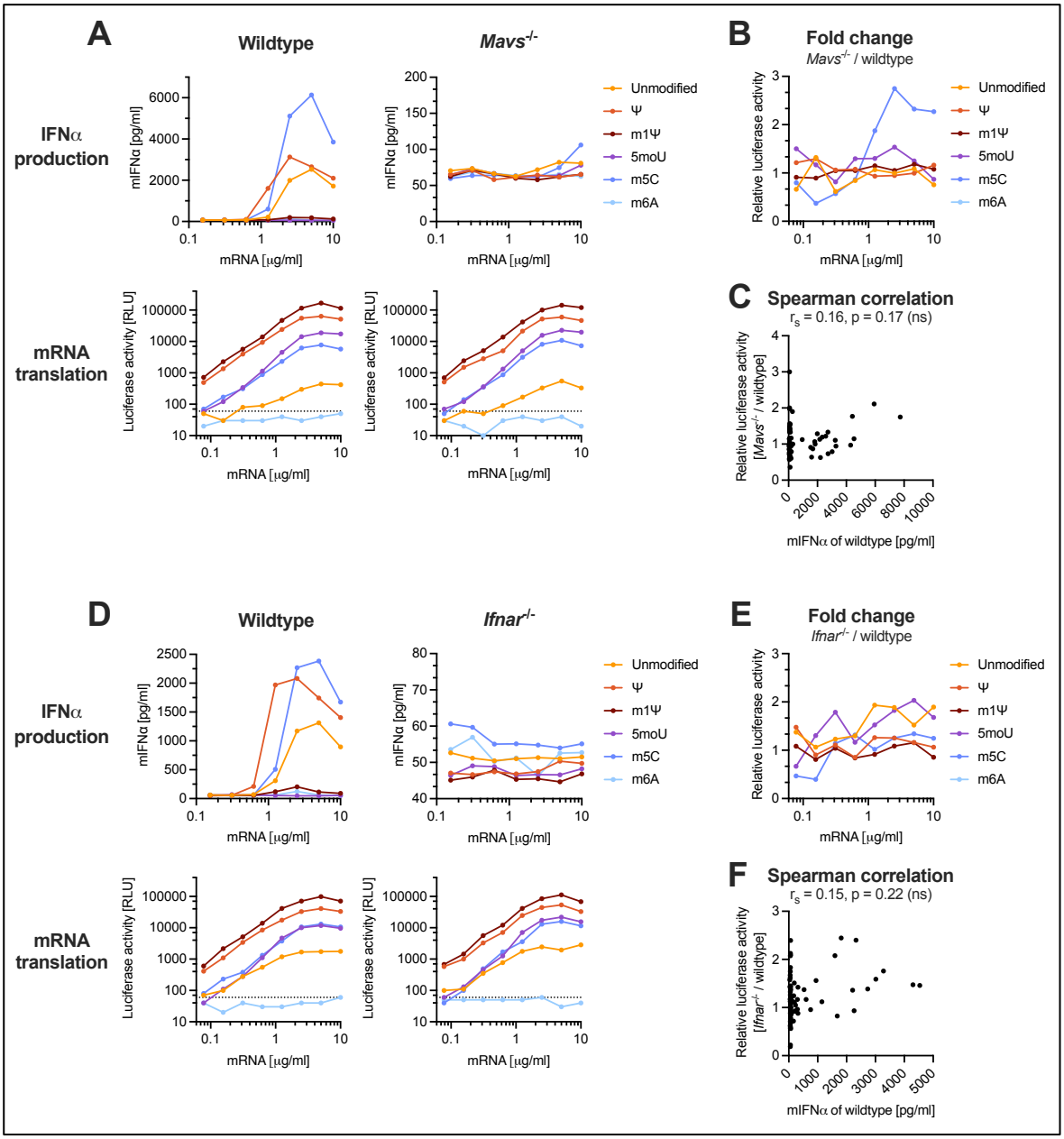

Figure 45: Deficiency of MAVS or IFNAR does not increase mRNA translation in BMDCs

(A) Wildtype and *Mavs*$^{-/-}$ BMDCs were transfected with EGFP-Fluc mRNA at concentrations ranging from 0.08 µg/ml to 10 µg/ml. After 18 hours, IFNα production was measured via ELISA and mRNA translation was quantified based on luciferase activity. Mean of two independent experiments. Dotted line indicates technical detection limit of the luciferase assay at 60 RLU. (B) Fold change of luciferase activity in *Mavs*$^{-/-}$ relative to wildtype BMDCs based on data depicted in (A). (C) Spearman correlation coefficient (r_s) and corresponding p-value was calculated for the fold change of luciferase activity in *Mavs*$^{-/-}$ cells depicted in (B) and IFNα production by wildtype cells depicted in (A). Data of m6A was excluded from the analysis due to the general absence of translation. None of the tested regression models (linear, exponential, sigmoidal, and first to third order polynomial) provided a sufficient fit ($R^2 > 0.5$) and the curves were thus omitted from the visualization. (D – F) Corresponding data using *Ifnar*$^{-/-}$ instead of *Mavs*$^{-/-}$ BMDCs, following the same methods and analyses as in (A-C).

3.3.3 *In vitro* translation of mRNA incorporating nucleoside modifications

In the following, a cell-free *in vitro* translation system was used to investigate the translation efficiency of modified mRNAs independent of innate immune restrictions. Thus, EGFP-Fluc mRNA was incubated in rabbit reticulocyte lysate (RRL), and firefly luciferase activity was quantified.
In line with preceding results (Figure 41, Figure 42), all modified mRNAs, except for m6A, were successfully translated in RRL (Figure 46A). Once again, uridine modifications yielded the highest translation. However, translation of 5moU-modified mRNA was considerably higher than all other modifications (Figure 46A), in contrast to preceding results observed *in cellulo*, where m1Ψ-modified mRNA presented the highest translational capacity (Figure 41, Figure 42). Additionally, translation of m5C-modified mRNA was reduced compared to unmodified mRNA (Figure 46A), in contrast to preceding results of *in cellulo* experiments (Figure 41, Figure 42) and other studies demonstrating a slightly increased translation of m5C-modified mRNA in RRL.[117]
To compare the relative increase in mRNA translation due to the incorporation of modified nucleosides between *in vitro* and *in cellulo* settings, the fold change of mRNA translation to the unmodified control was calculated for the luciferase activity in RRL depicted in Figure 46A and for corresponding data measured in PBMCs, BLaER1 cells, and BMDCs depicted in Chapter 3.3.1, Figure 42. As already observed, the highest translation increase relative to unmodified mRNA in RRL was exhibited by 5moU-modified mRNA (Figure 46B). In contrast, m1Ψ-modified mRNA exhibited the highest translation in all three tested cell types (Figure 46B, Figure 42). A similar phenomenon has been reported by Li *et al.*, where 5moU-modified mRNA outperformed m1Ψ-modified mRNA specifically in RRL but not in the tested cell types.[191] No other studies investigated the translation of 5moU-modified mRNA in RRL to date. Given that 5moU-modified mRNA did not induce strong innate immune activation in preceding experiments, the lack of innate restriction mechanisms in RRL would be an implausible cause for this discrepancy. However, differences in mRNA stability or translation machinery between RRL and tested cells are conceivable. Nonetheless, further research is required to elucidate the mechanisms by which 5moU-modified mRNA outperforms m1Ψ-modified mRNA specifically in RRL.

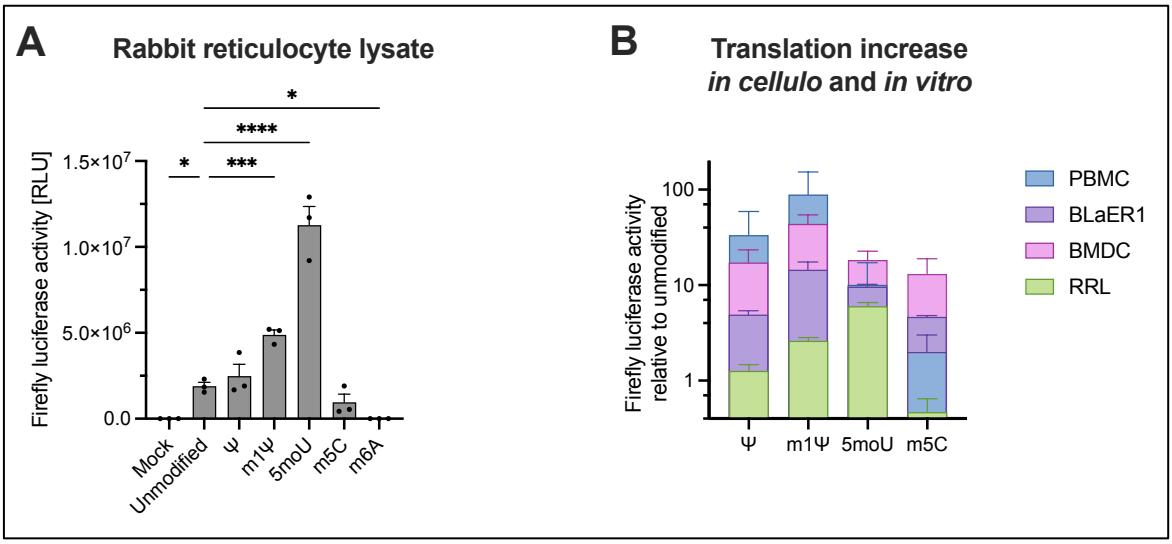

Figure 46: Nucleoside modifications differently modulate mRNA translation *in vitro* and *in cellulo*
(A) EGFP-Fluc mRNA incorporating indicated nucleoside modifications was incubated in rabbit reticulocyte lysate (RRL) and luciferase activity was quantified. Mean + SEM of three independent experiments. Statistical significance was determined by comparing every condition to the unmodified control and mock transfection using one-way ANOVA. (B) Overlay of fold changes in mRNA translation of modified mRNA relative to unmodified control calculated for *in vitro* translation depicted in (A) and *in cellulo* translation depicted in Figure 42. * $p < 0.05$, ** $p < 0.01$, *** $p < 0.001$, **** $p < 0.0001$.

In summary, the present findings suggest that, in addition to evading innate immune restrictions, modified nucleosides directly modulate mRNA translation efficiency, which is in line with existing experimental evidence.[117,147,191] Once again, the tested uridine modifications present the highest translational efficiency, therefore highlighting these modifications for mRNA therapeutics.

Nevertheless, it should be noted that although the RRL translation system is devoid of innate restrictions that require nuclear transcription, it does still possess antiviral restriction factors that act directly on translation. For example, several studies reported that RRL contains functional protein kinase R (PKR), a cytosolic dsRNA sensor that upon activation phosphorylates eIF2α (eukaryotic translation initiation factor 2α) and thereby inhibits overall translation.[147,192–194] Although the RRL by Promega contains additional hemin to inhibit phosphorylation of eIF2α by eIF2αK1 (eIF2α kinase 1), this does not affect PKR-mediated phosphorylation.[195] In line with this, the manual provided by RRL states that translation in RRL can be inhibited by large quantities of dsRNA.[196] Therefore, a modulation of dsRNA content or PKR activation by nucleoside modifications might skew the presented results and will be further investigated in the following chapter.

3.3.4 PKR-mediated restriction of modified mRNA translation

In addition to the innate restriction of mRNA translation induced by TLR and RLR activation, some nucleoside modifications have been proposed to directly reduce activation and effector mechanisms of antiviral restriction factors. For example, nucleoside modifications such as Ψ, m1Ψ, and m5C have been shown to reduce activation of PKR and thereby induce less translational restriction compared to unmodified mRNA.[118,147] Likewise, Ψ and m6A were found to reduce activation of OAS1 (2′-5′-Oligoadenylate synthetase 1) and its production of the second messenger 2-5A (2′-5′-linked oligoadenylate), which induces RNase L-mediated RNA degradation.[119] Furthermore, Ψ was reported to confer increased resistance to cleavage by RNase L.[119] However, for some of these findings, it is unclear whether the impact of nucleoside modifications is mediated by a direct effect on the enzymes or by a generally reduced dsRNA content.

To investigate the role of PKR for mRNA translation and a potential modulation by nucleoside modifications, the EGFP-Fluc mRNA was transfected into wildtype and *PKR*$^{-/-}$ THP-1 dual cells and firefly luciferase activity was quantified. Interestingly, the absence of PKR did not result in an enhanced translation of any mRNA, as confirmed by the calculated fold change (Figure 47), indicating the absence of relevant PKR activation by EGFP-Fluc mRNA in wildtype THP-1 cells.

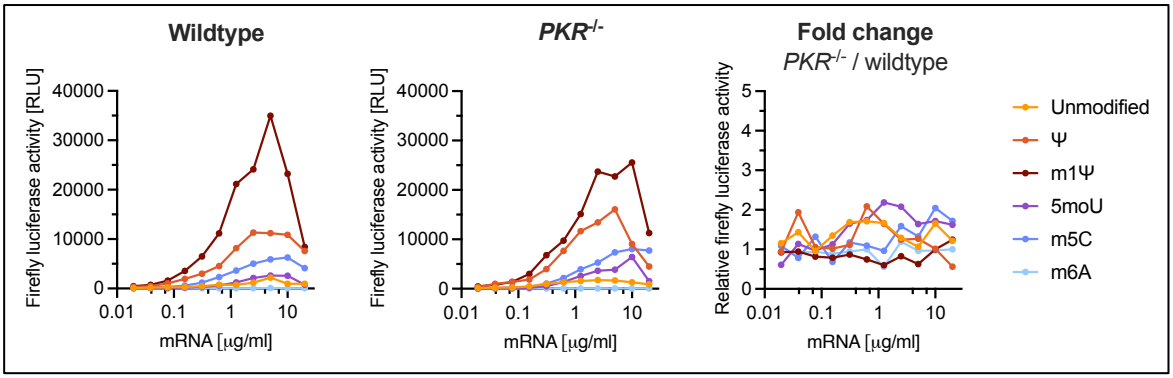

Figure 47: PKR does not restrict translation of EGFP-Fluc mRNA in THP-1 cells
Wildtype and *PKR*$^{-/-}$ THP-1 dual cells were transfected with EGFP-Fluc mRNA at concentrations ranging from 0.02 µg/ml to 20 µg/ml. After 18 hours, mRNA translation was quantified based on firefly luciferase activity and fold change of *PKR*$^{-/-}$ relative to wildtype cells was calculated. Mean of three independent experiments. Data were produced in collaboration with Katrin Ciupka and Charlotte Hunkler from the Schlee group.

Given that PKR activation leads to a translational inhibition of all mRNAs, Matsumiya *et al.* previously demonstrated that RIG-I-mediated production of type I IFNs is sensitive to concurrent PKR activation.[197] Therefore, activation of PKR can be measured based on a reduced innate immune response of wildtype relative to *PKR*$^{-/-}$ cells. Since the THP-1 dual cells stably express the Lucia luciferase under the control of an ISG54 minimal reporter and five ISREs (interferon-stimulated response elements), the activity of this enzyme was measured to estimate the type I IFN-mediated

JAK-STAT signaling. First, the suitability of this system to study PKR activation based on restricted immune responses was investigated by transfecting control RNAs. To do so, two known RIG-I ligands were used: a 24 bp and a 100 bp dsRNA, with only the latter exhibiting sufficient length to concurrently activate PKR.[51] Indeed, the 100 bp dsRNA, but not the 24 bp dsRNA, induced increased reporter expression in *PKR*$^{-/-}$ cells relative to wildtype cells (Figure 48A), confirming that the RIG-I-mediated immune response is restricted by concurrent activation of PKR.

In contrast, no PKR-mediated restriction was observed for the ISRE reporter activity induced by EGFP-Fluc mRNA, as evidenced by the calculated fold change of *PKR*$^{-/-}$ cells relative to wildtype (Figure 48B). Therefore, this finding underscores the absence of PKR activation by EGFP-Fluc mRNA.

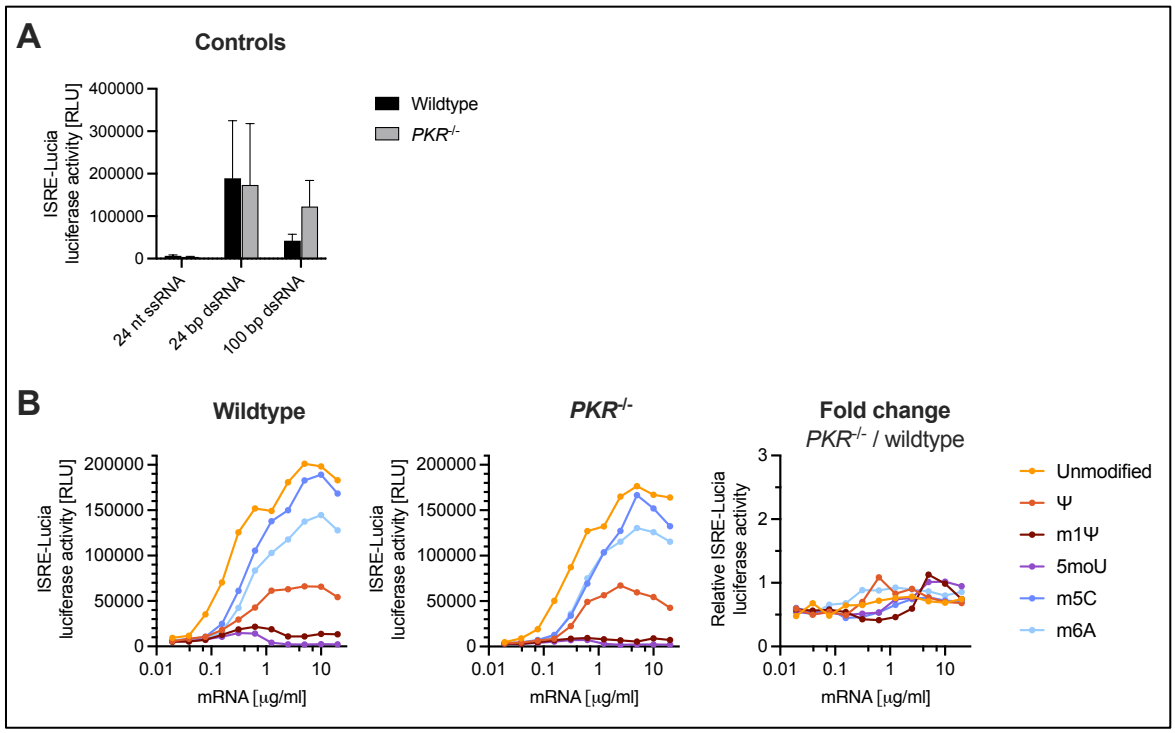

Figure 48: IFN signaling induced by EGFP-Fluc mRNA is not restricted by PKR in THP-1 cells
Wildtype and *PKR*$^{-/-}$ THP-1 dual cells were transfected with (A) indicated controls or (B) EGFP-Fluc mRNA at concentrations ranging from 0.02 µg/ml to 20 µg/ml. After 18 hours, type I IFN signaling was quantified based on ISRE-Lucia luciferase activity and fold change of *PKR*$^{-/-}$ relative to wildtype cells was calculated. Mean (+ SEM) of three independent experiments. Data were produced in collaboration with Katrin Ciupka and Charlotte Hunkler from the Schlee group.

Subsequently, it was hypothesized that the EGFP-Fluc mRNA did not contain sufficient quantities of dsRNA to induce substantial activation of PKR. To investigate this and assess the potential modulation of PKR activation by nucleotide modifications, the experiments in THP-1 dual cells were repeated using the previously described 512 bp duplex "ds512B". In addition to the ISRE-dependent Lucia luciferase, the THP-1 dual cells express the secreted embryonic alkaline phosphatase (SEAP) under the control of an IFNβ minimal promoter fused to five NFκB response elements,

which can be induced by TLR- or RLR-mediated NFκB signaling, as well as other PRRs. The activity of both enzymes was measured to investigate a broader range of cellular processes and enhance the reliability of the experiment.

Strikingly, both reporter activities exhibited a plateau and subsequent decline at RNA concentrations above 1 µg/ml for all immunogenic modifications in wildtype THP-1 cells, which was absent in *PKR*$^{-/-}$ cells (Figure 49). This finding demonstrates that all modified ds512B RNAs activate PKR to some extent and induce translational repression especially at high concentrations. Of note, no conclusion can be drawn regarding 5moU, as this modification did not induce innate responses.

To investigate the extent of PKR-mediated restriction of innate responses induced by ds512B RNA incorporating different nucleoside modifications, the fold change of the reporter activities was calculated for *PKR*$^{-/-}$ cells relative to wildtype. Interestingly, RNAs incorporating m5C or m6A exhibited a notably stronger PKR-mediated restriction than all other modifications (Figure 49), indicating an enhanced activation of PKR conferred by these modifications. Indeed, increased PKR activation by m6A has been indicated before, whereas m5C seemed to have reducing properties.[118,198,199] Given that previous experiments using anti-dsRNA dot blots revealed that m5C- and m6A-modified mRNAs exhibit reduced dsRNA content compared to unmodified mRNA (Figure 29), an enhanced activation of PKR by these modifications is rather unexpected and demonstrates a direct mechanistic enhancement of PKR activation by m5C and m6A (Figure 49).

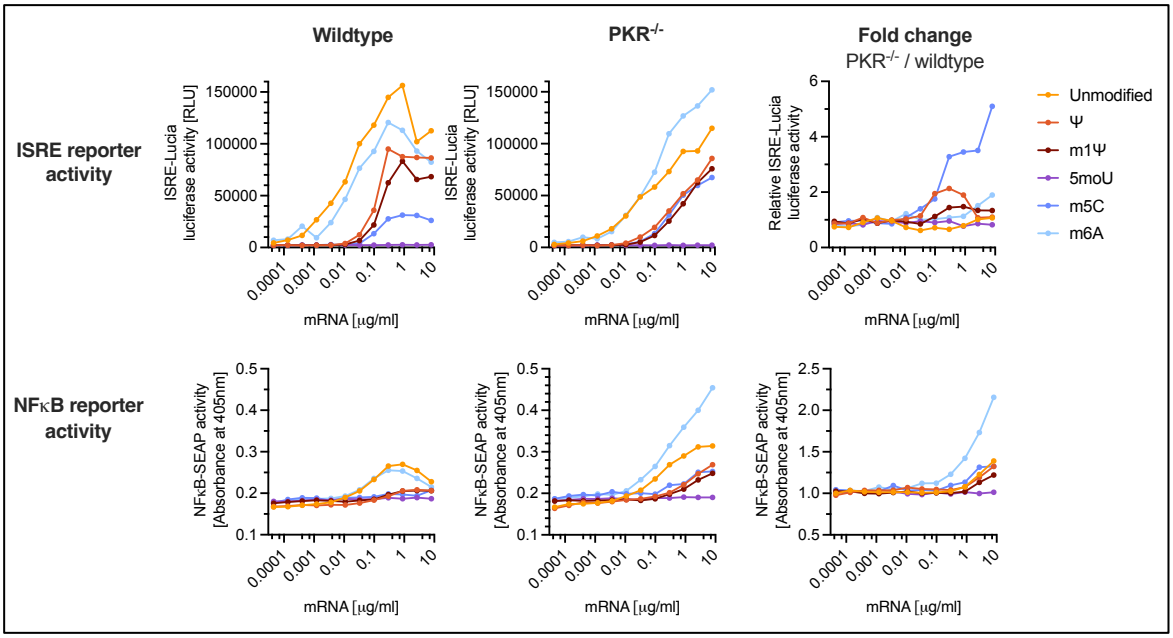

Figure 49: PKR activation by ds512B is enhanced by incorporation of m5C and m6A

(A) Wildtype and *PKR*$^{-/-}$ THP-1 dual cells were transfected with ds512B RNA at concentrations ranging from 0.0001 µg/ml to 8 µg/ml. After 18 hours, type I IFN signaling was quantified based on ISRE-Lucia luciferase activity and NFκB activity was quantified based on SEAP activity. Fold change of measured enzyme activities in *PKR*$^{-/-}$ relative to wildtype cells was calculated. Mean of three independent experiments. Data were produced in collaboration with Katrin Ciupka and Charlotte Hunkler from the Schlee group.

In summary, the presented evidence demonstrates that the EGFP-Fluc mRNA did not contain sufficient amounts of dsRNA to activate PKR. However, the system's sensitivity may not be representative for a systemic response, and even low amounts of PKR activation might be detrimental for the effectiveness of mRNA therapeutics. Therefore, reduced activation of PKR by nucleoside modifications could be beneficial for therapeutic application. Besides, since PKR activation was investigated only in human THP-1 cells, cell type- or species-specific effects could be possible and require further investigation. Nevertheless, this study demonstrates that all tested, immunogenic modifications were able to activate human PKR, with m5C and m6A actually exhibiting enhancing properties.

3.3.5 Combining m1Ψ with other nucleoside modifications for mRNA optimization

The combination of several nucleotide modifications into an mRNA in order to achieve the advantages of both modifications has been proposed before, especially for the combination of Ψ or m1Ψ with m5C. While a few application-focused *in vivo* studies successfully employed (m1)Ψ/m5C-modified mRNA, the benefit over incorporating only (m1)Ψ into the mRNA remains ambiguous.[73,74,125] For example, while Andries *et al.* reported that the combinations Ψ/m5C and m1Ψ/m5C lead to an increased mRNA translation compared to (m1)Ψ alone in five out of seven tested cell lines and primary cells, this was not reproducible in a murine *in vivo* setting, where m1Ψ alone exhibited significantly greater translation than all other modifications and combinations thereof.[83] Of note, the only murine cell line included by Andries *et al.* exhibited similar results as the murine *in vivo* experiments, potentially indicating species-specific effects.[83] However, one of the six tested human cell lines and primary cells also contradicted a benefit of Ψ/m5C or m1Ψ/m5C over m1Ψ alone. Similarly, Svitkin *et al.* demonstrated that a combination of Ψ/m5C or m1Ψ/m5C did not exhibit higher translation than (m1)Ψ alone in human HEK293T cells, and indicated excessive ribosome stalling and inefficient translation caused by the combination of m5C and m1Ψ.[147]

In the following, the aim was to investigate combinations of promising nucleoside modifications to further optimize the design of mRNA therapeutics by aiming at minimal innate immune stimulation and maximal translation. Given the considerably higher translation of m1Ψ over Ψ, only m1Ψ was investigated.

To assess the ambiguous aspects of m1Ψ/m5C-modified mRNA, the EGFP-Fluc mRNA was *in vitro* transcribed incorporating the respective modifications and transfected into PBMCs, BLaER1 cells, and BMDCs. Based on IFNα production and firefly luciferase activity, the effect of combined modifications on mRNA-induced innate immune responses and translation was assessed.

In human PBMCs and BLaER1 cells, the IFNα response to m1Ψ/m5C-modified mRNA was comparable to m1Ψ alone (Figure 50), in line with preceding results showing that m5C does not notably reduce RIG-I-dependent IFNα production in human cells (Figure 27C, D). In contrast, the IFNα response of murine BMDCs to m1Ψ-modified mRNA, which was previously shown to be MDA5-dependent (Figure 28B), was significantly reduced by combining m1Ψ with m5C (Figure 50), in line with preceding data demonstrating abrogation of MDA5 activation by m5C (Figure 28B). Additionally, m1Ψ/m5C-modified mRNA induced lower IFNα levels than m5C-modified mRNA (Figure 50), in line with m5C-modified mRNA being recognized by RIG-I in BMDCs (Figure 28B), and murine RIG-I activation being reduced by m1Ψ (Figure 31). These findings indicate that m1Ψ/m5C-modified mRNA combines the immunomodulatory effects of each individual modification, with m5C repressing activation of murine MDA5 and m1Ψ reducing activation of murine RIG-I.

Unfortunately, the translation of m1Ψ/m5C-modified mRNA was significantly lower than m1Ψ-modified mRNA in all cell types (Figure 50). In some cases, the luciferase activity induced by m1Ψ/m5C-modified mRNA was even below that observed for unmodified or m5C-modified mRNA. Together, these findings underscore that while m1Ψ/m5C-modified mRNA exhibits a favorably low innate immune stimulation in BMDCs, its translation is lower than mRNA incorporating only m1Ψ in both human and murine cells. Therefore, our data provide evidence that the combination of m1Ψ and m5C is suboptimal for mRNA therapeutics.

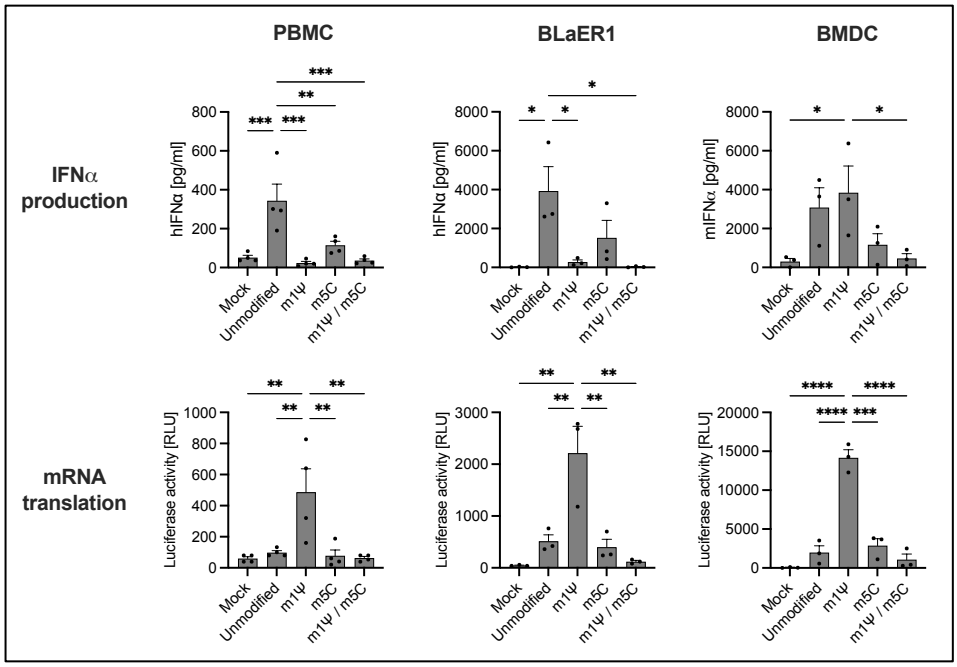

Figure 50: Combination of m1Ψ and m5C reduces mRNA translation compared to m1Ψ alone
PBMCs, BLaER1 cells and BMDCs were transfected with 0.8 μg/ml EGFP-Fluc mRNA incorporating indicated nucleoside modifications. After 18 hours, IFNα production was measured via ELISA and firefly luciferase activity was quantified. Mean + SEM of four donors or three independent experiments, respectively. Statistical significance was determined using one-way ANOVA. * $p < 0.05$, ** $p < 0.01$, *** $p < 0.001$, **** $p < 0.0001$.

Given the low innate immune stimulation and high translation of 5moU-modified mRNA, it was hypothesized that a combination of m1Ψ and 5moU would achieve optimal mRNA translation without the residual immune response observed for m1Ψ-modified mRNA. However, these modifications are both analogs of uridine. Therefore, a combination of both effectively halves the total content of each modification. To incorporate both modifications into the EGFP-Fluc mRNA, uridine was substituted by 50 % m1Ψ and 50 % 5moU while maintaining overall nucleotide concentrations during *in vitro* transcription. To control for the reduction of each individual modification, additional mRNAs incorporating 50 % m1Ψ or 5moU with 50 % uridine were generated, respectively.

In line with the outstanding capability of 5moU to reduce mRNA-induced innate immune responses, a combination of m1Ψ and 5moU induced notably lower IFNα levels than the m1Ψ-modified mRNA in both BLaER1 cells and BMDCs (Figure 51). Interestingly, 50 % of 5moU was still effective enough to induce less IFNα than 100 % m1Ψ-modified mRNA and almost as low as 100 % 5moU. In contrast, 50 % of m1Ψ were inefficient to fully maintain the inhibitory effects observed in human BLaER1 cells (Figure 51).

Unfortunately, the combination of m1Ψ and 5moU did not exhibit higher translation than m1Ψ- or 5moU-modified mRNA (Figure 51), similarly to the results observed for m1Ψ/m5C-modified mRNA. Interestingly, translation of 50 % 5moU-modified mRNA was equal to the respective fully modified mRNA, but only in human BLaER1 cells and not in BMDCs (Figure 51). In contrast, translation of 50 % m1Ψ-modified mRNA was significantly reduced compared to the m1Ψ-modified mRNA in both cell types, indicating that the effects of m1Ψ on mRNA-induced innate immune responses and mRNA translation correlate directly with the number of modifications incorporated (Figure 51).

Altogether, the m1Ψ/5moU-modified mRNA did not meet the expectations of an optimized mRNA. While the mRNA-induced cytokine response was successfully reduced compared to m1Ψ-modified mRNA, the translation efficiency was also notably lower. Moreover, m1Ψ/5moU-modified mRNA exhibited comparable levels of innate immune activation and translation as 5moU-modified mRNA. Consequently, combining m1Ψ and 5moU offers no advantage over each individual modification. Based on these findings, choosing the optimal modification depends on the specific application, either prioritizing maximal translation with residual innate immune activation (m1Ψ) or aiming at minimal immune activation at the cost of reduced translation efficiency (5moU).

Of note, it remains to be investigated whether different proportions of m1Ψ and 5moU, such as 75 % to 25 %, would improve mRNA translation while maintaining low innate immune stimulation.

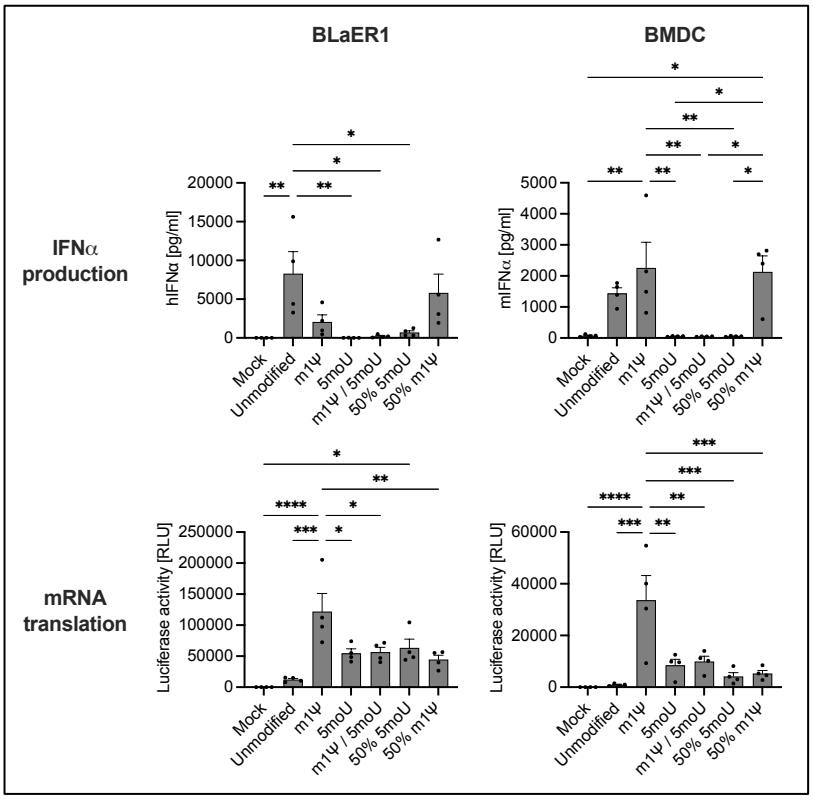

Figure 51: Combination of m1Ψ and 5moU efficiently reduces mRNA-induced innate immune stimulation, but does not improve mRNA translation

BLaER1 cells and BMDCs were transfected with 0.8 μg/ml EGFP-Fluc mRNA incorporating indicated nucleoside modifications. After 18 hours, IFNα production was measured via ELISA and firefly luciferase activity was quantified. Mean + SEM of four independent experiments, respectively. Statistical significance was determined using one-way ANOVA. * $p < 0.05$, ** $p < 0.01$, *** $p < 0.001$, **** $p < 0.0001$.

4. Discussion

4.1 Mechanisms of RIG-I-like receptor activation by mRNA vaccines

The inherent immunostimulatory properties of IVT-mRNA have limited its therapeutic applicability for several decades. Despite significant advancements in mRNA design, including the incorporation of a 5′ cap and modifications such as m1Ψ, the technology did not achieve widespread public application until the COVID-19 pandemic, when the urgent need for new treatment options led to the emergency authorization of mRNA-based vaccines. Although these vaccines have demonstrated remarkable efficacy, several questions regarding the innate immune responses to mRNA vaccines remained unanswered.

For example, while the incorporation of m1Ψ was thought to render the mRNA non-immunogenic, the collaborative work of the Bartok and Hartmann groups, to which this thesis work has contributed, demonstrates that the m1Ψ-modified COVID-19 mRNA vaccines by BioNTech and Moderna still induce innate immune responses (Chapter 1.4.4, Chapter 3.1).[83,200] Furthermore, this highly collaborative project revealed that the innate immune response to the COVID-19 mRNA vaccines is primarily mediated by RIG-I-like receptors (RLRs) (Chapter 1.4.4, Chapter 3.1). The important role of RLRs in mRNA sensing was further confirmed using an independent *in vitro* transcribed (IVT)-mRNA, demonstrating that this innate immune activation is ubiquitous to IVT-mRNA (Chapter 1.4.4, Figure 9; Chapter 3.1.1, Figure 13). In line with the broad expression of RLRs in all nucleated cells and their cytosolic localization, RLRs may represent the primary innate sensors for m1Ψ-modified mRNA vaccines.

Previous research regarding innate mRNA sensing mainly focused on Toll-like receptors (TLRs) and offers only limited information on RLR-mediated mRNA sensing and associated functional outcomes. This gap was addressed in collaboration with the Bartok group by providing mechanistic insight into RLR-mediated mRNA sensing. RLR activation was shown to be mediated by double-stranded (ds) RNA byproducts generated during *in vitro* transcription, as evidenced by a reduced innate immune stimulation after oligo(dT)-purification of BioNTech mRNA and the SC-IVT mRNA (Chapter 1.4.4, Figure 10; Chapter 3.1.2, Figure 17). In line with this, the Moderna vaccine, which employs oligo(dT)-purification during manufacturing, exhibited a lower innate immune stimulation than the BioNTech vaccine and the SC-IVT mRNA (Chapter 1.4.4: Figure 10, Chapter 3.1.2: Figure 17).

In order to investigate the functional outcomes of RLR-mediated mRNA sensing and their influence on mRNA vaccine efficacy, *in vivo* vaccination studies using mice were performed by Dr. Marcel Renn, Patrick Müller, and Yu Pan Tan, and part of their data is presented in Chapter 1.4.4 (Figure 7, Figure 8). In line with a previous publication, the activation of MDA5 by the COVID-19 mRNA

vaccines from BioNTech and Moderna was found to enhance the spike-specific adaptive immune response (Chapter 1.4.4, Figure 8), thus contributing to vaccine efficacy in an adjuvant-like manner.[67] This finding was further emphasized by the upregulation of activation markers on BMDCs following MDA5 activation by COVID-19 mRNA vaccines (Chapter 3.1.3: Figure 18). Thus, RLR activation by mRNA vaccines is able to improve vaccine efficacy via adjuvant-like effects. However, due to the observed species-specific differences (discussed in Chapter 4.2), it remains to be elucidated whether *in vivo* studies in murine models hold implications for the functional outcome of RIG-I-mediated mRNA sensing in humans.

Finally, it is important to note that the data presented in this thesis does not intend to nor does it provide sufficient evidence to evaluate the overall efficacy or functionality of the COVID-19 mRNA vaccines by BioNTech and Moderna. mRNA-induced innate immune stimulation may be a double-edged sword with serving both a role as an adjuvant to imitate viral infection while at the same time limiting the maximum tolerated vaccine dosage and translation efficiency. To find the optimal balance between these effects will require further systematic *in vivo* investigations. Several clinical studies confirmed the efficacy of the COVID-19 mRNA vaccines in inducing protection against SARS-CoV-2, and both vaccines successfully contributed to the containment of the pandemic.[79] Furthermore, since the COVID-19 mRNA vaccines by BioNTech and Moderna work exceptionally well, it is questionable whether a further reduction of innate immune sensing would be advantageous. The optimal extent of immune stimulation required for mRNA-based therapeutics has to be optimized for individual applications. Therefore, this study solely serves the characterization of innate immune responses to IVT-mRNA and provides mechanistic insights that will aid in the further development of mRNA therapeutics.

4.1.1 Methods to eliminate immunogenic dsRNA from *in vitro* transcribed mRNA

While a certain degree of innate immune stimulation by mRNA vaccines might be beneficial for effective adaptive responses, its extent has to be balanced in order to prevent inflammatory side-effects and not to compromise vaccine efficacy. For example, reducing the unspecific inflammatory properties of IVT-mRNA could enable the addition of defined immunostimulatory RNA species or other adjuvants. Apart from this, non-immunostimulatory mRNA is obligatory for applications such as protein replacement therapy. Therefore, several methods to reduce innate immune stimulation by IVT-mRNA have been investigated and will be discussed in the following.

Double-stranded RNA byproducts generated during *in vitro* transcription are a major cause of innate immune responses to IVT-mRNA that limit vaccine dosages and efficacy. The collaborative work of Bartok and Hartmann groups demonstrated that the elimination of immunogenic dsRNA by

oligo(dT)-purification significantly reduces innate immune stimulation by IVT-mRNA (Chapter 1.4.4, Figure 10; Chapter 3.1.2, Figure 17). Nevertheless, a residual amount of dsRNA and innate immune stimulation remained for the poly(A)+ fraction, in line with previous reports.[126] It is conceivable that RNA species that hybridized to the target mRNA were co-precipitated, resulting in double-stranded, immunogenic RNA regions.

While oligo(dT)-purification was effective in reducing mRNA-induced immune stimulation, the procedure is prone to unspecific material loss caused by inefficient binding and multiple washing steps, thereby reducing the overall mRNA yield and impeding reproducibility. Other methods to eliminate dsRNA content include HPLC purification and cellulose-based chromatography.[115,145,201] While HPLC purification has been reported to effectively reduce dsRNA content, it is currently not suitable for large-scale productions required for global vaccination campaigns.[115,145] Additionally, HPLC purification does not eliminate full-length antisense strands of the IVT-mRNA due their equal size, resulting in residual dsRNA and immune stimulation. The cellulose-based chromatography using ethanol-dissolved mRNA is thought to specifically bind dsRNA, while ssRNA is eluted, and has the potential for large-scale application.[145,146,201] However, its purification efficiency, *in vivo* applicability, and immune stimulation have not been investigated in detail yet. Therefore, oligo(dT)-purification is currently the most effective method to eliminate dsRNA from IVT-mRNA that is also suitable for large-scale productions.

In contrast, all these purification methods pose an extra step during manufacturing and considerably increase manufacturing time and cost while reducing reproducibility. Therefore, altering the *in vitro* transcription reaction conditions to reduce the generation of immunogenic dsRNA in the first place is a promising alternative. For example, previous studies proposed the reduction of $MgCl_2$ levels or employing polymerase mutants to reduce the generation of dsRNA.[25,202,203] Despite promising preliminary results, these methods require further investigation, especially in *in vivo* models.

Lastly, the incorporation of certain modified nucleosides into IVT-mRNA has been shown to reduce the generation of dsRNA byproducts and will be discussed in Chapter 4.3.

4.1.2 Role of 5′ capping for RIG-I-like receptor activation by *in vitro* transcribed mRNA

The addition of a 5′ cap-1 is required to enable efficient translation and to prevent innate immune stimulation via activation of RIG-I. However, uncapped 5′ppp-mRNA and cap-1 mRNA induced equal RIG-I-mediated IFNα levels in human BLaER1 cells (Figure 21B), although an increase in mRNA translation confirmed functional capping (Figure 21A). This discrepancy led to the hypothesis that the commonly used vaccinia capping enzyme is unable to operate on dsRNA species. Therefore, the capping efficiency was investigated using short ss- and dsRNA and LC/MS-based detection. Strikingly, this study demonstrates that the vaccinia capping enzyme is indeed unable to catalyze the transfer of a 7-methylguanosine to the 5′ end of dsRNA (Chapter 3.1.4, Figure 22). Interestingly, the phosphatase activity of the vaccinia capping enzyme was still active on blunt-end dsRNA, but a 3′ overhang of three nucleotides abolished this activity as well (Chapter 3.1.4, Figure 22). Therefore, the immunogenic dsRNA species contained within IVT-mRNA are not affected by enzymatic capping. These results provide valuable mechanistic insight into enzymatic capping of IVT-mRNA and the nature of RIG-I-activating byproducts. It remains to be investigated whether other commercially available capping enzymes, such as the Faustovirus capping enzyme, are capable of handling dsRNA species.[204] Besides, the Faustovirus capping enzyme is active at reaction temperatures of up to 55 °C, which might be sufficient to denature very short dsRNA below 20 bp. However, longer dsRNA requires a higher melting temperature of up to 98 °C.

In contrast, the role of cap-1 for activation of MDA5 remains ambiguous. While a few previous studies investigated MDA5 activation by viruses deficient in 2′-O-methyltransferases, other studies indicated that MDA5 binds to dsRNA internally contradicting a role of the 5′ end for ligand recognition by MDA5.[28–30] In addition, the putative inhibition of MDA5 activation by N1-2′-O-methylation postulated by Züst *et al.* is not supported by direct experimental evidence and indirect effects, such as MDA5-dependent upregulation of IFIT1 or other ISGs, remain conceivable.[30] While the present findings negate an inhibitory effect of cap-1 on MDA5 (Chapter 3.1.4), several limitations prevent a definitive conclusion. For example, since the vaccinia capping enzyme is unable to cap blunt-end or 3′-overhang dsRNA (Chapter 3.1.4, Figure 22), it is possible that the MDA5-activating RNA species remained uncapped, as is the case for RIG-I ligands. In contrast, since MDA5 binds to dsRNA internally, it could potentially bind to highly structured RNA possessing a single-stranded capped 5’ end followed by double-stranded regions.[28,29] This theory was investigated via consecutive digestion of mRNA with polyphosphatase and terminator exonuclease to eliminate uncapped transcripts. The equal MDA5 stimulation by treated and untreated mRNA could be attributed to the absence of cap-1-mediated inhibition (Chapter 3.1.4, Figure 23). However, it cannot be excluded that the exonuclease is unable to digest dsRNA, thereby preserving it in both samples.

In contrast, such an incapability to digest dsRNA would have resulted in an enrichment of immunogenic dsRNA and increased innate immune responses, which was not the case (Chapter 3.1.4, Figure 23). Furthermore, the primary application of the terminator exonuclease is the depletion of ribosomal RNA, which has extensive secondary structures.[205] To confirm the enzyme's capability to digest dsRNA, one could quantify the activation of RIG-I by untreated and treated IVT-mRNA in human cells. Since the effect of cap-1 on RIG-I is well characterized, the treated IVT-mRNA should not activate RIG-I, if the terminator exonuclease is able to digest dsRNA. In summary, while the current experimental evidence does not indicate an inhibitory effect of cap-1 on MDA5, further investigations are required to enable a definitive conclusion.

The vaccinia capping enzyme's inability to cap dsRNA raises the possibility that co-transcriptional capping might produce less uncapped dsRNA species in comparison. However, it is known that during co-transcriptional capping, the transcription sporadically initiates with a generic nucleotide instead of the cap analog, leading to the presence of uncapped transcripts. TriLink, the manufacturer of the currently most widely used cap analog CleanCap, claims up to 94 % capping efficiency, and previous studies comparing co-transcriptional and enzymatic capping of the target mRNA demonstrated equal efficiencies of > 90 % for both methods.[97,206] However, it remains unclear to what extent the employed methods detect the capping status of unspecific byproducts. In the present study, the co-transcriptionally capped BioNTech mRNA induced similarly high innate immune activation as the enzymatically capped SC-IVT, indicating that both preparations contain similar amounts of immunogenic dsRNA species (Chapter 3.1.2, Figure 17). While this experiment has been performed in murine BMDCs with MDA5 as the primary sensor, for which the effect of cap-1 remains unclear, a comparable level of immune stimulation between co-transcriptionally capped BioNTech mRNA and enzymatically capped SC-IVT has also been evidenced by RIG-I-dependent CXCL10 production in human BLaER1 cells by Dr. Thomas Zillinger (Chapter 1.4.4, Figure 9A).

Additionally, it is worth reiterating that the higher induction of innate immune responses by the co-transcriptionally capped BioNTech mRNA compared to the enzymatically capped Moderna mRNA (Chapter 1.4.4, Figure 9; Chapter 3.1.1, Figure 14) cannot be attributed to the different capping techniques, but instead results from oligo(dT)-purification employed specifically by Moderna (Chapter 1.4.4, Figure 10; Chapter 3.1.2, Figure 17), as demonstrated during the collaborative effort of the Bartok and Hartmann groups.

The comparison of capping efficiencies between co-transcriptional and enzymatic capping is largely limited by the challenges associated with quantifying the capping status of IVT-mRNA. The most direct method is the differentiation of capped and uncapped transcripts via LC/MS. However, IVT-mRNA represents a heterogeneous RNA population with sizes ranging up to several kilobases, which impedes the separation and identification of capped and uncapped RNAs. Therefore, the present study employed short, chemically synthesized RNAs to investigate the functionality of enzymatic capping. Other preliminary methods include the cleavage of the 5′ mRNA end prior to LC/MS

analysis or the detection of uncapped RNA based on ligation of radiolabeled or fluorescent probes to the 5′ end.[206–208] However, the cleavage of the former method is sequence-specific and therefore only depicts the 5′ end of the target mRNA and prematurely terminated transcripts, whereas other nonspecific transcripts are not included. Besides, these methods are not yet widely used and further characterization of their precision is required.

Finally, the selection of an appropriate capping method involves further considerations. While co-transcriptional capping represents a one-step approach to generate functional IVT-mRNA, preliminary data of this study indicated that co-transcriptional capping reduces mRNA yield while providing equal purity compared to standard *in vitro* transcription (data not shown). The observed mRNA yields for co-transcriptional capping were in line with previous reports and represented a 25 to 50 % reduction in total RNA amount compared to standard *in vitro* transcription.[97] Although enzymatic capping involves an additional reaction and purification step, the resulting material loss was usually limited to 10 – 20 % (data not shown). Therefore, besides the modulation of mRNA inflammatory potential by the capping method, the overall yield, purity, and laboriousness contribute to the applicability of each capping method. Nevertheless, further experiments are required to identify the optimal capping method tailored to the respective application.

Besides capping of the 5′ end, experimental evidence of the Bartok and Hartmann groups suggests phosphatase treatments as an effective measure to reduce activation of RIG-I by IVT-mRNA. The presented findings confirm functional dephosphorylation of dsRNA species by the polyphosphatase enzyme and demonstrate effective reduction of RIG-I-mediated immune responses (Chapter 3.1.1, Figure 15, Figure 16; Chapter 3.1.4, Figure 22). Therefore, employing polyphosphatase treatments as standard procedure during manufacturing has the potential to reduce undesired innate immune stimulation by IVT-mRNA preparations. Nevertheless, polyphosphatase digestion does require an additional reaction and purification step and increases manufacturing time and costs. Therefore, individual cost-benefit analyses will determine the optimal manufacturing conditions for mRNA therapeutics.

4.2 Species-specific differences of RLR-mediated mRNA sensing in humans and mice

The highly collaborative project of the Bartok and Hartmann groups revealed striking species-specific differences in the RLR-mediated sensing of IVT-mRNA between humans and mice: Firstly, human cells were shown to detect mRNA primarily via RIG-I, while murine cells utilized both RIG-I and MDA5 for mRNA detection, depending on the mRNA modification status (Chapter 1.4.4, Figure 9, Figure 11; Chapter 3.1, Figure 15, Figure 24, Figure 28). The experimental evidence collected in multiple different primary cells and cell lines indicates that the differential engagement of RLRs for innate mRNA sensing is not cell type- but indeed species-specific.

On top of this, the mRNA sensing was found to be modulated by m1Ψ in a species-specific manner: While the activation of human RIG-I was only partially reduced by incorporation of m1Ψ, murine RIG-I activation was completely abrogated (Chapter 1.4.4, Figure 11; Chapter 3.1, Figure 24, Figure 28). Furthermore, while activation of human MDA5 was also reduced by m1Ψ, murine MDA5 activation was actually enhanced (Chapter 1.4.4, Figure 11; Chapter 3.1, Figure 24, Figure 28). Therefore, in addition to the differential engagement of RLRs in humans and mice, the collaborative research effort of the Bartok and Hartmann groups demonstrated receptor-intrinsic differences between species, which were likewise independent of cell types, as evidenced by overexpression of human and murine RLRs in THP-1 cells (Chapter 3.2.3, Figure 33; Chapter 3.2.4, Figure 39).

In addition, the ensuing investigation of other commonly used nucleoside modifications revealed even more differences between human and murine RLR-mediated mRNA sensing and their modulation by nucleoside modifications. While the incorporation of 5moU into an optimal RIG-I ligand abrogated the activation of specifically murine RIG-I, human RIG-I was only slightly affected (Chapter 3.2.3, Figure 31, Figure 32, Figure 33). Murine RIG-I was also more susceptible to the other two uridine modifications tested, Ψ and m1Ψ, in contrast to human RIG-I. Additionally, activation of murine MDA5 by the ds-mRNA was significantly and strongly enhanced by Ψ and m1Ψ, while human MDA5 activation was unaffected by m1Ψ and only slightly enhanced by Ψ (Chapter 3.2.4, Figure 38).

Notably, no species-specific differences in RLR activation nor receptor-intrinsic ligand variations between human and murine RLRs have been described prior to the collaborative work of the Bartok and Hartmann groups.

Both RIG-I and MDA5 are considered highly relevant in both humans and mice, based on the susceptibility to viral infections of mice deficient in either RLR or patients harboring mutant RLRs.[209,210] The causes for the observed differences between human and murine RLR activation are currently unknown, but several possibilities exist. For example, the amino acid sequence of RLRs differs between humans and mice, with ~77 % homology for RIG-I and ~80 % homology for MDA5,

which might result in different ligand preferences.[211–214] Furthermore, differences in the protein sequence, functionality, or expression levels of downstream adapter proteins or regulatory proteins could affect RLR engagement during mRNA sensing. For example, activation of RIG-I is known to require the ubiquitination of its CTD as well as CARDs by several E3 ligases. Rajsbaum *et al.* reported that TRIM25 is the primary E3 ligase in humans responsible for RIG-I CARD ubiquitination, whereas mice predominantly depend on other ligases, such as Riplet.[215] This differential regulation of RIG-I ubiquitination could contribute to the species-specific RLR engagement between humans and mice. However, other mechanisms are conceivable and warrant further investigation.

Furthermore, it remains to be investigated which RLR functions besides sensing of IVT-mRNA are affected by species-specific differences. Future studies should include systematic comparisons of RLR activation between human and murine models to characterize the extent and mechanisms of these differences. A potential approach to address the underlying mechanisms could be the exchange of protein domains or specific amino acids between human and murine RLRs followed by an investigation of the functional outcome in overexpression studies.

Whatever the underlying mechanisms for the species-specific mRNA sensing in humans and mice may be, they likely evolved due to different evolutionary pressures. As humans and mice live in different environments and are exposed to different pathogens, this likely led to species-specific adaptations. In line with this, species-differences of other pattern recognition receptors have been described before. For example, murine STING exhibits enhanced responsiveness to bacterial cyclic dinucleotides, such as 3′-3′-cGAMP, compared to human STING, which demonstrates a higher selectivity for the endogenous second messenger 2′-3′-cGAMP depending on the respective polymorphism.[216–218] Furthermore, mice lack functional TLR8 but express the endosomal RNA sensor TLR13, which is absent in primates.[219,220] Since both TLR8 and TLR13 are endosomal sensors of bacterial RNA, this redundancy may have driven species-specific evolutionary selection. In addition, humans exhibit a significantly greater sensitivity of up to three magnitudes to the TLR4-ligand LPS than mice.[221] These species-specific differences in innate sensing highlight the evolutionary divergence between humans and mice, even within broadly conserved innate immune pathways.

Altogether, these findings hold important implications for translational research. Mice are valuable models for pre-clinical research and any species-specific difference impedes the extrapolation of research data to human application. This problem affects the safety and efficacy profiles of mRNA therapeutics and necessitates additional validation in human *in vitro* models. Additionally, characterization of species-specific differences is essential for improving the translatability of murine data into human clinical applications. While the employment of other animal models, such as the closely related primates, might present an alternative, this comes with several ethical and practical considerations.

Furthermore, differences between human and murine RLRs hold implications for certain autoinflammatory diseases caused by mutated RLRs, such as the Aicardi-Goutières syndrome. These diseases are often studied in representative murine models and raising awareness for this issue in researchers could facilitate the understanding and treatment of such diseases.

4.3 Modulation of innate immune responses by nucleoside modifications

4.3.1 Modulation of dsRNA content in IVT-mRNA by nucleoside modifications

The reduction in innate immune activation by IVT-mRNA incorporating modified nucleosides is believed to be caused by a reduced formation of dsRNA during *in vitro* transcription. In previous studies, a reduction of dsRNA content has been described for m1Ψ, 5moU, and m5C, whereas Ψ had ambiguous effects and m6A had no effect.[25,115,144–146] These findings were confirmed in the present study by performing dot blots with anti-dsRNA antibody J2 staining (Chapter 3.2.2**,** Figure 29, Figure 30). Additionally, the ambiguous effects of Ψ were found to be ligand-dependent (Chapter 3.2.2**,** Figure 29, Figure 30), in line with previous reports, whereas the effects of other modifications were consistent between ligands.[115]

However, the mechanisms leading to the modulation of dsRNA content by modified nucleosides remain unknown. A modulated polymerase activity or altered inter- or intramolecular RNA structures could affect the dsRNA-generating mechanisms, such as abortive termination, loop-back, or promoter-independent transcription. In addition, the presented data indicate that modified nucleosides not only regulate the dsRNA quantity but also quality. For example, while Ψ increased the overall dsRNA content in EGFP-Fluc mRNA (Chapter 3.2.2, Figure 29), its capacity to stimulate RIG-I was reduced (Chapter 3.2.1, Figure 28). Furthermore, m1Ψ-modified EGFP-Fluc mRNA had a reduced dsRNA content (Chapter 3.2.2, Figure 29) and reduced capability to activate RIG-I (Chapter 3.2.1, Figure 28), but activation of murine MDA5 was enhanced (Chapter 3.2.1, Figure 28). While other experimental evidence indicates a direct mechanistic enhancement of murine MDA5 activation by Ψ- and m1Ψ-modified ds-mRNA (Chapter 3.2.4, Figure 38), it is conceivable that Ψ and m1Ψ not only affect dsRNA quantity but also quality by specifically inhibiting the generation of short RIG-I ligands while facilitating generation of long dsRNA species. Of note, dsRNA species shorter than 40 bp are not detected by the anti-dsRNA antibody J2, while long dsRNA provides a proportionally greater signal.[179,222] It remains to be investigated how RNA length, sequence, or other currently unknown factors affect modulation of dsRNA content by nucleoside modifications. Initial

approaches to this investigation could include a dsRNA ladder of varying sizes and nucleotide content.

Consistent binding of J2 to dsRNA was confirmed for all modifications except 5moU, which exhibited a reduction in J2 binding affinity of approximately 45 % (Chapter 3.2.2, Figure 30). This new finding underscores the need to re-evaluate previous publications investigating dsRNA content in 5moU-modified IVT-mRNA and indicates that their conclusions should be interpreted with caution.[144,202] Of note, base pairing was not affected by 5moU based on the successful activation of human RIG-I by a 5moU-modified short dsRNA (Chapter 3.2.3, Figure 31). This finding demonstrates that the exact quantification of dsRNA content in an IVT-mRNA requires a standard dilution series of an equally modified dsRNA. Despite the inaccurate estimation of dsRNA content, 5moU-modified mRNA induced the lowest innate immune activation of all tested modifications in all tested human and murine cell types (Chapter 3.2.1, Figure 27, Figure 28), thus representing the most promising modification for mRNA therapeutics, regardless of the causative mechanisms.

4.3.2 Modulation of RIG-I-like receptor activation by nucleoside modifications

Modified nucleosides are known to reduce innate immune responses to IVT-mRNA, but their specific effects on individual PRRs remain only partially understood. Most research has focused on Ψ, leaving the impact of other modifications, such as 5moU, on specific PRRs largely unexplored (see Table 1). Furthermore, specifically the modulation of RLR activation by nucleoside modifications remains largely unexplored. Lastly, the mechanisms by which these modifications modulate the innate immune response, such as potential direct interference with receptor activation or reduced dsRNA generation during *in vitro* transcription, have been insufficiently characterized. Therefore, this study systematically compared innate immune responses to IVT-mRNA incorporating commonly used nucleoside modifications, with a particular focus on RLRs.

The mRNA-induced activation of both human and murine RIG-I was found to be reduced by uridine modifications and m6A, but not m5C (Chapter 3.2.1, Figure 27, Figure 28). While Ψ has been previously reported to reduce RIG-I activation, and the collaborative efforts of the Bartok and Hartmann groups demonstrated the same for m1Ψ, other modifications and their effect on RIG-I-mediated innate immune responses had been insufficiently characterized prior to this study.[13,117,126,149,150] Importantly, this study demonstrates for the first time that 5moU is the most efficient modification in reducing RIG-I activation by IVT-mRNA (Chapter 3.2.1, Figure 27, Figure 28), in line with its efficient reduction of dsRNA content (Chapter 3.2.2, Figure 29A,C-D). Since the generation of immunogenic byproducts during *in vitro* transcription had been largely unacknowledged at that time, the Ψ-mediated reduction of RIG-I activation had previously been

attributed to a direct inhibition of RIG-I binding or activation.[13,117] In contrast, the present study demonstrates that direct effects of the modifications on activation of human RIG-I are negligible and that the modulation is primarily dependent on the reduced generation of dsRNA byproducts, as evidenced by a 26 bp dsRNA incorporating modified nucleosides, representing an optimal RIG-I ligand (Chapter 3.2.3, Figure 31C, Figure 32A-B). The only exception to this is 5moU, which presented a statistically significant but moderate inhibition of human RIG-I activation of approximately 25 – 30 % (Chapter 3.2.3, Figure 31C, Figure 32A-B). While the modulation pattern of murine RIG-I by nucleotide modifications was similar to human RIG-I, meaning a reduced activation by uridine modifications and m6A, but not m5C (Chapter 3.2.3, Figure 31B, Figure 32C-D), the effects induced by uridine modifications were only partially dependent on a reduced dsRNA content (Chapter 3.2.3, Figure 31D, Figure 32C-D). Instead, uridine modifications seemed to directly interfere with activation of murine RIG-I via currently unknown mechanisms (Chapter 3.2.3, Figure 31D, Figure 32C-D). Strikingly, incorporation of 5moU into an optimal RIG-I ligand completely abolished activation of murine RIG-I even at high concentrations, indicating a strong direct impediment of RIG-I activation (Chapter 3.2.3, Figure 32C-D).

In BMDCs, the incorporation of m5C into IVT-mRNA shifted the innate immune response from MDA5 to RIG-I (Chapter 3.2.1, Figure 28B), indicating an enhanced activation of murine RIG-I by m5C. While a previous study indicated an enhanced binding of human RIG-I to m5C-modified RNA, the present study observed this enhanced activation by m5C specifically for murine but not human RIG-I (Chapter 3.2.1, Figure 28).[150] Furthermore, this effect was observed specifically for IVT-mRNA. Other RNAs, such as the 24 nt ssRNA, 26 bp dsRNA, 512 nt ssRNA (ss512B), or 512 bp dsRNA (ds512B) did not demonstrate enhanced activation of murine RIG-I in BMDCs upon incorporation of m5C (Chapter 3.2.3, Figure 31; Chapter 3.2.4; Figure 34), demonstrating that m5C does not directly enhance binding or activation of murine RIG-I and that this mRNA-specific phenomenon is mediated by currently unknown secondary mechanisms. An altered dsRNA content of IVT-mRNA by incorporation of m5C can be excluded as a cause based on anti-dsRNA J2 dot blots (Chapter 3.2.2, Figure 29). Nevertheless, it should once again be noted that RIG-I agonists shorter than 40 bp are not detected by the J2 antibody, and it remains to be investigated whether m5C specifically modulated the generation of short dsRNA in specifically IVT-mRNA.[179] This would be in line with the notion that nucleoside modifications modulate not only the quantity but also the nature of dsRNA byproducts.

Inhibitory effects of m6A on activation of RIG-I have been indicated by several previous publications. For example, Durbin *et al.* reported that m6A-modified RNAs exhibit a reduced binding affinity to RIG-I.[150] Furthermore, loss of the m6A writer METTL3 was found to enhance formation of endogenous dsRNA and cause innate immune activation via RIG-I.[141,223,224] Additionally, m6A modifications are presumably utilized by several viruses to evade recognition of RIG-I.[141,142,225–227] In contrast, the present study demonstrates the absence of direct mechanistic

inhibition of human or murine RIG-I by m6A (Chapter 3.2.3, Figure 31, Figure 32). Given that the previous studies do not provide direct experimental evidence of m6A-mediated inhibition of RIG-I activation, secondary mechanisms could be involved in the previously observed m6A-mediated reduction of innate immune responses. Indeed, several of such mechanisms have been proposed before. For example, m6A-modified RNAs were found to be sequestered by reader proteins, such as YTHDF2 and YTHDF3, thereby preventing binding to RIG-I and facilitating mRNA decay.[227–229] Furthermore, the mRNAs of IFNβ and several ISGs were found to be m6A-modified, resulting in an enhanced translation by currently unknown mechanisms, which would explain why a loss of m6A-writer proteins leads to a reduced and less-efficient innate immune response.[230,231] Besides, m6A was found to reduce A-to-I editing on endogenous dsRNA and alter degradation by nucleases, such as RNase L, which is known to produce RIG-I activating RNA species.[56,223,232] Further experiments are required to elucidate these mechanisms.

Although a previous study addressed the modulation of MDA5 activation by nucleoside modifications, this thesis reveals a significant discrepancy.[25] Contrary to earlier findings, *in vitro* transcribed ss- or ds512B are not optimal MDA5 ligands (Chapter 3.2.4; Figure 34). By recreating the experiments including RIG-I-deficient HEK 293T cells, this study demonstrates that Mu *et al.* unintentionally measured endogenous RIG-I activation by ss- or ds512B in HEK 293T cells and erroneously attributed the immune response to MDA5 (Chapter 3.2.4; Figure 37).[25] As a result, prior conclusions about MDA5 modulation by nucleoside modifications are incorrect. Notably, the same research group later showed that, while MDA5 binds and forms filaments on ds512B, this does not induce MDA5-dependent IFNβ-promoter activity, which they attributed to transfection reagent artifacts.[4] It appears that 500 bp dsRNA is insufficient for full MDA5 activation, consistent with reports indicating a requirement of at least 2000 bp dsRNA to shift activation from RIG-I to MDA5.[23] This discrepancy highlights that receptor binding and ATPase activity do not necessarily correlate with functional signaling and underscores the importance of including appropriate controls to avoid biased conclusions.

In conclusion, there was no prior knowledge about the impact of nucleoside modifications on MDA5 activation prior to the collaborative work of Bartok and Hartmann groups and this thesis. The effects of m1Ψ have been investigated while studying the COVID-19 vaccines (in collaboration with Bartok group), while this thesis proceeded to further examine m1Ψ and other commonly used nucleoside modifications.

The mRNA-induced activation of human MDA5 in BLaER1 cells was found to be reduced by all modifications (Chapter 3.2.1, Figure 28A). The inhibition of human MDA5 by Ψ and m1Ψ was largely mediated by a reduced dsRNA content of the IVT-mRNA, as demonstrated by a ds-mRNA, although a slight direct inhibition by m1Ψ was discernible (Chapter 3.2.4, Figure 38A, Figure 39B). The modifications 5moU, m5C, and m6A abrogated human MDA5 activation by ds-mRNA,

indicating a direct impediment of MDA5 activation independent of dsRNA content in IVT-mRNA (Chapter 3.2.4, Figure 38A, Figure 39B).

In BMDCs, mRNA-induced activation of murine MDA5 was enhanced by Ψ and m1Ψ via currently unknown mechanisms, and abrogated by 5moU, m5C, and m6A (Chapter 3.2.1, Figure 27B, Figure 28B). The enhanced activation of murine MDA5 by Ψ and m1Ψ was independent of dsRNA byproducts and also manifested for the ds-mRNA (Chapter 3.2.4, Figure 38B, Figure 39B). The mechanism of Ψ- and m1Ψ-mediated enhanced MDA5 activation currently remains unknown and requires further investigation (as discussed below). Equivalent to human MDA5, murine MDA5 activation was abrogated by incorporation of 5moU, m5C, and m6A in dsRNA, suggesting a direct mechanistic impediment of receptor activation (Chapter 3.2.4, Figure 38B, Figure 39B).

In conclusion, this study is the first to demonstrate that incorporation of 5moU, m5C, or m6A completely abrogates the activation of both human and murine MDA5 by rendering the dsRNA non-stimulatory rather than altering dsRNA content, potentially indicating a direct mechanistic inhibition of MDA5 by these modifications. In addition, Ψ and m1Ψ specifically enhance the activation of murine MDA5 in a species-specific manner and via direct effects.

For modifications that directly modulate RIG-I or MDA5 activation, further investigation is needed to determine the underlying mechanisms. To investigate the potential modulation of receptor binding affinity, techniques such as EMSA (electrophoretic mobility shift assay), protein-RNA co-precipitation, or electron microscopy could be employed. Additionally, the nucleoside modifications may impact receptor functionality, including ATP-dependent translocation or conformational changes, which can be studied using ATPase assays or limited trypsin digestion, as described previously.[25,150] Mutation of key amino acids involved in dsRNA recognition by RLRs could also shed light on how modified nucleosides modulate these receptors. Moreover, exchanging protein domains or amino acids between human and murine RLRs could help clarify the species-specific effects of 5moU on RIG-I, and of Ψ and m1Ψ on MDA5.

Lastly, while TLRs were not the main focus of this study, a holistic investigation of innate immune responses to IVT-mRNA and its modulation by nucleoside modifications is essential. While previous research regarding TLRs and certain nucleoside modifications exists, and the collaborative work of the Bartok and Hartmann groups extended this knowledge to m1Ψ, 5moU has not been investigated before. Thus, the present study demonstrates for the first time that incorporation of 5moU into IVT-mRNA inhibits activation of human TLR7 and TLR8. Given that both TLR7 and TLR8 bind uridine-containing RNA degradation products, it is not unexpected that uridine modifications are effective in inhibiting these receptors. However, it remains to be elucidated whether the modifications affect activation of TLR7 and TLR8 or modulate the degradation by endosomal nucleases. Lastly, engagement of TLR3 by IVT-mRNA was not detectable in the present study and thus requires further investigation.

In summary, the present study endorses m1Ψ and 5moU as promising modifications for mRNA therapeutics that aim for minimal innate immune stimulation. While reducing the activation of RLRs and TLRs, these modifications simultaneously offer an effective translation, as discussed below.

4.4 Translation of *in vitro* transcribed mRNA: modulation by nucleoside modifications and restriction by innate immune responses

Efficient translation is the foundation of mRNA therapeutics, ensuring that the genetic instructions encoded in the mRNA are rapidly converted into functional proteins. Optimization of mRNA translation can maximize the therapeutic efficacy, while enabling lower dosages and reducing side effects. All nucleoside modifications tested in this study, except m6A, have been previously found to enhance translation of IVT-mRNA.[83,117,144,188,189] Notably, m1Ψ is the first and, to date, only nucleoside modification utilized in an EMA-approved mRNA vaccine (COVID-19 vaccines by BioNTech and Moderna) and applied in human therapeutics.[59,60]

Consistent with previous publications, this study identifies m1Ψ and 5moU as the most effective modifications for enhancing mRNA translation (Chapter 3.3.1, Figure 41, Figure 42).[144,189] Both modifications hold promise for mRNA therapeutics, depending on the specific application and desired level of innate immune stimulation. While m1Ψ excels in boosting translation (Chapter 3.3.1, Figure 41, Figure 42), 5moU offers the lowest innate immune activation (Chapter 3.2.1, Figure 27). As a result, both are suitable for mRNA-based vaccines, but the minimal immune response conferred by 5moU may be particularly advantageous for protein replacement therapies. Although combining m1Ψ and 5moU in equal proportions did not improve mRNA translation compared to each individual modification (Chapter 3.3.5, Figure 51), different ratios should be further explored.

In contrast, m6A-modified mRNA was not translated (Chapter 3.3.1, Figure 41, Figure 42), despite the abundance of m6A in cellular mRNA and its function in innate evasion mechanisms of several viruses that maintain efficient replication.[139–142] Previous publications likewise demonstrated dysfunctional translation of m6A-modified IVT-mRNA.[117,185,187] Several studies show that natural m6A modifications are targeted to specific sites in endogenous mRNA that lie preferentially within UTRs.[233] Therefore, the location of m6A modifications within the mRNA could be critical for the outcome. In line with this, incorporating m6A modifications specifically in the 5′ UTR of IVT-mRNA was found to promote cap-independent translation.[234] Besides, modulation of mRNA translation by m6A was reported to depend on the position within codons and that multiple modifications within a single codon strongly reduce translation efficiency.[235] The hypothesis of site-specific m6A modulation could be further investigated by transcribing individual unmodified and modified mRNA parts and joining them via ligation, or modulating codon usage in order to

incorporate m6A at defined positions. Lastly, the poly(A)-tail was fully m6A-modified in the present study due to its templated-encoded transcription, which could potentially modulate RNA secondary structure or affinity to poly(A)-binding proteins and disable functional translation. This could be circumvented by transcribing an m6A-modified mRNA followed by enzymatic addition of an unmodified poly(A)-tail via the poly(A)-polymerase. Nevertheless, the absence of functional translation renders m6A currently ineffective for mRNA therapeutics.

The mechanisms by which nucleoside modifications modulate mRNA translation remain largely unknown. It has been proposed that the reduced innate immune stimulation and alleviated translational restriction are in part responsible.[117,118] While human BLaER1 cells indeed exhibited a MAVS- and IFNAR-mediated restriction of mRNA translation (Chapter 3.3.2, Figure 43A-B, Figure 44A-B), which was proportional to the extent of innate immune stimulation (Chapter 3.3.2, Figure 43C, Figure 44C), the relative translation pattern between unmodified and modified mRNA remained similar between wildtype and *MAVS*$^{-/-}$ or *IFNAR*$^{-/-}$ BLaER1 cells, respectively (Chapter 3.3.2, Figure 43A, Figure 44A), indicating that the positive effect is primarily mediated by a direct modulation of translation efficiency. In murine BMDCs, however, no MAVS- or IFNAR-mediated restriction of mRNA translation by innate immune activation was observed, consistent with the observation that the high inflammatory capacity of Ψ- and m1Ψ-modified mRNA did not hinder translation (Chapter 3.3.2, Figure 45A-B, D-E). It remains to be investigated whether this discrepancy between murine BMDCs and human BLaER1 cells is a cell type-specific effect or another species-specific divergence. Another possibility is that specifically activation of RIG-I, as is the case in human cells, leads to a translational restriction, while MDA5, the primary receptor in mice, does not or to a lesser extent. Supporting this, m5C-modified mRNA, the only variant that activated RIG-I in murine BMDCs, was also the only variant exhibiting a slight MAVS-mediated translational restriction in BMDCs (Chapter 3.3.2, Figure 45A-B). Potentially in line with this, Boehmer *et al.* reported that activation of RIG-I and subsequent type I IFN production primes the OAS/RNase L pathway, which then induces apoptosis via activation of OAS1 by the same 5′ppp-dsRNAs that initially activated RIG-I.[54] This mechanism might contribute to a RIG-I-specific restriction of mRNA translation, although this effect has only been described in tumor cells so far. In general, mRNA-induced cell death should be investigated, for example by flow cytometry employing annexin V staining. Besides, RIG-I- or MDA5-induced MAVS activation might involve currently unknown differences in the downstream signaling pathways resulting in the diverging functional outcomes. To explore this hypothesis, further studies should assess the impact of RLR activation on mRNA translation through additional transfection of RLR ligands while including *RIG-I*$^{-/-}$ and *MDA5*$^{-/-}$ cells alongside *MAVS*$^{-/-}$ in human and murine experimental models.

While activation of PKR is believed to contribute to the translational restriction of IVT-mRNA, this study found no supporting evidence. In contrast, the presented data suggest that the impact of PKR

activation by IVT-mRNA is negligible for mRNA translation (Chapter 3.3.4, Figure 47). Therefore, modulation of PKR activation was subsequently studied using a 512 bp dsRNA, which demonstrated PKR-mediated translational restriction for all immunogenic modifications (Chapter 3.3.4, Figure 49, Figure 47). While previous studies indicated that nucleoside modifications like Ψ could reduce PKR activation, the present study could not confirm this effect based on the ds512B (Chapter 3.3.4, Figure 49, Figure 47). Instead, m5C and m6A appeared to enhance PKR activation by the ds512B (Chapter 3.3.4, Figure 49, Figure 47), a finding previously indicated for m6A but not m5C.[118,198,199] However, it is possible that the experimental system used was not ideal for studying PKR activation. While PKR was activated by the ds512B in THP-1 dual cells, confirming the system's functionality, the sensitivity for detecting mRNA-induced PKR activation may have been insufficient. Additionally, since PKR activation was not directly quantified but inferred from reduced translation and RIG-I-mediated immune responses, the role of PKR in IVT-mRNA and its modulation by nucleoside modifications needs further investigation, for example analyzing PKR phosphorylation status after stimulation.

Finally, in rabbit reticulocyte lysate, which does not exhibit translational restriction due to TLR or RLR activation, but does possess functional PKR, nucleoside modifications similarly enhanced mRNA translation as observed *in cellulo* (Chapter 3.3.3, Figure 46A).[147,192–194] However, 5moU outperformed m1Ψ in this setting, in contrast to results obtained *in cellulo* (Chapter 3.3.3, Figure 46B). Due to the low innate immune stimulation by 5moU-modified mRNA (Chapter 3.2.1, Figure 27), it is unlikely that a reduced translational restriction in rabbit reticulocyte lysate is the cause for its superior translation compared to m1Ψ. Further research, including additional cell types, is required to explore this discrepancy. In conclusion, this finding confirms that, while mRNA-induced innate immune activation partially restricts mRNA translation, the benefits of nucleoside modifications are primarily due to their direct effects on the translational machinery. Nevertheless, the role of innate immune activation in mRNA translation should be further investigated *in vivo*, as *in vitro* studies only capture a subset of the broader system.

Moreover, the direct effects by which nucleoside modifications influence translation efficiency warrant further exploration. While m1Ψ has been shown to increase ribosome density on IVT-mRNA, other modifications have not been thoroughly studied.[147] Potential mechanisms include altered RNA-protein interactions, mRNA stability, secondary structure, and sub-cellular localization.[148] Additionally, the effects of mRNA sequence, nucleotide content, and codon usage on translation efficiency should be considered. Given the involvement of various enzymes in mRNA translation, additional mechanistic studies are necessary to fully understand how nucleoside modifications affect translation and RNA-protein interactions. Distinguishing between direct effects and those resulting from reduced innate immune activation remains a key challenge.

4.5 Conclusion & Outlook

The findings of this thesis and adjacent projects presented above may both potentially contribute to the better design of therapeutic mRNA as well as provide retrospective explanations for recent examples of vaccine development: During the COVID-19 pandemic, CureVac developed an mRNA vaccine encoding the SARS-CoV-2 spike protein but without m1Ψ incorporation. Administered at a lower dose (12 µg) than BioNTech (30 µg) and Moderna (100 µg), this relative reduction likely stemmed from the higher pro-inflammatory capacity of unmodified mRNA. CureVac's vaccine achieved only 48 % efficacy in phase III trials, compared to 94 % for BioNTech and Moderna, likely due to the lower dosage and reduced translation efficiency of unmodified mRNA.[79,236] While multiple factors may have influenced the efficacy, including emerging viral variants, the absence of nucleoside modifications may have heightened innate immune activation, limiting tolerable dosing and overall therapeutic success.

In another example, intravenous mRNA delivery to a multiple sclerosis mouse model without any innate immune stimulation induced peripheral tolerance against the encoded antigen, as evidenced by a reduction of antigen-specific effector T cells and an increase in regulatory T cells.[200] While beneficial for treating autoimmune diseases, these effects would be detrimental for vaccination settings.

These examples underscore the importance of fine-tuning the innate immune stimulation induced by mRNA vaccines. The ultimate goal for mRNA-based therapeutics is to tailor immune activation according to the therapeutic application: Vaccines benefit from precise and controllable activation of innate immune receptors to elicit an effective immune response. On the other hand, applications such as protein replacement therapy and cell fate reprogramming would benefit from non-immunogenic mRNA, since innate immune activation would likely limit protein translation. Designing such mRNAs tailored to the respective application requires extensive knowledge of innate mRNA sensing by pattern recognition receptors (PRRs).

The present thesis examines the innate immune activation triggered by *in vitro* transcribed (IVT)-mRNA, as utilized in the COVID-19 mRNA vaccines by BioNTech and Moderna, with a specific focus on RIG-I-like receptors (RLRs). In collaboration with the Bartok group, it was demonstrated that RLRs play primary roles in the sensing of mRNA vaccines and IVT-mRNA. RLRs were shown to be activated by double-stranded RNA byproducts generated during *in vitro* transcription. Several methods to reduce the inflammatory capacity of IVT-mRNA were investigated. For example, oligo(dT)-purification and dephosphorylation are presented as promising strategies to remove immunogenic dsRNA and reduce RIG-I activation. While the incorporation of nucleoside modifications has been previously shown to prevent activation of TLRs, this study, in collaboration with the Bartok group, characterizes the effects of commonly used modifications on RLR activation.

Particularly m1Ψ and 5moU were the most effective modifications in reducing RLR activation by IVT-mRNA, while simultaneously providing maximal translation. Furthermore, the mechanisms by which these commonly used modifications modulate RLR activation have been elucidated, such as direct impediments of receptor engagement or the reduced formation of dsRNA byproducts during transcription.

In addition, the collaborative work of the Bartok and Hartmann groups, along with this thesis, provides valuable insight into the fundamental mechanisms of RLR activation. The differential modulation of RIG-I and MDA5 by nucleoside modifications enhances our understanding of their distinct ligand recognition processes. Moreover, the observed species-specific differences in RLR engagement and ligand preferences have important implications for both basic research and clinical applications. Notably, the findings regarding MDA5 contribute to a deeper understanding of its activation, which remains less characterized compared to RIG-I. These insights are not only essential for advancing mRNA-based therapeutics but also contribute to the foundation for future basic research into RLR activation and ligand requirements.

Finally, the presented findings facilitate the design of IVT-mRNA that selectively activates specific receptors, thereby tailoring immune responses and optimizing vaccine efficacy and safety. For example, type I IFNs are the main cytokines induced by TLR3, TLR7, and RLRs, and promote a T_H1-biased immune profile, which is advantageous for the immune defense against intracellular pathogens, such as viruses.[1] In contrast, TLR8, while also inducing T_H1-associated cytokines such as IFNγ and IL-12p70, simultaneously triggers high quantities of TNFα and IL-6, contributing to systemic inflammation and potentially increasing adverse effects.[237] Of note, RLRs also induce TNFα and IL-6, but only small amounts. Careful modulation of these pathways is essential to harness their benefits while minimizing unintended immunological consequences. The presented results also enable the design of a non-immunogenic mRNA, which could be used for mRNA vaccines in which protein expression and immune activation originate from two separate components. For instance, combining a non-immunogenic mRNA with a precise amount of immunogenic RNA species, such as RIG-I ligands, presents a promising approach for controllable adjuvanticity.[238] Additionally, non-immunogenic mRNA could be paired with specific adjuvants that, for example, trigger a T_H2-polarized response, thereby optimizing the immune defense against extracellular pathogens. These approaches may offer significant advantages by allowing more precise control over both antigen production and immune response modulation.

In conclusion, this study provides essential insights that will aid in the development of optimized IVT-mRNA with precise immunostimulatory properties or non-immunogenic profiles, paving the way for safer and more effective mRNA therapeutics.

5. Appendix

5.1 Supplementary Material

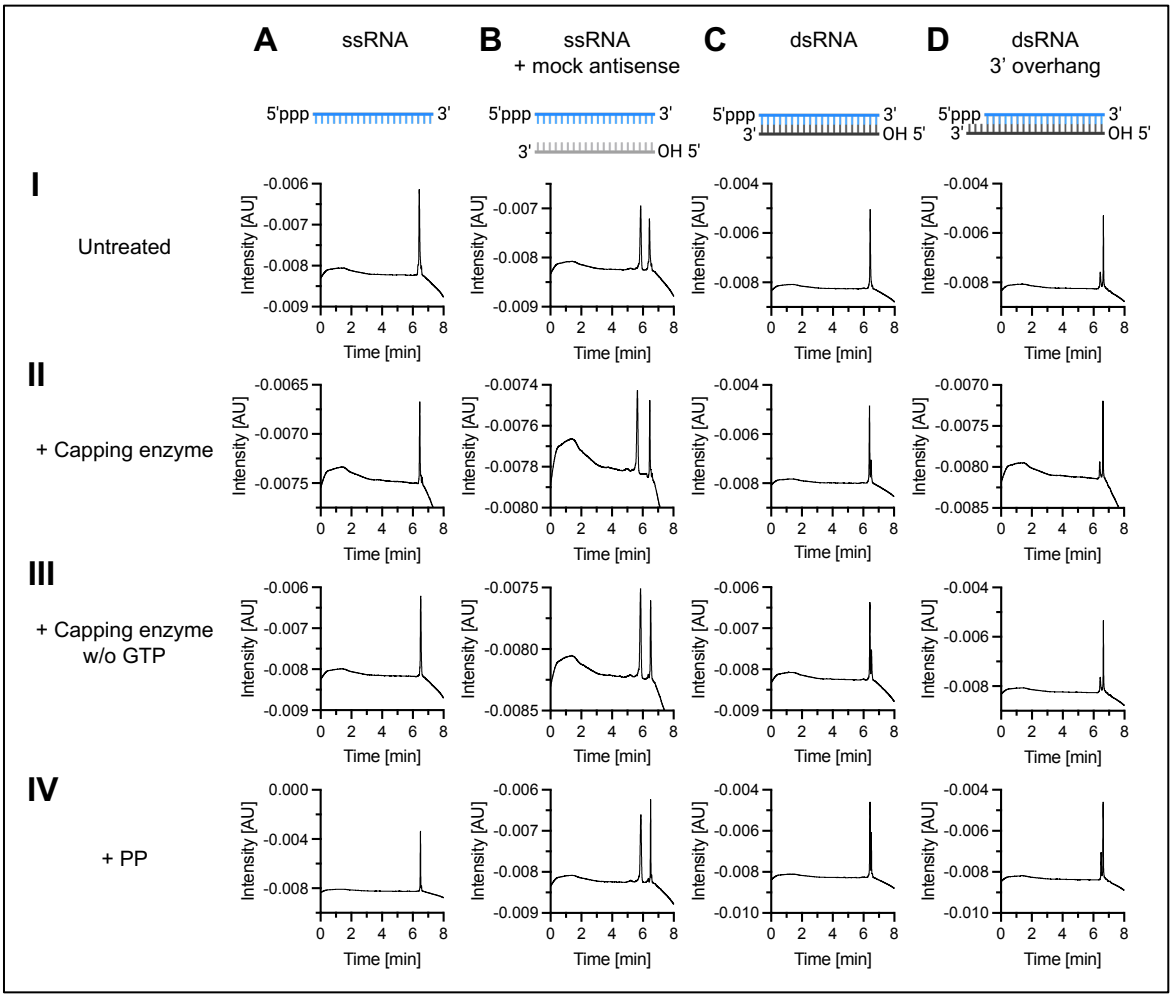

Figure 52: UV traces corresponding to deconvoluted ESI$^-$ RNA masses of LC/MS analysis
Synthetic 24 nt RNAs indicated in I – IV were treated as indicated in A – D and subjected to LC/MS analysis. Data depict the UV trace at 260 nm (I) ssRNA, (II) ssRNA with mock antisense, (III) blunt-end dsRNA, (IV) dsRNA with a 3 nt 3′ overhang. (A) Untreated RNAs, (B) standard capping using the vaccinia capping enzyme, (C) capping without GTP, (D) polyphosphatase (PP) digestion. Data are representative of three independent experiments.

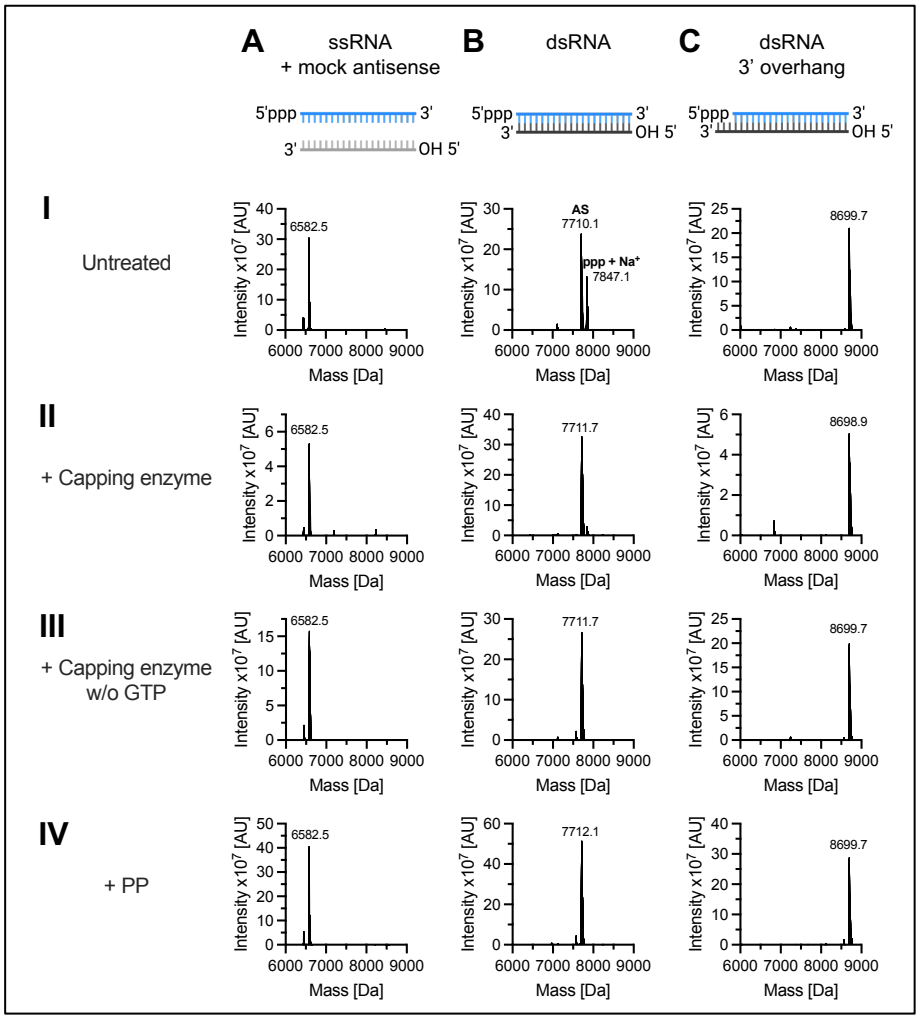

Figure 53: Deconvoluted ESI- masses of the corresponding antisense strands
Synthetic 24 nt RNAs indicated in I – IV were treated as indicated in A – D and subjected to LC/MS analysis. Data depict the deconvoluted ESI^- masses of the main peak assigned to the RNA antisense strand (depicted in grey or black, respectively). (I) ssRNA, (II) ssRNA with mock antisense, (III) blunt-end dsRNA, (IV) dsRNA with a 3 nt 3′ overhang. (A) Untreated RNAs, (B) standard capping using the vaccinia capping enzyme, (C) capping without GTP, (D) polyphosphatase (PP) digestion. Data are representative of three independent experiments.

5.2 Abbreviations

2-5A	2′-5′-linked oligoadenylate
5moU	5-Methoxy-uridine
ACE2	Angiotensin-converting enzyme 2
APC	Antigen-presenting cell
ATF4	Activating transcription factor 4
ATP	Adenosine triphosphate
AUC	Area under the curve
BCR	B cell receptor
BLaER1	B cell Leukemia C/EBPαER clone 1
BMDC	Bone marrow-derived dendritic cell
BMM	Bone marrow-derived macrophage
Bp	Base pairs
CARD	Caspase activation and recruitment domain
CD	Cluster of differentiation
cGAS	Cyclic GMP-AMP synthase
Cluc	Cypridina luciferase
COVID-19	Coronavirus disease-2019
CQ	Chloroquine
CTD	C-terminal domain
CTL	Cytotoxic $CD8^+$ T lymphocyte
DC	Dendritic cell
DEPC	Diethyl pyrocarbonate
DMEM	Dulbecco's Modified Eagle Medium
DMSO	Dimethyl sulfoxide
DNA	Deoxyribonucleic acid
DOTAP	1,2-dioleoyl-3-trimethylammonium-propane
Ds	Double-stranded
DSPC	Distearoylphosphatidylcholine
EDTA	Ethylenediaminetetraacetic acid
EGFP	Enhanced green fluorescent protein
eIF2α	Eukaryotic initiation factor 2α
eIF2αK1	Eukaryotic initiation factor 2α kinase 1
ELISA	Enzyme-linked immunosorbent assay
EMCV	Encephalomyocarditis virus
EMSA	Electrophoretic mobility shift assay
FCS	Fetal calf serum
Fluc	Firefly luciferase
Gluc	Gaussia luciferase
GMCSF	Granulocyte-macrophage colony-stimulating factor
GTP	Guanosine triphosphate
HPLC	High-performance liquid chromatography
H	Hour(s)
HT-DNA	Herring testes deoxyribonucleic acid
IFIT1	Interferon-induced protein with tetratricopeptide repeats 1

IFN	Interferon
IFNAR	Interferon-α/β receptor
Ig	Immunoglobulin
IKK	IκB kinase
IL	Interleukin
IRAK	Interleukin-1 receptor associated kinase
IRF	Interferon-regulatory factor
ISG	Interferon-stimulated gene
ISRE	Interferon-stimulated response element
IVT-mRNA	*In vitro* transcribed mRNA
JAK	Janus kinase
Kb	Kilo bases
LC/MS	Liquid chromatography / mass spectrometry
LGP2	Laboratory of genetics and physiology 2
LNP	Lipid nanoparticle
LRR	Leucine-rich repeat
M-CSF	Macrophage Colony Stimulating Factor
m1Ψ	N1-methyl-pseudouridine
m5C	5-Methyl-cytidine
m6A	N6-methyl-adenosine
MAVS	Mitochondrial antiviral-signaling protein
MDA5	Melanoma differentiation-associated protein 5
MFI	Mean fluorescent intensity
MHC	Major histocompatibility complex
Min	Minute(s)
MPL	Monophosphoryl lipid A
mRNA	Messenger RNA
MyD88	Myeloid differentiation primary response 88
NA	Not available
NFκB	Nuclear factor kappa-light-chain-enhancer of activated B cells
NK cell	Natural killer cell
NLRP3	NOD-like receptor family pyrin domain containing 3
Nt	Nucleotides
NTP	Nucleotide triphosphate
OAS1	2′-5′-Oligoadenylate synthetase 1
PBMC	Peripheral blood mononuclear cells
PBS	Phosphate buffered saline
PCR	Polymerase chain reaction
pDC	Plasmacytoid dendritic cell
PEG	Polyethylene glycol
PKR	Protein kinase R
Poly(A:U)	Polyadenylic–polyuridylic acid
Poly(I:C)	Polyinosinic:polycytidylic acid
PP	Polyphosphatase
PTO	Phosphothioate
Rcf	Relative centrifugal force
RIG-I	Retinoic-inducible gene I
RIPK3	Receptor-interacting serine/threonine-protein kinase 3

RLR	RIG-I-like receptor
RNA	Ribonucleic acid
RPMI	Roswell Park Memorial Institute 1640 Medium
RRL	Rabbit reticulocyte lysate
RT	Room temperature
S1P1R	Sphingosine-1-phosphate receptor 1
SAM	S-adenosylmethionine
SARS-CoV-2	Severe acute respiratory syndrome coronavirus 2
SC-IVT	SARS-CoV-2 *in vitro* transcript
SEAP	Secreted embryonic alkaline phosphatase
Sec	Seconds
SEM	Standard error of the mean
ss	single-stranded
STAT	Signal transducers and activators of transcription
TBK1	TANK-binding kinase 1
TCR	T cell receptor
TE	Terminator exonuclease
T_H cell	T helper cell
TIR	Toll/IL-1 receptor
TLR	Toll-like receptor
TNFα	Tumor necrosis factor α
TRAF	TNF receptor-associated factor
TRIF	TIR-domain containing adapter-inducing interferon-β
WHO	World Health Organization
ZAP	Zinc finger antiviral protein
ZBP1	Z-DNA/RNA binding protein 1
Ψ	Pseudouridine

5.3 References

1. Murphy, K., Weaver, C. & Berg, L. J. *Janeway's Immunobiology*. (Norton & Company, 2022).

2. Yoneyama, M. *et al.* The RNA helicase RIG-I has an essential function in double-stranded RNA-induced innate antiviral responses. *Nat. Immunol.* **5**, 730–737 (2004).

3. Yoneyama, M. *et al.* Shared and Unique Functions of the DExD/H-Box Helicases RIG-I, MDA5, and LGP2 in Antiviral Innate Immunity. *J. Immunol.* **175**, 2851–2858 (2005).

4. Ahmad, S. *et al.* Breaching Self-Tolerance to Alu Duplex RNA Underlies MDA5-Mediated Inflammation. *Cell* **172**, 797-810.e13 (2018).

5. Mannion, N. M. *et al.* The RNA-Editing Enzyme ADAR1 Controls Innate Immune Responses to RNA. *Cell Reports* **9**, 1482–1494 (2014).

6. Chung, H. *et al.* Human ADAR1 Prevents Endogenous RNA from Triggering Translational Shutdown. *Cell* **172**, 811-824.e14 (2018).

7. Schlee, M. Master sensors of pathogenic RNA – RIG-I like receptors. *Immunobiology* **218**, 1322–1335 (2013).

8. Schlee, M. & Hartmann, G. The Chase for the RIG-I Ligand—Recent Advances. *Mol. Ther.* **18**, 1254–1262 (2010).

9. Meylan, E. *et al.* Cardif is an adaptor protein in the RIG-I antiviral pathway and is targeted by hepatitis C virus. *Nature* **437**, 1167–1172 (2005).

10. Kawai, T. *et al.* IPS-1, an adaptor triggering RIG-I- and Mda5-mediated type I interferon induction. *Nat. Immunol.* **6**, 981–988 (2005).

11. Seth, R. B., Sun, L., Ea, C.-K. & Chen, Z. J. Identification and Characterization of MAVS, a Mitochondrial Antiviral Signaling Protein that Activates NF-κB and IRF3. *Cell* **122**, 669–682 (2005).

12. Alberts, B. *et al. Molecular Biology Of The Cell*. (W. W. Norton & Company, 2022).

13. Hornung, V. *et al.* 5'-Triphosphate RNA Is the Ligand for RIG-I. *Science* **314**, 994–997 (2006).

14. Schlee, M. *et al.* Recognition of 5′ Triphosphate by RIG-I Helicase Requires Short Blunt Double-Stranded RNA as Contained in Panhandle of Negative-Strand Virus. *Immunity* **31**, 25–34 (2009).

15. Goubau, D. *et al.* Antiviral immunity via RIG-I-mediated recognition of RNA bearing 5′-diphosphates. *Nature* **514**, 372–375 (2014).

16. Marques, J. T. *et al.* A structural basis for discriminating between self and nonself double-stranded RNAs in mammalian cells. *Nat. Biotechnol.* **24**, 559–565 (2006).

17. Binder, M. *et al.* Molecular Mechanism of Signal Perception and Integration by the Innate Immune Sensor Retinoic Acid-inducible Gene-I (RIG-I)*. *J. Biol. Chem.* **286**, 27278–27287 (2011).

18. Ren, X., Linehan, M. M., Iwasaki, A. & Pyle, A. M. RIG-I Selectively Discriminates against 5′-Monophosphate RNA. *Cell Rep.* **26**, 2019-2027.e4 (2019).

19. Cui, S. *et al.* The C-Terminal Regulatory Domain Is the RNA 5′-Triphosphate Sensor of RIG-I. *Mol. Cell* **29**, 169–179 (2008).

20. Regt, A. K. de *et al.* A conserved isoleucine in the binding pocket of RIG-I controls immune tolerance to mitochondrial RNA. *Nucleic Acids Res.* **51**, 11893–11910 (2023).

21. Schuberth-Wagner, C. *et al.* A Conserved Histidine in the RNA Sensor RIG-I Controls Immune Tolerance to N1-2′O-Methylated Self RNA. *Immunity* **43**, 41–51 (2015).

22. Im, J. H. *et al.* Mechanisms of length-dependent recognition of viral double-stranded RNA by RIG-I. *Sci. Rep.* **13**, 6318 (2023).

23. Kato, H. *et al.* Length-dependent recognition of double-stranded ribonucleic acids by retinoic acid–inducible gene-I and melanoma differentiation–associated gene 5. *J. Exp. Med.* **205**, 1601–1610 (2008).

24. Plumet, S. *et al.* Cytosolic 5′-Triphosphate Ended Viral Leader Transcript of Measles Virus as Activator of the RIG I-Mediated Interferon Response. *PLoS ONE* **2**, e279 (2007).

25. Mu, X., Greenwald, E., Ahmad, S. & Hur, S. An origin of the immunogenicity of in vitro transcribed RNA. *Nucleic Acids Res* **46**, gky177- (2018).

26. Bartok, E. & Hartmann, G. Immune Sensing Mechanisms that Discriminate Self from Altered Self and Foreign Nucleic Acids. *Immunity* **53**, 54–77 (2020).

27. Pichlmair, A. *et al.* Activation of MDA5 Requires Higher-Order RNA Structures Generated during Virus Infection. *J. Virol.* **83**, 10761–10769 (2009).

28. Peisley, A. *et al.* Cooperative assembly and dynamic disassembly of MDA5 filaments for viral dsRNA recognition. *Proc. Natl. Acad. Sci.* **108**, 21010–21015 (2011).

29. Peisley, A. *et al.* Kinetic mechanism for viral dsRNA length discrimination by MDA5 filaments. *Proc. Natl. Acad. Sci.* **109**, E3340–E3349 (2012).

30. Züst, R. *et al.* Ribose 2′-O-methylation provides a molecular signature for the distinction of self and non-self mRNA dependent on the RNA sensor Mda5. *Nat Immunol* **12**, 137–143 (2011).

31. Szretter, K. J. *et al.* 2′-O Methylation of the Viral mRNA Cap by West Nile Virus Evades Ifit1-Dependent and -Independent Mechanisms of Host Restriction In Vivo. *PLoS Pathog.* **8**, e1002698 (2012).

32. Luthra, P., Sun, D., Silverman, R. H. & He, B. Activation of IFN-β expression by a viral mRNA through RNase L and MDA5. *Proc. Natl. Acad. Sci.* **108**, 2118–2123 (2011).

33. Lazear, H. M., Schoggins, J. W. & Diamond, M. S. Shared and Distinct Functions of Type I and Type III Interferons. *Immunity* **50**, 907–923 (2019).

34. Maadidi, S. E. *et al.* A Novel Mitochondrial MAVS/Caspase-8 Platform Links RNA Virus–Induced Innate Antiviral Signaling to Bax/Bak-Independent Apoptosis. *J. Immunol.* **192**, 1171–1183 (2014).

35. Vince, J. E. & Tschopp, J. IRF-3 partners Bax in a viral-induced dance macabre. *EMBO J.* **29**, 1627–1628 (2010).

36. Besch, R. *et al.* Proapoptotic signaling induced by RIG-I and MDA-5 results in type I interferon–independent apoptosis in human melanoma cells. *J. Clin. Investig.* **119**, 2399–2411 (2009).

37. Kumar, S. *et al.* IPS-1 differentially induces TRAIL, BCL2, BIRC3 and PRKCE in type I interferons-dependent and -independent anticancer activity. *Cell Death Dis.* **6**, e1758–e1758 (2015).

38. Bauer, S. & Hartmann, G. *Toll-like Receptors (TLRs) and Innate Immunity*. (Springer, 2008).

39. Kawai, T., Ikegawa, M., Ori, D. & Akira, S. Decoding Toll-like receptors: Recent insights and perspectives in innate immunity. *Immunity* **57**, 649–673 (2024).

40. Sakaniwa, K. *et al.* TLR3 forms a laterally aligned multimeric complex along double-stranded RNA for efficient signal transduction. *Nat. Commun.* **14**, 164 (2023).

41. Liu, J. *et al.* A five-amino-acid motif in the undefined region of the TLR8 ectodomain is required for species-specific ligand recognition. *Mol. Immunol.* **47**, 1083–1090 (2010).

42. Tanji, H. *et al.* Toll-like receptor 8 senses degradation products of single-stranded RNA. *Nat. Struct. Mol. Biol.* **22**, 109–115 (2015).

43. Zhang, Z. *et al.* Structural Analysis Reveals that Toll-like Receptor 7 Is a Dual Receptor for Guanosine and Single-Stranded RNA. *Immunity* **45**, 737–748 (2016).

44. Shibata, T. *et al.* Guanosine and its modified derivatives are endogenous ligands for TLR7. *Int. Immunol.* **28**, 211–222 (2016).

45. Greulich, W. *et al.* TLR8 Is a Sensor of RNase T2 Degradation Products. *Cell* **179**, 1264-1275.e13 (2019).

46. Ostendorf, T. *et al.* Immune Sensing of Synthetic, Bacterial, and Protozoan RNA by Toll-like Receptor 8 Requires Coordinated Processing by RNase T2 and RNase 2. *Immunity* **52**, 591-605.e6 (2020).

47. Tong, A.-J. *et al.* Nucleotide modifications enable rational design of TLR7-selective ligands by blocking RNase cleavage. *J. Exp. Med.* **221**, e20230341 (2023).

48. Freund, I. *et al.* 2′-O-methylation within prokaryotic and eukaryotic tRNA inhibits innate immune activation by endosomal Toll-like receptors but does not affect recognition of whole organisms. *RNA* **25**, 869–880 (2019).

49. Rimbach, K., Kaiser, S., Helm, M., Dalpke, A. H. & Eigenbrod, T. 2'-O-Methylation within Bacterial RNA Acts as Suppressor of TLR7/TLR8 Activation in Human Innate Immune Cells. *J. Innate Immun.* **7**, 482–493 (2015).

50. Safran, S. A., Eckert, D. M., Leslie, E. A. & Bass, B. L. PKR activation by noncanonical ligands: a 5′-triphosphate requirement versus antisense contamination. *RNA* **25**, 1192–1201 (2019).

51. Lemaire, P. A., Anderson, E., Lary, J. & Cole, J. L. Mechanism of PKR Activation by dsRNA. *J. Mol. Biol.* **381**, 351–360 (2008).

52. Donnelly, N., Gorman, A. M., Gupta, S. & Samali, A. The eIF2α kinases: their structures and functions. *Cell. Mol. Life Sci.* **70**, 3493–3511 (2013).

53. Reuver, R. de & Maelfait, J. Novel insights into double-stranded RNA-mediated immunopathology. *Nat. Rev. Immunol.* 1–15 (2023) doi:10.1038/s41577-023-00940-3.

54. Boehmer, D. F. R. *et al.* OAS1/RNase L executes RIG-I ligand–dependent tumor cell apoptosis. *Sci. Immunol.* **6**, (2021).

55. Meng, H. *et al.* Regulation of the Interferon-Inducible 2′–5′-Oligoadenylate Synthetases by Adenovirus VAI RNA. *J. Mol. Biol.* **422**, 635–649 (2012).

56. Malathi, K., Dong, B., Gale, M. & Silverman, R. H. Small self-RNA generated by RNase L amplifies antiviral innate immunity. *Nature* **448**, 816–819 (2007).

57. Fenner, F. Global Eradication of Smallpox. *Rev. Infect. Dis.* **4**, 916–930 (1982).

58. Pollard, A. J. & Bijker, E. M. A guide to vaccinology: from basic principles to new developments. *Nat. Rev. Immunol.* **21**, 83–100 (2021).

59. European Medicines Agency. European Public Assessment Report: Comirnaty, EMA/392045/2023. (2021).

60. European Medicines Agency. European Public Assessment Report: Spikevax, EMA/360647/2023. (2021).

61. Li, H., Willingham, S. B., Ting, J. P.-Y. & Re, F. Cutting Edge: Inflammasome Activation by Alum and Alum's Adjuvant Effect Are Mediated by NLRP3. *J. Immunol.* **181**, 17–21 (2008).

62. Giannini, S. L. *et al.* Enhanced humoral and memory B cellular immunity using HPV16/18 L1 VLP vaccine formulated with the MPL/aluminium salt combination (AS04) compared to aluminium salt only. *Vaccine* **24**, 5937–5949 (2006).

63. Vollmer, J. & Krieg, A. M. Immunotherapeutic applications of CpG oligodeoxynucleotide TLR9 agonists. *Adv. Drug Deliv. Rev.* **61**, 195–204 (2009).

64. Zhao, T. *et al.* Vaccine adjuvants: mechanisms and platforms. *Signal Transduct. Target. Ther.* **8**, 283 (2023).

65. Ribi, E. *et al.* Peptides as requirement for immunotherapy of the guinea-pig line-10 tumor with endotoxins. *Cancer Immunol., Immunother.* **7**, 43–58 (1979).

66. Ribi, E. *et al.* Preparation and antitumor activity of nontoxic lipid A. *Cancer Immunol., Immunother.* **12**, 91–96 (1982).

67. Li, C. *et al.* Mechanisms of innate and adaptive immunity to the Pfizer-BioNTech BNT162b2 vaccine. *Nat Immunol* **23**, 543–555 (2022).

68. Pulendran, B., Arunachalam, P. S. & O'Hagan, D. T. Emerging concepts in the science of vaccine adjuvants. *Nat. Rev. Drug Discov.* **20**, 454–475 (2021).

69. Brisse, M., Vrba, S. M., Kirk, N., Liang, Y. & Ly, H. Emerging Concepts and Technologies in Vaccine Development. *Front. Immunol.* **11**, 583077 (2020).

70. Qin, F. *et al.* A Guide to Nucleic Acid Vaccines in the Prevention and Treatment of Infectious Diseases and Cancers: From Basic Principles to Current Applications. *Front. Cell Dev. Biol.* **9**, 633776 (2021).

71. Lu, B. *et al.* The next-generation DNA vaccine platforms and delivery systems: advances, challenges and prospects. *Front. Immunol.* **15**, 1332939 (2024).

72. Pardi, N., Hogan, M. J., Porter, F. W. & Weissman, D. mRNA vaccines — a new era in vaccinology. *Nat. Rev. Drug Discov.* **17**, 261–279 (2018).

73. Warren, L. *et al.* Highly Efficient Reprogramming to Pluripotency and Directed Differentiation of Human Cells with Synthetic Modified mRNA. *Cell Stem Cell* **7**, 618–630 (2010).

74. Zangi, L. *et al.* Modified mRNA directs the fate of heart progenitor cells and induces vascular regeneration after myocardial infarction. *Nat. Biotechnol.* **31**, 898–907 (2013).

75. Rizvi, F. *et al.* Murine liver repair via transient activation of regenerative pathways in hepatocytes using lipid nanoparticle-complexed nucleoside-modified mRNA. *Nat. Commun.* **12**, 613 (2021).

76. Gillmore, J. D. *et al.* CRISPR-Cas9 In Vivo Gene Editing for Transthyretin Amyloidosis. *N. Engl. J. Med.* **385**, 493–502 (2021).

77. Sahin, U., Karikó, K. & Türeci, Ö. mRNA-based therapeutics — developing a new class of drugs. *Nat Rev Drug Discov* **13**, 759–780 (2014).

78. World Health Organization. WHO Director-General's opening remarks at the media briefing on COVID-19, 11 March 2020. https://www.who.int/director-general/speeches/detail/who-director-general-s-opening-remarks-at-the-media-briefing-on-covid-19---11-march-2020 (2020).

79. Chaudhary, N., Weissman, D. & Whitehead, K. A. mRNA vaccines for infectious diseases: principles, delivery and clinical translation. *Nat Rev Drug Discov* **20**, 817–838 (2021).

80. Meyerowitz, E. A., Scott, J., Richterman, A., Male, V. & Cevik, M. Clinical course and management of COVID-19 in the era of widespread population immunity. *Nat. Rev. Microbiol.* **22**, 75–88 (2024).

81. Steiner, S. *et al.* SARS-CoV-2 biology and host interactions. *Nat. Rev. Microbiol.* **22**, 206–225 (2024).

82. Rijkers, G. T. *et al.* Antigen Presentation of mRNA-Based and Virus-Vectored SARS-CoV-2 Vaccines. *Vaccines* **9**, 848 (2021).

83. Andries, O. *et al.* N1-methylpseudouridine-incorporated mRNA outperforms pseudouridine-incorporated mRNA by providing enhanced protein expression and reduced immunogenicity in mammalian cell lines and mice. *J Control Release* **217**, 337–344 (2015).

84. Connors, J. *et al.* Lipid nanoparticles (LNP) induce activation and maturation of antigen presenting cells in young and aged individuals. *Commun. Biol.* **6**, 188 (2023).

85. DIMITRIADIS, G. J. Translation of rabbit globin mRNA introduced by liposomes into mouse lymphocytes. *Nature* **274**, 923–924 (1978).

86. Wolff, J. A. *et al.* Direct Gene Transfer into Mouse Muscle in Vivo. *Science* **247**, 1465–1468 (1990).

87. Martinon, F. *et al.* Induction of virus-specific cytotoxic T lymphocytes in vivo by liposome-entrapped mRNA. *Eur. J. Immunol.* **23**, 1719–1722 (1993).

88. Chamberlin, M. & Ring, J. Characterization of T7-specific ribonucleic acid polymerase. 1. General properties of the enzymatic reaction and the template specificity of the enzyme. *J. Biol. Chem.* **248**, 2235–44 (1973).

89. Milligan, J. F., Groebe, D. R., Witherell, G. W. & Uhlenbeck, O. C. Oligoribonucleotide synthesis using T7 RNA polymerase and synthetic DNA templates. *Nucleic Acids Res.* **15**, 8783–8798 (1987).

90. Cheetham, G. M. T., Jeruzalmi, D. & Steitz, T. A. Structural basis for initiation of transcription from an RNA polymerase–promoter complex. *Nature* **399**, 80–83 (1999).

91. Kuzmine, I., Gottlieb, P. A. & Martin, C. T. Binding of the Priming Nucleotide in the Initiation of Transcription by T7 RNA Polymerase*. *J. Biol. Chem.* **278**, 2819–2823 (2003).

92. Jiang, M., Rong, M., Martin, C. & McAllister, W. T. Interrupting the template strand of the T7 promoter facilitates translocation of the DNA during initiation, reducing transcript slippage and the release of abortive products11Edited by M. Gottesman. *J. Mol. Biol.* **310**, 509–522 (2001).

93. Imburgio, D., Anikin, M. & McAllister, W. T. Effects of Substitutions in a Conserved DX2GR Sequence Motif, Found in Many DNA-dependent Nucleotide Polymerases, on Transcription by T7 RNA Polymerase. *J. Mol. Biol.* **319**, 37–51 (2002).

94. Brieba, L. G., Padilla, R. & Sousa, R. Role of T7 RNA Polymerase His784 in Start Site Selection and Initial Transcription †. *Biochemistry* **41**, 5144–5149 (2002).

95. Jackson, R. J., Hellen, C. U. T. & Pestova, T. V. The mechanism of eukaryotic translation initiation and principles of its regulation. *Nat Rev Mol Cell Bio* **11**, 113–127 (2010).

96. Stepinski, J., Waddell, C., Stolarski, R., Darzynkiewicz, E. & Rhoads, R. E. Synthesis and properties of mRNAs containing the novel "anti-reverse" cap analogs 7-methyl(3'-O-methyl)GpppG and 7-methyl (3'-deoxy)GpppG. *RNA (N. York, NY)* **7**, 1486–95 (2001).

97. Henderson, J. M. *et al.* Cap 1 Messenger RNA Synthesis with Co-transcriptional CleanCap® Analog by In Vitro Transcription. *Curr. Protoc.* **1**, e39 (2021).

98. Sikorski, P. J. *et al.* The identity and methylation status of the first transcribed nucleotide in eukaryotic mRNA 5′ cap modulates protein expression in living cells. *Nucleic Acids Res.* **48**, 1607–1626 (2020).

99. TriLink Biotechnologies. CleanCap® AG Product Insert. (2025).

100. TriLink Biotechnologies. CleanCap® GG Product Insert. (2025).

101. Sahin, U. *et al.* COVID-19 vaccine BNT162b1 elicits human antibody and TH1 T cell responses. *Nature* **586**, 594–599 (2020).

102. Moss, B., Gershowitz, A., Wei, C.-M. & Boone, R. Formation of the guanylylated and methylated 5′-terminus of vaccinia virus mRNA. *Virology* **72**, 341–351 (1976).

103. Ensinger, M. J., Martin, S. A., Paoletti, E. & Moss, B. Modification of the 5'-terminus of mRNA by soluble guanylyl and methyl transferases from vaccinia virus. *Proc. Natl. Acad. Sci.* **72**, 2525–2529 (1975).

104. Corbett, K. S. *et al.* SARS-CoV-2 mRNA vaccine design enabled by prototype pathogen preparedness. *Nature* **586**, 567–571 (2020).

105. Shuman, S. Catalytic activity of vaccinia mRNA capping enzyme subunits coexpressed in Escherichia coli. *J. Biol. Chem.* **265**, 11960–11966 (1990).

106. Lenk, R. *et al.* Understanding the impact of in vitro transcription byproducts and contaminants. *Front. Mol. Biosci.* **11**, 1426129 (2024).

107. Koh, H. R. *et al.* Correlating Transcription Initiation and Conformational Changes by a Single-Subunit RNA Polymerase with Near Base-Pair Resolution. *Mol. Cell* **70**, 695-706.e5 (2018).

108. Cazenave, C. & Uhlenbeck, O. C. RNA template-directed RNA synthesis by T7 RNA polymerase. *Proc. Natl. Acad. Sci.* **91**, 6972–6976 (1994).

109. Triana-Alonso, F. J., Dabrowski, M., Wadzack, J. & Nierhaus, K. H. Self-coded 3′-Extension of Run-off Transcripts Produces Aberrant Products during in Vitro Transcription with T7 RNA Polymerase (∗). *J Biol Chem* **270**, 6298–6307 (1995).

110. Gholamalipour, Y., Karunanayake Mudiyanselage, A. & Martin, C. T. 3′ end additions by T7 RNA polymerase are RNA self-templated, distributive and diverse in character—RNA-Seq analyses. *Nucleic Acids Res.* **46**, gky796- (2018).

111. Karikó, K., Buckstein, M., Ni, H. & Weissman, D. Suppression of RNA Recognition by Toll-like Receptors: The Impact of Nucleoside Modification and the Evolutionary Origin of RNA. *Immunity* **23**, 165–175 (2005).

112. Karikó, K., Ni, H., Capodici, J., Lamphier, M. & Weissman, D. mRNA Is an Endogenous Ligand for Toll-like Receptor 3*. *J Biol Chem* **279**, 12542–12550 (2004).

113. Kranz, L. M. *et al.* Systemic RNA delivery to dendritic cells exploits antiviral defence for cancer immunotherapy. *Nature* **534**, 396–401 (2016).

114. Pollard, C. *et al.* Type I IFN Counteracts the Induction of Antigen-Specific Immune Responses by Lipid-Based Delivery of mRNA Vaccines. *Mol. Ther.* **21**, 251–259 (2013).

115. Karikó, K., Muramatsu, H., Ludwig, J. & Weissman, D. Generating the optimal mRNA for therapy: HPLC purification eliminates immune activation and improves translation of nucleoside-modified, protein-encoding mRNA. *Nucleic Acids Res* **39**, e142–e142 (2011).

116. Pichlmair, A. *et al.* RIG-I-Mediated Antiviral Responses to Single-Stranded RNA Bearing 5’-Phosphates. *Science* **314**, 997–1001 (2006).

117. Karikó, K. *et al.* Incorporation of Pseudouridine Into mRNA Yields Superior Nonimmunogenic Vector With Increased Translational Capacity and Biological Stability. *Mol Ther* **16**, 1833–1840 (2008).

118. Anderson, B. R. *et al.* Incorporation of pseudouridine into mRNA enhances translation by diminishing PKR activation. *Nucleic Acids Res* **38**, 5884–5892 (2010).

119. Anderson, B. R. *et al.* Nucleoside modifications in RNA limit activation of 2′-5′-oligoadenylate synthetase and increase resistance to cleavage by RNase L. *Nucleic Acids Res.* **39**, 9329–9338 (2011).

120. Moseman, E. A., Wu, T., Torre, J. C. de la, Schwartzberg, P. L. & McGavern, D. B. Type I interferon suppresses virus-specific B cell responses by modulating CD8+ T cell differentiation. *Sci. Immunol.* **1**, (2016).

121. Fallet, B. *et al.* Interferon-driven deletion of antiviral B cells at the onset of chronic infection. *Sci. Immunol.* **1**, (2016).

122. Crouse, J., Kalinke, U. & Oxenius, A. Regulation of antiviral T cell responses by type I interferons. *Nat. Rev. Immunol.* **15**, 231–242 (2015).

123. Ishii, K. J. & Akira, S. TLR Ignores Methylated RNA? *Immunity* **23**, 111–113 (2005).

124. Weissman, D. *et al.* HIV Gag mRNA Transfection of Dendritic Cells (DC) Delivers Encoded Antigen to MHC Class I and II Molecules, Causes DC Maturation, and Induces a Potent Human In Vitro Primary Immune Response. *J Immunol* **165**, 4710–4717 (2000).

125. Moradian, H., Roch, T., Lendlein, A. & Gossen, M. mRNA Transfection-Induced Activation of Primary Human Monocytes and Macrophages: Dependence on Carrier System and Nucleotide Modification. *Sci Rep-uk* **10**, 4181 (2020).

126. Nelson, J. *et al.* Impact of mRNA chemistry and manufacturing process on innate immune activation. *Sci Adv* **6**, eaaz6893 (2020).

127. Bon, A. L. *et al.* Type I Interferons Potently Enhance Humoral Immunity and Can Promote Isotype Switching by Stimulating Dendritic Cells In Vivo. *Immunity* **14**, 461–470 (2001).

128. Bon, A. L. *et al.* Cutting Edge: Enhancement of Antibody Responses Through Direct Stimulation of B and T Cells by Type I IFN. *J. Immunol.* **176**, 2074–2078 (2006).

129. Bon, A. L. *et al.* Cross-priming of CD8+ T cells stimulated by virus-induced type I interferon. *Nat. Immunol.* **4**, 1009–1015 (2003).

130. Bacher, N. *et al.* Interferon-α Suppresses cAMP to Disarm Human Regulatory T Cells. *Cancer Res.* **73**, 5647–5656 (2013).

131. Longhi, M. P. *et al.* Dendritic cells require a systemic type I interferon response to mature and induce CD4+ Th1 immunity with poly IC as adjuvant. *J. Exp. Med.* **206**, 1589–1602 (2009).

132. Rajagopal, D. *et al.* Plasmacytoid dendritic cell–derived type I interferon is crucial for the adjuvant activity of Toll-like receptor 7 agonists. *Blood* **115**, 1949–1957 (2010).

133. The Nobel Prize in Physiology or Medicine 2023 - NobelPrize.org. https://www.nobelprize.org/prizes/medicine/2023/summary/.

134. Sun, H., Li, K., Liu, C. & Yi, C. Regulation and functions of non-m6A mRNA modifications. *Nat. Rev. Mol. Cell Biol.* 1–18 (2023) doi:10.1038/s41580-023-00622-x.

135. Kierzek, E. *et al.* The contribution of pseudouridine to stabilities and structure of RNAs. *Nucleic Acids Res* **42**, 3492–3501 (2014).

136. Morais, P., Adachi, H. & Yu, Y.-T. The Critical Contribution of Pseudouridine to mRNA COVID-19 Vaccines. *Front. Cell Dev. Biol.* **9**, 789427 (2021).

137. Cappannini, A. *et al.* MODOMICS: a database of RNA modifications and related information. 2023 update. *Nucleic Acids Res.* **52**, D239–D244 (2023).

138. McCown, P. J. *et al.* Naturally occurring modified ribonucleosides. *Wiley Interdiscip. Rev.: RNA* **11**, e1595 (2020).

139. Desrosiers, R., Friderici, K. & Rottman, F. Identification of Methylated Nucleosides in Messenger RNA from Novikoff Hepatoma Cells. *Proc. Natl. Acad. Sci.* **71**, 3971–3975 (1974).

140. Dominissini, D. *et al.* Topology of the human and mouse m6A RNA methylomes revealed by m6A-seq. *Nature* **485**, 201–206 (2012).

141. Qiu, W. *et al.* N6-methyladenosine RNA modification suppresses antiviral innate sensing pathways via reshaping double-stranded RNA. *Nat Commun* **12**, 1582 (2020).

142. Li, N. *et al.* METTL3 regulates viral m6A RNA modification and host cell innate immune responses during SARS-CoV-2 infection. *Cell Reports* **35**, 109091 (2021).

143. Mao, Y. *et al.* m6A in mRNA coding regions promotes translation via the RNA helicase-containing YTHDC2. *Nat. Commun.* **10**, 5332 (2019).

144. Moradian, H., Roch, T., Anthofer, L., Lendlein, A. & Gossen, M. Chemical modification of uridine modulates mRNA-mediated proinflammatory and antiviral response in primary human macrophages. *Mol Ther - Nucleic Acids* **27**, 854–869 (2022).

145. Baiersdörfer, M. *et al.* A Facile Method for the Removal of dsRNA Contaminant from In Vitro-Transcribed mRNA. *Mol Ther - Nucleic Acids* **15**, 26–35 (2019).

146. Luo, D. *et al.* Lateral flow immunoassay for rapid and sensitive detection of dsRNA contaminants in in vitro-transcribed mRNA products. *Mol. Ther. - Nucleic Acids* **32**, 445–453 (2023).

147. Svitkin, Y. V. *et al.* N1-methyl-pseudouridine in mRNA enhances translation through eIF2α-dependent and independent mechanisms by increasing ribosome density. *Nucleic Acids Res* **45**, gkx135 (2017).

148. Mauger, D. M. *et al.* mRNA structure regulates protein expression through changes in functional half-life. *Proc National Acad Sci* **116**, 24075–24083 (2019).

149. Peisley, A., Wu, B., Yao, H., Walz, T. & Hur, S. RIG-I Forms Signaling-Competent Filaments in an ATP-Dependent, Ubiquitin-Independent Manner. *Mol. Cell* **51**, 573–583 (2013).

150. Durbin, A. F., Wang, C., Marcotrigiano, J. & Gehrke, L. RNAs Containing Modified Nucleotides Fail To Trigger RIG-I Conformational Changes for Innate Immune Signaling. *Mbio* **7**, e00833-16 (2016).

151. Arunachalam, P. S. *et al.* Systems vaccinology of the BNT162b2 mRNA vaccine in humans. *Nature* **596**, 410–416 (2021).

152. Kumar, H. *et al.* Essential role of IPS-1 in innate immune responses against RNA viruses. *J. Exp. Med.* **203**, 1795–1803 (2006).

153. Hemmi, H. *et al.* Small anti-viral compounds activate immune cells via the TLR7 MyD88–dependent signaling pathway. *Nat. Immunol.* **3**, 196–200 (2002).

154. Rapino, F. *et al.* C/EBPα Induces Highly Efficient Macrophage Transdifferentiation of B Lymphoma and Leukemia Cell Lines and Impairs Their Tumorigenicity. *Cell Rep.* **3**, 1153–1163 (2013).

155. Rapino, F. *et al.* C/EBPα Induces Highly Efficient Macrophage Transdifferentiation of B Lymphoma and Leukemia Cell Lines and Impairs Their Tumorigenicity. *Cell Rep.* **19**, 1281 (2017).

156. Zal, T., Volkmann, A. & Stockinger, B. Mechanisms of tolerance induction in major histocompatibility complex class II-restricted T cells specific for a blood-borne self-antigen. *J. Exp. Med.* **180**, 2089–2099 (1994).

157. Gitlin, L. *et al.* Essential role of mda-5 in type I IFN responses to polyriboinosinic:polyribocytidylic acid and encephalomyocarditis picornavirus. *Proc. Natl. Acad. Sci.* **103**, 8459–8464 (2006).

158. Liehl, P. *et al.* Innate Immunity Induced by Plasmodium Liver Infection Inhibits Malaria Reinfections. *Infect. Immun.* **83**, 1172–1180 (2015).

159. Martin, M. Cutadapt removes adapter sequences from high-throughput sequencing reads. *EMBnetJ.* **17**, 10–12 (2011).

160. Love, M. I., Huber, W. & Anders, S. Moderated estimation of fold change and dispersion for RNA-seq data with DESeq2. *Genome Biol.* **15**, 550 (2014).

161. Putri, G. H., Anders, S., Pyl, P. T., Pimanda, J. E. & Zanini, F. Analysing high-throughput sequencing data in Python with HTSeq 2.0. *Bioinformatics* **38**, 2943–2945 (2022).

162. Danecek, P. *et al.* Twelve years of SAMtools and BCFtools. *GigaScience* **10**, giab008 (2021).

163. Dobin, A. *et al.* STAR: ultrafast universal RNA-seq aligner. *Bioinformatics* **29**, 15–21 (2012).

164. Bussmann, L. H. *et al.* A Robust and Highly Efficient Immune Cell Reprogramming System. *Cell Stem Cell* **5**, 554–566 (2009).

165. Omo-Lamai, S. *et al.* Lipid Nanoparticle-Associated Inflammation is Triggered by Sensing of Endosomal Damage: Engineering Endosomal Escape Without Side Effects. *bioRxiv* 2024.04.16.589801 (2024) doi:10.1101/2024.04.16.589801.

166. Sharma, P., Hoorn, D., Aitha, A., Breier, D. & Peer, D. The immunostimulatory nature of mRNA lipid nanoparticles. *Adv. Drug Deliv. Rev.* **205**, 115175 (2024).

167. Shuman, S. Catalytic activity of vaccinia mRNA capping enzyme subunits coexpressed in Escherichia coli. *J. Biol. Chem.* **265**, 11960–6 (1990).

168. Welbourne, E. N. *et al.* Anion exchange HPLC monitoring of mRNA in vitro transcription reactions to support mRNA manufacturing process development. *Front. Mol. Biosci.* **11**, 1250833 (2024).

169. Wei, L., Zhang, M., Zhang, H., Zhao, H. & Mei, Y. A poly(A) polymerase and oligo(dT)-dependent method for the purification of engineering circular RNAs that enhances protein expression in eukaryotic cells. *bioRxiv* 2024.12.27.630476 (2024) doi:10.1101/2024.12.27.630476.

170. Qu, J. *et al.* Quality by design for mRNA platform purification based on continuous oligo-dT chromatography. *Mol. Ther. - Nucleic Acids* **35**, 102333 (2024).

171. Schmidt, A. *et al.* 5′-triphosphate RNA requires base-paired structures to activate antiviral signaling via RIG-I. *Proc. Natl. Acad. Sci.* **106**, 12067–12072 (2009).

172. Ramanathan, A., Robb, G. B. & Chan, S.-H. mRNA capping: biological functions and applications. *Nucleic Acids Res.* **44**, 7511–7526 (2016).

173. Hou, X., Zaks, T., Langer, R. & Dong, Y. Lipid nanoparticles for mRNA delivery. *Nat. Rev. Mater.* **6**, 1078–1094 (2021).

174. Jurk, M. *et al.* Human TLR7 or TLR8 independently confer responsiveness to the antiviral compound R-848. *Nat. Immunol.* **3**, 499–499 (2002).

175. Hornung, V. *et al.* Sequence-specific potent induction of IFN-α by short interfering RNA in plasmacytoid dendritic cells through TLR7. *Nat. Med.* **11**, 263–270 (2005).

176. Hemmi, H. *et al.* A Toll-like receptor recognizes bacterial DNA. *Nature* **408**, 740–745 (2000).

177. Liu, K. *et al.* Skewed endosomal RNA responses from TLR7 to TLR3 in RNase T2-deficient macrophages. *Int. Immunol.* **33**, 479–490 (2021).

178. Schmidt, O. Genetik und Molekularbiologie. (2017) doi:10.1007/978-3-662-50274-7.

179. Bonin, M. *et al.* Determination of preferential binding sites for anti-dsRNA antibodies on double-stranded RNA by scanning force microscopy. *RNA* **6**, 563–570 (2000).

180. Wienert, B., Shin, J., Zelin, E., Pestal, K. & Corn, J. E. In vitro–transcribed guide RNAs trigger an innate immune response via the RIG-I pathway. *PLoS Biol.* **16**, e2005840 (2018).

181. Aliabadi, H. M. Polymers and Nanomaterials for Gene Therapy. in 55–80 (2016). doi:10.1016/b978-0-08-100520-0.00003-5.

182. Blasius, A. L. & Beutler, B. Intracellular Toll-like Receptors. *Immunity* **32**, 305–315 (2010).

183. Yoneyama, M., Kato, H. & Fujita, T. Physiological functions of RIG-I-like receptors. *Immunity* **57**, 731–751 (2024).

184. Kužnik, A. *et al.* Mechanism of Endosomal TLR Inhibition by Antimalarial Drugs and Imidazoquinolines. *J. Immunol.* **186**, 4794–4804 (2011).

185. Kormann, M. S. D. *et al.* Expression of therapeutic proteins after delivery of chemically modified mRNA in mice. *Nat Biotechnol* **29**, 154–157 (2011).

186. Bérouti, M. *et al.* Lysosomal endonuclease RNase T2 and PLD exonucleases cooperatively generate RNA ligands for TLR7 activation. *Immunity* (2024) doi:10.1016/j.immuni.2024.04.010.

187. Slobodin, B. *et al.* Transcription Impacts the Efficiency of mRNA Translation via Co-transcriptional N6-adenosine Methylation. *Cell* **169**, 326-337.e12 (2017).

188. Melamed, J. R. *et al.* Lipid nanoparticle chemistry determines how nucleoside base modifications alter mRNA delivery. *J Control Release* **341**, 206–214 (2022).

189. Sioud, M., Juzeniene, A. & Sæbøe-Larssen, S. Exploring the Impact of mRNA Modifications on Translation Efficiency and Immune Tolerance to Self-Antigens. *Vaccines* **12**, 624 (2024).

190. Ashley, C. L., Abendroth, A., McSharry, B. P. & Slobedman, B. Interferon-Independent Upregulation of Interferon-Stimulated Genes during Human Cytomegalovirus Infection is Dependent on IRF3 Expression. *Viruses* **11**, 246 (2019).

191. Li, B., Luo, X. & Dong, Y. Effects of Chemically Modified Messenger RNA on Protein Expression. *Bioconjugate Chem.* **27**, 849–853 (2016).

192. Ilan, L. *et al.* PKR activation and eIF2α phosphorylation mediate human globin mRNA splicing at spliceosome assembly. *Cell Res.* **27**, 688–704 (2017).

193. Ben-Asouli, Y., Banai, Y., Hauser, H. & Kaempfer, R. Recognition of 5′-terminal TAR structure in human immunodeficiency virus-1 mRNA by eukaryotic translation initiation factor 2. *Nucleic Acids Res.* **28**, 1011–1018 (2000).

194. Davis, S. & Watson, J. C. In vitro activation of the interferon-induced, double-stranded RNA-dependent protein kinase PKR by RNA from the 3’ untranslated regions of human alpha-tropomyosin. *Proc. Natl. Acad. Sci.* **93**, 508–513 (1996).

195. Sharp, T. V., Xiao, Q., Jeffrey, I., Gewert, D. R. & Clemens, M. J. Reversal of the double-stranded-RNA-induced inhibition of protein synthesis by a catalytically inactive mutant of the protein kinase PKR. *Eur. J. Biochem.* **214**, 945–948 (1993).

196. Promega. Rabbit Reticulocyte Lysate System, Instructions for Use of Products L4960 and L4151. (2017).

197. Matsumiya, T. *et al.* The double-stranded RNA-dependent protein kinase PKR negatively regulates the protein expression of IFN-β induced by RIG-I signaling. *FASEB J.* **37**, e22780 (2023).

198. Nallagatla, S. R. & Bevilacqua, P. C. Nucleoside modifications modulate activation of the protein kinase PKR in an RNA structure-specific manner. *Rna* **14**, 1201–1213 (2008).

199. Nallagatla, S. R. *et al.* Native Tertiary Structure and Nucleoside Modifications Suppress tRNA's Intrinsic Ability to Activate the Innate Immune Sensor PKR. *PLoS ONE* **8**, e57905 (2013).

200. Krienke, C. *et al.* A noninflammatory mRNA vaccine for treatment of experimental autoimmune encephalomyelitis. *Science* **371**, 145–153 (2021).

201. Linares-Fernández, S. *et al.* Combining an optimized mRNA template with a double purification process allows strong expression of in vitro transcribed mRNA. *Mol. Ther. - Nucleic Acids* **26**, 945–956 (2021).

202. Wang, G. *et al.* mRNA produced by VSW-3 RNAP has high-level translation efficiency with low inflammatory stimulation. *Cell Insight* **1**, 100056 (2022).

203. Wu, M. Z., Asahara, H., Tzertzinis, G. & Roy, B. Synthesis of low immunogenicity RNA with high-temperature in vitro transcription. *Rna* **26**, 345–360 (2020).

204. New England Biolabs. Faustovirus Capping Enzyme, M2081. https://www.neb.com/en/products/m2081-faustovirus-capping-enzyme (2024).

205. Biosearch Technologies. Terminator 5′-Phosphate-Dependent Exonuclease Manual. (2024).

206. Vlatkovic, I. *et al.* Ribozyme Assays to Quantify the Capping Efficiency of In Vitro-Transcribed mRNA. *Pharmaceutics* **14**, 328 (2022).

207. Beverly, M., Dell, A., Parmar, P. & Houghton, L. Label-free analysis of mRNA capping efficiency using RNase H probes and LC-MS. *Anal. Bioanal. Chem.* **408**, 5021–5030 (2016).

208. Grudzien, E. *et al.* Novel cap analogs for in vitro synthesis of mRNAs with high translational efficiency. *RNA* **10**, 1479–1487 (2004).

209. Onomoto, K., Onoguchi, K. & Yoneyama, M. Regulation of RIG-I-like receptor-mediated signaling: interaction between host and viral factors. *Cell. Mol. Immunol.* **18**, 539–555 (2021).

210. Asgari, S. *et al.* Severe viral respiratory infections in children with IFIH1 loss-of-function mutations. *Proc. Natl. Acad. Sci.* **114**, 8342–8347 (2017).

211. UniProt: RIG-I (Homo sapiens). https://www.uniprot.org/uniprotkb/O95786/entry.

212. UniProt: RIG-I (Mus musculus). https://www.uniprot.org/uniprotkb/Q6Q899/entry.

213. UniProt: MDA5 (Homo sapiens). https://www.uniprot.org/uniprotkb/Q9BYX4/entry.

214. UniProt: MDA5 (Mus musculus). https://www.uniprot.org/uniprotkb/Q8R5F7/entry.

215. Rajsbaum, R. *et al.* Species-Specific Inhibition of RIG-I Ubiquitination and IFN Induction by the Influenza A Virus NS1 Protein. *PLoS Pathog.* **8**, e1003059 (2012).

216. Ablasser, A. *et al.* cGAS produces a 2′-5′-linked cyclic dinucleotide second messenger that activates STING. *Nature* **498**, 380–384 (2013).

217. Gao, P. *et al.* Structure-Function Analysis of STING Activation by c[G(2′,5′)pA(3′,5′)p] and Targeting by Antiviral DMXAA. *Cell* **154**, 748–762 (2013).

218. Yi, G. *et al.* Single Nucleotide Polymorphisms of Human STING Can Affect Innate Immune Response to Cyclic Dinucleotides. *PLoS ONE* **8**, e77846 (2013).

219. Heil, F. *et al.* Species-Specific Recognition of Single-Stranded RNA via Toll-like Receptor 7 and 8. *Science* **303**, 1526–1529 (2004).

220. Oldenburg, M. *et al.* TLR13 Recognizes Bacterial 23S rRNA Devoid of Erythromycin Resistance–Forming Modification. *Science* **337**, 1111–1115 (2012).

221. Vaure, C. & Liu, Y. A Comparative Review of Toll-Like Receptor 4 Expression and Functionality in Different Animal Species. *Front. Immunol.* **5**, 316 (2014).

222. Schönborn, J. *et al.* Monoclonal antibodies to double-stranded RNA as probes of RNA structure in crude nucleic acid extracts. *Nucleic Acids Res.* **19**, 2993–3000 (1991).

223. Gao, Y. *et al.* m6A Modification Prevents Formation of Endogenous Double-Stranded RNAs and Deleterious Innate Immune Responses during Hematopoietic Development. *Immunity* **52**, 1007-1021.e8 (2020).

224. Zhu, L. *et al.* METTL3 suppresses pancreatic ductal adenocarcinoma progression through activating endogenous dsRNA-induced anti-tumor immunity. *Cell Oncol* 1–13 (2023) doi:10.1007/s13402-023-00829-2.

225. Lu, M. *et al.* N6-methyladenosine modification enables viral RNA to escape recognition by RNA sensor RIG-I. *Nat Microbiol* **5**, 584–598 (2020).

226. Chen, S. *et al.* N6-methyladenosine modification of HIV-1 RNA suppresses type-I interferon induction in differentiated monocytic cells and primary macrophages. *Plos Pathog* **17**, e1009421 (2021).

227. Kim, G.-W., Imam, H., Khan, M. & Siddiqui, A. N 6-Methyladenosine modification of hepatitis B and C viral RNAs attenuates host innate immunity via RIG-I signaling. *J Biol Chem* **295**, 13123–13133 (2020).

228. Chen, Y. G. *et al.* N6-Methyladenosine Modification Controls Circular RNA Immunity. *Mol. Cell* **76**, 96-109.e9 (2019).

229. Wang, X. *et al.* N6-methyladenosine-dependent regulation of messenger RNA stability. *Nature* **505**, 117–120 (2014).

230. McFadden, M. J. *et al.* Post-transcriptional regulation of antiviral gene expression by N6-methyladenosine. *Cell Reports* **34**, 108798 (2021).

231. Winkler, R. *et al.* m6A modification controls the innate immune response to infection by targeting type I interferons. *Nat Immunol* **20**, 173–182 (2019).

232. Xiang, J.-F. *et al.* N 6-Methyladenosines Modulate A-to-I RNA Editing. *Mol Cell* **69**, 126-135.e6 (2018).

233. Meyer, K. D. *et al.* Comprehensive Analysis of mRNA Methylation Reveals Enrichment in 3′ UTRs and near Stop Codons. *Cell* **149**, 1635–1646 (2012).

234. Meyer, K. D. *et al.* 5′ UTR m6A Promotes Cap-Independent Translation. *Cell* **163**, 999–1010 (2015).

235. Hoernes, T. P. *et al.* Eukaryotic Translation Elongation is Modulated by Single Natural Nucleotide Derivatives in the Coding Sequences of mRNAs. *Genes-basel* **10**, 84 (2019).

236. Kremsner, P. G. *et al.* Efficacy and safety of the CVnCoV SARS-CoV-2 mRNA vaccine candidate in ten countries in Europe and Latin America (HERALD): a randomised, observer-blinded, placebo-controlled, phase 2b/3 trial. *Lancet Infect. Dis.* **22**, 329–340 (2022).

237. Coch, C. *et al.* Human TLR8 Senses RNA From Plasmodium falciparum-Infected Red Blood Cells Which Is Uniquely Required for the IFN-γ Response in NK Cells. *Front. Immunol.* **10**, 371 (2019).

238. Tockary, T. A. *et al.* Comb-structured mRNA vaccine tethered with short double-stranded RNA adjuvants maximizes cellular immunity for cancer treatment. *Proc. Natl. Acad. Sci.* **120**, e2214320120 (2023).

5.4 Danksagung

Ich danke **Herrn Prof. Dr. Gunther Hartmann** für die Möglichkeit, meine Doktorarbeit an seinem Institut für klinische Chemie und klinische Pharmakologie anfertigen zu dürfen. Außerdem danke ich meinen Gutachtern für ihre Zeit und Mühe zur Bewertung dieser Arbeit. Diese sind, neben **Herrn Prof. Dr. Hartmann**, **Herr Prof. Dr. Michael Famulok**, **Frau Prof. Dr. Irmgard Förster** und **Frau PD Dr. Anke Schiedel**.

Mein besonderer Dank gilt meinem Betreuer **Dr. Thomas Zillinger**. Seine fachliche Expertise und engagierte Betreuung haben mich bereits während meines Praktikums und meiner Masterarbeit überzeugt, sodass ich schließlich auch meine Doktorarbeit unter seiner Anleitung verfassen durfte. Mit einer gelungenen Balance aus Unterstützung und Freiraum hat er meine wissenschaftliche und persönliche Entwicklung maßgeblich gefördert.

Weiterer Dank gilt außerdem **Prof. Dr. Eva Bartok**, die gemeinsam mit **Herrn Hartmann** die Leitung, Organisation und wissenschaftliche Auswertung des Impfstoff-Projekts übernommen hat und aktuell noch die einzelnen Bausteine zum finalen Manuskript zusammensetzt. Zudem hat sie viel Zeit und Mühe in die Korrektur dieser Arbeit investiert und ihre zahlreichen Anmerkungen haben deutlich zu deren Qualität beigetragen.

Außerdem möchte ich allen anderen Kollegen der **AG Hartmann**, **AG Bartok** und **AG Schlee** für die produktive wissenschaftliche Zusammenarbeit danken, insbesondere meinen Co-Erst-Autoren **Thomas Zillinger, Sofía Soler** und **Marcel Renn.** Ich danke **Martin Schlee**, **Katrin Ciupka** und **Charlotte Hunkler** für ihr Mitwirken bei der Untersuchung von PKR-Aktivierung durch modifizierte mRNA. **Christine Wuebben** danke ich für den wissenschaftlichen Austausch und wertvolle Hilfe im Labor, insbesondere bei der LC/MS Analytik (an dieser Stelle auch ein Danke an **Dirk Radzey**). Besonders hervorheben möchte ich außerdem **Bastian Putschli**, der mich im Labor tatkräftig unterstützt hat, sowie **Heike Prange** und **Sidika Choussein**, die für einen reibungslosen Laboralltag sorgen. Ich danke außerdem allen Kollegen, die tatkräftig beim Einsammeln der Impfstoff-Reste geholfen haben, sowie den Kliniken, die diese mitten im Pandemie-Chaos bereitgestellt haben. Auch wenn ich nicht jeden einzeln nennen kann, bin ich all meinen Kollegen dankbar für ihre Unterstützung.

Ich bin außerdem sehr dankbar für die Möglichkeit, mehrere nationale und internationale Konferenzen besucht haben zu dürfen, die ich als äußerst lehrreich und inspirierend empfand, und bei denen ich schöne Erinnerungen mit der Arbeitsgruppe gesammelt habe. Diese wurden mir von **Prof. Hartmann**, **Thomas Zillinger** sowie dem **TRR 237** ermöglicht.

Ich danke allen ehemaligen und derzeitigen Kollegen der AG Hartmann und anderer Arbeitsgruppen für die gute Laune und positive Energie im Arbeitsalltag sowie auf Konferenzreisen, für gemeinsame Unternehmungen außerhalb des Instituts, und die entstandenen Freundschaften. Ein ganz besonders

herzlicher Dank gilt: **Evi, Connie, Madeleine, Sandra, Svenja, Felix, Sofia (Sechi), Sofía (Soler), Christine, Charlotte, Katrin, Samira,** und **Kasia**. Mit euch macht die Arbeit einfach mehr Spaß!
Meinen Freunden danke ich für den unterhaltsamen Ausgleich zum intensiven Arbeitsalltag und die ermutigenden Worte, allen voran natürlich **Patrick**. Deine ruhige und besonnene Art war besonders in stressigen Phasen eine unersetzliche Unterstützung. Ich danke dir für deinen Rückhalt, deinen Humor und für die gemeinsame Zeit, die ich wirklich sehr genieße und schätze.
Zum Schluss danke ich meinen Eltern **Edmund und Ingrid.** Danke für eure Unterstützung in jeder Lebenslage, dass ihr mich und meine Ausbildung immer gefördert habt und dass ich mich immer auf euch verlassen kann.